Understanding the disease mechanisms of cerebellar ataxia through induced pluripotent stem cell models



Maggie Mei-Ki Wong

St Hugh's College

University of Oxford

A thesis submitted for the degree of

Doctor of Philosophy

Trinity 2018

Declaration

The work in this thesis was performed in the Department of Physiology, Anatomy and Genetics. Except where acknowledgement is made, all of the work presented is my own and has not been submitted for any other degree in this or any other University or institute of learning.

Acknowledgement

This thesis is dedicated to my beloved family and friends who supported me unconditionally throughout my DPhil studies. I would like to thank especially my supervisors Professors Esther Becker and Kevin Talbot for their wonderful guidance and patience. Without my colleague Lauren Watson, awesome private mentor Mattéa Finelli and great friends Dasha Svistunova and Liam Argent, I would not be able to finish my DPhil studies. Finally, special thanks to Ole Sudland who accompanied me on this emotional journey.

Understanding the disease mechanisms of cerebellar ataxia through induced pluripotent stem cell models

Maggie Mei-Ki Wong

St Hugh's College

University of Oxford

A thesis submitted for the degree of *Doctor of Philosophy*

Trinity 2018

Abstract

The cerebellar ataxias are a heterogeneous group of incurable disorders that are characterised by progressive dysfunction and degeneration of Purkinje cells. Although numerous causative genes have been identified, the underlying pathogenic mechanisms remain incompletely understood, due to the limited availability of human brain tissue and the lack of reliable disease models. Accumulating evidence has suggested that subtypes of autosomal dominant ataxias (SCAs) are likely to be caused by shared pathogenic pathways. Focused on spinocerebellar ataxia type 14 (SCA14), a subtype of SCAs, this work aimed to understand the aetiology of SCA14 and related SCAs using novel disease models derived from human induced pluripotent stem cells (iPSCs). SCA14 is caused by mutations in protein kinase C gamma (PKCγ), a central molecule in signalling pathways that are important for Purkinje cell development and function. Using iPSCs derived from patients carrying two distinct SCA14 mutations (H36R and H101Q), this work has revealed three novel interconnected disease mechanisms. (1) SCA14 mutations promoted formation of PKCγ foci, which accumulate in the cytoplasm. (2) Mutant PKCγ showed increased kinase activity resulting in increased phosphorylation of substrates. (3) The mislocalisation of hyperactive mutant PKCγ is likely to affect the phosphorylation of its targets at the membrane and the cytoplasm. Importantly, results obtained in SCA14 iPSCs faithfully recapitulated the pathological findings observed in the patient post-mortem cerebellum. Finally, to determine the developmental changes in Purkinje cells, human Purkinje cells were generated from control and SCA14 iPSCs using a novel simplified protocol. Notably, the dendritic development and survival of human SCA14 Purkinje cells were significantly compromised in long-term culture. CRISPR/Cas9-mediated genome editing was also employed to correct the mutations and produce isogenic controls of SCA14 iPSCs. Together, this work highlighted the importance of a faithful disease model and the value of a patient material-driven approach for understanding the aetiology of neurological disorders. In the future, these patient iPSCs would be an ideal platform for further investigation of molecular pathways and therapeutic development for SCA14 and other cerebellar ataxias.

Table of Contents

Declaration ..... **ii**

Acknowledgement ..... **iii**

Table of Contents ..... **v**

List of Figures ..... **ix**

List of Tables ..... **xii**

List of Abbreviations ..... **xiii**

Chapter 1 Introduction **1**

1.1 The cerebellum 1

1.1.1 Overview 1

1.1.2 Organisation of the cerebellum 1

1.2 Cerebellar ataxias 3

1.2.1 Spinocerebellar ataxias (SCAs) 4

1.3 Spinocerebellar ataxia type 14 (SCA14) 14

1.3.1 Genetic basis of SCA14 15

1.4 Protein kinase C gamma (PKCγ) 16

1.4.1 Protein kinase C (PKC) family 16

1.4.2 Structure of PKCγ 17

1.4.3 Regulation of PKCγ 21

1.4.4 Expression and functions of PKCγ in the central nervous system 25

1.5 Current disease models of SCA14 31

1.5.1 Loss-of-function models 31

1.5.2 Transgenic mouse models of SCA14 32

1.6 Proposed pathogenic mechanisms of SCA14 34

1.6.1 Accumulation of mutant PKCγ foci 34

1.6.2 Impairment in mutant protein degradation 36

1.6.3 Abnormal regulation and mobility of mutant PKCγ 37

1.6.4 Altered kinase activity and substrate binding of mutant PKCγ 39

1.6.5 Aberrant calcium homeostasis and signalling 41

1.6.6 Oxidative stress and cell apoptosis 42

1.6.7 Aberrant cerebellar synaptic plasticity 43

1.7 Disease modelling of SCA14 and other cerebellar ataxias using human iPSCs 54

1.8 Aims of study 56

Chapter 2 Common Materials and Methods **60**

2.1 Methods 60

2.1.1 DNA preparation 60

2.1.2 RNA preparation 60

2.1.3 Reverse transcription (RT) 60

2.1.4 Real time quantitative PCR (qPCR) 61

2.1.5 PCR 61

2.1.6 Culture of human iPSCs 62

2.2 Materials 63

Chapter 3 Generation of human induced pluripotent stem cells (iPSCs) from SCA14 patients **68**

3.1 Introduction 68

3.2 Specific Materials and Methods 73

3.2.1 Reprogramming of skin fibroblasts from SCA14 patients into iPSCs 73

3.2.2 Quality control tests 74

3.2.2.1 Karyotyping 75

3.2.2.2 Mycoplasma testing 75

3.2.2.3 Sendai virus clearance 76

3.2.2.4 FACS flow cytometry 76

3.3 Results 76
3.3.1 Reprogramming of SCA14 patients' skin fibroblasts into iPSCs 76
3.3.2 Characterisation of reprogrammed SCA14-iPSCs (quality control tests) 79
3.3.2.1 Karyotyping 79
3.3.2.2 Mycoplasma test 81
3.3.2.3 Sendai virus clearance 82
3.3.2.4 Expression of pluripotency markers (Tra-1-60 and Nanog) 83
3.3.2.5 Determination of genotypes using Sanger sequencing 85
3.4 Chapter Discussion 87
3.4.1 The impact of reprogramming on disease modelling: epigenetic memory of iPSCs 87
3.4.2 Genomic mutations arising in iPSCs during reprogramming 90
3.4.3 Genome editing in iPSCs 91
3.4.4 High-throughput drug screening using iPSCs 91
3.5 Conclusions 93
Chapter 4 Generating isogenic controls for SCA14 iPSCs using CRISPR/Cas9 genome editing 94
4.1 Introduction 94
4.1.1 CRISPR/Cas9 system for genome editing 94
4.2 Specific Materials and Methods 98
4.2.1 Design of gRNAs and repair donors 98
4.2.2 Preparation of sgRNAs and Cas9 nuclease-expressing plasmids 105
4.2.2.1 Annealing of oligonucleotides 105
4.2.2.2 Preparation of cut vectors 105
4.2.2.3 Ligation of annealed oligonucleotides into CRISPR vectors 106
4.2.2.4 Transformation and expansion of DH5-α cells 106
4.2.3 Cell transfection 107
4.2.3.1 Lipofectamine-based transfection of human HEK293T cells 107
4.2.3.2 Nucleofection of iPSC clones 108
4.2.4 Transient Puromycin-selection and expansion of iPSC clones 109
4.2.5 Screening of modified iPSC clones 109
4.2.5.1 Extraction of genomic DNA 109
4.2.5.2 High-resolution melt (HRM) analysis 110
4.2.5.3 T7 endonuclease assays 111
4.2.5.4 Detection of restriction digestion sites introduced 112
4.2.5.5 Tracking of Indels by Decomposition (TIDE) analysis 112
4.3 Results 113
4.3.1 Producing isogenic controls for SCA14 iPSCs using a CRISPR plasmid approach 113
4.3.1.1 Design of gRNAs and repair donor templates for producing isogenic controls for SCA14 iPSCs 114
4.3.1.2 Preparation of constructs 118
4.3.2 Assessing the targeting efficiency of gRNAs in HEK293T cells 120
4.3.3 Producing an isogenic control for SCA14 H36R iPSCs 124
4.3.3.1 Nucleofection and puromycin selection of SCA14 iPSCs 124
4.3.3.2 Screening of modified iPSC clones 126
4.3.4 Producing isogenic controls for SCA41 R762H iPSCs using direct transfection of ribonucleoprotein complexes 129
4.3.4.1 Design of the gRNAs and repair donors 130
4.3.4.2 Testing targeting efficiency of gRNAs in HEK293-BFP cells 133
4.4 Chapter Discussion 136
4.5 Conclusions 139
Chapter 5 SCA14 pathology in patient cerebellum and iPSCs 140
5.1 Introduction 140
5.2 Specific Materials and Methods 143
5.2.1 Phorbol 12-myristate 13-acetate (PMA) and Phorbol 12,13-Dibutyrate (PDBu) treatment of iPSCs 143
5.2.2 Preparation of cerebellar and cell lysates 143
5.2.3 Preparation of Triton-soluble supernatant and --insoluble pellets 144

5.2.4 Dephosphorylation of proteins using Lambda phosphatase 144
5.2.5 SDS-PAGE and immunoblotting 145
5.2.6 Immunostaining 146
5.2.7 Image quantification 147
5.2.8 Statistical analysis 147
5.3 Results 147
5.3.1 SCA14 pathology in patient post-mortem cerebellum 147
5.3.2 PKCγ is endogenously and ubiquitously expressed in the cytoplasm of control and SCA14 iPSCs 151
5.3.3 SCA14 mutations reduce membrane targeting of mutant PKCγ 156
5.3.4 Degradation of mutant PKCγ foci 158
5.3.4.1 Mutant PKCγ foci do not co-localise with ubiquitin 158
5.3.4.2 Mutant PKCγ foci are not removed by autophagy 159
5.3.4.3 Reduced co-localisation of mutant PKCγ foci with lysosomes despite increased lysosomal formation 163
5.3.5 SCA14 mutations increase kinase activity of mutant PKCγ 166
5.3.6 SCA14 mutations in PKCγ increase phosphorylation of its substrate TRPC3 in iPSCs 169
5.4 Chapter Discussion 175
5.4.1 SCA14 mutations promote formation of PKCγ foci 175
5.4.2 Accumulation of PKCγ foci in the cytoplasm 178
5.4.3 SCA14 mutations reduce membrane association of mutant PKCγ 180
5.4.4 Increased kinase activity of PKCγ and excessive downstream signalling 182
5.5 Conclusions 186
Chapter 6 Understanding the pathogenic mechanisms underlying SCA14 using human iPSC-derived Purkinje cells 189
6.1 Introduction 189
6.1.1 The role of SCA14 mutations in Purkinje cell development 189
6.1.2 Cerebellar development 190
6.1.2.1 Early cerebellar specification 191
6.1.2.2 Specification of cerebellar progenitors 193
6.1.2.3 Migration and maturation of Purkinje cells 194
6.1.2.4 Maturation and dendritic development of Purkinje cells 195
6.1.3 Existing protocols for generating cerebellar neurons using human iPSCs 199
6.2 Specific Materials and Methods 201
6.1.1 Differentiation of human iPSCs into Purkinje cells 201
6.1.1.1 Dissociation of human iPSCs 201
6.1.1.2 Formation and culture of embryoid bodies 201
6.1.1.3 Dissociation and co-culture of Purkinje cells 202
6.1.2 Immunocytochemistry 204
6.1.3 Image quantification 205
6.1.4 Statistical analysis 205
6.3 Results 206
6.3.1 Generation of Purkinje cells from human iPSCs 206
6.3.2 Populations of progenitors within control and SCA14 embryoid bodies express early midbrain-hindbrain markers on day 21 208
6.3.3 Control and SCA14 iPSC-derived neural progenitors express markers of Purkinje cell precursors on day 35 210
6.3.4 Human cells express specific markers and show distinctive features of Purkinje cells from day 50 onwards 212
6.3.5 The development and survival of human SCA14 Purkinje cells are compromised .217
6.3.6 Differential expression of PKCγ in control and SCA14 Purkinje cells on day 100 .221
6.4 Chapter Discussion 225
6.4.1 A simplified protocol for the reproducible generation of cerebellar Purkinje cells *in vitro* 225
6.4.2 Further improvements to the Purkinje cell differentiation protocol 226
6.4.3 Developing a differentiation protocol for three-dimensional cerebellar organoids from human iPSCs 230

6.4.4 Effect of SCA14 mutations on the development and survival of human Purkinje cells 231
6.5 Conclusions 236
Chapter 7 Discussion 237
7.1 Summary and significance 237
7.2 Shared disease mechanisms and potential therapies of SCAs 239
7.2.1 Accumulation of protein foci 239
7.2.2 Aberrant phosphorylation of substrates in Purkinje cell-enriched pathways 240
7.3 Conclusion 244
References 245
Appendix 277

List of Figures

Figure 1.1 Schematic of the major cell types and circuitry of the cerebellum. 3
Figure 1.2 Schematic illustration of SCA14 mutations discovered to-date corresponding to different PKCγ protein domains. 16
Figure 1.3 Structure of PKCγ. 20
Figure 1.4 Schematic illustration of the priming phosphorylation events of PKCγ. 22
Figure 1.5 Schematic illustration of the life cycle of PKCγ. 23
Figure 1.6 Simplified illustration of dendritic development via mGluR1-PKCγ-mediated signalling. 28
Figure 1.7 Several SCA14 mutations are located in the residues that are highly conserved and around the binding surfaces with lipid cofactors of PKCγ. 38
Figure 1.8 Pedigree of the four-generation British family with a SCA14 H101Q mutation that was included in this study. 57
Figure 1.9 H36R and H101Q are located at the equivalent positions in the two cysteine-rich subdomains of PKCγ. 58
Figure 1.10 Schematic representation of experimental plans of this study. 59
Figure 3.1 Methods of *in vitro* reprogramming. 72
Figure 3.2: Reprogramming of SCA14 patients' skin fibroblasts into iPSCs using Sendai virus. 78
Figure 3.3: Karyotype analysis of iPSC lines used in the study. 80
Figure 3.4: Sendai virus and transcription factors were cleared from iPSC lines. 83
Figure 3.5: Histograms of FACS results. 84
Figure 3.6: Sequencing results for genotyping. 86
Figure 4.1 Schematic representation of CRISPR/Cas9 genome engineering for generating isogenic controls, selection methods and a flowchart of experiments. 95
Figure 4.2 Procedures for producing isogenic controls. 113
Figure 4.3 The genotypes and the intended corrections of the SCA14 mutations H36R and H101Q. 115
Figure 4.4 Design of gRNAs, DNA repair template and primers for correcting the SCA14 mutations. 117
Figure 4.5 Cloning strategy of gRNA- and Cas9-expressing plasmids. 119
Figure 4.6 Combinations of WT SpCas9, SpCas9n and gRNAs produced indels as detected by HRM analysis and T7 assay. 122
Figure 4.7 PRKCG01-1, a SCA14 iPSC line harbouring the H36R mutation, was transfected with gRNA- and SpCas9n-expressing plasmids using nucleofection and selected for puromycin-resistant cells. 125

Figure 4.8 Schematic of the screening strategy for edited iPSC clones. 127
Figure 4.9 Deletions but no single nucleotide edits were detected in iPSCs clones transfected with both forward and reverse donors. 129
Figure 4.10 Genomic sequences of control iPSCs, SCA41 iPSCs and HEK293-BFP cells were obtained by Sanger sequencing and used for designing CRISPR strategies to correct the R762H mutation in SCA41 iPSCs. 132
Figure 4.11 T7 assay showed that none of the gRNA-Cas9 combinations successfully produced indels. 134
Figure 4.12 PflMI digestion, Sanger sequencing and TIDE analysis showed that none of the gRNA-Cas9 combinations resulted in the desired gene edits. 135
Figure 4.13 Schematic of the revised design of CRISPR/Cas9 system for correcting the SCA41 (R762H) mutation in the *TRPC3* gene. 138
Figure 5.1 Cerebellar pathology in SCA14 150
Figure 5.2 Mutant PKCγ forms cytoplasmic foci in iPSCs. 154
Figure 5.3 DMSO treatment does not affect iPSC cellular phenotypes. 155
Figure 5.4 SCA14 mutations reduce membrane association of PKCγ. 157
Figure 5.5 Mutant PKCγ foci do not colocalise with ubiquitin. 159
Figure 5.6 Mutant PKCγ foci do not colocalise with LC3II-positive autophgosomes and autophagosome formation is not induced following PKCγ activation. 162
Figure 5.7 SCA14 PKCγ foci only partially colocalise with lysosomes despite significant lysosome enlargement. 165
Figure 5.9 SCA14 mutations enhance kinase activity of PKCγ. 168
Figure 5.10 Phosphorylation of TRPC3, a known substrate of PKCγ, is increased in SCA14 iPSCs. 174
Figure 5.11 Model of the functional effect of PKCγ mutations. 188
Figure 6.1 Schematic representation of the specification of the cerebellar territory. 192
Figure 6.2 Overview of cerebellar neuronal differentiation protocol. 207
Figure 6.3 Control- and SCA14 iPSC-derived neural progenitors express similar levels of early midbrain-hindbrain markers on day 21 209
Figure 6.4 Control and SCA14 iPSC-derived neural progenitors express early specific markers of Purkinje cell precursors on day 35 211
Figure 6.5 Optimisation of terminal differentiation of human iPSC-derived cerebellar Purkinje cells from day 35 onwards. 217
Figure 6.6 The development and survival of SCA14 Purkinje cells were compromised in long-term culture. 221
Figure 6.7 Control and SCA14 cerebellar progenitors showed similar expression pattern of PKCγ on days 21 and 35 but not during terminal differentiation. 223

Figure 6.8 Overview of improved cerebellar neuronal differentiation protocol..... 228
Supplementary Figure 5.1: PKCγ is not degraded via autophagy. 277
Supplementary Figure 6.1: Results of cerebellar progenitors derived from individual iPSC clones. 278

List of Tables

Table 1-1 List of known SCA genes and mutations 6
Table 1-2 Table of known SCA14 mutations and their effects in patients, cell and/or animal models. 44
Table 2-1 A list of primers used in this study 63
Table 2-2 A list of antibodies used in this study. 66
Table 3-1 Results of mycoplasma test 81
Table 3-2 Quality control tests performed on patient iPSC lines 93
Table 4-1 List of CRISPR nucleases from additional bacterial species and their PAM sequences. 97
Table 4-2 List of primers that were used to amplify fragments of DNA surrounding the target mutations for Sanger sequencing. 99
Table 4-3 List of crRNAs targeting the SCA14 H36R and H101Q mutations in the human *PRKCG* gene and the SCA41 R762H mutation in the human *TRPC3* gene designed using the CRISPR Design Tool. 101
Table 4-4 List of single-stranded DNA repair donor templates used in this study. 104
Table 4-5 List of primers used to amplify fragments surrounding the CRISPR cleavage sites in exon 1 and exon 4 of the human *PRKCG* gene for HRM analysis. 111
Table 4-6 List of primers used to amplify fragments surrounding the CRISPR cleavage sites in exon 1 and exon 4 of the human *PRKCG* and *TRPC3* genes respectively. 111
Table 4-7 List of gRNAs targeting SCA14 mutations designed and tested. 118
Table 4-8 List of gRNA- and Cas9- expressing constructs that were generated. 120
Table 4-9 Summary of the transfection conditions and targeting efficiency of gRNAs tested in HEK293T cells using HRM analysis and T7 assay. 123
Supplementary Table 5.1 Demographics and post-mortem interval for control and SCA14 brains used in this study. 277

List of Abbreviations

AMPARs: AMPA-type receptors
BDNF: brain-derived neurotrophic factor
BFP: blue fluorescent protein
BMP: bone morphogenetic protein
CMA: chaperone-mediated autophagy
CNTF: ciliary neurotrophic factor
CRF: corticotropin-releasing factor
CRISPR: Clustered Regularly Interspaced Short Palindromic Repeat
crRNA: CRISPR RNA
DAG: diacylglycerol
DGKγ: diacylglycerol kinase gamma
DSB: double-stranded break
E: embryonic day
EDTA: ethylenediaminetetraacetic acid
EEA1: early endosome antigen 1
EGL: external granular layer
EGTA: ethylene glycol-bis(β-aminoethyl ether)-N,N,N',N'-tetraacetic acid
Engrailed-1: En1
Engrailed-2: En2
ER: endoplasmic reticulum
ESC: embryonic stem cell
eSpCas9: enhanced SpCas9
FACS: fluorescence-activated cell sorting
Fgf: fibroblast growth factor
FRET: fluorescence resonance energy transfer
Gbx2: gastrulation brain homeobox 2
GDNF: glial derived neurotrophic factor
GFP: green fluorescent protein
gRNA: guide RNA
H_2O_2: hydrogen peroxide
HDF: human dermal fibroblasts
HDR: homology-directed repair
HRM analysis: high resolution melt analysis
HSC70: heat shock cognate 70
HSP40: heat shock protein 40
Hsp90: heat shock protein 90
Indel: insertions or deletions
IP_3: inositol trisphosphate
IP_3R1: inositol 1,4,5-trisphosphate
iPSCs: induced pluripotent stem cells
LAMP2: lysosome-associated membrane protein 2
LC3: microtubule-associated protein 1 light chain 3
Lmx1b: lim homeobox 1b
LTD: long-term depression
LTP: long-term potentiation
MARCKS: myristoylated alanine-rich C kinase substrate
MEF: mouse feeder cells
mGluR1: metabotropic glutamate receptor 1
mGluR5: metabotropic glutamate receptor 5
MHB: midbrain-hindbrain boundary
MOI: multiplicity of infection
MRI: magnetic resonance imaging
NHEJ: non-homologous end joining
NMDAR: NMDA-type receptors
NT: neurotrophin
Otx2: orthodenticle homeobox 2
P/S: penicillin/streptomycin
p75NTR: p75 neurotrophin receptor
PAM: protospacer adjacent motif
PBMCs: peripheral blood mononuclear cells

PDBu: phorbol 12,13-dibutyrate
PDK-1: phosphoinositide-dependent kinase-1
PHLPP: PH domain leucine-rich repeat protein phosphatase
PIP_2: phosphatidylinositol 4,5-bisphosphate
PKC: protein kinase C
PKCα: protein kinase C alpha
PKCβ: protein kinase C beta
PKCγ: protein kinase C gamma
PLC: phospholipase C
PMA: phorbol 12-myristate 13-acetate
PolyQ: polyglutamine
PP2A: protein phosphatase 2A
PPase: phosphatase
PS: phosphatidylserine
RNP: ribonucleoprotein
ROS: reactive oxygen species
RT: reverse transcription
SaCas9: Staphylococcus aureus Cas9
SAG: smoothened agonist
SCA: spinocerebellar ataxia
SCA14: spinocerebellar ataxia type 14
SCA6: spinocerebellar ataxia type 6
SCNT: somatic cell nuclear transfer
SDF1: stromal cell-derived factor
SDS-PAGE: sodium dodecyl sulfate polyacrylamide gel electrophoresis
SpCas9: Streptococcus pyogenes Cas9
SpCas9n: SpCas9 nickase
SQSTM1: sequestosome-1
T3: thyroid hormone L-3,3',5-triiodothyronine
T7EI: T7 endonuclease 1
TGFβ: transforming growth factor β
TIDE: Tracking of Indels by Decomposition
TRPC3: C3-type transient receptor potential channel
TRα1: thyroid hormone receptor α1
UPS: ubiquitin-proteasome system
UTP: untranslated region
Wnt1: wingless homologue 1
WT: wildtype

Chapter 1 Introduction

1.1 The cerebellum

1.1.1 Overview

The cerebellum, which means the 'little brain' in Latin, plays an important role in motor coordination and learning. The cerebellum is essential for coordinating communications between the sensory and motor systems. It receives inputs from other parts of the nervous system and integrating these inputs to fine-tune motor activity. Instead of initiating or controlling the basal elements of movements, the cerebellum coordinates their spatial accuracy and timing. Damage to the cerebellum leads to disorder in motor coordination and learning as well as impairments in language, emotion processing, spatial and executive functions such as in the Cerebellar Cognitive Affective Syndrome (CCAS) in humans (Schmahmann and Sherman, 1998; Stoodley et al., 2016).

1.1.2 Organisation of the cerebellum

The cerebellum is located at the base of the brain and behind the pons. It is connected to the brainstem by three pairs of peduncles. The cerebellum is composed of the outer grey matter (cerebellar cortex), with white matter underneath and three pairs of embedded deep nuclei (from medial to lateral, the fastigial, interposed, and dentate nuclei) (Beckinghausen and Sillitoe, 2018; Sillitoe and Joyner, 2007). Structurally, it is subdivided into a central vermis flanked by two hemispheres (Cerminara et al., 2015). The cerebellum of higher vertebrates is folded into folia and subdivided into three lobes and ten lobules (I- X) (Cerminara et al., 2015; Larsell, 1952). The cerebellum can also be divided into three regions according to their functions: vestibulocerebellum that regulates balance and eye movements, spinocerebellum that controls

body and limb movements, and cerebrocerebellum that is involved in planning movements and evaluating sensory information for action (Michael-Titus et al., 2010).

The human cerebellum constitutes 10% of total brain volume but contains more neurons than the rest of the brain combined (Herculano-Houzel, 2009). The cerebellar cortex is highly organised and has three well-defined layers (Fig. 1.1). The five major cerebellar cell types include the inhibitory stellate and basket cells, Golgi and Purkinje cells, and the excitatory granule cells (Cerminara et al., 2015; Eccles, 1967; Palay and Chan-Palay, 1974; Ramnani, 2006; Ramon y Cajal, 1911; Voogd and Glickstein, 1998). These cerebellar cells have stereotypic and distinct morphologies, and discrete localisation within the cerebellar cortex (Leto et al., 2016; Sillitoe and Joyner, 2007). The outermost molecular layer contains stellate and basket cells, two types of inhibitory interneurons that form GABAergic synapses onto Purkinje cell dendrites. The middle Purkinje cell layer contains the cell bodies of Purkinje cells, which is the most prominent cell type of the cerebellum, aligned in a monolayer. The extensive, flattened dendritic arbours of Purkinje cells project into the molecular layer, where they receive synaptic inputs from parallel fibres of granule cells and climbing fibres of inferior olive. Below the Purkinje cell layer is the granule cell layer, which contains granule cells (the main excitatory interneurons of the cerebellar cortex) and Golgi cells. Precise connections between the major neurons are arranged in repeating circuit modules throughout the cerebellum (Goldowitz and Hamre, 1998; Michael-Titus et al., 2010; Ramon y Cajal, 1911; Sillitoe and Joyner, 2007).

The cerebellum receives two types of excitatory inputs: mossy fibres originating from the precerebellar nuclei and climbing fibres coming from the inferior olive. Purkinje cells integrate these inputs and provide the sole output of the cerebellar cortex (Eccles, 1973; Witter et al., 2016). Their inhibitory axons terminate on neurons in the cerebellar nuclei, which then project to other regions of the brain (Caligiore et al., 2017). The cerebellum is connected with the majority of the cerebral cortex, forming closed-loop cerebello-thalamo-cortico-pontine-

cerebellar circuits (Buisseret-Delmas and Angaut, 1993; Palesi et al., 2015; Salamon et al., 2007; Snider and Eldred, 1952). Different cerebellar functional regions can be broadly defined based on their patterns of connectivity with the cerebral cortex and the spinal cord, giving rise to a functional topography in the cerebellum (Doron et al., 2010; Stoodley and Schmahmann, 2010; Stoodley et al., 2012). Disruptions in cerebellar processing or connectivity therefore lead to many different disorders, one of which is cerebellar ataxia, i.e. a loss of control over movement.

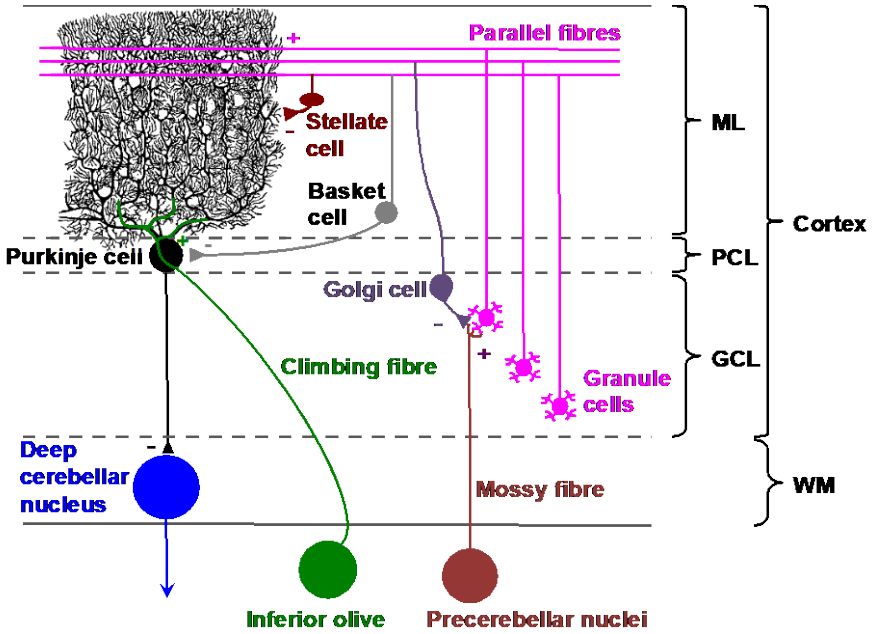


Figure 1.1 Schematic of the major cell types and circuitry of the cerebellum.

Granule cells receive input from the mossy fibres coming from the precerebellar nuclei. Purkinje cells receive two excitatory inputs from climbing fibres originating in the inferior olive and parallel fibres coming from granule cells. Purkinje cells form the sole output of the cerebellar cortex conveyed to deep cerebellar nuclei. Excitatory (+) and inhibitory (−) inputs are indicated. Minor cerebellar cell types including unipolar brush cells and Lugaro cells are not depicted. GCL: granule cell layer; ML: molecular layer; PCL: Purkinje cell layer; WM: white matter. Adapted from (Becker and Stoodley, 2013).

1.2 Cerebellar ataxias

Ataxia, means “loss of order” in Greek, is used clinically to describe aberrant and poor coordination of limb movements (Carlson et al., 2009). Cerebellar ataxia is caused by dysfunction either within the cerebellum or in its afferent and efferent pathways (Carlson et al.,

2009). The cerebellar ataxias are a highly heterogeneous group of disorders that can be acquired or caused by genetic mutations, which compose a significant proportion of the disorders (Sailer and Houlden, 2012; Taroni et al., 2013). Depending on the expression patterns and functions of the mutated proteins, ataxias can affect only the cerebellum (pure cerebellar ataxias) or display as complex forms that involve multiple systems. Hereditary ataxias are clinically and genetically heterogeneous. Mutations in many genes can all lead to cerebellar ataxias and yet mutations in the same gene may present a range of clinical features. Hereditary cerebellar ataxias can be categorised into autosomal dominant, autosomal recessive, X-linked and mitochondrial forms according to their pattern of heritance (Didonna and Opal, 2016; Sailer and Houlden, 2012; Sandford and Burmeister, 2014b; Taroni et al., 2013). Currently, the genetic cause of around 40% of clinical cases of ataxia has yet been identified suggesting that many more causative genes await identification (Huang and Verbeek, 2018; Sailer and Houlden, 2012; Sandford and Burmeister, 2014a).

1.2.1 Spinocerebellar ataxias (SCAs)

Spinocerebellar ataxias (SCAs), also known as autosomal dominant ataxias, are a group of hereditary neurodegenerative disorders that are caused by the dysfunction and degeneration of the cerebellum, predominantly Purkinje cells. To date, over 46 subtypes of SCAs caused by mutations in distinct genes have been identified (Huang and Verbeek, 2018; Taroni et al., 2013) (Table 1.1). The genetically heterogeneous SCAs show a wide range of clinical features. SCA patients are characterised by progressive loss of motor coordination and balance. Other symptoms such as involuntary eye movements and dysarthria have also been reported (Taroni et al., 2013).

SCAs can be genetically categorised into two groups: non-conventional SCAs and those caused by conventional mutations. Non-conventional SCAs can be further divided into two groups:

polyglutamine and intronic repeat SCAs depending on whether the expansion repeats are located in the coding or non-coding regions (Sailer and Houlden, 2012; Taroni et al., 2013). Polyglutamine SCAs are caused by coding CAG repeat expansions encoding long polyglutamine tracts in SCA1-3, 6, 7 and 17. Disease severity and age of onset correlate with the size of the repeat expansion (Sailer and Houlden, 2012; Taroni et al., 2013). On the other hand, expansions of non-coding repeats in untranslated regions (UTPs) or intronic regions lead to intronic repeat SCAs including SCA8 (CTG or CAG repeats), SCA10 (ATTCT repeats), SCA12 (CAG repeats), SCA31 (TGGAA repeats), SCA36 (GGCCTG repeats), and SCA37 (ATTTC repeats) (Sailer and Houlden, 2012; Taroni et al., 2013). In recent years, increasing number of SCAs caused by conventional mutations have been identified by next generation sequencing (Chelban et al., 2018; Duarri et al., 2012; Huang and Verbeek, 2018; Jiang et al., 2014; Lee et al., 2012; Nemeth et al., 2013; Nibbeling et al., 2017; Sandford and Burmeister, 2014a; Wang et al., 2010; Yang et al., 2013b). These genetically distinct SCAs all result in progressive dysfunction and eventually degeneration of Purkinje cells (Matilla-Duenas et al., 2014). However, the underlying molecular mechanisms are still unclear.

Table 1-1 List of known SCA genes and mutations

SCA type	Gene name	OMIM number	Locus	Mutation type	Protein name	Function	Reference
SCA1	ATXN1	164400	6p22.3	(polyQ)n	Ataxin-1	Transcription regulation	(Orr et al., 1993)
SCA2	ATXN2	183090	12q24.12	(polyQ)n	Ataxin-2	RNA metabolism	(Pulst et al., 1996; Sanpei et al., 1996)
SCA3	ATXN3	607047	14q32.12	(polyQ)n	Ataxin-3	De-ubiquitination, transcription regulation	(Kawaguchi et al., 1994)
SCA5	SPTBN2	600224	11q13.2	Deletion, MM	B-spectrin, non-erythrocytic 2	Neuronal membrane skeleton	(Ikeda et al., 2006)
SCA6	CACNA1A	183086	19p13.13	(polyQ)n	Voltage-dependent P/Q-type calcium channel subunit alpha-1A	Calcium signalling/homeostasis	(Zhuchenko et al., 1997)
SCA7	ATXN7	164500	3p14.1	(polyQ)n	Ataxin-7	Transcription regulation	(David et al., 1997)
SCA8	KLHL1AS	608768	13q21	(CTG/CAG)n[a]	Ataxin-8	-	(Koob et al., 1999)
SCA10	ATXN10	603516	22q13.31	(ATTCT)n [a]	Ataxin-10	Neuritogenesis	(Matsuura et al., 2000)
SCA11	TTBK2	604432	15q15.2	Frameshift/ deletion	Tau-tubulin kinase 2	Tau phosphorylation	(Houlden et al., 2007)
SCA12	PPP2R2B	604326	5q32	(CAG)n [a]	Serine/threonine-protein phosphatase 2A 55 kDa regulatory subunit B beta isoform	Regulation of PP2 activity, transcription regulation	(Holmes et al., 1999)
SCA13	KCNC3	605259	19q13.33	MM	Potassium voltage-gated channel subfamily C member 3	Potassium signalling/homeostasis	(Waters et al., 2006)

SCA type	Gene name	OMIM number	Locus	Mutation type	Protein name	Function	Reference
SCA14	PRKCG	605361	19q13.42	MM	Protein kinase C gamma type	Phosphorylation, signal transduction	(Chen et al., 2003)
SCA15/16/29	ITPR1	606658	3p26.1	Deletion	Inositol 1,4,5-trisphosphate receptor type 1	Intracellular calcium homeostasis	(Huang et al., 2012; Iwaki et al., 2008; van de Leemput et al., 2007)
SCA17	TBP	607136	6q27	(polyQ)n	TATA-box-binding protein	Transcription regulation	(Nakamura et al., 2001)
SCA18	IFRD1	607458	7q22-q32	MM	interferon-related developmental regulator gene-1	-	(Brkanac et al., 2009)
SCA19/22	KCND3	607346	1p13.2	MM/ deletion	Potassium voltage-gated channel subfamily D member 3	Potassium signalling/homeostasis	(Duarri et al., 2012; Lee et al., 2012)
SCA20	DAGLA	608687	11q12	12 gene duplication	Sn1-specific diacylglycerol lipase alpha	Chromosomal duplication	(Knight et al., 2008)
SCA21	TMEM240	607454	1p36.33	MM	Transmembrane protein 240	-	(Delplanque et al., 2014)
SCA23	PDYN	610245	20p13-p12.2	MM/ frameshift	Proenkephalin-B	Potassium signalling/homeostasis	(Bakalkin et al., 2010)
SCA26	eEF2	609306	19p13.3	MM	Elongation factor 2	Translation elongation	(Hekman et al., 2012)
SCA27	FGF14	609307	13q33.1	MM	Fibroblast growth factor 14	Signal transduction	(van Swieten et al., 2003)
SCA28	AFG3L2	610246	18p11.21	MM	AFG3-like protein 2	ATP-dependent protease activity	(Di Bella et al., 2010)
SCA31	BEAN	117210	16q21	(TGGAA)n [a]	Protein BEAN1	-	(Sato et al., 2009)

SCA type	Gene name	OMIM number	Locus	Mutation type	Protein name	Function	Reference
SCA34	ELOVL4	133190	6q14.1	MM	Elongation of very long chain fatty acids protein 4	Synthesis of very long chain saturated fatty acids and very long chain polyunsaturated fatty acids	(Cadieux-Dion et al., 2014)
SCA35	TGM6	613908	20p13	MM	Protein-glutamine gamma-glutamyltransferase 6	Cross-linking of proteins and the conjugation of polyamines to proteins	(Wang et al., 2010)
SCA36	NOP56	614153	20p13	(GGCCTG)n [a]	Nucleolar protein 56	Involved in the early to middle stages of 60S ribosomal subunit biogenesis	(Kobayashi et al., 2011)
SCA37	DAB1	615945	1p32.2	(ATTTC)n [a]	Disabled homolog 1	-	(Seixas et al., 2017)
SCA38	ELOVL5	615957	6p12.1	MM	Elongation of very long chain fatty acids protein 5	Elongation of long-chain polyunsaturated fatty acids	(Di Gregorio et al., 2014)
SCA40	CCDC88C	616053	14q32.11-q32.12	MM	Protein Daple	Negative regulator of canonical Wnt signalling pathway	(Tsoi et al., 2014)
SCA41	TRPC3	616410	4q27	MM	Short transient receptor potential channel 3	Non-selective calcium permeable cation channel, calcium signalling/ homeostasis	(Fogel et al., 2015)
SCA42	CACNA1G	616795	17q21.33	MM	Voltage-dependent T-type calcium channel subunit alpha-1G	Calcium signalling/ homeostasis	(Coutelier et al., 2015)
SCA43	MME	617018	3q25.2	MM	Metalloprotease neprilysin	A neutral endopeptidase that cleaves and inactivates various neuropeptides and peptide hormones	(Depondt et al., 2016)

SCA type	Gene name	OMIM number	Locus	Mutation type	Protein name	Function	Reference
SCA44	GRM1	617691	6q24.3	MM	Metabotropic glutamate receptor 1	G-protein coupled receptor for glutamate	(Watson et al., 2017)
SCA45	FAT2	604269	5q33.1	MM	Protocadherin Fat 2	Cell adhesion, implicated in cerebellar development	(Nibbeling et al., 2017)
SCA46	PLD3	615698	19q13.2	MM	Phospholipase D3	Involved in hydrolysis of membrane phospholipids and processing of amyloid-beta precursor protein	(Nibbeling et al., 2017)
NA	KIF26B	614026	1q44	MM	Kinesin-like protein KIF26B	Organelle trafficking along microtubules	(Nibbeling et al., 2017)
NA	EP300	602700	22q13.2	MM/ frameshift	Histone acetyltransferase p300	Transcription regulation	(Nibbeling et al., 2017)
NA	FAT1	600976	4q35.2	MM	Protocadherin Fat 1	Cellular polarization, directed cell migration and modulating cell-cell contact	(Nibbeling et al., 2017)

MM = missense mutations; polyQ = polyglutamine; [a] = noncoding; (…) n = repeat expansions; NA = not assigned. Modified from (Huang and Verbeek, 2018; Matilla-Duenas et al., 2014).

1.2.1.1 Shared pathogenic pathways in SCAs

Genetically diverse SCAs show overlapping pathological and clinical phenotypes, suggesting that the seemingly divergent genes may converge to several shared pathogenic pathways. A number of major pathogenic mechanisms have been proposed, including altered protein homeostasis, toxic RNA gain-of function, transcriptional dysregulation as well as impaired calcium homeostasis and signalling (Bushart et al., 2016; Huang and Verbeek, 2018; Matilla-Duenas et al., 2014).

The misfolding and accumulation of protein aggregates is a hallmark of polyglutamine SCAs (Huang and Verbeek, 2018; Orr, 2012; Taroni et al., 2013). The expanded tract of polyglutamine expansions is prone to protein misfolding. Misfolded proteins form small oligomers and large neuronal inclusions, and accumulate throughout and outside cells. However, it remains debatable whether protein aggregates cause Purkinje cell degeneration in SCAs (Matilla-Duenas et al., 2014; Sisodia, 1998; Taroni et al., 2013). Several studies have shown that small soluble oligomers, but not insoluble inclusions, may be cytotoxic by sequestering transcription factors as well as proteins involved in protein degradation processes (Chai et al., 2001; Perez et al., 1998; Schmidt et al., 2002; Zander et al., 2001). This suggests that these longer polyglutamine mutations may exert a dominant negative effect on other proteins and inhibit their normal functions (Ashkenazi et al., 2017; Fujigasaki et al., 2001; Matilla-Duenas et al., 2014; Perez et al., 1998; Uchihara et al., 2001). Moreover, the age-decline protein degradation system might not be efficient to remove the accumulating inclusions. The accumulation of inclusions might then impose cellular stress in Purkinje cells and thereby contribute to SCA pathogenesis. In contrary, some studies suggest that disease severity is independent of the presence of inclusions in mouse models and insoluble inclusions might even be protective (Cummings et al., 2001; Klement et al., 1998; Matilla-Duenas et al., 2014; Orr, 2012; Saudou et al., 1998). It therefore remains controversial whether protein aggregates in SCAs are detrimental (Matilla-Duenas et al., 2014; Sisodia, 1998; Taroni et al., 2013).

Finally, calcium homeostasis is central to proper neuronal function including the establishment and maintenance of synaptic transmission. Calcium triggers electrical activity-dependent gene expression including genes that expressed early during development and those important for neuronal plasticity. Neuronal calcium transients come from many extracellular and intracellular sources. The calcium balance is tightly controlled by a number of calcium buffers and transporters (Bushart et al., 2016; Matilla-Duenas et al., 2014). Dysregulation of calcium homeostasis and signalling in Purkinje cells is a major disease mechanism underlying conventional SCAs (Bushart et al., 2016; Kasumu and Bezprozvanny, 2012; Matilla-Duenas et al., 2014; Meera et al., 2016; Taroni et al., 2013). Many of the genes affected in conventional SCAs encode for components controlling extracellular and intracellular calcium entry as well as calcium signalling pathways. The genes that affect calcium entry at the plasma membrane include voltage-gated calcium channels *CACNA1A* in SCA6 (Zhuchenko et al., 1997) and *CACNA1G* in SCA42 (Coutelier et al., 2015), voltage-gated potassium channels *KCNC3* in SCA13 (Waters et al., 2006), *KCND3* in SCA19/22 (Duarri et al., 2012; Lee et al., 2012) and calcium permeable channel *TRPC3* in SCA41 (Fogel et al., 2015). Calcium release is further propagated by release from intracellular stores. Several SCA genes are involved in calcium release from intracellular stores, including *ITPR1* encoding inositol 1,4,5-trisphosphate receptor type 1 in SCA15/16/29 (Huang et al., 2012; Iwaki et al., 2008; van de Leemput et al., 2007) and *AFG3L2* coding for AFG3 like matrix AAA peptidase subunit 2 in SCA28 that regulates mitochondrial calcium influx (Di Bella et al., 2010). Mutations in glutamate receptors upstream of calcium release also cause SCAs, including β-III spectrin *SPTBN2* in SCA5 (Ikeda et al., 2006), *DAGLA* in SCA20 (Knight et al., 2008) and metabotropic glutamate receptor *GRM1* in SCA44 (Watson et al., 2017). Moreover, calcium imbalance was also reported in SCA14 caused by mutations in protein kinase C gamma (PKCγ) that is important for signal transduction (Chen et al., 2003). In addition to conventional SCAs, deranged calcium signalling has also been reported in polyglutamine SCAs such as SCA1, 2 and 3 (Kasumu and Bezprozvanny, 2012; Matilla-Duenas et al., 2014; Meera et al., 2016). Significant reduction in

calcium buffers and components in calcium-signalling pathways has been shown in SCA1 transgenic mice (Lin et al., 2000; Serra et al., 2004; Serra et al., 2006). Interaction of mutant ataxin-1 and ataxin-2 with IP_3R1 on the endoplasmic reticulum (ER) membrane that induces increased calcium release from the ER is lost (Chen et al., 2008; Liu et al., 2009; van de Loo et al., 2009). Alterations in calcium-potassium balance caused by mutations in calcium and potassium channels might increase neuronal excitability and affect neuronal firing properties that alter functions of Purkinje cells. The calcium imbalance might activate calcium-dependent cell death processes and cause degeneration of Purkinje cells (Bushart et al., 2016; Matilla-Duenas et al., 2014). Moreover, calcium-signalling pathways might influence transcription via the mitogen-activated protein kinase (MAPK/ERK) cascade, which transduces signals from the plasma membrane to the nucleus (Wiegert and Bading, 2011). This suggests that pathways of calcium signalling and transcriptional regulation might converge. These convergent pathways result in early synaptic neurotransmission deficits, progressive dysfunction and ultimately degeneration of Purkinje cells in SCAs (Bushart et al., 2016; Huang and Verbeek, 2018; Matilla-Duenas et al., 2014; Meera et al., 2016; Taroni et al., 2013). However, it is still unclear why Purkinje cells are particularly vulnerable and the molecular mechanisms that lead to Purkinje cell dysfunction and death remain to be elucidated.

To understand why Purkinje cells are particularly vulnerable in SCAs, it is essential to understand their unique structure, position in the cerebellum and physiology. Each Purkinje cell contains a large pear-shaped cell body and an extensively branched dendritic arbour with numerous spines growing from one side of the cell body and axon growing from the other side (Ramon y Cajal, 1911). Purkinje cells are structurally and functionally the centres of the cerebellar network. Their cell bodies are aligned in the Purkinje cell layer, which is located in the middle of the cerebellar cortex (Eccles, 1967; Palay and Chan-Palay, 1974; Voogd and Glickstein, 1998). Purkinje cells integrate inputs from parallel and climbing fibres, and generate the sole output of the cerebellar cortex to the deep cerebellar nuclei (Sotelo and Rossi, 2013). These outputs are then projected to the brainstem and the cerebral cortex via the thalamus

(Bostan et al., 2010; Buisseret-Delmas and Angaut, 1993; Cerminara et al., 2015; Hoshi et al., 2005). The interaction between Purkinje cells with parallel and climbing fibres generates plasticity that is important for motor leaning. The signals generated by Purkinje cells are required for motor planning and accuracy of movements. Physiologically, Purkinje cells display high intrinsic activity and spontaneous action potential firing even in the absence of synaptic input (Latham and Paul, 1971; Zhou et al., 2014; Zhou et al., 2015). Alterations in spontaneous Purkinje cell firing, which have been reported in several models of SCAs and animals showing ataxia, might therefore affect Purkinje cell and cerebellar functions, and cause cerebellar ataxia. Nonetheless, the underlying molecular pathways remain to be clarified. Moreover, pathways enriched in Purkinje cells might also contribute to their selective vulnerability. A recent comparative analysis of cell-type specific and enriched transcripts identified 491 genes specific to Purkinje cells (Doyle et al., 2008; Huang and Verbeek, 2018). Among these, four are known SCA genes (*ITPR1*, *AFG3L2*, *TRPC3* and *CACNA1G*) and encode important regulators of calcium homeostasis and signalling (Huang and Verbeek, 2018; Schorge et al., 2010), further highlighting the importance of proper calcium handling to Purkinje cell function and survival. Further investigation into human Purkinje cell-specific genes might identify pathways that are important to their function and survival, of which disruptions might contribute to SCA pathogenesis.

To date, limited information exists with regard to the function of SCA genes in the human brain. A recent cerebellar transcriptomic analysis revealed that 40% of SCA genes, particularly those involved in ion channel activity, were most highly expressed in the human cerebellum (Bettencourt et al., 2014). Moreover, gene co-expression network analysis identified two gene co-expression modules that were enriched in the human cerebellum, including genes involved in the ubiquitin-proteasome system, and calcium homeostasis and signalling (Bettencourt et al., 2014). This further highlights the importance of impaired degradation of aggregates and aberrant calcium homeostasis in SCA pathogenesis. Further investigations would aid the

identification of interactions of these genes specific to Purkinje cells, which might explain the Purkinje cell vulnerability in SCAs.

1.3 Spinocerebellar ataxia type 14 (SCA14)

A SCA subtype that displays pure cerebellar ataxia with the affected gene situated at the center of signaling pathways important for Purkinje cell function might be a good entry point to elucidate the convergent pathways underlying SCAs. Spinocerebellar ataxia type 14 (SCA14) is a form of autosomal dominant ataxia that affects less than 5% of people affected with ataxia (Taroni et al., 2013). SCA14 was first described by Yamashita et al. (2000) in a four-generation Japanese family with nine affected patients. The age of onset varies from childhood to adulthood ranging from 10 to 70 while lifespan is not affected. SCA14 patients usually show benign phenotypes and remain ambulant (Chen et al., 2012a; Taroni et al., 2013). SCA14 is clinically heterogeneous as with most SCAs. SCA14 patients display progressive loss of gait and limb coordination resulting from the dysfunction and degeneration of Purkinje cells in the cerebellum. In addition to ataxia, a spectrum of other clinical symptoms such head and limbs tremor, dystonia, myoclonus, speech and eye movement disturbances, reduced vibration sense, seizures, peripheral neuropathy, Parkinsonism, depression and cognitive impairment were also observed in SCA14 patients (Chelban et al., 2018; Chen et al., 2005; Chen et al., 2012a; Ganos et al., 2014; Rosenberg and Khemani, 2015; Stevanin et al., 2004; Taroni et al., 2013; Yabe et al., 2003).

Brain MRI in all affected individuals showed mild to moderate cerebellar atrophy, predominantly in the vermis, while atrophy of the cerebral cortex or the brain stem is usually absent (pure cerebellar ataxia) (Asai et al., 2009; Koht et al., 2012; Morita et al., 2006; Stevanin et al., 2004; Ueda et al., 2013; van de Warrenburg et al., 2003; Wedding et al., 2013; Yamashita et al., 2000). In rare cases, two patients carrying a Q127R mutation in the highly conserved C1B regulatory domain also exhibited atrophy in the brain stem (Yabe et al., 2003). Moreover,

N-isopropyl-p-[123I]-iodoamphetamine single-photon emission computed tomography revealed decreased blood flow exclusively in the upper cerebellum of a SCA14 patient (Ueda et al., 2013). Human post-mortem cerebellar tissues of SCA14 are scarce. Thus far, cerebellar tissue from only one SCA14 patient, which showed loss of Purkinje cells, has been reported (Brkanac et al., 2002; Chen et al., 2003). However, further human pathological findings regarding disease mechanisms are not available.

1.3.1 Genetic basis of SCA14

SCA14 was originally linked to mutations in the chromosome 19q13.4-qter by Yamashita et al. (2000). Subsequent analysis showed that SCA14 was caused by mutations in the *PRKCG* gene encoding protein kinase C gamma (PKCγ) (Chen et al., 2003). The *PRKCG* gene contains 18 exons. To date, more than 40 missense mutations and deletions have been identified throughout the coding region of *PRKCG* (Fig. 1.2). The majority of the known SCA14 mutations are missense mutations and most of them lie within exon 4-5. Four in-frame amino acid deletions were found in the *PRKCG* gene including F48del in exon 1 (Ganos et al., 2014), del K100-H101 (Chen et al., 2005), F113del in exon 4 (Ganos et al., 2014) and M697Iex in exon 18. SCA14 has been suggested to be caused by gain of function mutations, rather than haploinsufficiency, or a combination of both as heterozygous PKCγ-null animals are neurologically normal (Asai et al., 2009; Schrenk et al., 2002; Yabe et al., 2003). Moreover, truncating mutations have not been reported.

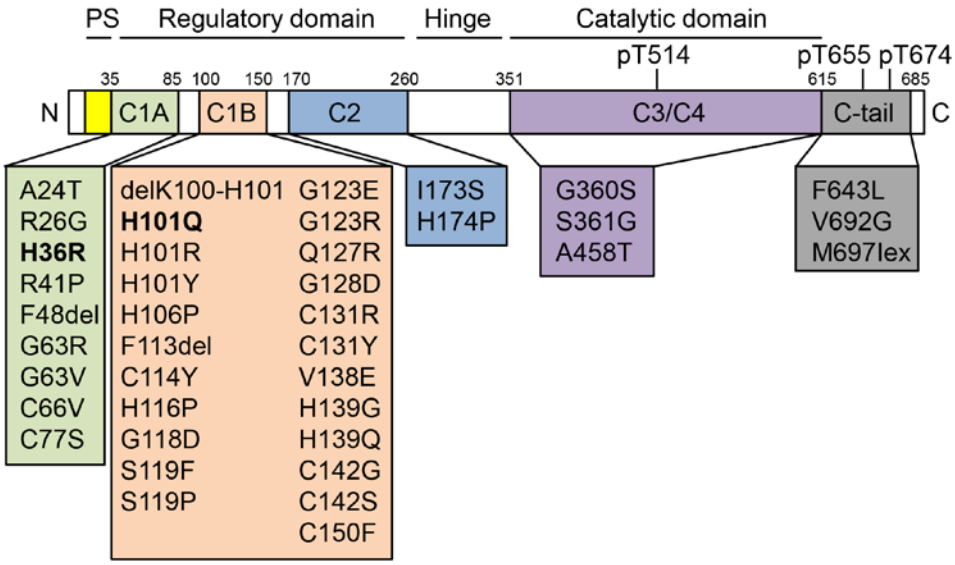


Figure 1.2 Schematic illustration of SCA14 mutations discovered to-date corresponding to different PKCγ protein domains.

(A) Known SCA14 mutations are grouped according to their location within different colour-coded PKCγ protein domains. The two mutations (H36R and H101Q) that are included in this study are highlighted in bold. C1A (green) and C1B (orange), which bind diacylglycerol (DAG) or phorbol esters, and C2 domain (blue) that bind calcium ions, collectively form the regulatory domain. C3/C4 indicates the catalytic domain (purple). The regulatory and catalytic domains are connected by a hinge region. The three phosphorylation sites at T514 (pT514), T655 (pT655) and T674 (pT674) residues are shown. The starting and ending numbers of the amino acid residues are indicated. N: N-terminus; PS: pseudosubstrate; C: C-terminus.

1.4 Protein kinase C gamma (PKCγ)

1.4.1 Protein kinase C (PKC) family

PKCγ belongs to the family serine/threonine kinases protein kinase C (PKC), which plays critical roles in several cellular signalling transduction pathways including cell proliferation, differentiation and apoptosis (Newton, 2010; Steinberg, 2008). Ten PKC isozymes are grouped into three classes: conventional PKCs, novel PKCs and atypical PKCs according to their domain composition and cofactors that regulate their activities (Newton, 2010; Sanchez-Bautista et al., 2009). Conventional PKCs include PKCα, the alternatively spliced PKCβI and βII (two splice variants of the same gene that differ in the last 43 amino acids) and PKCγ. In the cerebellum, all isoforms of the conventional PKCs are expressed with different cellular and subcellular localisation (Callender and Newton, 2017; Ding et al., 2005; Metzger and

Kapfhammer, 2003). PKCα is ubiquitously expressed at moderate levels throughout the cerebellum including in Purkinje cells (Bareggi et al., 1996; Gundlfinger et al., 2003; Hirono et al., 2001; Huang et al., 1988; Huang, 1989; Wetsel et al., 1992). PKCβI and βII are expressed only in granule cells with distinctive subcellular localisation (Ase et al., 1988; Barmack et al., 2000; Gundlfinger et al., 2003; Huang et al., 1988; Wetsel et al., 1992). PKCβI is localised to cell bodies and small dendrites, whereas PKCβII is only detected in parallel fibres and presynaptic endings (Barmack et al., 2000). PKCγ is exclusively and highly expressed in Purkinje cells throughout their cell bodies and dendrites (Cardell et al., 1997; Hashimoto et al., 1988; Kose et al., 1988; Schrenk et al., 2002). The exclusive and abundant expression of PKCγ indicates that it might be important for Purkinje cell function.

1.4.2 Structure of PKCγ

Similar to other members of conventional PKCs, PKCγ is composed of two functionally distinctive domains: a regulatory domain (approximately 35 kDa) and a catalytic domain (approximately 45 kDa), connected by a flexible hinge region (Fig. 1.2) (Callender and Newton, 2017; Newton, 2018). The structural conformation of PKCγ is important for its subcellular localisation, affinity for the plasma membrane and the regulation of its kinase activity.

In front of the regulatory domain, there is a 17 amino acid-long pseudosubstrate region near the N-terminal. The pseudosubstrate resembles the consensus substrate sequence but with an alanine at the position of the phosphoacceptor site (House and Kemp, 1990), which maintains PKCγ in an inactive state. The pseudosubstrate is therefore a key molecular switch in the regulation of PKCγ.

The regulatory domain contains diacylglycerol (DAG) (C1 domain) and calcium sensors (C2 domain) for membrane targeting. The C1 domain is further divided into two cysteine-rich subdomains: C1A and C1B, which are structurally complementary (Ananthanarayanan et al.,

2003; Sanchez-Bautista et al., 2009). The C1 domain binds DAG/phorbol ester and the anionic phospholipid phosphatidylserine (PS) (Johnson et al., 2000). Although isolated C1A subdomain has higher affinity for DAG and phorbol ester (Dries et al., 2007), only C1B subdomain binds these substrates in the context of the full-length protein (Kikkawa et al., 1983; Konig et al., 1985; Newton, 2018). The solution structure of the PKCγ C1B subdomain shows that it is composed of five β-strands and one α-helix (Fig. 1.3A) (Tanabe et al.; Xu et al., 1997). Residues S111, T113, F114, L122, Y123 and G124 that form a narrow hydrophilic groove at the top of the C1B domain serves as a phorbol ester-binding site for anchoring PKCγ to the plasma membrane (Xu et al., 1997; Zhang et al., 1995). The upper half of the C1B domain forms a largely hydrophobic surface and interacts with phospholipids (Xu et al., 1997). Binding of zinc ions to the two zinc ion-coordinating sites stabilises the two type I β turns and structure of the C1B subdomain (Xu et al., 1997; Zhang et al., 1995).

The C2 domain mediates calcium-dependent binding to anionic phospholipids and phosphatidylinositol 4,5-bisphosphate (PIP_2) (Evans et al., 2006; Farah and Sossin, 2012; Gallegos and Newton, 2008; Sanchez-Bautista et al., 2006). Similar to other conventional PKCs, the C2 domain of PKCγ contains a β-sheet comprised of eight anti-parallel β-strands connected by various surface loops (Fig. 1.3B). Three loops at the top of the β-strands, which are known as the calcium-binding regions (1, 2 and 3), contain five aspartate residues that allow for multiple calcium bindings through their carboxylate groups (Kazi, 2011; Pike et al., 2007). Coordination of calcium ions in the C2 domain causes a dramatic increase in the affinity of conventional PKCs for phospholipids.

The catalytic domain (C3/C4) is highly conserved among PKC isoforms. It contains a N-terminal lobe composed of β-sheets, an ATP binding site, a lysine that is prone to mutations for phosphoryl-transfer and a gatekeeper residue that controls the accessibility of the ATP binding pocket. The catalytic domain binds ATP and controls phosphorylation during maturation and activation of PKCγ. The amino acid sequences of the catalytic domain of PKC isoforms are

highly conserved (more than 60%) within the family. The crystal structure of the PKCβII catalytic domain, which has a similar amino acid sequence as PKCγ, shows folding into a classical bi-lobal fold. The smaller N-terminal lobe, which is composed of five β-strands and two α-helices, is connected to the larger C-terminal lobe containing eight α-helices by a hinge region (Grodsky et al., 2006; Leonard et al., 2011) (Fig. 1.3C). The active site consists of an ATP-binding site and a peptide-substrate binding site. It has been shown that basic residues at the N- or C-terminal ends of the phosphoacceptor site of substrates are particularly important for PKC phosphorylation. One of the key sites of priming phosphorylation of PKCγ is located at threonine 514 (T514) within the activation loop in the catalytic domain (Newton, 2010, 2018; Steinberg, 2008).

The C-terminal tail, also known as the V5 domain, is another key regulatory element of PKCγ (Newton, 2010, 2018; Steinberg, 2008). It serves as a docking surface for proteins that regulates PKCγ and as a tether to structural determinants in the catalytic domain (Kannan et al., 2007; Newton, 2018). The C-terminal tail contains a conserved PXXP motif that interacts with a conserved tyrosine in the α-helix of the catalytic domain. This creates a binding surface for chaperones heat shock protein 90 (Hsp90) and Cdc37 for the priming phosphorylation of PKCγ. In addition, the C-terminal tail also serves as the docking site for phosphoinositide-dependent kinase-1 (PDK-1) (Gao et al., 2001), prolylisomerase Pin1 (Abrahamsen et al. 2012), heat shock protein 70 (Hsp70) (Gao and Newton, 2006), and mTORC2 component, Sin1 (Cameron et al., 2011). The C-terminal tail contains two highly conserved phosphorylation sites, the turn motif and hydrophobic motif (Bornancin and Parker, 1997; Edwards and Newton, 1997). The phosphorylation at these two sites anchors the C-terminal tail onto the top of the N-terminal lobe where it interacts with the C1B domain (Leonard et al., 2011). This interaction stabilizes the catalytic core and facilitates ATP and substrate binding (Kannan et al., 2007; Newton, 2018). The C-terminal tail is also important for the protein insolubility of PKCγ. Activated PKCγ are moved to Triton-insoluble pellets following phorbol ester activation. This

translocation is enhanced by an exposed C-terminal tails (Jezierska et al., 2014), suggesting that C-terminal tail is important for regulating the subcellular localisation of PKCγ.

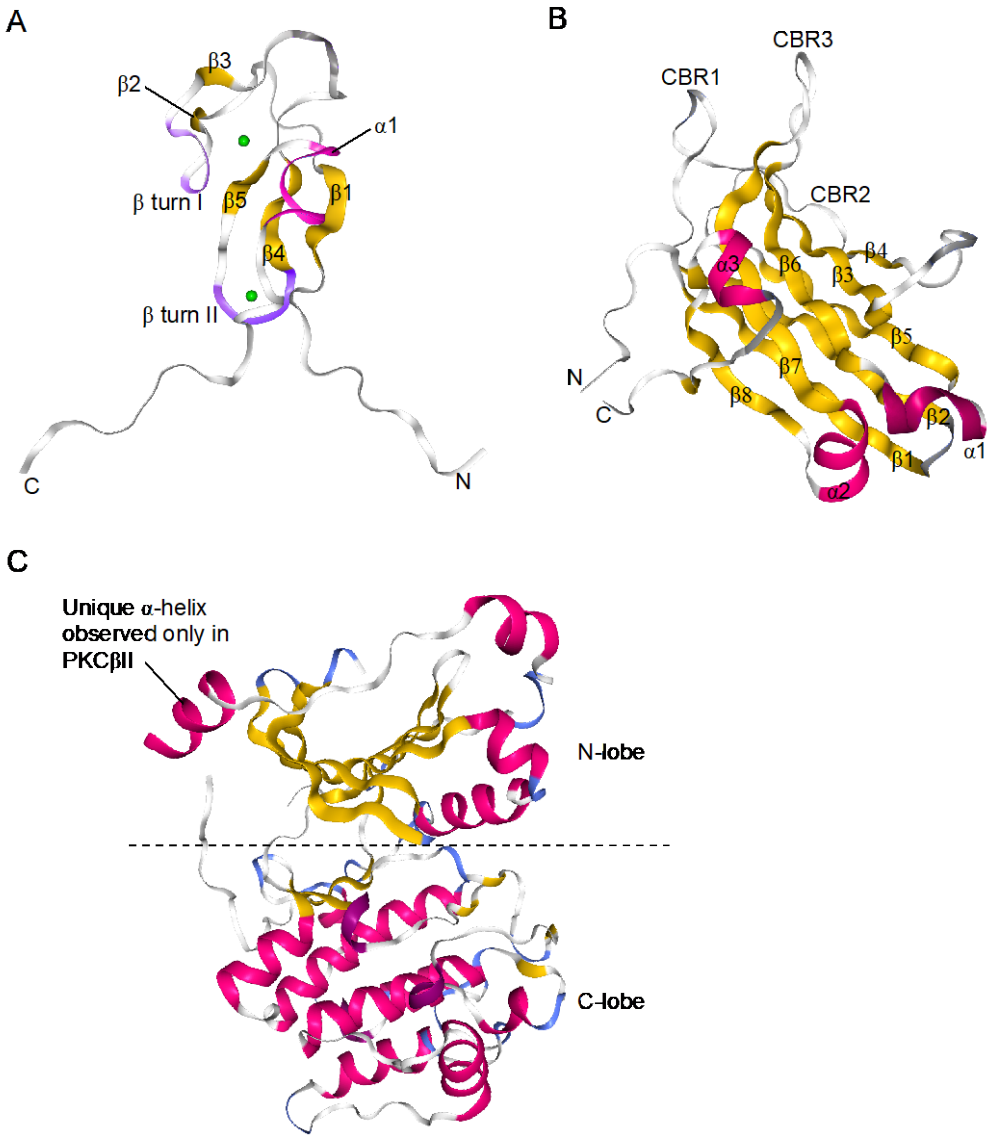


Figure 1.3 Structure of PKCγ.

(A) Ribbon representation of the C1B subdomain of PKCγ from Protein Data Bank (PDB) 1TBN (Xu et al., 1997). The C1B subdomain of PKCγ is composed of five β-strands (β1-β5, yellow) and one α-helix (magenta). Binding to zinc ions (green) stabilizes the two β turns (I and II, purple). N: N-terminal; C: C-terminal. (B) Ribbon representation of the C2 domain of f PKCγ rom PDB 2UZP (Pike et al., 2007). The C2 domain is composed of eight anti-parallel β-strands (β1-β8, yellow) and three one α-helixes (α1-α3, magenta). Three calcium-binding regions (CBR1-CBR3) are also indicated. N: N-terminal; C: C-terminal. (C) Ribbon representation of the PKCβII catalytic domain has a similar amino acid sequence as PKCγ, from PDB 2I0E (Grodsky et al., 2006). The catalytic domain folds into a classical bi-lobal fold. The smaller N-terminal lobe, which is composed of five β-strands (yellow) and two α-helices (magenta), is connected to the larger C-terminal lobe containing eight α-helices (magenta) by a hinge region. 3D structures were visualised using the NGL viewer (Rose et al., 2016).

1.4.3 Regulation of PKCγ

1.4.3.1 Priming phosphorylation and maturation of PKCγ

Phosphorylation of PKCγ is crucial to maintaining its conformation as well as regulating its subcellular localisation, kinase activity and degradation. PKCγ undergoes a series of phosphorylation events to become stable, mature and responsive to activation (Fig. 1.4). Newly synthesized PKCγ moves from the cytoplasm to the plasma membrane in an "open" conformation in which the substrate-binding cavity is not occupied by the autoinhibitory pseudosubstrate (Newton, 2003; Newton, 2010). The molecular chaperone HSP90 and co-chaperone CDC37 bind to the PXXP motif in the C-terminal tail to prepare immature PKCγ for the first phosphorylation. The open conformation allows a membrane-bound kinase, PDK-1 to access the docking site on the hydrophobic loop in the C-terminal tail and phosphorylate the activation loop at T514 located at the centre of the catalytic domain. PDK-1 is then released from the docking site and allows the subsequent autophosphorylation events to take place: first at the turn motif (T655) and then at the hydrophobic motif (T674) in the C-terminal tail (Newton, 2010). The C-terminal modifications depend on the intrinsic kinase activity of PKCγ. Autophosphorylation at T655 and T674 is mediated by an intramolecular reaction (Behn-Krappa and Newton, 1999), and the kinase complex mTORC2 (Ikenoue et al., 2008; Sarbassov et al., 2004). Once phosphorylated, PKCγ adopt a closed conformation that the pseudosubstrate binds the substrate-binding cavity, and the C1 and C2 domains become masked (Newton, 2018). This conformational change allows the lower affinity sensor, the C1B domain, to be the primary DAG binder (Antal et al., 2014). Moreover, the phosphorylation sites are now protected from dephosphorylation and the enzyme is resistant to degradation. The resulting mature PKCγ is released from the membrane to the cytoplasm and is now responsive to activation (Newton, 2010, 2018).(Callender and Newton, 2017)

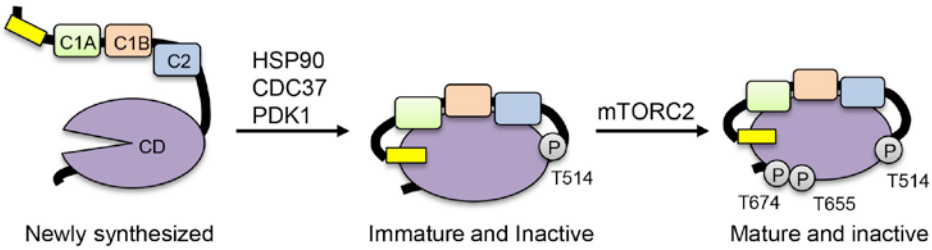


Figure 1.4 Schematic illustration of the priming phosphorylation events of PKCγ.

Newly synthesized PKCγ is in an open conformation, in which all its regulatory modules are unmasked. PKCγ is then processed by three ordered phosphorylation events that depend on the binding of chaperones HSP90 and CDC37 to a conserved PXXP motif in the kinase domain, the kinase complex mTORC2, and the activation loop kinase, PDK-1. Phosphorylation at these priming sites, the activation loop (T514), the turn motif (T655) and the hydrophobic motif (T674) allows PKCγ to adopt an autoinhibited conformation. Specifically, the pseudosubstrate (yellow) is clamped in the substrate-binding cavity of the catalytic domain (purple), and the DAG-sensing C1A (green) and C1B (orange) domains become masked. The masking of the C1 domains effectively prevents basal signalling in the absence of agonists. The resulting mature PKCγ is then responsive to activation.

1.4.3.2 Reversible activation of PKCγ

Membrane translocation is a hallmark of PKCγ dynamics. Mature but inactive PKCγ resides in the cytosol (Fig. 1.5). The hydrolysis of PIP_2 downstream of G-protein-coupled receptors (GPCRs) generates calcium ions and DAG resulting in a two-step activation of PKCγ. The activation of PKCγ is initiated by the binding of calcium to the C2 domain, which induces the rapid translocation of PKCγ from the cytoplasm to the plasma membrane, where PKCγ interacts with phospholipids. The C2 domain is displaced from the catalytic domain and thereby exposes a PIP_2-binding surface. The interaction of the C2 domain with PIP_2 thus localises PKCγ at the plasma membrane. PKCγ is further activated by the subsequent binding of its membrane-embedded ligand DAG to the C1 domain, primarily the C1B. This engagement of the C1B subdomain to the membrane provides the energy to release the pseudosubstrate from the catalytic domain resulting in the open (active) conformation (Newton, 2010). PKCγ then phosphorylates and activates diacylglycerol kinase gamma (DGKγ), which in turn converts DAG into phosphatidic acid (Yamaguchi et al., 2006), resulting in PKCγ dissociation from the membrane. PKCγ returns to its autoinhibited conformation following the decay of its second messengers (Newton, 2018).

1.4.3.3 Down-regulation of PKCγ

The open, membrane-bound conformation of PKCs is sensitive to dephosphorylation by phosphatases by two orders of magnitude (Dutil et al., 1994). Prolonged activation results in dephosphorylation and subsequent degradation of PKCs (Hansra et al., 1999). Studies with PKCβII have revealed that the first step in down-regulation is the dephosphorylation at the hydrophobic motif catalysed by the PH domain leucine-rich repeat protein phosphatase (PHLPP) (Gao et al., 2008). This dephosphorylation renders the partially dephosphorylated PKC detergent-insoluble (Hansra et al., 1996; Hansra et al., 1999). Subsequent dephosphorylation at the turn motif and activation loop by protein phosphatase 2A (PP2A) produces a fully dephosphorylated PKC that is degraded via the ubiquitin-proteasomal pathway (Abrahamsen et al., 2012). Modulation of the levels of PHLPP in mammalian cells directly regulates the levels of PKC (Gao et al., 2008). Sumoylation also controls the lifetime of conventional PKCs: phosphorylated PKCα is sumoylated on a conserved lysine in the catalytic domain (Lys65). Dephosphorylation at the priming sites reduces sumoylation, which then promotes ubiquitination and thus degradation of PKCs (Wang et al., 2016). The binding of chaperone HSP70 to the dephosphorylated turn motif stabilises conventional PKCs and promotes their re-phosphorylation resulting in signalling-competent enzymes again (Fig. 1.5).

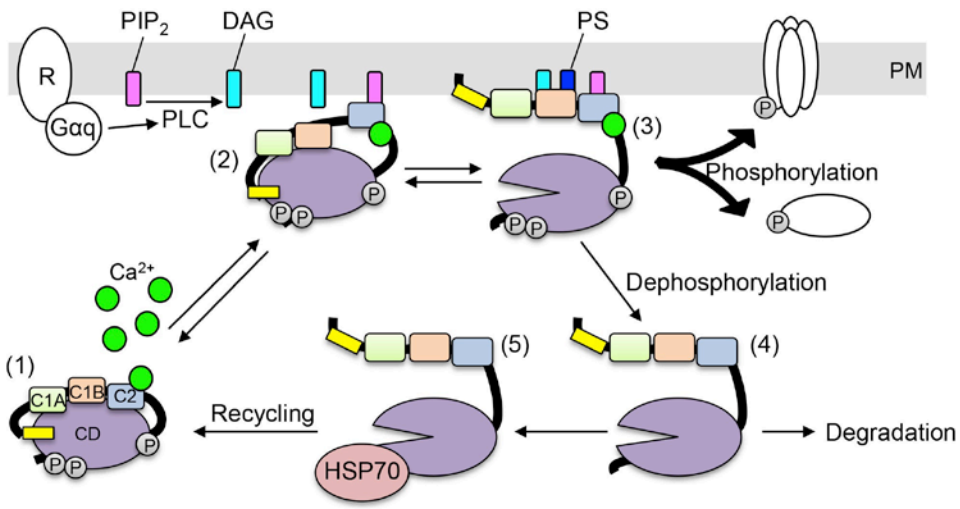


Figure 1.5 Schematic illustration of the life cycle of PKCγ.

(1) Mature PKCγ resides in the cytosol in an autoinhibited conformation. Bindings of agonists to Gαq-coupled receptors (R) such as mGluR1 leads to phospholipase C (PLC)-catalysed hydrolysis of PIP_2 generating DAG and indirectly, increase of cytosolic calcium (Ca^{2+}). Ca^{2+} bind to PKCγ and promote translocation of PKCγ to

the plasma membrane. (2) The calcium-bound C2 domain engages with PIP_2 at the plasma membrane and (3) facilitates the binding of PKCγ to its membrane-embedded ligand, DAG, via primarily the C1B domain. The pseudosubstrate is then released from the substrate-binding cavity of the catalytic domain. Activated PKCγ phosphorylates downstream substrates such as TRPC3. PKCγ returns to its autoinhibited conformation following the decay of its second messengers. (4) The membrane-bound conformation of PKCγ is sensitive to dephosphorylation. Prolonged activation leads to the first dephosphorylation event on the hydrophobic motif catalysed by phosphatase PHLPP, followed by dephosphorylation by PP2A. Fully dephosphorylated PKCγ is degraded via the ubiquitin-proteasomal pathway. (5) Alternatively, binding of HSP70 to the dephosphorylated turn motif allows PKCγ to become re-phosphorylated, thereby sustaining the signalling lifetime of the enzyme.

1.4.3.4 Propagation of PKCγ signals in Purkinje cells

The propagation of PKCγ signals along dendrites of Purkinje cells is important for signal transduction from distal region of dendrites to the cell bodies for cerebellar development and plasticity. Using live imaging of Purkinje cells in cerebellar slices of tetracycline-inducible neuron-specific PKCγ-GFP transgenic mice, PKCγ translocation in Purkinje cells was induced by parallel fibre activation via the metabotropic glutamate receptor 1 (mGluR1) pathway (Sakai et al., 2004). The activation of mGluR1 induces a reversible and transient translocation of PKCγ from the cytosol to the plasma membrane in the dendritic shaft of Purkinje cells. This translocation can be propagated peripherally from the stimulated branch to neighbouring synapses that are not stimulated. In addition, translocation of PKCγ propagates from the distal region of the dendritic tree along the dendrites to the proximal trunk close to the soma of Purkinje cells. Interestingly, translocation of PKCγ ends at the proximal dendrites and does not occur in the cell bodies of Purkinje cells, suggesting that PKCγ translocation in the proximal dendrites and Purkinje cell soma may be modulated by other synaptic inputs. Moreover, PKCγ translocation in Purkinje cell dendrites is regenerative with a relatively long refractory period, but it is still unclear how these properties are implicated in cerebellar development and plasticity (Sakai et al., 2004).

1.4.4 Expression and functions of PKCγ in the central nervous system

In vertebrates, PKCγ is highly expressed in the brain and the spinal cord (Ding et al., 2005; Saito et al., 1988). Within the brain, PKCγ is found in the cerebellum, hippocampus and cerebral cortex (Saito and Shirai, 2002). In the cerebellum, PKCγ is exclusively and highly expressed in Purkinje cells (Barmack et al., 2000; Cardell et al., 1997; Hashimoto et al., 1988; Kose et al., 1988; Sakai et al., 2004; Schrenk et al., 2002). PKCγ is ubiquitously localized in the cytoplasm of the cell bodies, throughout dendrites and in growth cones of Purkinje cell axons (Kose et al., 1988; Shimohama et al., 1990). PKCγ is also found in the nucleus of primary rat Purkinje cells suggesting a role in nuclear events such as regulation of gene expression (Kose et al., 1988; Nishizuka, 1988; Shimohama et al., 1990). The expression of PKCγ is relatively low at birth, which then increases over the first two weeks. PKCγ expression peaks during the third postnatal week, which is the period of extensive dendritic growth in Purkinje cells (Hashimoto et al., 1988; Huang et al., 1988; Moriya and Tanaka, 1994). In fact, PKCγ plays important roles in Purkinje cell dendritic development (Metzger, 2010; Metzger and Kapfhammer, 2000, 2003). Moreover, functional disruption of PKCγ resulted in motor dysfunction and ataxia in rodents as well as in humans (reviewed in (Chen et al., 2012a)), suggesting that PKCγ is important to cerebellar function. However, the molecular mechanisms by which PKCγ controls these processes are still poorly understood.

1.4.4.1 PKCγ in cerebellar development: regulation of Purkinje cell dendritic growth

Purkinje cell dendrites are highly branched and form an arbour-like structure. The complexity of the dendritic tree of Purkinje cells is mediated by the number and distribution of synaptic inputs (Metzger, 2010). These highly branched dendritic arbours are critical for neuronal signal integration and firing patterns (Metzger, 2010). The maturation of the dendritic trees is essential in determining connectivity patterns in the adult brain. Intrinsic gene control mechanisms play an important role in basal Purkinje cell dendritic outgrowth while afferent innervation and activity are required for full maturation of Purkinje cell dendrites during development (Metzger,

2010; Metzger and Kapfhammer, 2000, 2003). However, the molecular mechanisms of these complex processes that control dendritic development of Purkinje cells are incompletely understood. Conventional PKCs have been shown to modulate Purkinje cell dendritic development via synaptic activation and transduce calcium signals to the downstream signalling cascade (Metzger, 2010; Metzger and Kapfhammer, 2000, 2003). Activation of conventional PKCs using phorbol ester reversibly inhibited dendritic growth resulting in a small dendritic tree with short dendrites and few branches in rat cerebellar organotypic slice cultures (Metzger and Kapfhammer, 2000). In contrast, inhibition of conventional PKCs facilitated dendritic branching without a major effect on the overall size of dendritic arbour (Metzger and Kapfhammer, 2000). Further analysis suggested that PKCγ was the major isoform that was targeted by PKC inhibition. Similar overgrowth of Purkinje cell dendritic trees accompanied with increased branching was observed in PKCγ-deficient mice (Gundlfinger et al., 2003). Moreover, pharmaceutical inhibition did not promote further growth of dendritic trees (Gundlfinger et al., 2003). This suggests that PKCγ is the limiting factor but not the only PKC isoform involved in the control of Purkinje cell dendritic growth. Later studies demonstrated that PKC activation in slice cultures from PKCγ-deficient mice still led to strong inhibition of dendritic complexity of Purkinje cell arbours (Gundlfinger et al., 2003). This suggests that another PKC isozyme that is expressed in Purkinje cells: PKCα could also modulate dendritic outgrowth of Purkinje cells (Gundlfinger et al., 2003). Therefore, these studies support a model that the activity of abundantly expressed PKCγ negatively regulates the intrinsic growth of Purkinje cell dendrites before parallel fibre inputs develop. Less abundant PKCα forms a reserve pool that can be activated by synaptic input of parallel fibres (Gundlfinger et al., 2003; Metzger, 2010).

1.4.4.2 PKCγ in cerebellar development: elimination of multiple climbing fibre innervation of Purkinje cells

Proximal Purkinje cell dendrites undergo a dynamic modification of innervation by climbing fibres originating from the interior olive of the medulla during postnatal development (Metzger, 2010; Metzger and Kapfhammer, 2003). In the first postnatal week in rodents, developing Purkinje cells are innervated by multiple climbing fibres. The excessive climbing fibre synapses are then gradually eliminated. By the end of the third postnatal week, mature Purkinje cells receive input from a single climbing fibre (Metzger, 2010; Metzger and Kapfhammer, 2003). Interestingly, PKCγ-deficient mice, which displayed motor incoordination, showed multiple climbing fibre innervations of Purkinje cells persistent into adulthood (Chen et al., 1995). This suggests that PKCγ controls the elimination of excessive climbing fibre innervation. This impaired climbing fibre elimination in PKCγ-deficient mice could be rescued by overexpression of PKCα in Purkinje cells, but not under normal physiological condition (Takahashi et al., 2017). This is likely to be due to the low expression level of PKCα in developing Purkinje cells (Chen et al., 1995; Takahashi et al., 2017). Moreover, PKCγ showed two-fold higher Ca^{2+} affinity than PKCα and might therefore be more likely to be activated under physiological conditions (Gundlfinger et al., 2003; Kohout et al., 2002). These findings indicate that PKCγ is the central regulatory element of climbing fibre elimination from Purkinje cells during development (Hirai, 2017; Metzger, 2010; Metzger and Kapfhammer, 2003; Saito and Shirai, 2002; Takahashi et al., 2017). Subsequent studies have demonstrated that this process is regulated by modulation of excitatory inputs from parallel fibres through activity of the mGluR1 pathway (Sirzen-Zelenskaya et al., 2006), which also controls motor coordination in adulthood (Ichise et al., 2000; Nakao et al., 2007). Activation of mGluR1 and the subsequent activation of downstream effectors Gαq, phospholipase C (PLC) and PKCγ in Purkinje cells are involved in the elimination of climbing fibre innervation (Hirai, 2017; Metzger, 2010; Saito and Shirai, 2002) (Fig. 1.6). The deficiency of any component in this signaling cascade leads to the persistent multiple innervations of Purkinje cells by climbing fibres and motor incoordination as observed in mutant or transgenic mice (De Zeeuw et al., 1998; Hashimoto et

al., 2009; Hashimoto et al., 2000; Hirono et al., 2001; Ichise et al., 2000; Kano et al., 1995; Kano et al., 1997; Kano et al., 2008; Kano et al., 1998; Kashiwabuchi et al., 1995; Kose et al., 1988; Offermanns et al., 1997).

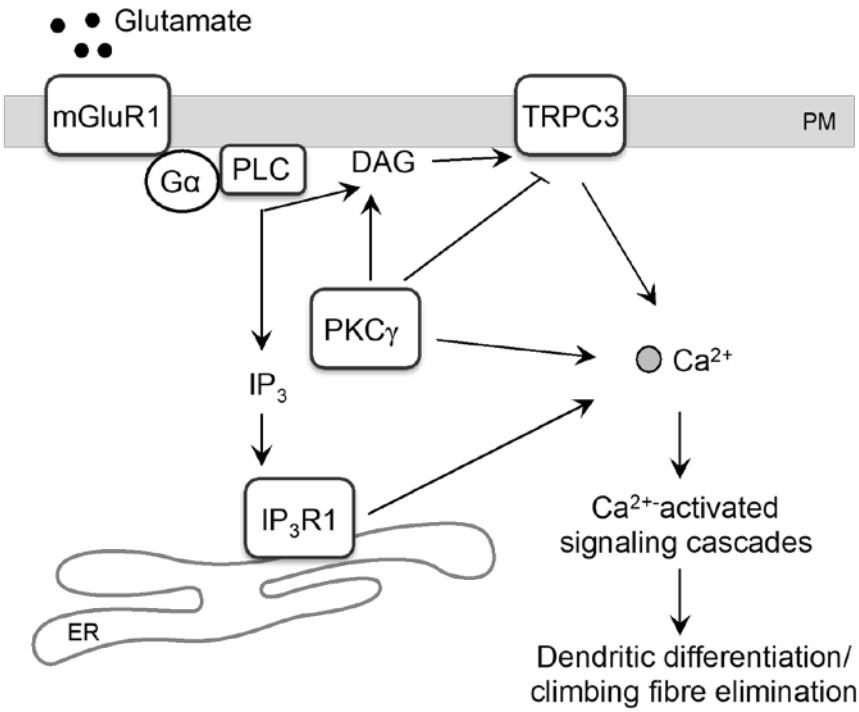


Figure 1.6 Simplified illustration of dendritic development via mGluR1-PKCγ-mediated signalling.

mGluR1 at Purkinje cell postsynaptic site activates PLC via G protein to produce IP_3 and DAG. DAG activates TRPC3 channel causing calcium influx. IP_3 binds to its receptor IP_3R1 in the endoplasmic reticulum (ER), which then releases calcium into the cytosol. PKCγ is activated by calcium and translocates to the plasma membrane, where it binds to DAG via its regulatory domain and then phosphorylates TRPC3. The PKCγ-mediated phosphorylation, acting as a negative feedback mechanism, inhibits TRPC3 and blocks further calcium influx. Therefore, the cytoplasmic calcium homeostasis is maintained. PKCγ-mediated phosphorylation of other substrates can also occur throughout the cells. This might affect calcium signalling and subsequently modulate Purkinje cell dendritic development. IP_3: inositol triphosphate; DAG: diacylglycerol; PLC: phospholipase C; Ca^{2+}: calcium ions. Modified from (Becker, 2015).

1.4.4.3 PKCγ in synaptic plasticity

Synaptic plasticity, which is important for learning, depends on the selective strengthening and weakening of synapses (Kessels and Malinow, 2009). Excitatory synapses contain AMPA-type receptors (AMPARs) to transmit signals and NMDA-type receptors (NMDARs) to trigger long-term changes in synaptic transmission: long-term potentiation (LTP) and long-term depression (LTD) (Gerrow and Triller, 2010; Kessels and Malinow, 2009). While the insertion of AMPARs to synaptic membranes result in LTP, its removal leads to LTD (Gerrow and Triller, 2010; Kessels and Malinow, 2009). Pharmaceutical and electrophysiological studies have shown that AMPAR phosphorylation by PKC is involved in LTP and LTD. Activation of PKC caused synaptic transmission resembling LTP in hippocampal slices and pyramidal cells directly injected with phorbol ester (Hu et al., 1987; Linden et al., 1986; Linden et al., 1987; Malenka et al., 1986) while inhibition of PKC prevented the induction of LTP (Malinow et al., 1989). Hippocampal LTP was significantly diminished under usual test conditions in PKCγ-deficient mice (Abeliovich et al., 1993). However, it could be induced by a period of low frequency stimulation (Abeliovich et al., 1993), suggesting that PKCγ is a regulator of LTP but is not required by LTP production. Activation of PKCγ was shown to increase membrane expression of GluR4 subunit of AMPARs in HEK293 cells (Correia et al., 2003) and induce trafficking of AMPARs into excitatory synapses in embryonic zebrafish (Patten and Ali, 2009). This suggests the involvement of PKCγ in membrane insertion of AMPARs during LTP.

Cerebellar LTD at parallel fibre-Purkinje cell synapses along the distal dendrites of Purkinje cells is a form of cerebellar plasticity and plays an important role in motor learning (Ito, 2001; Schonewille et al., 2011; Yamaguchi et al., 2016). It is induced by conjunctive stimulation of parallel fibres and climbing fibres, which triggers activation of mGluR1. The resulting increase in calcium concentration and PKC activation causes phosphorylation of serine 880 in the C-terminal PDZ ligand motif of AMPAR GluR2 (Hirai, 2001; Matsuda et al., 2000; Matsuda et al., 1999; Tatsukawa et al., 2006). This phosphorylation event promotes the binding of PICK1 with GluR2 and leads to PICK1-dependent endocytosis of postsynaptic AMPARs (Chung et

al., 2003; Hirai, 2001; Xia et al., 2000). Phosphorylation of GluR2 subunit by PKC is critical for the expression of LTD in hippocampal CA1 and pyramidal neurons (Chung et al., 2000; Kim et al., 2001). The inhibition of PKC activity in Purkinje cells impaired cerebellar LTD and motor learning (De Zeeuw et al., 1998; Goossens et al., 2001; Koekkoek et al., 2003). Extensive studies have shown that the LTD induction is regulated by a positive feedback signalling loop based on mutual activation of PKC and mitogen-activated protein kinase (MAPK) cascades (Hansel et al., 2006; Kuroda et al., 2001; Leitges et al., 2004; Tanaka and Augustine, 2008; Tanaka et al., 2007). PKC-mediated phosphorylation of a calcium-sensing molecule CaMKIIβ, induced by activation of mGluR1 at the parallel fibre-Purkinje cell synapses, promoted spine formation and elongation in Purkinje cells via F-actin bundling (Kawaguchi and Hirano, 2013; Sugawara et al., 2017). However, although motor coordination was impaired in PKCγ-deficient mice, eye blink conditional indicative of motor learning remains intact. Moreover, cerebellar LTD was normal in PKCγ-deficient mice but was absent in PKCα-deficient mice (Abeliovich et al., 1993; Metzger, 2010; Metzger and Kapfhammer, 2000), suggesting that PKCα, but not PKCγ, is responsible for the expression of cerebellar LTD (Leitges et al., 2004; Schonewille et al., 2011; Takahashi et al., 2017). This difference results from the unique presence of the PDZ-binding motif in PKCα that allows the formation of PKCα/PICK1 complex (Dong et al., 1997; Hanley, 2008) and the subsequent phosphorylation of the GluA2 C-terminus of AMPARs (Matsuda et al., 1999). Therefore, although PKCα and PKCγ share considerable amount of phosphorylation targets, their distinct functions in Purkinje cells might be partly due to a different subset of phosphorylation targets.

1.5 Current disease models of SCA14

Despite the numerous SCA14 mutations discovered, the molecular impacts of these mutations on the protein structure and functions of PKCγ, and the pathogenesis of SCA14 remain to be elucidated. Since SCA14 is rare and mild, the lack of human brain tissue has impinged the investigation of its pathogenesis. Most of the studies concerning the molecular impacts of SCA14 mutations on the structure, localisation, dynamics and kinase activities of PKCγ were performed in *in vitro* cell models such as kidney COS-7, Chinese hamster ovary CHO, HeLa and neuronal SH-SY5Y cells. Despite the important insights to the potential mechanisms provided by the structural and functional analyses of PKCγ, the inconsistency of results shown in these non-neuronal cell lines suggest that the effect of PKCγ mutations may be cell-type specific and that *in vitro* studies of irrelevant cell types may not be the best approach to understand the molecular mechanism of SCA14.

To investigate the normal function of PKCγ, a PKCγ-knockout mouse model (Abeliovich et al., 1993) and a rat model harboring a spontaneous *agu* mutation that gives rise to a truncated PKCγ (Craig et al., 2001) have been used. Moreover, three transgenic mouse models of SCA14 have been generated to determine the Purkinje cell-specific phenotypes caused by SCA14 mutations *in vivo* (Ji et al., 2014; Shimobayashi and Kapfhammer, 2017; Zhang et al., 2009). In addition, primary mouse Purkinje cell cultures overexpressing SCA14 mutants have also been used. Localisation and aggregation of the mutant proteins, number, morphological changes, electrophysiology, and calcium signalling of Purkinje cells were examined.

1.5.1 Loss-of-function models

PKCγ-knockout mice are neurologically normal and present only mild ataxic phenotypes such as mildly abnormal gait and incoordination (Abeliovich et al., 1993). The cerebellum of these mice exhibited abnormal persistence of multiple climbing fibre innervations onto Purkinje cells (Kano et al., 1995). Purkinje cell dendritic trees were enlarged and had an increased number of

dendritic growth and branching (Schrenk et al., 2002). This suggests that SCA14 is caused by gain-of-function mutations, rather than haploinsufficiency (Asai et al., 2009; Schrenk et al., 2002; Yabe et al., 2003).

A rat model harbouring the spontaneous *agu* mutation showed movement impairments and is defective in dopamine release (Payne et al., 2000; Payne et al., 1998). These rats showed age-progressive dysfunction and death of neurons in the midbrain (substantia nigra pars compacta) (Craig et al., 2001). A nonsense mutation G851T at codon 281 in the *Prkcg* gene was later identified in the AS/AGU rats (Craig et al., 2001). The G481T mutation produces a new stop codon at position 281 that creates a truncated protein of 280 amino acids. The protein, if produced, would terminate five residues C-terminal to the last strand of the β-sheet structure of the C2 regulatory domain. PKCγ staining was absent in Purkinje cells of the *agu* mutant in contrast to the strong staining in the wildtype using an antibody recognizing the C-terminal (Craig et al., 2001). The truncated protein was predicted to possess a severe or complete loss of PKCγ function due to the loss of catalytic domain. However, it was unclear whether the truncated protein was expressed at all. Overall, it remains to be determined whether the movement impairments were a result of the loss of PKCγ function in Purkinje cells.

1.5.2 Transgenic mouse models of SCA14

PKCγ-H101Y transgenic mice using a universal CMV promoter were generated by Zhang et al. (2009) to determine the effect of the H101Y mutation on PKCγ in Purkinje cells. Motor function of the transgenic mice was tested with the tail suspension test. Transgenic mice tended to clasp their hind limbs when they were hung upside down by the tails in contrast to the splaying out of hind limbs in wildtype mice. However, tail suspension test is not commonly used to assess motor coordination. Rotarod and walking beam tests that are traditional tests for motor coordination should be used instead (Huang, 1989). In the PKCγ-H101Y transgenic mice, the number of Purkinje cells decreased and altered morphologies of cell bodies were

observed at four weeks of age. Endogenous mutant PKCγ was expressed in the soma and dendrites of Purkinje cells, which was similar to wildtype at the age of four weeks. The mutant PKCγ was not expressed under the control of a Purkinje cell-specific promoter. Therefore, although mutant PKCγ was expressed mainly in the Purkinje cell layer, it was uncertain whether the observed mild motor incoordination was a result of an altered Purkinje cell function caused by the mutant protein. Moreover, the presence of mutant PKCγ foci, which is commonly assessed in other studies, was not examined. Therefore, the credibility of the model needs further investigation.

Ji et al. (2014) reported a double transgenic mouse model with a human S361G mutation in the catalytic domain under the control of a Purkinje cell-specific promoter Pcp2. Moreover, inducible expression of mutant PKCγ was allowed using a Tet-Transactivator system (Pcp2-tTA/TRE-PKCγ). The transgenic mice did not show gross cerebellar atrophy or a major loss of Purkinje cells. All cerebellar cell types were present with normal lamination. However, the size and complexity of the dendritic trees of the diseased Purkinje cells in slice cultures were drastically reduced. The thicker primary dendritic branches and shorter secondary dendritic branches resembled Purkinje cells from control mice treated with PKC activator. This suggests that the altered morphology of Purkinje cell dendrites might be caused by increased intrinsic PKCγ activity. Despite the lack of gross cerebellar atrophy, these mice showed a mild cerebellar ataxia revealed by testing on the rotarod and on the walking beam. This suggests that faulty synaptic function and connectivity rather than the loss of Purkinje cells might cause the ataxic phenotypes. Nevertheless, electrophysiological properties and synaptic connectivity of Purkinje cells in these mice should be examined to test this hypothesis.

Finally, the generation of a SCA14 mouse model with a human G118D mutation under the control of a Purkinje cell-specific Pcp2 promoter and a tTA/TRE system was recently reported (Pcp2-tTA/TRE-PKCγ) (Shimobayashi and Kapfhammer, 2017). No phenotypes or morphological alterations were reported in these mice. Only a slight decrease in gross area of

Purkinje cells in slice cultures and in dissociated developing Purkinje cells from juvenile transgenic mice was detected. The credibility of this mouse model therefore needs further investigation.

1.6 Proposed pathogenic mechanisms of SCA14

Several pathogenic mechanisms underlying SCA14 including protein misfolding and aggregation, impaired autophagy, altered kinase activity and deranged calcium signalling have been proposed. Interestingly, some of these mechanisms have been described in other SCAs, suggesting that SCA14 is a good entry point to elucidate the potential common factors in disease pathogenesis. Table 1.2 summarises the findings of pathogenic mechanisms of SCA14 mutations using *in vitro* analyses, cellular models, primary neurons and patient post-mortem cerebellar tissues identified to-date.

1.6.1 Accumulation of mutant PKCγ foci

The accumulation of mutant PKCγ foci has been one of the major proposed pathogenic mechanisms underlying SCA14. The majority of SCA14 mutations, including H36R and H101Q, have been shown to cause the formation of cytoplasmic PKCγ foci *in vitro*, in heterologous cell models as well as in developing and mature primary cultured mouse Purkinje cells (Doran et al., 2008; Nemeth et al., 2013; Ogawa et al., 2013; Seki et al., 2005a; Seki et al., 2009; Seki et al., 2007). Two types of mutant PKCγ foci are usually observed in overexpression systems: small dot-like foci in the cytoplasm and perinuclear large foci (Doran et al., 2008; Nemeth et al., 2013; Ogawa et al., 2013; Seki et al., 2005a; Seki et al., 2009; Seki et al., 2007). Long-term time-lapse imaging showed that the small dot-like foci of mutant PKCγ-GFP was first observed in the cytoplasm, which then accumulated in perinuclear regions leading to the formation of large foci (Seki et al., 2007). In addition, SCA14 mutations were reported to accelerate amyloid-like fibril formation of mutant PKCγ, which were positive for

amyloid-like fibril binding agents Congo red and Trehalose (Seki et al., 2010a; Seki et al., 2010b), *in vitro* and in cell models (Takahashi et al., 2015) as well as weakly in cultured primary mouse Purkinje cells (Seki et al., 2009).

The mutant PKCγ foci have been suggested to induce cellular stress and apoptosis. Protein foci of three SCA14 mutants (H101Y, S119P and G128G) induced ER stress and apoptosis in mammalian cell lines and neuronal cells (Lin et al., 2007; Lin and Takemoto, 2007; Seki et al., 2007). Mutant PKCγ foci co-localised with an ER marker BiP/GRP78 and caused elevation of apoptotic markers in hippocampal neurons overexpressing these three SCA14 mutants (Lin and Takemoto, 2007). In addition, cell death increased following aggregate formation and accumulation in CHO (Seki et al., 2007), HT22 (Lin and Takemoto, 2007), lens epithelial (Lin et al., 2007) and SH-SY5Y cells (Takahashi et al., 2015) expressing mutant PKCγ (R41P, H101Y, S119P, G128D, Q127R, F643L). The extent of cell death was suggested to depend on the expression level of mutant PKCγ. Moreover, cultured primary mouse Purkinje cells expressing SCA14 mutants also showed fragmented and condensed nuclei, which was considered as a marker of apoptosis. These apoptotic Purkinje cells contained mutant aggregates and less Calbindin staining compared to controls (Seki et al., 2009). The cell death signals have been suggested to propagate to neighbouring cells via gap junctions (Lin et al., 2007; Lin and Takemoto, 2007; Nguyen et al., 2004). Inhibitors of protein oligomerization and aggregation such as Congo Red and trehalose were found to alleviate aggregation of mutant proteins, reverse improper dendritic development and inhibit apoptotic cell death in cultured primary Purkinje cells (Seki et al., 2010a; Seki et al., 2010b). Nevertheless, it is still unclear whether mutant PKCγ foci/aggregates are present in Purkinje cells of SCA14 patients.

In contrary, mutant PKCγ foci were not observed in cellular models overexpressing other SCA14 mutants (Verbeek et al., 2008; Verbeek et al., 2005). In addition, mutant PKCγ led to lower dendritic spine density of Purkinje cells with parallel fibres as well as reduced area, length, and branches of dendritic trees of dissociated primary cultured mouse Purkinje cells in

a foci-independent manner (Seki et al., 2009). Therefore, the pathological importance of mutant PKCγ foci remains controversial.

1.6.2 Impairment in mutant protein degradation

The loss of Purkinje cells observed in human SCA14 patients and transgenic mice, as well as increased cell death reported in cultured cells might be a result of impaired degradation of mutant PKCγ. Degradation of misfolded or partially unfolded proteins has been shown to be impaired in many neurodegenerative diseases including SCAs (Ciechanover and Kwon, 2015; Dantuma and Bott, 2014; Menzies et al., 2017; VerPlank et al., 2017; Zheng et al., 2016). In healthy individuals, misfolded proteins can be degraded by various cellular proteolytic pathways. Misfolded proteins are recognised by molecular chaperones that deliver substrates to the ubiquitin-proteasome system (UPS), chaperone-mediated autophagy (CMA) and macroautophagy (referred to autophagy hereafter) depending on their size, solubility and the nature of misfolding. Soluble and monomeric misfolded proteins are primarily degraded by the UPS and CMA, while aggregates of misfolded proteins are predominantly degraded by autophagy (Ciechanover and Kwon, 2015, 2017; Kwon and Ciechanover, 2017).

In the UPS, polyubiquitin chains are added to proteins in three steps by the cooperative actions of three groups of enzymes: the ubiquitin-activating enzymes (E1), the ubiquitin-transferring enzymes (E2), and the ubiquitin ligases (E3). The polyubiquitinated proteins are then unfolded into polypeptide chains and cleaved into short peptides while passing through the proteasome (Kwon and Ciechanover, 2017). Thus far, only two studies have investigated the degradation of mutant PKCγ overexpressed in *in vitro* cell models. Mutant PKCγ was reported to be ubiquitinated, and proteasome inhibition caused accumulation of mutant PKCγ foci in CHO cells (Seki et al., 2007). This in turn resulted in the induction of ER stress and apoptotic cell death (Seki et al., 2009; Seki et al., 2007). However, it is unclear why mutant PKCγ foci were not cleared despite being ubiquitinated.

In autophagy, aggregates of misfolded proteins are sequestered in autophagosomes, which then fuse with lysosomes, where substrates are digested by lysosome hydrolases (Appelqvist et al., 2013; Button et al., 2017; Ciechanover and Kwon, 2015, 2017; Dantuma and Bott, 2014; Hu et al., 2015; Menzies et al., 2017; Zheng et al., 2016). To date, only one study has reported the potential involvement of autophagy in SCA14. Degradation of mutant PKCγ (S119P) foci was promoted by autophagy inducers in MEF and SH-SY5Y cells (Yamamoto et al., 2010). However, it is unclear whether mutant PKCγ foci can be targeted to autophagosomes and removed by autophagy under physiological condition in the absence of autophagy inducer.

Specific misfolded proteins that expose a unique degradation peptide can be degraded via the CMA. The peptide motif is recognised by molecular chaperones and directly delivered into lysosomes for degradation. However, the role of the CMA in the removal of mutant PKCγ foci has not been explored.

Overall, it is unknown whether mutant PKCγ foci/aggregates exist and if present, are effectively degraded or not in human Purkinje cells. Moreover, it is still unclear how the impairment of protein degradation processes, if present, eventually causes Purkinje cell dysfunction and degeneration in SCA14.

1.6.3 Abnormal regulation and mobility of mutant PKCγ

The majority of the known SCA14 mutations cluster in the region corresponds to the C1 domain of PKCγ. Several of these mutations are located in the highly conserved residues and around the binding surfaces with lipid cofactors of PKCγ (Steinberg, 2008) (Fig. 1.7). However, the molecular impact of these SCA14 mutations on the protein structure and function of PKCγ remains unclear. Three-dimensional structural modeling of H101Y and G128D PKCγ suggested conformational changes in the zinc-finger region (H101, C131, C134 and C150 for

site 1, and H139, C114, C117 and C142 for site 2) (Lin et al., 2007). These findings are in agreement with a previous report showing that the DAG/phorbol ester activation in the PKCγ H101Y mutant was altered (Lin and Takemoto, 2005). The modelled structure of the S119P mutant showed loosening of the global fold and overall conformational changes in the C1B subdomain structure, indicating disruption of the C1B Zinc-finger stress switch and a collapse in the DAG/phorbol ester-binding loop (S110, T112, F113, L121, Y122, and G123) (Lin et al., 2007). This is in contrast to the previous models, which did not confirm C1B folding changes for this mutant (Chen et al., 2003).

Fluorescence resonance energy transfer (FRET) and translocation analyses demonstrated that the mobility of mutant PKCγ in Purkinje cell dendrites was remarkably reduced, probably because of oligomer formation (Seki et al., 2009). Also, translocation of mutant PKCγ in response to high potassium-induced depolarization was attenuated (Seki et al., 2009). Since the propagation of PKCγ translocation plays an important role in signal transduction of Purkinje cells, soluble oligomers of mutant PKCγ would impair cellular functions of Purkinje cells by attenuating translocation and reducing the phosphorylation of membrane substrates. This would result in abnormal dendritic development and spine density of Purkinje cells (Sakai et al., 2011). In addition, mutant PKCγ was shown to impose a dominant negative effect on wildtype PKCγ. The presence of exogenous PKCγ mutated at the C1B subdomain prevented the normal function and activation of endogenous wildtype PKCγ by inhibiting autophosphorylation of both wildtype and mutant PKCγ at T514 (Lin et al., 2007). This suggests that mutant PKCγ might alter the responsiveness to activation and mobility of wildtype PKCγ.



Figure 1.7 Several SCA14 mutations are located in the residues that are highly conserved and around the binding surfaces with lipid cofactors of PKCγ.

Sequence alignment of PKCγ C1A and C1B subdomains. Conserved cysteine and histidine residues are shaded in grey. Lipid cofactor binding sites are indicated by green shading. Binding regions of PKCγ to14-3-3 protein are indicated by black boxes. Known SCA14 mutations that lie within the C1A and C1B subdomains are indicated in red.

1.6.4 Altered kinase activity and substrate binding of mutant PKCγ

Although kinase activity of mutant PKCγ has been shown to be higher than wildtype PKCγ in *in vitro* cell models (Adachi et al., 2008; Shimobayashi and Kapfhammer, 2017; Verbeek et al., 2005) and implicated in one study using SCA14 transgenic mice (Ji et al., 2014), it remains unclear whether increased kinase activity directly causes abnormal development, function and loss of Purkinje cells in SCA14. A number of SCA14 mutations in the C1 domains including H101Q have been reported to show higher kinase activity using *in vitro* kinase activity assays in COS-7 and CHO cells, in the absence and presence of activation with phorbol ester (PMA) treatment (Adachi et al., 2008; Verbeek et al., 2005). However, the phosphorylation levels at T514, T655 and T674 of some of these mutants were similar to (Verbeek et al., 2005) or lower than wildtype PKCγ (Lin et al., 2007; Seki et al., 2005a; Verbeek et al., 2008). A recent study comparing dendritic development of mouse Purkinje cells overexpressing mutant PKCγ suggests that mutations in different domains affect dendritic development differentially (Shimobayashi and Kapfhammer, 2017). The authors reported that although the tested mutations showed increased kinase activity *in vitro*, some of the SCA14 mutants still resulted in dendritic tree area of primary cultured mouse Purkinje cells that were comparable to controls. However, the causal relationship between dendritic development and pathogenesis of SCA14 is not well established. Therefore, it remains to be elucidated whether increased activity of PKCγ leads to SCA14. Moreover, the overall area of Purkinje cell dendritic trees may not be the ideal measurement and should not be the only parameter for evaluating dendritic development of Purkinje cells. Instead, thickness, length and degree of branching of Purkinje cells, which are widely used parameters, should be taken into consideration as demonstrated in another study (Ji et al., 2014).

It is noteworthy that although PKCγ is highly expressed in brain and spinal cord (Ding et al., 2005; Li et al., 2005; Saito and Shirai, 2002), atrophy is confined to Purkinje cells in the

cerebellum in SCA14 patients (Chen et al., 2012a). This suggests that interactions between mutant PKCγ and its substrates might be restricted to or be highly abundant in Purkinje cells. Alternatively, the interactions result in downstream signalling that is exceptionally important to Purkinje cells and the alternations might be particularly detrimental to this particular neuronal cell type.

A number of proteins such as GluR4 subunit of AMPARs, metabotropic glutamate receptor 5 (mGluR5), non-muscle myosin heavy chain II-B (Myosin-10), myristoylated alanine-rich C kinase substrate (MARCKS), GSP43/B-50, high-mobility group protein HMG-I, RC3/neurogranin, glycogen synthetase, aprataxin, C3-type transient receptor potential channel (TRPC3), connexin-43, connexin-46, scaffolding protein 14-3-3, DGKγ and CaMKIIβ have been identified as PKCγ substrates (Adachi et al., 2008; Asai et al., 2009; Correia et al., 2003; Kim et al., 2005; Lin and Takemoto, 2005; Marais et al., 1990; Nguyen et al., 2004; Ramakers et al., 1999; Saleh et al., 2001; Sugawara et al., 2017; Trebak et al., 2005; Venkatachalam et al., 2003; Verbeek et al., 2008; Williams and Coluccio, 1995; Xiao et al., 2000; Yamaguchi et al., 2006).

PKCγ binds and phosphorylates the GluR4 subunit of AMPARs in rat cerebellum. Activation of PKCγ induced membrane expression of the GluR4 subunit of AMPARs (Correia et al., 2003), which might be involved in synaptic plasticity. DGKγ is phosphorylated and activated by PKCγ, both of which are abundant in Purkinje cells. Active DGKγ regulated the re-translocation of PKCγ from the plasma membrane to the cytosol (Yamaguchi et al., 2006). Mutant PKCγ might affect its interaction with DGKγ and in turn alter its membrane residence time. PKCγ phosphorylates connexin-43 leading to disassembly of gap junction plaques and decreased gap junction activity in cultured lens epithelial cells (Lin and Takemoto, 2005). A calcium-permeable non-selective cation channel TRPC3 that controls calcium balance showed reduced phosphorylation in COS-7 cells overexpressing H101Y and G128D mutant PKCγ (Adachi et al., 2008). Aprataxin, which is a DNA repair protein causative for a type of

autosomal recessive ataxia, was found to be a preferential substrate for mutant PKCγ, but not wildtype PKCγ (Asai et al., 2009). The increased phosphorylation of aprataxin inhibited its nuclear entry and sensitized cells to oxidative stress by increasing unrepaired DNA damage (Asai et al., 2009). Phosphorylation of MARCKS, which is multifunctional protein involved in cell motility and membrane trafficking, and that of a more downstream target ERK was decreased in HeLa cells overexpressing mutant PKCγ (G118D, V138E and C142S) (Verbeek et al., 2008). However, contradictory results were also reported in SH-SY5Y (S119F and M697Iex) (Asai et al., 2009) and HeLa cells (S119F, S119P and G128D) (Yamamoto et al., 2014) overexpressing different SCA14 mutants. This suggests that the alternations in interactions of PKCγ with its substrates may be cell-type and mutation specific. However, it remains unclear whether interactions with these substrates are pathological and how these interactions cause dysfunction and death of Purkinje cells in SCA14 patients. Identification of the Purkinje cell-specific substrates of PKCγ may clarify the pathogenic roles of mutant PKCγ in known cellular pathways.

1.6.5 Aberrant calcium homeostasis and signalling

Calcium imbalance has been one of the suggested pathogenic mechanisms for Purkinje cell dysfunction and degeneration in SCAs (refers to section 1.2.1.1) (Bushart et al., 2016; Kasumu and Bezprozvanny, 2012; Matilla-Duenas et al., 2014; Meera et al., 2016; Taroni et al., 2013). Thus far, only one study has explored the role of calcium homeostasis in SCA14 aetiology (Adachi et al., 2008). Wildtype PKCγ negatively regulated calcium-induced calcium entry via phosphorylation of TRPC3 in COS-7 cells co-expressing wildtype PKCγ and TRPC3. Cells overexpressing mutant PKCγ with mutations in different domains showed contrasting results. Mutant PKCγ with mutated C1 domain (R41P, del100-101, H101Q, H101Y, G118G, S119F, S119P, G123E, G123R, Q127R, G128D, C131R, V138E, C150F) failed to inhibit calcium influx due to prolonged membrane retention. Despite these C1 mutants showed higher kinase activity, they could not regulate intracellular calcium level. Moreover, a mutation in the

catalytic domain (G360S) caused sustained calcium entry resulting from the loss of its kinase activity. Subsequent analyses showed that the inability of mutant PKCγ to maintain calcium homeostasis was a result of significant decrease in TRPC3 phosphorylation by PKCγ C1B mutants (H101Y and G128D). This reduced PKCγ-mediated inhibitions thus led to the sustained opening of TRPC3 channel and consequently calcium overload. On the other hand, cells expressing S361G- and F643L-PKCγ with an intact C1 domain and high kinase activity completely blocked calcium entry resulting in calcium underload compared to controls (Adachi et al., 2008). Taken together, these findings suggest that both sustained and over-inhibition of calcium influx may cause calcium imbalance in SCA14. Nevertheless, it has not been shown whether calcium homeostasis and signalling is aberrant in SCA14 Purkinje cells.

1.6.6 Oxidative stress and cell apoptosis

Oxidative stress is induced by an imbalanced redox states, involving either excessive generation of reactive oxygen species (ROS) or dysfunction of the antioxidant system (Calabrese et al., 2005; Kim et al., 2015). The brain is exceptionally vulnerable to the effects of ROS due to its high oxygen demand, its abundance of peroxidation-susceptible lipid cells and the relatively low levels of glutathione, which is an endogenous antioxidant that eliminates ROS (Chen et al., 2012b; Kim et al., 2015; Sahebkar et al., 2018). Oxidative stress has been linked to aging and neurodegenerative diseases including Alzheimer's and Parkinson's diseases (Chen et al., 2012b; Kim et al., 2015; Sahebkar et al., 2018). Cumulative oxidative stress may induce cellular damage, impairment of the DNA repair system, and mitochondrial dysfunction, all of which have been known as key factors in acceleration of the aging process and the development of neurodegenerative disorders (Federico et al., 2012; Kim et al., 2015; Patten et al., 2010). Hydrogen peroxide (H_2O_2) is an uncharged and freely diffusible ROS that is relatively high in the brain. Sublethal exposure of cells to H_2O_2 causes changes in the oxidation state of proteins (Cumming et al., 2004). PKCγ has been suggested to be an oxidative stress sensor (Lin and Takemoto, 2005; Lin and Takemoto, 2007; Linda et al., 2017). PKCγ was activated by H_2O_2

via the C1 domain in lens epithelial cells (Lin and Takemoto, 2005). The activated and oxidized PKCγ translocated to membranes, forms disulphide bonds and was targeted to caveolin-1 and connexin-43-containing lipid rafts. The subsequent phosphprylation of connexin-43 by PKCγ at serine 368 led to gap junction plaque disassembly and inhibition of gap junction activity (Lin and Takemoto, 2005). Further studies showed that PKCγ C1B mutants (H101Y, S119P and G128D) were irresponsive to H_2O_2 activation and exerted a dominant negative effect on wildtype PKCγ, causing the abolition of H_2O_2-induced phosphorylation of connexin-43 and -50. This thus led to sustained opening of gap junctions, which allowed propagation of apoptotic signals (Lin et al., 2007; Lin and Takemoto, 2007). Nonetheless, the contribution of oxidative stress in SCA14 has not been explored directly. It is unclear whether chronic exposure and accumulation of ROS might lead to vulnerability of Purkinje cells in SCA14.

1.6.7 Aberrant cerebellar synaptic plasticity

Cerebellar LTD at parallel fibre-Purkinje cell synapses is induced by simultaneous stimulation of parallel fibres and climbing fibres, which triggers activation of mGluR1 (refer to section 1.4.4.3 for details). While the loss of function of PKCγ does not affect cerebellar LTD in PKCγ-deficient mice (Abeliovich et al., 1993; Leitges et al., 2004), a gain-of-function SCA14 mutation (S119P) was shown to disrupt LTD expression at parallel fibre-Purkinje cell synapses (Shuvaev et al., 2011). mGluR1-mediated slow excitatory postsynaptic currents (EPSCs) were also increased (Shuvaev et al., 2011). This disruption of LTD might be a dominant negative effect of mutant PKCγ on PKCα by disturbing its membrane association (Shuvaev et al., 2011). As a result, motor learning might be disrupted. Further investigation into other SCA14 mutations is needed to confirm if these also disrupt cerebellar LTD and whether it is via the same mechanism shown in the aforementioned study.

Table 1-2 Table of known SCA14 mutations and their effects in patients, cell and/or animal models.

Mutation	Exon	Domain	Publications where the mutations were first reported	Cell lines	Primary neurons	Animal models
A24T	1	C1A	(Chelban et al., 2018)	-		
R26G	1	C1A	(Sailer et al., 2012)	-	-	-
H36R	**1**	**C1A**	**(Nemeth et al., 2013)**	• Presence of the mutated SCA14 protein foci in HEK cells (Nemeth et al., 2013)	-	-
R41P	1	C1A	(Chen et al., 2005)	• Mutated C1A peptide failed to bind phorbol ester. Full-length mutant PKCγ formed cytotoxic foci (Nakazono et al., 2018; Takahashi et al., 2015) • Increased kinase activity but sustained calcium-induced calcium influx (Adachi et al., 2008)	-	-
F48del	1	C1A	(Ganos et al., 2014)	-	-	-
G63R	1	C1A	(Nibbeling et al., 2017)	• Loss of phorbol ester-induced membrane translocation of mutant protein. Cytoplasmic aggregates in HEK293T cells (Nibbeling et al., 2017)	-	-
G63V	2	C1A	(Nolte et al., 2007)	• Mutated C1A peptide formed foci and failed to bind PDBu (Takahashi et al., 2015) but full length mutant PKCγ did not form foci in COS-7 cells (Verbeek et al., 2005) • Loss of phorbol ester-induced membrane translocation in HEK293T cells (Nibbeling et al., 2017)	-	-
C66Y	2	C1A	(Ganos et al., 2014)	-	-	-
C77S	3	C1A	(Wieczorek et al., 2007)	-	-	-
del K100-H101	4	C1B	(Chen et al., 2005)	• Increased kinase activity but sustained calcium-induced calcium influx (Adachi et al., 2008)	-	-

Mutation	Exon	Domain	Publications where the mutations were first reported	Cell lines	Primary neurons	Animal models
H101Q	**4**	**C1B**	**(Alonso et al., 2005)**	• Normal PKCγ mRNA expression while mutant protein levels gradually dropped in HEK293 cells (Alonso et al., 2005) • Presence of mutant protein foci (Nemeth et al., 2013; Seki et al., 2005a) • Small dot-like foci co-localised with early endosomes but not late endosomes (Seki et al., 2005a). Foci were not ubiquitinated in HEK and mouse neuroblastoma cells (Becker, unpublished) • Oxidative stress-induced membrane ruffling was abolished (Doran et al., 2008) • Increased kinase activity with or without calcium channel activator and sustained calcium channel-induced calcium influx (Adachi et al., 2008)	-	-
H101R	4	C1B	(Chelban et al., 2018)	• Non-ubiquitinated small cytoplasmic dot-like foci and massive perinuclear foci in HEK and mouse neuroblastoma cells (Becker, unpublished).	-	-
H101Y	4	C1B	(Chen et al., 2003)	• Controversial foci formation: massive perinuclear foci that co-localised with Golgi marker in CHO, COS-7 and SH-SY5Y cells (Seki et al., 2005a; Takahashi et al., 2015) but absent in COS-7 cells (Verbeek et al., 2005) • Increased cell death (Takahashi et al., 2015) • Enhanced calcium-induced membrane translocation but reduced residence time on plasma membrane. Sustained calcium influx (Adachi et al., 2008) • Controversial kinase activity (Asai et al., 2009; Seki et al., 2005a). Mutation has a dominant negative effect on endogenous wildtype PKCγ enzyme activity. Irresponsive to oxidative stress leading to uncontrolled and open gap junctions in cells, which caused apoptosis (Lin et al., 2007; Lin and Takemoto, 2005; Lin and Takemoto, 2007) • Conformational changes in the zinc-finger region (Lin et al., 2007)	• Phosphorylation of Cx57, a connexin at gap junction, on serines was inhibited in cerebellar slice culture (Sohl et al., 2004)	• Altered morphology and loss of Purkinje cells in vivo at four weeks of age. Transgenic mice tend to clasp their hind limbs in tail suspension test. Decreased kinase activity leading to loss of connexin-57 hosphorylation. ER stress was induced and enhanced by oxidative stress (Zhang et al., 2009)

Mutation	Exon	Domain	Publications where the mutations were first reported	Cell lines	Primary neurons	Animal models
H106P	4	C1B	(Chelban et al., 2018)	• Non-ubiquitinated small cytoplasmic dot-like foci and massive perinuclear foci in HEK and mouse neuroblastoma cells (Becker, unpublished)	-	-
F113del	4	C1B	(Ganos et al., 2014)	-	-	-
C114Y	4	C1B	(Klebe et al., 2005)	• Foci formation of mutated C1B peptides (Takahashi et al., 2015)	-	-
H116P	4	C1B	(Ganos et al., 2014)	-	-	-
G118D	4	C1B	(van de Warrenburg et al., 2003)	• Increased cell death (Seki et al., 2005a) • Cytoplasmic dot-like foci in CHO, COS-7 and SH-SY5Y cells. Enhanced foci formation after receptor-mediated transient translocation (Seki et al., 2005a). No foci in HeLa cells (Verbeek et al., 2005) • Enhanced phorbol ester-induced translocation (Verbeek et al., 2008) and prolonged calcium-induced membrane localization in CHOhm1 cells (Adachi et al., 2008) • Mutant protein co-localised with F-actin at membrane ruffles in COS-7 cells (Verbeek et al., 2005) • Sustained calcium influx (Adachi et al., 2008) • Controversial phosphorylation status and kinase activity of mutant PKCγ (Adachi et al., 2008; Asai et al., 2009; Seki et al., 2005a; Verbeek et al., 2005) Reduced phosphorylation of PKC reporter and MAPK signalling (Verbeek et al., 2008)	• Normal gross area of dissociated developing dissociated Purkinje cells overexpressing mutant PKCγ (Shimobayashi and Kapfhammer, 2017)	• Slightly decreased gross area of Purkinje cells in dissociated and slice cultures from juvenile transgenic mice (Shimobayashi and Kapfhammer, 2017)

Mutation	Exon	Domain	Publications where the mutations were first reported	Cell lines	Primary neurons	Animal models
S119F	4	C1B	(Hiramoto et al., 2006)	• Massive perinuclear foci (Asai et al., 2009; Seki et al., 2005a) co-localised with Golgi while dot-like foci did not co-localise with Golgi, lysosome, and early or late endosomes in CHO, COS-7 and SH-SY5Y cells (Seki et al., 2005a) • Susceptible to oxidative stress due to reduced DNA repair mechanism (Asai et al., 2009) and increased cell death (Seki et al., 2005a) • Controversial kinase activity (Adachi et al., 2008; Asai et al., 2009; Seki et al., 2005a). Increased phosphorylation of aprataxin and their nuclear localisation as well as phosphorylation of MARCKS (Asai et al., 2009). • Impaired phorbol ester-induced perinuclear translocation of pMRACKS, remodelling of actin cytoskeleton and macropinocytosis in HeLa cells (Yamamoto et al., 2014) • Sustained calcium-induced calcium influx (Adachi et al., 2008)	-	-
S119P	4	C1B	(Chen et al., 2003)	• Dot-like and large foci(Doran et al., 2008; Ogawa et al., 2013; Seki et al., 2005a; Seki et al., 2007; Yamamoto et al., 2010) induced ER stress and caspase 3-mediated cell apoptosis in CHO and neuronal HT22 cells (Seki et al., 2009; Seki et al., 2007). Both UPS and autophagy are involved in degradation of small dot-like but not large foci (Seki et al., 2009; Seki et al., 2007; Yamamoto et al., 2010), which were promoted by autophagic inducers (Yamamoto et al., 2010). Foci did not co-localise with Golgi, lysosome, and early or late endosomes (Seki et al., 2005a). Congo Red and trehalose reduced oligomerisation of mutant PKCγ and thereby lessening cell death in SH-5YSY cells (Seki et al., 2010a; Seki et al., 2010b). Elevated level of Hsp70 independent of the present of foci. Hsp70 strongly co-localised with foci in SH-SY5Y cells (Ogawa et al., 2013)	• Soluble oligomers and cytoplasmic foci co-localised with ubiquitin and proteasome 20S in primary cultured mouse Purkinje cells, predominantly in soma. Abnormal dendritic development regardless of foci formation (Seki et al., 2009) • Increased Purkinje cell apoptosis (Seki et al., 2009) • Reduced mobility of mutant PKCγ in Purkinje cell soma	• No gait ataxia. Impaired rotarod performance in juvenile mice • Presence of foci in soma and dendritic tree, primarily at branch points of developing Purkinje cells *in vivo* • Developmental stage-sensitive abnormal dendritic development, climbing fibre elimination and apoptosis of Purkinje cells.

Mutation	Exon	Domain	Publications where the mutations were first reported	Cell lines	Primary neurons	Animal models
				• Prolonged calcium-induced membrane localization (Adachi et al., 2008). Impaired phorbol ester-induced perinuclear translocation of in HeLa cells (Yamamoto et al., 2014) • Controversial basal kinase activity (Adachi et al., 2008; Lin et al., 2007; Seki et al., 2005a) • Irresponsive to oxidative stress (Lin et al., 2007) and caused oxidative stress-induced cell apoptosis due to sustained opening of gap junctions (Lin et al., 2007; Lin and Takemoto, 2007) • Failed to mediate remodelling of actin cytoskeleton and activate macropinocytosis in response to phorbol ester stimulation. Loss of co-localisation with pMARKCs in HeLa cells (Yamamoto et al., 2014) • Introduce a conformationally restricted Proline residue into the beta-sheet near to the phorbol ester-binding site (Chen et al., 2003). Loosening of the global fold and overall conformational changes in the C1B domain structure (Lin et al., 2007) • Sustained calcium-induced calcium influx (Adachi et al., 2008)	and dendrites (Seki et al., 2009) • Congo red and trehalose reduced foci formation and cell apoptosis, improved the mobility of mutant PKCγ reversed the improper development of dendrites in primary cultured Purkinje cells without foci (Seki et al., 2010a; Seki et al., 2010b) • Elevated expression of Hsp70 independent of foci formation in E14 primary cultured mouse Purkinje cells (Ogawa et al., 2013) • Normal gross area of developing dissociated Purkinje cells (Shimobayashi and Kapfhammer, 2017)	• Disrupted LTD expression at parallel fibre-Purkinje cell synapses *in vivo* • Exerted a dominant negative effect on wildtype PKCγ (Shuvaev et al., 2011)
G123E	4	C1B	(Klebe et al., 2005)	• Sustained calcium-induced calcium influx (Adachi et al., 2008)	-	-
G123R	4	C1B	(Klebe et al., 2005)	• Increased kinase activity but sustained calcium-induced calcium influx (Adachi et al., 2008)	-	-

Mutation	Exon	Domain	Publications where the mutations were first reported	Cell lines	Primary neurons	Animal models
Q127R	4	C1B	(Yabe et al., 2003)	• Cytoplasmic dot-like foci that did not co-localise with Golgi, lysosome, early or late endosomes in CHO, COS-7 and SH-SY5Y cells. Accelerated formation of amyloid-like fibrils in cell lines and in vitro, which was reduced by Congo Red treatment (Takahashi et al., 2015) • Increased cell death (Asai et al., 2009; Seki et al., 2005a) • Less autophosphorylation at T674 (Seki et al., 2005a) • Increased kinase activity (Asai et al., 2009) • Prolonged calcium-induced membrane localization. Increased kinase activity but sustained calcium-induced calcium influx (Adachi et al., 2008)	-	-
G128D	4	C1B	(Chen et al., 2003)	• Controversial foci formation: small dot-like and large foci(Doran et al., 2008; Ogawa et al., 2013; Seki et al., 2005a; Seki et al., 2007), which induces ER stress and cell apoptosis in CHO cells and HT22 cells (Seki et al., 2009; Seki et al., 2007) while no foci was found in COS7 and HEK cells (Doran et al., 2008; Nemeth et al., 2013) • Foci were ubiquitinated but only dot-like foci co-localise with proteasome 20S (Seki et al., 2009; Seki et al., 2007). Foci did not co-localised with Golgi, lysosome, and early or late endosomes (Seki et al., 2005a). Upregulation of Hsp70 regardless of foci formation. Hsp70 strongly co-localised with foci in SH-SY5Y cells (Ogawa et al., 2013) • Impaired phorbol ester-induced perinuclear translocation (Yamamoto et al., 2014) but enhanced calcium-induced membrane translocation (Adachi et al., 2008) • Controversial kinase activity (Adachi et al., 2008; Lin et al., 2007; Lin and Takemoto, 2007). Mutant protein has a dominant negative effect on endogenous wildtype PKCγ enzyme activity (Lin et al., 2007).	• Soluble oligomers and cytoplasmic foci predominantly in soma of primary cultured mouse Purkinje cells. Foci co-localised with ubiquitin and proteasome 20S (Seki et al., 2009) • Increased cell apoptosis (Seki et al., 2009) • Reduced membrane-translocation in soma and dendrites (Seki et al., 2009) • Abnormal dendritic development of Purkinje cells regardless of foci formation, which was improved by trehalose (Seki et al., 2010a; Seki et al., 2009)	-

Mutation	Exon	Domain	Publications where the mutations were first reported	Cell lines	Primary neurons	Animal models
				• Less phosphorylation of TRPC3 (Adachi et al., 2008). Impaired actin reorganisation and macropinocytosis following phorbol ester stimulation in HeLa cells (Yamamoto et al., 2014). Irresponsive to oxidative stress leading to uncontrolled and open gap junctions in cells, which caused apoptosis (Lin et al., 2007; Lin and Takemoto, 2007) • Lower affinity to endogenous DAG and phorbol ester TRPC3 (Adachi et al., 2008) due to conformational changes near the hydrophobic binding cleft (Chen et al., 2003) and the zinc-finger region (Lin et al., 2007)		
C131R	4	C1B	(Dalski et al., 2006)	• Increased basal kinase activity (Adachi et al., 2008; Asai et al., 2009) • Sustained calcium-induced calcium influx (Adachi et al., 2008)	-	-
C131Y	4	C1B	(Klebe et al., 2005)	-	-	-
V138E	5	C1B	(Vlak et al., 2006)	• Contradictory foci formation (Jezierska et al., 2014; Takahashi et al., 2015; Verbeek et al., 2008). Mutant protein was resistant to phorbol ester-induced dephosphorylation and accumulated in the insoluble fraction in a phosphorylated state, which was improved by chaperone PDK1 overexpression (Jezierska et al., 2014) • Enhanced phorbol-ester-induced translocation of PKCγ (Jezierska et al., 2014; Verbeek et al., 2008)(Verbeek et al., 2008; Jezierska et al., 2014) but C2 domain-induced translocation was not affected (Verbeek et al., 2008) • Controversial kinase activity: increased basal kinase activity (Adachi et al., 2008) and interaction with PDK1 (Jezierska et al., 2014) but reduced phosphorylation of PKC reporter and MAPK signalling (Verbeek et al., 2008) • Sustained calcium-induced calcium influx (Adachi et al., 2008)	• Normal gross area of developing dissociated Purkinje cells (Shimobayashi and Kapfhammer, 2017)	-

Mutation	Exon	Domain	Publications where the mutations were first reported	Cell lines	Primary neurons	Animal models
H139G	5	C1B	(Koht et al., 2012)	-	-	-
H139Q	5	C1B	(Wedding et al., 2013)	-	-	-
C142S	5	C1B	(Verbeek et al., 2008)	• No foci. Enhanced phorbol-ester-induced translocation of PKCγ but C2 domain-induced translocation was not affected. Reduced phosphorylation of PKC reporter and MAPK signalling (Verbeek et al., 2008)	-	-
C150F	5	C1B	(Fahey et al., 2005)	• Cytoplasmic small dot-like and large foci (Asai et al., 2009; Doran et al., 2008; Nemeth et al., 2013). Small dot-like foci co-localised with early endosomes (Doran et al., 2008) • Increased cell death in response to oxidative stress (Asai et al., 2009) • Higher intrinsic kinase activity (Adachi et al., 2008; Asai et al., 2009; Fahey et al., 2005; Verbeek et al., 2005) • Enhanced calcium-induced membrane translocation (Adachi et al., 2008; Verbeek et al., 2005) • Mutant PKCγ co-localised with F-actin at membrane ruffles in response to phorbol ester stimulation in COS-7 cells (Verbeek et al., 2005) • Sustained calcium influx (Adachi et al., 2008) when activated by calcium.	-	-
I173S	5	C2	(Ueda et al., 2013)	-	-	-
H174P	5	C2	(van Gaalen et al., 2013)	-	-	-
G360S	10	Catalytic	(Klebe et al., 2005)	• Contradictory kinase activity (Adachi et al., 2008; Asai et al., 2009) • Reduced membrane residence time (Adachi et al., 2008) • Calcium underload (Adachi et al., 2008)	• Normal gross area of developing dissociated mouse Purkinje cells (Shimobayashi and Kapfhammer, 2017)	-

Mutation	Exon	Domain	Publications where the mutations were first reported	Cell lines	Primary neurons	Animal models
S361G	10	Catalytic	(Chen et al., 2005)	• Inconsistent foci formation: no foci in COS-7 cells (Doran et al., 2008) but few small dot-like cytoplasmic and large foci in mouse neuroblastoma cells (Becker, unpublished) • Increased kinase activity but normal calcium homeostasis in CHOhm1 cells (Adachi et al., 2008)	• Significantly decreased gross area of developing dissociated mouse Purkinje cells (Shimobayashi and Kapfhammer, 2017)	• Mild ataxic phenotypes in rotarod and walking beam test (Ji et al., 2014) • No gross cerebellar atrophy or loss of Purkinje cells *in vivo* (Ji et al., 2014) • Abnormal dendritic development of Purkinje cells in slice cultures (Ji et al., 2014; Shimobayashi and Kapfhammer, 2017)and dissociated cultures (Shimobayashi and Kapfhammer, 2017) • Increased kinase -activity (Ji et al., 2014) • Upregulated gene and protein expression of carbonic anhydrase related protein 8 (Car8) and *ITPR1 in vivo* (Shimobayashi et al., 2016).
F643L	18	Catalytic	(Stevanin et al., 2004)	• Controversial foci formation: Triton-insoluble large perinuclear foci (Seki et al., 2005a; Takahashi et al., 2015) that co-localised with Golgi (Seki et al., 2005a) while dot-like foci did not co-localise with Golgi, lysosome, and early or late endosomes (Seki et al., 2005a). No foci in COS-7 cells (Doran et al., 2008) • Increased cell death (Takahashi et al., 2015) • Less phosphorylation of mutant PKCγ (Seki et al., 2005a) but increased kinase activity (Adachi et al., 2008; Asai et al., 2009)	• Significantly smaller developing Purkinje cells in dissociated cultures (Shimobayashi and Kapfhammer, 2017)	-

Mutation	Exon	Domain	Publications where the mutations were first reported	Cell lines	Primary neurons	Animal models
				• Normal calcium homeostasis in CHOhm1 cells (Adachi et al., 2008)		
V692G	18	C terminus	(Klebe et al., 2005)	• Controversial kinase activity (Adachi et al., 2008; Asai et al., 2009) • Normal calcium homeostasis (Adachi et al., 2008)	-	-
M697Iex	18	C terminus	(Asai et al., 2009)	• Cytoplasmic mutant protein foci (Asai et al., 2009) • Increased cell death upon oxidative stress due to recued DNA repair mechanism (Asai et al., 2009) • Increased kinase activity. Higher phosphorylation of aprataxin and MARCKS (Asai et al., 2009) • Mislocalisation of aprataxin (Asai et al., 2009)	-	-

The studies in bold letters included the mutations H36R and H101Q. *19 out of 20 tested PKCγ mutations showed an increased constitutive activity of PKCγ and increased calcium levels in the cytoplasm in a cell based assay (Adachi et al., 2008).

1.7 Disease modelling of SCA14 and other cerebellar ataxias using human iPSCs

Although animal and *in vitro* cell models have provided important insights into the molecular mechanisms underlying SCA14 and other cerebellar ataxias, the results obtained are inconclusive and do not fully recapitulate the neuropathological features observed in SCA14 patients. Therefore, a more reliable disease model is urgently needed to better understand the molecular pathogenic mechanisms underlying SCA14. Human induced pluripotent stem cells (iPSCs) derived from patients contain the disease-causing mutations expressed at endogenous levels in contrast to artificial overexpression of exogenous genes in cell models that makes the interpretation of mutant protein aggregation difficult. Human iPSCs can be differentiated into disease-relevant cell types, particularly Purkinje cells, which is the major cell type affected in cerebellar ataxia. This will allow comparison to controls for the identification of disease phenotypes specific to human Purkinje cells, which are otherwise difficult to obtain.

To date, fewer than 20 studies have been reported using human iPSCs from patients with cerebellar ataxias. The majority of these have been performed in neurons without specification and in other cell types. None of these studies have yet successfully recapitulated the specific cerebellar neuronal dysfunction and degeneration known to characterise these conditions. Most of these studies focused on autosomal recessive ataxias, while only a handful of these studies characterised iPSCs or iPSC-derived neurons from patients with polyglutamine SCAs (reviewed in (Lukovic et al., 2016; Watson et al., 2015b; Wong et al., 2017). Thus far, only one study has succeeded in generating cerebellar Purkinje cells from two SCA6 patients harbouring a polyglutamine expansion in the calcium channel Cav2.1 and examined the disease phenotypes (Ishida et al., 2016). Of note, the SCA6 Purkinje cells only showed abnormal dendritic development upon stress, but not under normal culture conditions, suggesting that environmental triggers might be crucial to causing disease phenotypes. This is consistent with

the lack of structural abnormalities in Purkinje cells of Cav2.1 knockout mice during development (Fletcher et al., 2001; Jun et al., 1999; Todorov et al., 2012) and therefore disease phenotypes might not be apparent when human iPSC-derived Purkinje cells are relatively young despite expressing mature Purkinje cell markers. In addition, accumulation of cytoplasmic aggregates of expanded Cav2.1 is critical to Purkinje cell degeneration in SCA6 but not the altered functions of the expanded Cav2.1 (Ishikawa et al., 1999; Ishikawa et al., 2001). However, it remains unclear if the SCA6 iPSC-derived Purkinje cells can recapitulate the disease phenotypes observed in human post-mortem brain material as well as in SCA6 animal models. These include the cytoplasmic aggregation of Cav2.1 channel, nuclear localisation of the cleaved Cav2.1 C-terminus and the resulting disruption of gene expression (Matilla-Duenas et al., 2014; Taroni et al., 2013).

As presented above, previous studies of SCA14 have predominantly relied on *in vitro* cell models of irrelevant cell types. Only few transgenic mouse models have been generated (based on three out of 40 known SCA14 mutations) (Ji et al., 2014; Seki et al., 2009; Zhang et al., 2009), which do not recapitulate major aspects of the human disease. Only one patient post-mortem cerebellum has been reported (Chen et al., 2003) (refer to section 1.5). However, apart from a loss of Purkinje cells, no other pathological findings were observed (Chen et al., 2003), likely due to the unsatisfactory quality of the post-mortem materials. Thus far, neither patient-derived iPSCs nor iPSC-derived neurons have been reported for SCA14.

1.8 Aims of study

The lack of reliable disease models has hampered our understanding of the disease mechanisms underlying SCA14 and the development of much-needed therapies. In light of this, my project has taken a new approach to dissect the pathogenic mechanisms underlying SCA14 by employing human iPSC-derived models.

My work focused on two distinct SCA14 mutations: H36R (Nemeth et al., 2013) and H101Q (Alonso et al., 2005) (Table 1.2). Both of these are located within the DAG-sensing regulatory C1 domain (Fig. 1.2). The H36R mutation results from an A-to-G transversion in exon 1, resulting in a histidine-to-arginine change at codon 36 of PKCγ, which lies within the C1A subdomain. The affected patient showed late-onset but rapidly progressive motor incoordination in addition to cerebellar atrophy (Nemeth et al., 2013). The second mutation, H101Q, has a C-to-G variation in exon 4, leading to a histidine-to-glutamine change at codon 101 in the C1B subdomain of PKCγ. Patients carrying this H101Q mutation displayed a slowly progressive pure cerebellar ataxia (Alonso et al., 2005). Three patients from a four-generation British family, in which 19 members had cerebellar ataxia, were included in this study (Talbot, unpublished data) (Fig. 1.7A). All affected individuals carried the H101Q mutation. Skin fibroblasts were obtained from two patients of this family (Fig. 1.8A) and cerebellar atrophy was evident on MRI (Fig. 1.8B). Post-mortem cerebellar tissue was obtained from a patient who died of 'natural causes' at the age of 90 years (Fig. 1.8A).

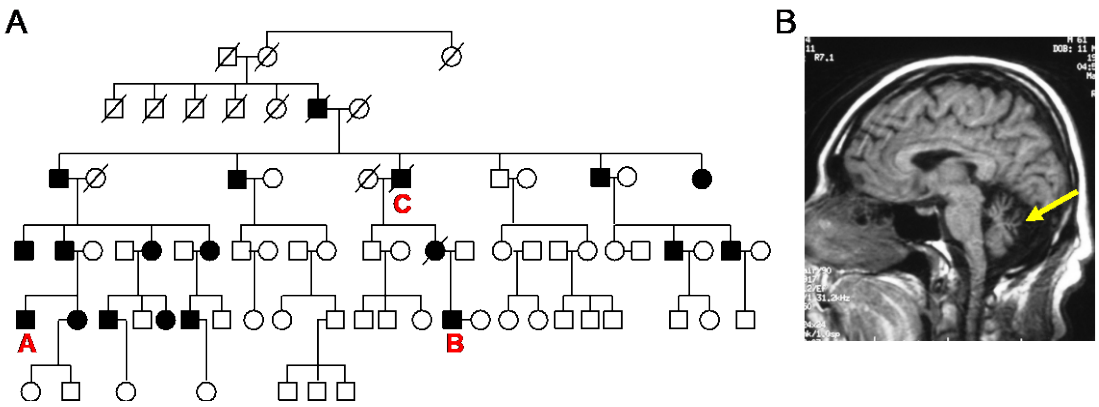


Figure 1.8 Pedigree of the four-generation British family with a SCA14 H101Q mutation that was included in this study.

(A) Three patients A, B and C (in red) from a four-generation British family with the H101Q mutation were included in this study. Skin fibroblasts were obtained from patients A and B. Brain MRI was performed on patient B. Post-mortem cerebellar tissue was obtained from patient C. Unaffected individuals are labelled in white while affected individuals are in black. Slashes indicate deceased individuals. Circles: females; square: males. (B) Brain MRI image of patient B showed cerebellar atrophy (yellow arrow).

The C1A and C1B subdomains are structurally and functionally complementary. Three-dimensional structural modelling showed that the histidine at position 36 in the C1A subdomain lies at the equivalent position to the histidine at position 101 in the C1B subdomain (Nemeth et al., 2013), suggesting that the two mutations have a similar functional effect (Fig. 1.9). In this study, it was hypothesized that SCA14 mutations in the C1 domain altered the properties and conformation of the regulatory domain, and facilitated aggregation of mutant PKCγ. This might thus change mobility and membrane retention time of PKCγ, and hence interactions with its membrane substrates. SCA14 mutations might also affect the kinase activity of PKCγ and therefore its interactions with other substrates, not only at the plasma membrane. The resulting aberrant signalling downstream of PKCγ might thereby cause dysfunction of Purkinje cells and SCA14.

A

C1A *34* SHKFTARFFKQPTFCSHCTDFIWGIGKQGLQCQVCSFVVHRRCHEFVTFEC *86*
C1B *99* KHKFRLHSYSSPTFCDHCGSLLYGLVHQGMKCSCCEMNVHRRCVRSVPSLC *151*

B

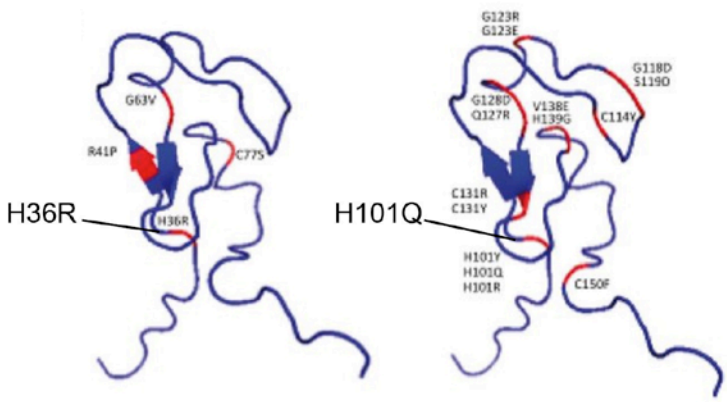


Figure 1.9 H36R and H101Q are located at the equivalent positions in the two cysteine-rich subdomains of PKCγ.

(A) Sequence alignment of the region containing the C1A (upper) and C1B (lower) subdomains. The two histidine residues that are mutated in H36R and H101Q are located at the equivalent positions in the two C1 subdomains (highlighted in grey). (B) Comparison of the three-dimensional structure of the C1A and C1B subdomains in *PRKCG* demonstrates the identical position of H36 in the C1A (left) and H101 in C1B (right) subdomains, respectively. Other SCA14-causing mutations in the C1A and C1B subdomains are also indicated.

Objectives:

1. To reprogramme fibroblasts and characterise iPSCs from SCA14 patients

2. To generate appropriate isogenic controls using CRISPR/Cas9 genome editing

3. To develop an *in vitro* disease model of SCA14 using patient iPSCs

4. To investigate the functions of mutant PKCγ in patient iPSC-derived Purkinje cells in order to identify the disease pathways underlying SCA14

In this study, iPSC lines were first generated from skin fibroblasts of four SCA14 patients with two distinct mutations: H36R and H101Q (Fig. 1.10). CRISPR/Cas9-mediated genome editing was then employed to correct the mutations and produce isogenic controls of SCA14 iPSCs. Functional studies were next performed to investigate the cellular phenotypes caused by the mutant PKCγ in iPSCs. Finally, to determine the developmental changes of human Purkinje cells caused by SCA14 mutations, control and SCA14 iPSCs were differentiated into human Purkinje cells using a novel simplified protocol. Importantly, the results obtained from iPSCs and iPSC-derived Purkinje cells were compared to pathological findings obtained from human SCA14 post-mortem cerebellar tissue to verify the disease phenotypes. Taken together, this work is the first to dissect the pathogenic mechanisms underlying SCA14 using human iPSCs and iPSC-derived Purkinje cells derived from patients.

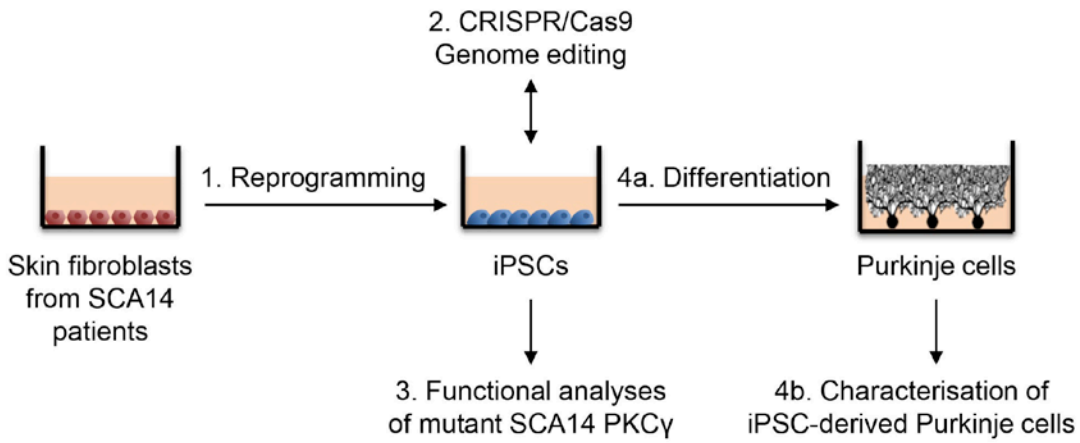


Figure 1.10 Schematic representation of experimental plans of this study.

Skin fibroblasts obtained from SCA14 patients were reprogrammed into iPSCs (1), which were then subjected to functional analyses (3). iPSCs were differentiated into Purkinje cells via self-inductive signaling that drives Purkinje cell fate (4a). Morphology and marker expression of iPSC-derived Purkinje cells were characterized (4b). To generate isogenic controls, CRISPR/Cas9 genome engineering was applied (2).

Chapter 2 Common Materials and Methods

2.1 Methods

2.1.1 DNA preparation

Genomic DNA was prepared using the DNeasy Blood & Tissue Kit (Qiagen) according to the manufacturer's protocol. Briefly, deep frozen cell pellets containing at least $2x10^6$ cells were thawed and equilibrated to room temperature and resuspended in 1x PBS. The cell mixture was lysed with proteinase K at room temperature for two minutes. RNase was added to produce RNA-free genomic DNA. Buffer AL was added for precipitation at 56 °C. The mixture was left at room temperature for 30 minutes after adding ethanol. The mixture was vortexed gently between steps. Vortex after spinning through column was avoided to ensure the integrity of genomic DNA. The precipitate was then spun through a column, washed with washing buffers and resuspended in nuclease-free water to obtain more than 100 ng/μl genomic DNA.

2.1.2 RNA preparation

RNA was prepared using the RNeasy Mini Kit (Qiagen) or RNeasy Micro Kit (Qiagen) depending on starting numbers of cells according to the manufacturer's protocol. Briefly, cell pellets were thawed and lysed. Absolute ethanol was added to precipitate total RNA, which was then spun through a column. DNase was added to digest genomic DNA. The total RNA was washed for three times and then eluted in 30 μl of nuclease-free water. The RNA concentration was then measured, and the RNA was ready for reverse transcription (RT).

2.1.3 Reverse transcription (RT)

The total RNA prepared was converted into cDNA using the High-Capacity RNA-to-cDNA Kit (Applied Biosystems) according to the manufacturer's protocol. Briefly, 2 μg of total RNA,

10 µl of 2x RT buffer and 1 µl of 20x RT enzyme mix were mixed. Nuclease-free water was added to bring the mixture to 20 µl per reaction. The mixture was incubated at 37 ºC for 60 minutes, followed by 90 ºC for 5 minutes. The cDNA products were stored at 4 ºC until used.

2.1.4 Real time quantitative PCR (qPCR)

The cDNA was diluted to 10 ng/µl in nuclease-free water and subsequently used for qPCR. 10 µl 2x Fast SYBR® Green Master Mix (Applied Biosystems), 1 µl each of forward and reverse primer (10 µM), 10 ng/µl cDNA template and water was mixed to give a 20 µl reaction mix. The mixture was vortexed and then centrifuged (1000 x *g*) for 1 minute at 4 ºC. The qPCR machine (Applied Biosystems) was set to 95 ºC for 20 seconds, 40 cycles of denaturation (95ºC) for 3 seconds, annealing for 30 seconds and extension (72 ºC) for 30 seconds, followed by melt curve analysis (95 ºC for 15 seconds, 60 ºC for 1 minute), to show that only the desired products were amplified (single peak in melt curve). The relative quantities were determined according to the RT-qPCR step-one protocol using Ct values that was normalised to beta-actin to obtain the ΔΔCt with reference to positive controls. The positive controls were prepared from fibroblasts seven days after viral transduction when the virus was still present and at its maximum.

2.1.5 PCR

Regions of exon 1 and exon 4 of the *PRKCG* and exon 9 of the *TRPC3* genes were amplified using the Expand High Fidelity PCR System (Sigma) or Phusion Hot Start II DNA Polymerase (Thermo Fisher Scientific) and the primers listed in Table 2.1. The size of the products was then confirmed using 1-2.5% agarose (Sigma) electrophoresis depending on the size of PCR products amplified. The PCR products were subsequently purified using the QIAquick PCR Purification Kit (Qiagen), resuspended in nuclease-free water and stored at -20 ºC until used.

2.1.6 Culture of human iPSCs

Human iPSCs were reprogrammed from fibroblasts grown from skin biopsies collected in the John Radcliffe Hospital neurology clinic under ethical approval (REC Ref 12/WA/0186), and maintained in feeder-free conditions on hESC-qualified Matrigel (Corning), in supplemented mTeSR-1 medium (StemCell Technologies). Cells were passaged 1:3 every three to five days, using 0.5 mM ethylenediaminetetraacetic acid (EDTA) (Invitrogen) (Beers et al., 2012).

2.2 Materials

Table 2-1 A list of primers used in this study.

Gene	Forward Primer (5'-3')	Reverse Primer (5'-3')	Applications	Reference
ATOH1	TGTTATCCCGTCGTTCAACAAC	TGGGCGTTTGTAGCAGCTC	qPCR	(Muguruma et al., 2015)
c-Myc	TAACTGACTAGCAGGCTTGTCG	TCCACATACAGTCCTGGATGATGATG	qPCR	CytoTune®2.0 user manual
EN1	GCTTGTCCTCCTTCTCGTTC	TGGTCAAAACTGACTCGCAG	qPCR	(Watson et al., 2018)
EN2	CCGGCGTGGGTCTACTGTA	GGCCGCTTGTCCTCTTTGTT	qPCR	(Muguruma et al., 2015)
KIRREL2	GGGGCTAGTTCAGTGGACTAA	CACGGGCCTAATGTGGAGG	qPCR	(Muguruma et al., 2015)
Klf4	TTCCTGCATGCCAGAGGAGCCC	AATGTATCGAAGGTGCTCAA	qPCR	CytoTune®2.0 user manual
KOS	ATGCACCGCTACGACGTGAGCGC	ACCTTGACAATCCTGATGTGG	qPCR	CytoTune®2.0 user manual
LHX5	GTGCGCGAAGAAGTCGTAGT	CGAGTCTGAGATGTTGGGGT	qPCR	(Watson et al., 2018)
NANOG	CAGCCCCGATTCTTCCACCAG	CGGAAGATTCCCAGTCGGGTT	qPCR	(Watson et al., 2018)
OCT4	GACAGGGGGAGGGGAGGAGC	CTTCCCTCCAACCAGTTGCCC	qPCR	(Watson et al., 2018)
OLIG2	GATAGTCGTCGCAGCTTTCG	CCTGAGGCTTTTCGGAGC	qPCR	(Watson et al., 2018)
PRKCG	GCTATCGGCCTCTTCTTCCT	AGGACCACCAATCGACAGAC	qPCR	-
PRKCG exon 1	AGAAAGGCAGGATCCTGGTC	CGGCGTGATAGGAGTCTGCA	PCR	-
PRKCG exon 4	GCTGACCTAGAGAGCAAGGC	CTTTGGAAGGGCCCTGGCA	PCR	-
PTF1A	TGAGTTGTTTTTCATCAGTCCA	CAGGCCCAGAAGGTCATC	qPCR	-
SeV-1	GGATCACTAGGTGATATCGAGC	ACCAGACAAGAGTTTAAGAGATATGTATC	qPCR	CytoTune®2.0 user manual
SeV-2	AGACCCTAAGAGGACGAAGACAGA	ACTCCCATGGCGTAACTCCATAG	qPCR	(Nishimura et al., 2011; Nishimura et al., 2013)

SKOR2	AGCCCAGTTCACCATCCAT	GCTGTTGTCATCCTTTGTAGATAC	qPCR	(Watson et al., 2018)
WNT1	CAACCGAGGCTGTCGAGAAA	GTGCAGGATTCGATGGAACCT	qPCR	(Muguruma et al., 2015)
β-actin	GCCGCCAGCTCACCATGGATG	CCATCACGCCCTGGTGCCTGG	qPCR	(Watson et al., 2018)

Table 2-2 A list of antibodies used in this study.

Antibody/ isotype	Company	Catalogue number	Host species	Dilution	Applications
Primary Antibodies					
Atoh1	EMD Millipore	AB5692	Rabbit	1:200	IF
Calbindin	Swant	CB38	Rabbit	Both 1:5000	IF/ WB
Calbindin	Swant	300	Mouse	1:400	IF
En1	Abcam	ab70993	Rabbit	1:50	IF
En2	Santa Cruz	sc-8111	Goat	1:50	IF
Foxp2	Abcam	ab1307	Goat	1:5000	IF
Gbx2	Santa Cruz	H00002637-M01	Goat	1:50	IF
Human Nuclear Antigen	Abcam	ab191181	Mouse	1:200	IF
IgG647	Cell Signalling	2985S	Rabbit	1:300	FC
IgM488	Biolegend	401617	Mouse	1:250	FC
Kirrel2	R&D Systems	MAB2564	Mouse	1:50	IF
Lamp2[H4B4]	Abcam	ab25631	Mouse	1:100/ 1:500	IF/ WB
LC3	Nanotool	0231-100/LC3-5F10	Mouse	1:200	IF
LC3B	Novus biologicals	NB100-2220	Rabbit	1:5000	WB
Lhx5	EMD Millipore	AB5762	Rabbit	1:100	IF
NANOG^{647}	Cell Signalling	5448S	Rabbit	1:150	FC
Olig2	R&D Systems	AF2418	Goat	1:40	IF
PKCγ (C19)	Santa Cruz	sc-211	Rabbit	1:100/ 1:500	IF/ WB
PKCγ (C4)	Santa Cruz	sc-166385	Mouse	1:50	IF
pT514-PKCγ	Abcam	ab109539	Rabbit	1:1000	WB
pT674-PKCγ	Abcam	ab5797	Rabbit	1:500	WB
Sodium potassium ATPase	Abcam	ab76020	Rabbit	1:100	IF
Tra-1-60^{488}	Biolegend	B119983	Mouse	1:100	FC
Tuj1	Covance	MMS-435P	Mouse	1:1000	IF
Ubiquitin	Abcam	ab7780	Rabbit	1:500	IF/ WB
β-actin	Abcam	ab3280	Mouse	1:1000	WB

Antibody/ isotype	Company	Catalogue number	Host species	Dilution	Applications
Secondary Antibodies					
anti-Goat Alexa 594	Invitrogen	A-11058	Donkey	1:1000	IF
anti-Mouse Alexa 488	Invitrogen	A-11001	Goat	1:1000	IF
anti-Mouse Alexa 594	Invitrogen	R37121	Goat	1:1000	IF
anti-Rabbit Alexa 488	Invitrogen	R37116	Goat	1:1000	IF
anti-Rabbit Alexa 594	Invitrogen	A-11012	Goat	1:1000	IF
anti-Mouse HRP	GE Healthcare	NA931-1ML	Sheep	1:10000	WB
anti-Rabbit HRP	GE Healthcare	NA934-1ML	Donkey	1:10000	WB

FC: flow cytometry, IF: immunofluorescence, IHC: immunohistochemistry, WB: Western blotting

Chapter 3 Generation of human induced pluripotent stem cells (iPSCs) from SCA14 patients

3.1 Introduction

A comprehensive understanding of the disease aetiology and pathophysiology is essential for developing a cure or effective treatment, both of which require tractable and faithful disease models. To understand the disease mechanisms that cause the patient-specific disease phenotypes, the ideal tools are primary patient cells. However, primary patient cells, particularly human brain cells, and post-mortem tissues are difficult to obtain, particularly in rare hereditary neurological disorders such as cerebellar ataxias (Avior et al., 2016). In addition, human post-mortem tissues capture the end point of the disease but cannot provide information of disease progression and pathogenic mechanisms that affect early stages of the disorders (Siller et al., 2013). In order to study the pathogenic mechanisms underlying genetic neurological disorders, various disease models have been produced using human immortal cell lines and animals (Avior et al., 2016; Sterneckert et al., 2014). Human transformed cell lines of irrelevant cell types expressing a disease-causing gene of interest have been used as *in vitro* cell models of human diseases. However, many of the disease mechanisms and phenotypes of neurological disorders are cell type-specific. *In vitro* cell models of irrelevant cell types might therefore not be the ideal system for studying brain disorders (Sterneckert et al., 2014; Watson et al., 2015b; Wong et al., 2017). Mammalian genomes are highly conserved across species. Therefore, animal models such as mice, rats and non-human primates, which can be used for the examination of disease mechanisms at different developmental stages *in vivo* and behaviour analyses, have been valuable tools for modelling human diseases (Avior et al., 2016; Sterneckert et al., 2014). Nonetheless, despite the genomic similarity, the physiology of animals differs from that of human in many organ functions, many of which are phenotypically observable and could preclude the recapitulation of human disease phenotypes in animal

models (Avior et al., 2016; Wong et al., 2017). In addition, many drugs effective in cell and animal models do not work in human patients in clinical trials (Sterneckert et al., 2014; Wong et al., 2017). Thus, there is an urgent need to develop reliable disease models, ideally using human cells.

Human pluripotent stem cells can be differentiated into any human disease-relevant cell types in large quantity and are therefore ideal tools for disease modelling and developing therapies (Sterneckert et al., 2014). In particular, monogenic diseases with high penetrance and clear disease phenotypes such as SCA14 are especially suitable to use stem cell-based models for the assessment of *in vitro* observable phenotypes (Avior et al., 2016). Human pluripotent stem cells include embryonic stem cells (ESCs) and induced pluripotent stem cells (iPSCs). ESCs are derived from the inner cell mass of a blastocyst pre-implantation. The derivation of human ESCs was first described by Thomson and colleagues (Thomson et al., 1998). Isolated ESCs from healthy individuals can be genetically edited at a specific locus, generating *de novo* mutations. Alternatively, disease-specific ESCs can be identified during the *in vitro* fertilization process by pre-implantation genetic diagnosis or pre-implantation genetic screening. However, their wider application in cell therapy and regenerative medicine has been restricted by the limited availability, ethical concerns and immunological incompatibility of ESCs (Avior et al., 2016; Siller et al., 2013).

Somatic cells can acquire ESC-like properties through nuclear reprogramming by three major approaches: somatic cell nuclear transfer (SCNT), cell fusion and introduction of defined transcription factors (Fig. 3.1) (Avior et al., 2016; Krishnakumar and Blelloch, 2013; Siller et al., 2013; Smith et al., 2016). In SCNT, nuclei of somatic cells are inserted into the cytoplasm of enucleated oocytes and directed to totipotency rapidly (Narbonne et al., 2012). Successfully reprogrammed SCNT zygotes can develop into blastocysts (pluripotent), where ESCs can be derived from the inner cell mass. The blastocyst can then develop into a cloned animal. However, SCNT is technically challenging and utilizes a limited gametic resource, and is

therefore not ideal for the generation of stem cells in large quantity (Krishnakumar and Blelloch, 2013; Smith et al., 2016). The second approach is through the fusion of ESCs with a somatic cell. Reprogramming is initiated when the two nuclei are still physically separated (heterokaryon phase). Global epigenetic remodelling then occurs and is followed by the activation of pluripotency genes, which requires DNA synthesis (Tada et al., 1997). The somatic and pluripotent nuclei fuse after cell division, and the pluripotent network is then consolidated within the somatic genome (Krishnakumar and Blelloch, 2013; Smith et al., 2016). This method still requires the use of ESCs so the ethical concerns and limited availability remain. Yet, cell fusion experiments highlighted the importance of ESC trans-factors for reprogramming the somatic genome (Krishnakumar and Blelloch, 2013) that later led to the identification of master transcription factors that drive pluripotency (Takahashi and Yamanaka, 2006). Yamanaka and colleagues first demonstrated the reprogramming of adult human dermal fibroblasts into iPSCs by transfection of four transcription factors, namely *OCT3/4*, *SOX2*, *KLF4*, and *c-MYC* (Takahashi et al., 2007; Takahashi and Yamanaka, 2006). These four genes have been shown to contribute to the long-term maintenance of ESC phenotypes and the rapid proliferation of ESCs in culture. Human iPSCs produced using this method are indistinguishable from human ESCs in morphology, proliferation, gene expression, chromatic modification profiles and global chromatin configuration (Liang and Zhang, 2013). Importantly, somatic cells obtained from human patients can be reprogrammed into iPSCs and subsequently differentiated into any cell types desired. This approach therefore allows for the investigation of pathogenic mechanisms even for diseases involving cell types that are difficult to access and potentially personalised-therapies, and thus has revolutionised the field of modern biology. The derivation of iPSCs can be done using various methods from different parental cell types, most commonly fibroblasts or blood cells (Avior et al., 2016; Brix et al., 2015; Nakagawa et al., 2008; Stadtfeld et al., 2008; Yu et al., 2007). Efficient cell reprogramming requires the sustained and simultaneous expression of exogenous factors for 10-20 days. Retrovirus and lentivirus were used originally (Takahashi et al., 2007; Takahashi and Yamanaka, 2006). However, these vectors can be integrated into the host genome and the

integrated reprogramming genes might affect the differentiation potential of iPSCs. Non-integrative reprogramming methods such as the use of Sendai viruses, episomal vectors and direct delivery of transcription factor mRNA or protein have therefore been developed (Brix et al., 2015; Nakagawa et al., 2008; Stadtfeld et al., 2008; Yu et al., 2007). Another reprogramming approach using small molecular cocktails rather than ectopic transcription factors has also been developed (Hou et al., 2013a).

For this work, Sendai virus was used. Sendai virus is a non-segmented negative-strand RNA virus that can infect a wide range of animal cells but is not pathogenic to humans. Of note, Sendai virus allows for transient but strong gene expression without integrating into the host genome and is therefore an ideal tool for somatic cell reprogramming (Nishimura et al., 2011; Nishimura et al., 2013). The viral backbone is cleared from host cells after several passages.

The goal of this chapter was to generate iPSCs from human dermal fibroblasts obtained from SCA14 patients. Four patients with two distinct missense mutations (H36R and H101Q) were included in this work. The two patients carrying the H36R mutations were mother and son. The two male patients harbouring the H101Q mutation came from the same family as explained in section 1.8 of Chapter 1 (Fig. 1.8). Patient information can be found in Fig. 3.2H. Following reprogramming, isolated iPSC clones were characterized following a standardised pipeline. Parts of the results presented in this chapter were included in a manuscript submitted to a peer-reviewed journal.

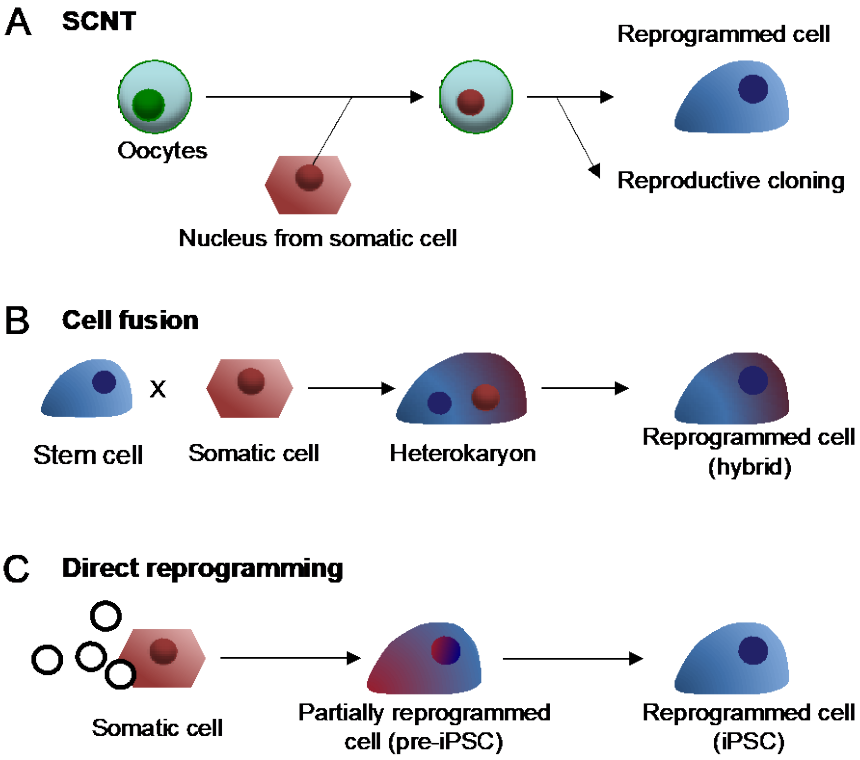


Figure 3.1 Methods of *in vitro* reprogramming.

A somatic nucleus can be reverted to an early embryonic state via three approaches: somatic cell nuclear transfer (SCNT), cell fusion and ectopic expression of transcription factors (direct reprogramming). (A) In SCNT, somatic nuclei are transferred into enucleated oocytes. Upon oocyte activation, maternal factors globally remodel the somatic genome. Successfully reprogrammed SCNT zygotes have restored totipotency and express select pluripotency factors, such as *Oct4*. After three to four days, the inner cell mass is formed in the blastocyst and developmental potency is restricted, producing pluripotent cells from which ESCs can be derived. (B) Fusion of somatic cells with stem cells of different origin produces heterokaryon, of which nuclei of the fused cells are still separated and the expression of pluripotency genes are reactivated. The somatic and pluripotent nuclei fuse after cell division, and additional genes are then reprogrammed to consolidate the pluripotent network within the somatic genome forming a hybrid-reprogrammed cell. (C) A more recent technique is the induction of iPSCs by the overexpression of a defined set of transgenes including *OCT4*, *SOX2*, *KLF4* and *MYC*. The transition from a factor-dependent, non-pluripotent state to iPSCs requires multiple divisions and an extended latency period under persistent ectopic expression of all four transgenes. Complete reprogramming of the somatic nucleus only occurs in a small percentage of cells that acquire stabilised global epigenetic features. Modified from (Cantone and Fisher, 2013).

3.2 Specific Materials and Methods

3.2.1 Reprogramming of skin fibroblasts from SCA14 patients into iPSCs

Experiments described in this chapter were performed by myself and Stephanie Hoekstra, a former MSc student in the group, following the guidance of Jane Vowles, Cathy Browne and Dr. Sally Cowley at the James Martin Stem Cell Facility. I performed the reprogramming and characterisation of iPSCs derived from patients PRKCG01 and PRKCG02. The reprogramming of skin fibroblasts into iPSCs from patients SCA14-1 and SCA14-2 was carried out by Stephanie Hoekstra. I then finished the characterisation and expansion of all iPSC lines produced.

Reagents were purchased from Thermo Fisher Scientific, unless stated otherwise. Reprogramming of skin fibroblasts from patients PRKCG01 and PRKCG02 was performed using the CytoTune®-iPS 2.0 Sendai Reprogramming Kit according to manufacturer's protocols. Briefly, patients' skin fibroblasts were thawed and expanded. Two days prior to viral transduction, the fibroblasts were detached and seeded at a range of densities on 12-well plates ($0.75x10^5$, $1.0x10^5$, $1.25x10^5$, $1.5x10^5$, $2.0x10^5$) and grown for two days to 90% confluency. Sendai virus was added to fibroblasts on day 0 at a multiplicity of infection (MOI) of 3 per $1.0x10^5$ cells and incubated overnight. Virus was removed the next day. A well of untransfected fibroblasts was kept for each density for monitoring cell division. Skin fibroblasts from patients SCA14-1 and SCA14-2 were reprogrammed using the SeVdp(KOSM)302L Sendai virus system (Dafinca et al., 2016; Nishimura et al., 2011; Nishimura et al., 2013). This system contains the genes for all four reprogramming transcription factors (*Klf4, Oct4, Sox2, c-Myc*), expressed from a single transcript and packaged into a single Sendai virus, thereby ensuring gene dosage ratio consistency. The system also possesses a target for mir302, ensuring viral RNA is efficiently degraded once cells are reprogrammed to pluripotency (when mir302 is

expressed). This ensures complete removal of exogenous genetic material within a few passages. Transduced fibroblasts were cultured in fibroblast medium [ADMEM, 10% foetal calf serum, 1% Glutamax, 1% penicillin/streptomycin (P/S)]. 8000 reprogrammed cells per ml were transferred to a layer of mouse embryonic feeder cells (CF1 MEF) (Merck) on 0.1% gelatin coated 6-well plates and cultured in KOSR medium [KnockOut Dulbecco's modified Eagle's medium (DMEM), 10% KnockOut Serum Replacement; 0.1% Non-Essential Amino Acids, 2 mM GlutaMax-I, 0.5 mM beta-mercaptoethanol, 10 ng/ml Basic Fibroblast Growth Factor (bFGF) (R&D), 1% P/S] on day 7. The remaining cells were pelleted for positive control for Sendai virus clearance assay. Half of the media were changed every two days until day 13. MEF cells were set up in T75 flasks on day 7 and cultured in KOSR medium. The medium was collected every day for seven days as conditioned medium to feed iPSCs on feeder cells after sterilization. Reprogrammed cells were fed with conditioned medium supplemented with 10 ng/ml bFGF for around two weeks. Colonies emerged at around day 26 were ready for manual passaging onto Matrigel (Corning)-coated 12-well plates (feeder-free conditions). For passage number five to eight, two vials of iPSCs (2.0-3.0x10^6 cells each) were frozen and the remaining well were expanded. Three clones of iPSCs were expanded in mTeSR-1 medium (StemCell Technologies) supplemented with 1% P/S for three to four weeks until reaching six 10-cm dishes. Cells were detached using 0.5 mM EDTA or pre-warmed TrypLE Express. iPSCs were then frozen in freezing medium containing 20% DMSO and 60% foetal bovine serum (2.0-3.0x10^6 cells per vial), and then stored in liquid nitrogen for long term. Three cell pellets per clone were prepared and stored at -80^{o}C at the time of freezing for genomic DNA and total RNA preparation. iPSC expansion and cell pelleting was repeated if clones showed abnormal karyotypes (see Figure 3.2A for the timeline of reprogramming).

3.2.2 Quality control tests

One vial of each iPSC clone was thawed. iPSCs were seeded in a 1:4 ratio in a Matrigel-coated 6-well plate and cultured in mTeSR-1 medium to monitor cell viability. 10μM ROCK inhibitor

(Sigma) was added to reduce cell death on the day of thawing. Subsequently, the cell medium was used for mycoplasma testing. DNA and RNA of iPSCs were used for karyotyping and determination of Sendai viral clearance, respectively. Fixed iPSCs were used for flow cytometry experiments to determine cell pluripotency. All quality control tests were done on the passage numbers shown in Table 3.3.

3.2.2.1 Karyotyping

Genomic DNA was prepared as described in section 2.1.1 in Chapter 2. The DNA prepared was sent to Illumina for karyotyping. Human OmniExpress-24.v1.1 DNA Analysis Kit (WG-315-1101) was used. The results were analysed using KaryoStudio 1.3 and GenomeStudio software (Illumina). iPSC line SNP profiles were compared to the original pool of fibroblasts, which confirmed the identity of the iPSC to the original fibroblasts. Amplification, deletion and heterozygosity were shown as green, orange and grey bands, respectively, in the karyograms. Only iPSC lines containing SNPs fewer than 1,000,000 nucleotides were considered normal and qualified for subsequent quality control tests.

3.2.2.2 Mycoplasma testing

The MycoAlert™ assay (Lonza) was used to detect mycoplasma in used culture media according to the manufacturer's protocol. Briefly, 1 ml of the culture media collected from the cell culture of $2.0x10^6$ iPSCs was centrifuged (400 x *g*, 5 minutes). MycoAlert reagent (100 µl) was added to 1 ml of the collected supernatant. Five minutes later, the luminescence was measured before (reading 1) and after (reading 2) adding the substrate (100 µl). The ratios of the readings were calculated using the following equation: Ratio = reading 2/ reading 1. If the ratio was smaller than 1, the sample was considered negative for mycoplasma.

3.2.2.3 Sendai virus clearance

Total RNA was extracted and reverse-transcribed into cDNA as described in sections 2.1.2 and 2.1.3. qPCR were performed as described in section 2.1.5 in Chapter 2 to amplify virus backbones and transgenes *c-Myc*, *Klf4*, *KOS* and *SeV-1* (for those reprogrammed with CytoTune®-iPS 2.0) and *SeV-2* (for those reprogrammed with SeVdp(KOSM)302L Sendai virus system) using primers listed in Table 2.1 (Dafinca et al., 2016; Nishimura et al., 2011; Nishimura et al., 2013)

3.2.2.4 FACS flow cytometry

$2.0x10^6$ iPSCs were harvested using 1 ml TrypLE. The cell pellet was fixed in 2% PFA (Sigma) and then permeabilized in ice-cold absolute methanol (Sigma). $0.5x10^6$ fixed cells were washed in FACS buffer [1% foetal calf serum (FCS) (Hyclone), 10 µg/ml IgG from human serum (Sigma) and 0.01% sodium azide in PBS] three times to remove methanol and then resuspended in 100 µl FACS buffer. Antibody- and isotype (control)-mixes were prepared separately in the required dilutions (see Table 2.1). 5 µl of the antibody mix and isotype mix were added to into different rows of a 96-deep-well plate. 45µl cell suspension were added to each well and mixed properly. The plate was incubated in dark at room temperature for an hour with shaking. The stained cells were then washed with FACS buffer twice with centrifugation (400 x *g*) and analysed using FACSCalibur (BD Biosciences). The data were analysed using FlowJo software (FlowJo Enterprise) to obtain the scatter plots, histograms, cell counts and viability. Gating was done manually to include the majority of the cells and exclude the outliners.

3.3 Results

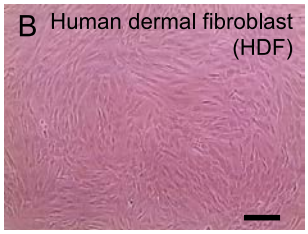
3.3.1 Reprogramming of SCA14 patients' skin fibroblasts into iPSCs

This work included four patients harbouring two distinct SCA14 mutations: H36R and H101Q. The skin fibroblasts of patients harbouring the H36R mutation (PRKCG01 and PRKCG02)

were reprogrammed with Sendai virus using CytoTune®-iPS 2.0 (Invitrogen) (Fig. 3.2B). 13 days after viral transduction, small colonies of reprogrammed cells (black arrow) merged on MEFs (Fig. 3.2C). 18 days after transduction, colonies were ready for manually picking and passaging onto Matrigel-coated culture plates (Fig. 3.2D). iPSCs showed well-defined and relatively large nuclei. The edge of each iPSC colony was clear and irregular in shape. Each colony contained closely packed iPSCs (Fig. 3.2E). The iPSCs were expended in the following weeks until the cells were confluent in six 10-cm culture dishes (Fig. 3.2F). The cells were then frozen into 2.0-3.0x10^6 cells per cryovial (more than thirty vials per clone) and stored in liquid nitrogen for future use. Four iPSC clones for patient PRKCG01 and three clones for patient PRKCG02 were generated.

The skin fibroblasts of patients SCA14-1 and SCA14-2 harbouring the H101Q mutation were reprogrammed using the SeVdp(KOSM)302L Sendai virus system (Nishimura et al., 2011; Nishimura et al., 2013). These iPSCs were expanded and frozen in the same conditions as mentioned (experimental details see Specific Methods and Materials in this chapter). Cell pellets were also prepared for subsequent characterisation. Two iPSC clones each for patients SCA14-1 and SCA14-2 were generated.

The table in Figure 3.2H summarises the details of the patients, mutations and reprogramming methods. Information of control iPSCs derived from age- and sex-matched healthy donors that were provided by the James Martin Stem Cell Facility, University of Oxford is also included.

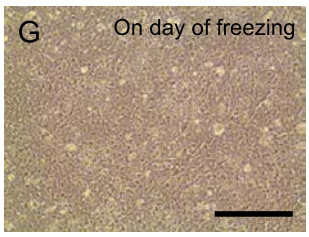


C

D

E

F



H

Mutation	Donors	Age	Sex	Reprogramming method
H36R (exon 1)	PRKCG01	71	F	Cytotune 2.0
	PRKCG02	44	M	Cytotune 2.0
H101Q (exon 4)	SCA14-1	47	M	SeVdpmir302L virus
	SCA14-2	71	M	SeVdpmir302L virus
Control	AH017	67	F	SeVdpmir302L virus
Control	OX3	49	M	SeVdpmir302L virus
Control	SFC841	36	M	Cytotune 1.0

Figure 3.2: Reprogramming of SCA14 patients' skin fibroblasts into iPSCs using Sendai virus.

(A) Timeline of reprogramming showing the major procedures and media used. (B) Human dermal fibroblasts (HDF) two days before viral transduction. Reprogrammed cells emerged at day 13 (black arrow) (C) and grew into a large colony of iPSCs (day 18) on MEF monolayer (D). Colonies of iPSCs were picked and manually passaged onto Matrigel-coated surface in feeder-free conditions and grew into a single colony (E). (F and G) showed iPSCs one day after passaging and on the day of freezing. (H) Details of patients and healthy donors, as well as reprogramming methods included in this study. MEF: mouse feeder cells.

3.3.2 Characterisation of reprogrammed SCA14-iPSCs (quality control tests)

3.3.2.1 Karyotyping

Karyotyping was performed to assess the chromosomal stability of the reprogrammed iPSC lines. The extracted DNA was sent to Illumina for karyotyping. The results were then analysed using KaryoStudio. 11 out of 19 patient iPSC lines sent for SNP array showed normal karyotypes. The abnormal karyotypes in the iPSC lines that showed abnormal karyotypes were mainly due to duplication of a small fragment on chromosome 20, which is vulnerable in iPSCs during mitosis (data not shown). The karyograms of the parental fibroblasts and the reprogrammed patient iPSC lines from four patients: PRKCG01 and PRKCG02 (H36R) (Fig. 3.3A) as well as SCA14-1 and SCA14-2 (H101Q) (Fig. 3.3B) displayed normal karyotypes. Karyotyping of control iPSC lines AH017-3 and OX3-7 was also conducted after iPSC expansion and showed normal karyotypes (Fig. 3.3C).

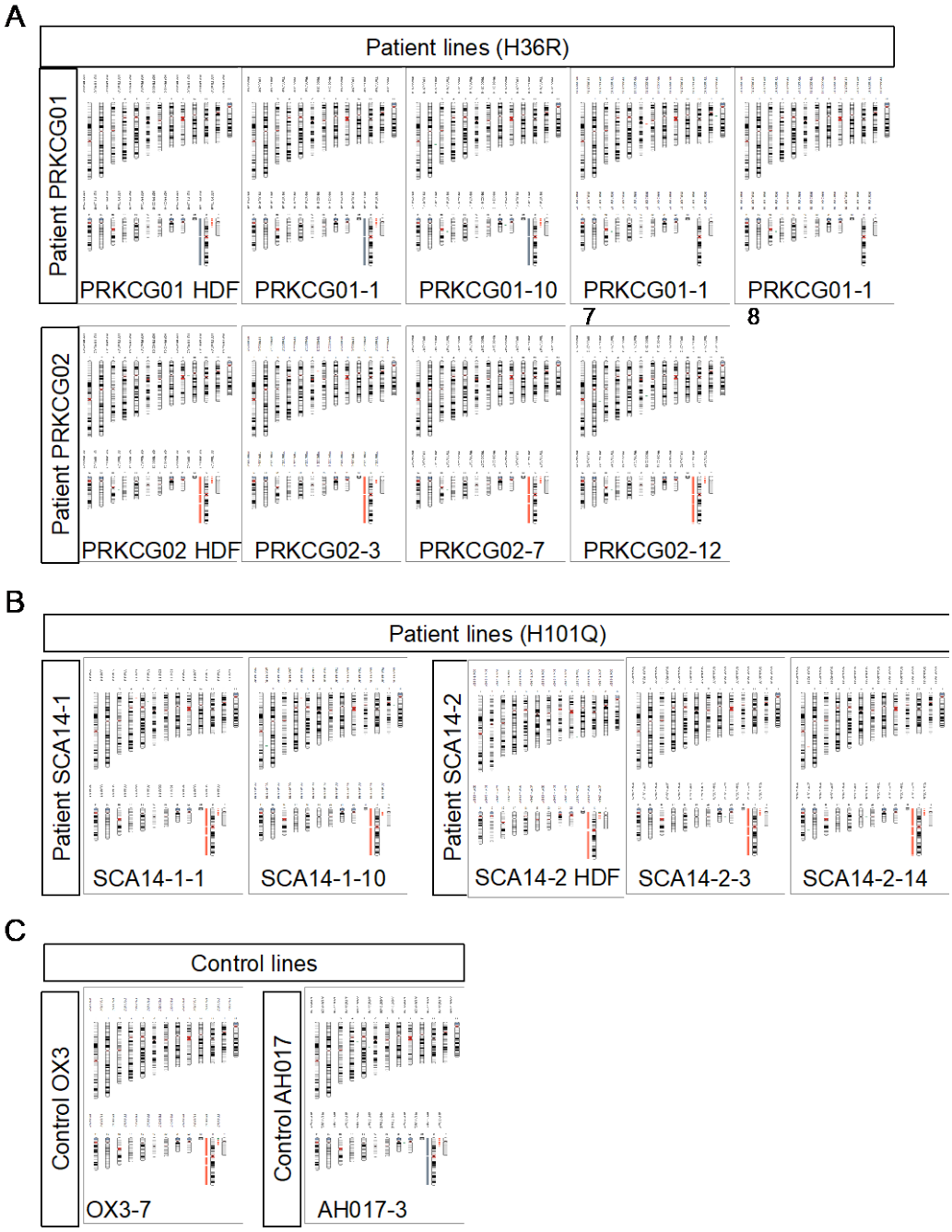


Figure 3.3: Karyotype analysis of iPSC lines used in the study.

The karyograms of parental fibroblasts and 11 patient iPSC clones are shown: (A) patients harbouring the H36R mutation; (B) patients harbouring the H101Q mutation. (C) Karyograms of two control iPSC lines: AH017-3 and OX3-7. All showed normal karyotypes. Amplifications (green), deletions (orange) and loss of heterozygosity regions (grey) are shown alongside the relevant chromosome (except that in females the X chromosomes are annotated in grey, and single-copy sex chromosomes are shown in orange). Any changes larger than 1,000,000 nucleotides were considered abnormal. HDF: human dermal fibroblasts.

3.3.2.2 Mycoplasma test

Mycoplasma are the smallest and simplest prokaryotes that are the most commonly found contamination in cell culture. Mycoplasma cause changes in chromosomes, growth rate, morphology and cell metabolism of iPSCs. Mycoplasma are not visible by microscopy. Indications of contamination include decrease in cell proliferation, morphological changes, cell aggregation or poor cell transfection efficiencies. Contaminating mycoplasma can be indirectly detected by measuring the activity of mycoplasmal enzymes, i.e. the rate of the conversion of ADP to ATP. The media of iPSCs was collected and subsequently tested using the luminometric Mycoalert kit (Lonza). All iPSC lines tested were free of mycoplasma (Table 3.1).

Table 3-1 Results of mycoplasma test

Sample	Passage number	Reading 1	Reading 2	Ratio	Result
Positive control	-	10.59	240.9	22.75	Negative
Negative control	-	5.738	6.48	1.13	Negative
PRKCG01-1	P13	1.639	0.91	0.56	Negative
PRKCG01-10	P13	3.984	1.883	0.47	Negative
PRKCG01-17	P12	3.283	1.395	0.42	Negative
PRKCG01-18	P12	1.578	0.953	0.6	Negative
PRKCG02-3	P12	1.215	0.689	0.57	Negative
PRKCG02-7	P14	4.133	2.272	0.55	Negative
PRKCG02-12	P12	3.497	1.723	0.49	Negative
SCA14-1-1	P20+13	1.07	0.316	0.3	Negative
SCA14-2-3	P19+9	2.629	1.06	0.4	Negative
SCA14-2-13	P25	10.28	1.68	0.16	Negative
SCA14-2-14	P19+9	1.052	0.366	0.35	Negative

No mycoplasma was detected in patient iPSC lines. Reading 1 and reading 2 show luminescence before and after adding the substrate. Ratio=Reading 1/Reading 2. If the ratio is smaller than 1, the sample is considered negative for mycoplasma.

3.3.2.3 Sendai virus clearance

Sendai virus is a RNA virus, which does not integrate into the genome of its hosts, producing "footprint-free" iPSCs. The Sendai viral backbone is lost naturally (Nishimura et al., 2011; Nishimura et al., 2013) after around twelve passages if using the CytoTune®-iPS 2.0 system. iPSCs that were reprogrammed using the SeVdp(KOSM)302L Sendai virus system appeared to clear the Sendai viral backbone after at least 20 passages. To show that the iPSCs were virus-and-transgene-free, any potential exogenous residues were amplified by means of qPCR. RNA was extracted from cell pellets of patient iPSC lines and RT-qPCR was performed using the primers for Sendai viral backbone (SeV) and transcription factors (KOS: Klf4, Oct3/4, Sox2, c-Myc). As the iPSCs were reprogrammed using two different methods, two different sets of primers were used. An extra copy of transcription factors Klf4, Oct3/4 and Sox2 is included in the CytoTune®-iPS 2.0 reprogramming method to increase the reprogramming efficiency. Therefore, separate primers for those three transcription factors were included in the detection of exogenous transgenes using RT-qPCR for iPSC clones generated with this method. As all four transcription factors were packaged in a single vector in the SeVdp(KOSM)302L Sendai virus system (Nishimura et al., 2011; Nishimura et al., 2013), only primers detecting the part of viral backbone (SeV) were included for analysing the iPSC clones generated using this method. SeV, Klf4, Oct3/4, Sox2 or c-Myc were not detected in any of the iPSC lines (Fig. 3.4). β-actin was used as an endogenous control for each iPSC line to show successful cDNA synthesis and as an internal reference for normalisation. Fibroblasts at one-day post transduction were used as the positive controls.

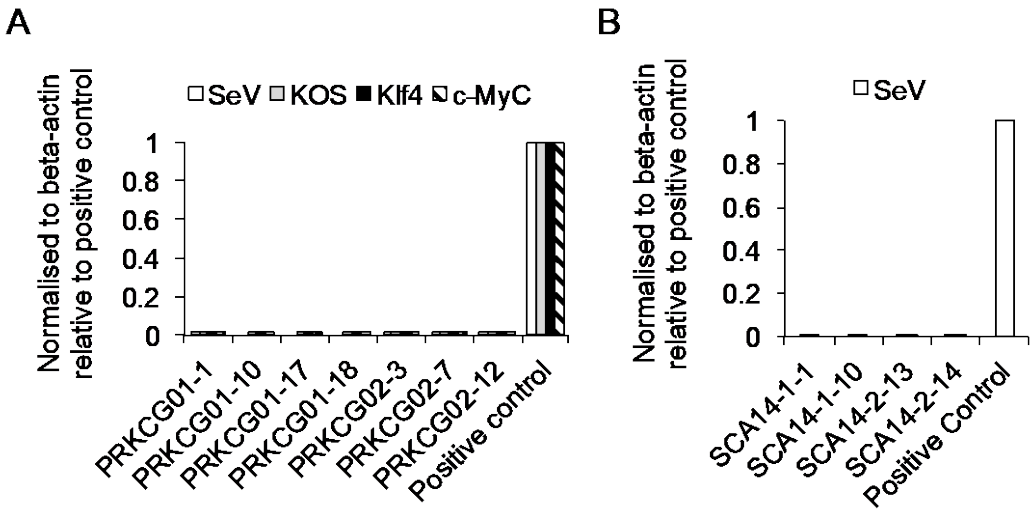


Figure 3.4: Sendai virus and transcription factors were cleared from iPSC lines.

The expression levels of Sendai virus backbone (SeV) as well as four transcription factors: KOS (Klf4, Oct3/4, Sox2), Klf4 and cMyc were checked using qPCR. (A) The patient clones reprogrammed using Cytotune 2.0 were free of both viral backbone and transgenes after at least twelve passages. (B) Patient clones reprogrammed using the SeVdp(KOSM)302L Sendai virus system were cleared of viral backbone after at least 20 passages. The C_T values were normalised to β-actin and relative to the positive controls (fibroblasts one day after viral transduction).

3.3.2.4 Expression of pluripotency markers (Tra-1-60 and Nanog)

The expression of transcription factors Tra-1-60 and Nanog indicates stem cell pluripotency (Dafinca et al., 2016; Nishimura et al., 2011; Nishimura et al., 2013). To assess the viability and the proportion of reprogrammed cells that express both pluripotency markers, fluorescence-activated cell sorting (FACS) was employed. The iPSCs were fixed and then immunolabelled with antibodies against Tra-1-60 and Nanog before FACS analysis. The results were analysed using the FlowJo software (FlowJo Enterprise). More than 95% of the cells of each iPSC line were positive for both pluripotency markers Tra-1-60 and Nanog (Fig. 3.5).

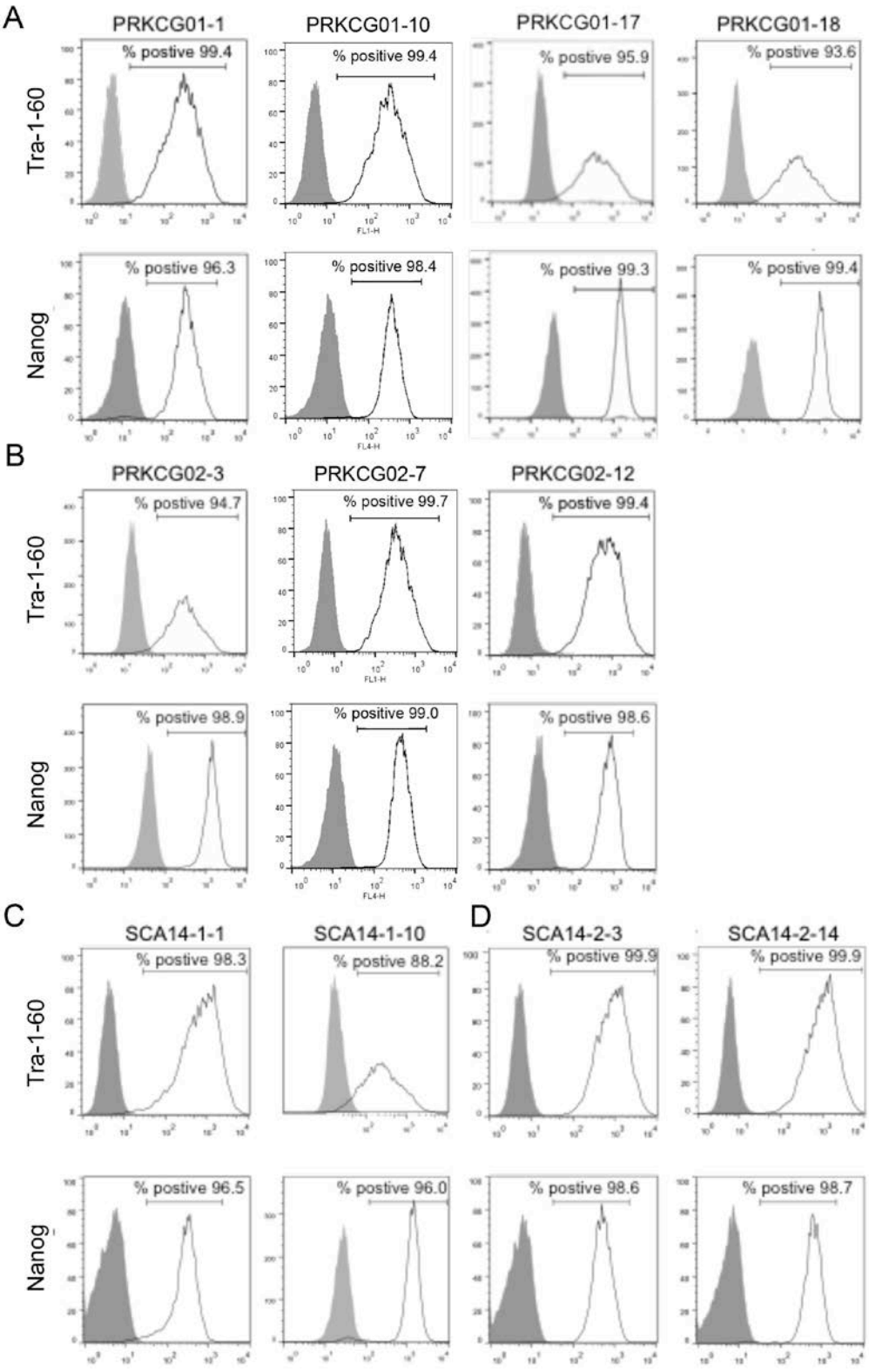


Figure 3.5: Histograms of FACS results.

The smoothed histograms of the FACS results of each clone displayed the frequency of the events in each fluorescence channel (y-axis) versus fluorescence intensity (x-axis). More than 85% of the cells of each patient iPSC clone were positive for both pluripotency markers Tra-1-60 and Nanog. The grey peaks show the data of isotypes (controls) while the white peak show the counts of either Tra-1-60 (FLH-1) or Nanog (FLH-4). (A) Patient PRKCG01 (H36R); (B) patient PRKCG02 (H36R); (C) patient SCA14-1 (H101Q); (D) patient SCA14-2 (H101Q).

3.3.2.5 Determination of genotypes using Sanger sequencing

Sanger sequencing confirmed the genotype of each iPSC line. The exons containing the corresponding mutation, exon 1 for H36R and exon 4 for H101Q, were amplified by PCR and then subjected to sequencing. All PRKCG01 and PRKCG02 clones showed A/G double peaks (heterozygous mutation) at nucleotide position 107 in exon 1 (red arrows, B-F) while all SCA14-1 and SCA14-2 clones showed C/G double peaks at position 303 in exon 4 (blue arrows, L-O) in the *PRKCG* PCR products (Fig.3.6). In addition to the SCA14 mutations, a C-to-T silent SNP (rs2547362) was found at nucleotide position 72 in exon 1 in both PRKCG01 (Fig. 3.6P) and PRKCG02 (black arrows) (Fig. 3.6Q) iPSC lines. No additional mutations were found in exon 4 of both SCA14-1 and SCA14-2 iPSCs.

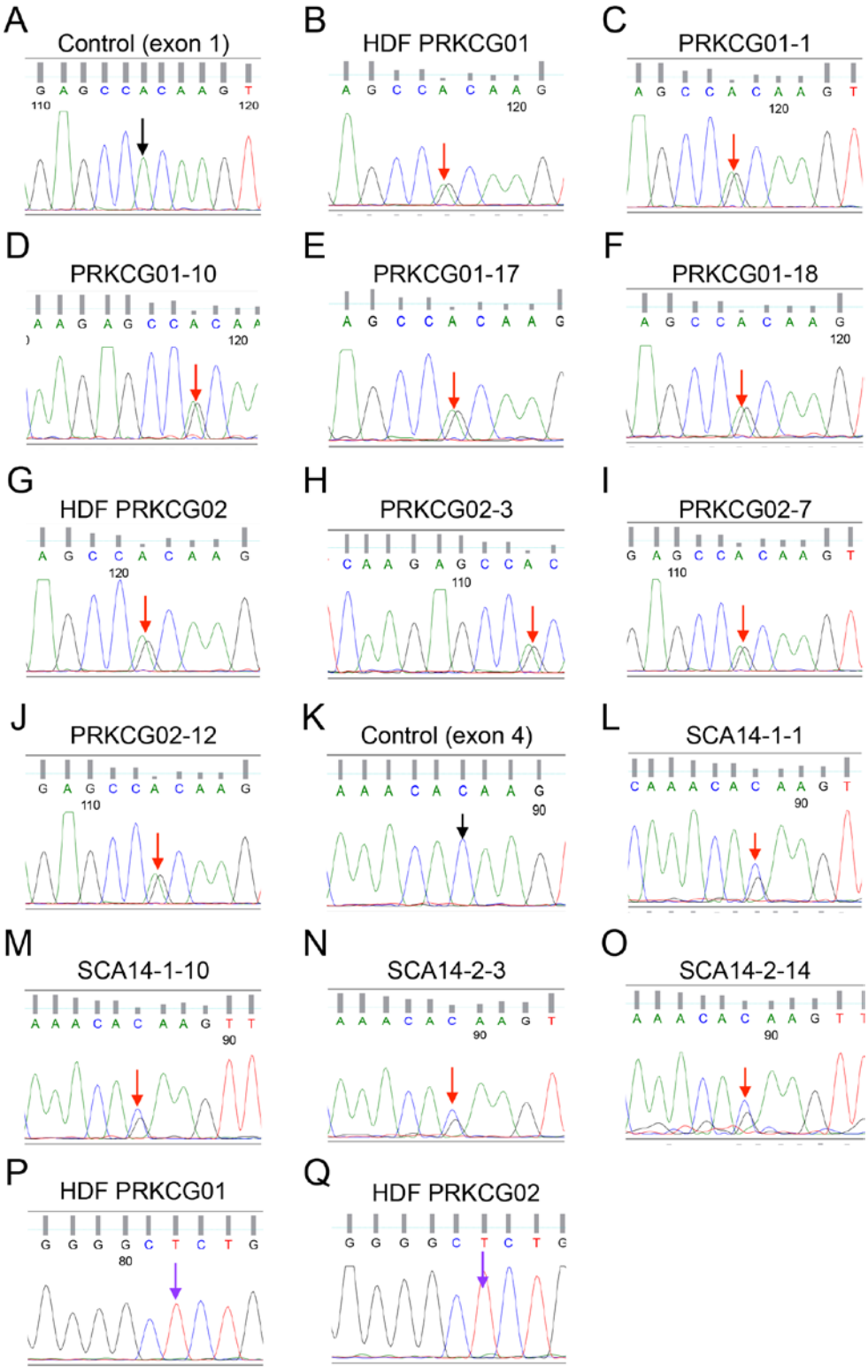


Figure 3.6: Sequencing results for genotyping.

The genotypes of the patient iPSC lines were confirmed by Sanger sequencing. (A) Positive control showing the wildtype nucleotide at nucleotide 107 in exon 1 (black arrow). (B-F) Patients' fibroblasts and iPSC lines of PRKCG01 and PRKCG02 contain the heterozygous H36R mutation (A/G) in exon 1 (red arrows). (K) Positive control showing the wildtype nucleotide at position 303 in exon 4 (black arrow). (L-O) SCA14-1 and SCA14-2 patient iPSC lines contain the H101Q mutation (C/G) at position 303 in exon 4 (red arrows). (K and J) A silent C/T variation at nucleotide 72 in exon 1 was identified in both patients carrying the H36R mutation (purple arrows). HDF: human dermal fibroblasts.

3.4 Chapter Discussion

In this chapter, eleven iPSC lines in total were generated from four SCA14 patients carrying two distinct mutations in the regulatory domain of PKCγ. At least two clones were produced for each patient. All patient iPSC lines passed a standard pipeline of quality control tests. These patient iPSCs displayed normal karyotypes, were free of mycoplasma and clear from exogenous transgenes and Sendai virus backbone from the reprogramming. The reprogrammed cells expressed markers Tra-1-60 and Nanog confirming their pluripotency. All reprogrammed patient lines retained their disease genotypes.

3.4.1 The impact of reprogramming on disease modelling: epigenetic memory of iPSCs

The molecular mechanisms driving reprogramming of somatic cells into iPSCs by defined factors are still incompletely understood. Nevertheless, it has been revealed that residual somatic epigenetic memory may sometimes persist in iPSCs, which can potentially affect their differentiation capacity and utility as disease models (Avior et al., 2016).

The pluripotent state of ESCs is enforced by epigenetic factors closely linked to pluripotency transcriptional factor network. Resetting the epigenetic state of somatic cells to that of ESCs will generate iPSCs that possess ESC-like properties (Brix et al., 2015). Reprogramming somatic cells into an ESC-like state requires the erasure of somatic epigenetic marks and the establishment of those characteristics of pluripotency. This involves a genome-wide remodelling of the epigenetic landscape within the cells, which then leads to global changes of gene expression (Brix et al., 2015). Although iPSCs are very similar to ESCs in terms of pluripotency, self-renewal and differentiation capacity, the process of reprogramming may lead to several differences. These include the persistence of epigenetic memory from the somatic cells of origin in iPSCs, differential DNA methylation signatures and a different extent of

genetic aberrations. These differences might sometimes give rise to phenotypic differences before or following differentiation (Avior et al., 2016; Siller et al., 2013).

During reprogramming, the somatic genome undergoes various epigenetic modifications including genome-wide DNA methylation and histone modifications (Brix et al., 2015; Liang and Zhang, 2013). When the reprogramming factors are introduced into somatic cells, they drive the cells to overcome the first epigenetic barrier by inducing unstable modulation of the original somatic state, with local rather than global epigenetic changes. This initial modulation depends on the sustained expression of the reprogramming factors. The somatic cell chromatin is reorganised to an ESC-like state with loosely packed heterochromatin, characterised by the presence of histone trimethylation and abundant euchromatin modifications (Brix et al., 2015; Liang and Zhang, 2013). These changes can assist in removing potent memory of prior transcriptional activity in the parental somatic cell. Meanwhile, somatic-identity genes such as mesenchymal genes are downregulated by OCT4 and SOX2, and the cell cycle is accelerated by MYC, after which epithelial genes are activated, in part by KLF4 and inhibition of TGFβ signalling. At either of these stages, non-pluripotent intermediates still depend on the sustained expression of the reprogramming factors. However, the genes expressed by the original cell type are not always completely suppressed and their expression sometimes persists, which might explain the low efficiency of reprogramming (Brix et al., 2015; Krishnakumar and Blelloch, 2013; Liang and Zhang, 2013; Smith et al., 2016). These intermediate epithelial cells, in which expression of *NANOG* is upregulated, show increased cell proliferation as accelerated by MYC. These cells overcome the second barrier to activate pluripotency, which requires the endogenous expression of a set of pioneer genes including *SOX2, NANOG, ESRRB, UTF1, LIN28* and *DPPA2* (Buganim et al., 2012). Cells that fail to overcome this barrier become partially reprogrammed and contribute to cell heterogeneity (Liang and Zhang, 2013). Upon activation of the pluripotency network and withdrawal of exogenous reprogramming factors (Golipour et al., 2012), reprogramming cells can self-renew independently of the introduced reprogramming factors. Finally, these reprogramming cells require the elimination of somatic

epigenetic memory, reactivation of the X-chromosome in females and re-establishment of histone modifications at developmental genes to become reprogrammed cells with full functional pluripotency (Smith et al., 2016). Nonetheless, these nascent iPSCs may still retain some somatic cell memory and chromatin modification pattern. Remnant DNA methylation patterns specific to the parental cells have been observed in established iPSCs (Liang and Zhang, 2013). These somatic traits can be removed by additional passages or treatment with inhibitors before becoming refined iPSCs possessing *bona fide* pluripotency similar to ESCs. This epigenetic memory of the parental cells may contribute to a biased differentiation potential towards the originating lineages (Bilic and Izpisua Belmonte, 2012; Liang and Zhang, 2013). In particular, early passage iPSCs may not respond to differentiation cues like ESCs (Bilic and Izpisua Belmonte, 2012). Furthermore, it has been shown that certain genomic loci in iPSCs bear abnormal DNA methylation pattern, which is neither a feature of ESCs nor that of the parental somatic cells. These aberrant traits are adopted during the reprogramming process and may lead to altered gene expression and functional phenotypes (Bilic and Izpisua Belmonte, 2012; Liang and Zhang, 2013). The sites and regions of differential methylation have been shown to depend on the genetic variation of donor cells, derivation methods and culture conditions, age of donor cells as well as the number of passages (Brix et al., 2015). Several patient iPSC clones derived from patients SCA14-1 and SCA14-2 using the SeVdp(KOSM)302L Sendai virus system were particularly vulnerable to differentiation into fibroblast-looking cells (data not shown). This could result from the persistence of parental somatic epigenetic memory due to incomplete reprogramming. Indeed, unlike the more recent CytoTune®-iPS 2.0 system, which contains an extra set of c-Myc and Klf4 vectors for stronger expression of the two factors, the SeVdp(KOSM)302L system possesses only one set of these factors. This might thus lead to less efficient reprogramming and the generation of partially reprogrammed cells that are prone to differentiate back to fibroblasts. In addition, some of the control and patient iPSC lines did not differentiate well into cerebellar lineages (data not shown) and were therefore excluded in this study. This limited differentiation capacity might be a result of aberrant epigenetic signatures.

Combinations of different transgenes and the use of small molecules to interfere with the epigenetics have been developed to improve the iPSC reprogramming efficiency (Brix et al., 2015). Increasing knowledge in the epigenetic regulation of cell identity might allow the switch of cell fate via or bypass the totipotent or pluripotent state (Morris and Daley, 2013).

3.4.2 Genomic mutations arising in iPSCs during reprogramming

Reprogramming is a lengthy process involving multiple steps and rounds of cell division, which are prone to error. Robust quality control tests are therefore essential to ensure the iPSCs generated possess normal and ESC-like features. Karyotyping is an important quality control test of iPSC generation to confirm the integrity of chromosomes and the lack of genomic mutations. Genomic mutations can arise from the reprogramming processes and/or the *in vitro* expansion of cells (Ben-David and Benvenisty, 2008; Bilic and Izpisua Belmonte, 2012). These mutations can range from chromosomal aneuploidy, subchromosomal deletions or duplications to single base mutations. These mutations could be advantageous to cell proliferation and survival in *in vitro* culture conditions (Ben-David and Benvenisty, 2008). Several of the iPSC clones selected for the SCA14 patient with the H101Q mutation failed the karyotyping test showing large deletions or duplications. This is consistent with the high reported rate of genomic abnormalities (Gore et al., 2011; Hussein et al., 2011; Laurent et al., 2011; Mayshar et al., 2010). In addition, to minimise the potential impact of genomic mutations accumulate during expansion, the passage number of all iPSC lines included in this study were below 40. A recent report has shown that the initial genomic instability and continued progression result from DNA replication stress, and defective condensation and segregation due to altered levels of actin cytoskeletal genes (Lamm et al., 2016). Nevertheless, the correlation between the cause of the high occurrence of genetic aberrations and reprogramming methods such as combination of transcription factors, or iPSC expansion method remains to be elucidated. Further

investigation into the molecular mechanisms of reprogramming methods will improve the efficiency of reprogramming and reduce mutations arisen during the processes.

3.4.3 Genome editing in iPSCs

Differences in genetic background might contribute to phenotypic differences in studies using one or few iPSC lines (Musunuru, 2013; Zhang et al., 2017b). As mentioned above, the process of generating, expanding and passaging iPSC lines can result in the accumulation of genetic mutations, as well as varying genomic methylation patterns depending on identity of parent somatic cells. Moreover, age, gender and ethnicity of donors; differences in reprogramming methods, passage number and adaptation to culture of the iPSC lines might also contribute to varying phenotypes such as transcriptional profiles (Musunuru, 2013; Zhang et al., 2017b). The use of appropriate controls is therefore important for accurate disease modelling using iPSCs. Ideally, isogenic controls should be produced by either correcting the mutations in patient iPSCs, or introducing the mutations into control iPSCs using genome-editing techniques. This should produce iPSC lines that only differ in the disease-causing mutations and allows for rigorous phenotypic comparisons between cell lines.

3.4.4 High-throughput drug screening using iPSCs

Animal models are frequently used for drug screening. However, many diseases such as SCA14 lack a suitable animal model. Moreover, the use of animal models is often not feasible for high-throughput drug screening due to the lack of easily assessable phenotypes, complex physiology and procedures involved (Avior et al., 2016). In contrast, iPSCs and iPSC-derived models can be used to identify clear phenotypes, which can be automatically measured and quantified *in vitro.* Potential drugs can be identified by two approaches: candidate drug approach and high-throughput screening, both of which have their own advantages and limitations (Avior et al., 2016). Candidate drug approach is used to find potent drugs from a defined set of drugs when

specific pathogenic pathways have been narrowed down. This allows for the screening of a small number of drugs but evaluation of complex phenotypes using a fewer cells. This approach can be used to validate regulatory approved drugs for the potentially rapid transition from *in vitro* models to clinical trials. However, novel drug discovery might then be limited. Alternatively, a large quantity of drugs can be screened in an unbiased fashion and assessment of rescue or alleviation of phenotypes can be automated. This allows for the discovery of new drugs when prior knowledge of disease mechanisms is not necessary but a large number of cells and clear cellular phenotypes are needed (Avior et al., 2016).

3.5 Conclusions

Overall, iPSCs and iPSC-derived neurons represent exciting tools for the modelling of neurological disorders including cerebellar ataxias where patient cells are not readily accessible. When coupled with genome editing technology, disease-causing mutations, particularly for monogenic diseases such as cerebellar ataxias, can be corrected in patient-derived iPSC lines or introduced in control lines to accurately assess disease phenotypes in identical genetic backgrounds. Moreover, iPSC-derived cell models offer new opportunities for the medium to large scale screening of potential drugs for this currently incurable group of disorders. In this chapter, iPSCs from four SCA14 patients were successfully produced and characterised. At least two clones for each patient iPSC line were generated: four clones for PRKCG01, three clones for PRKCG02, two clones for SCA14-1 and two clones for SCA14-2. All patient iPSC lines passed all the quality control tests, which are summarised in Table 3.2. These iPSCs are ready for subsequent analyses including the correction of mutations using CRISPR/Cas9 genome editing, functional analysis of mutant PKCγ, differentiation into Purkinje cells and thereby dissecting the disease pathways underlying SCA14.

Table 3-2 Quality control tests performed on patient iPSC lines

Clones	Mutation	Karyotyping	Mycoplasma test	Sendai virus clearance	Pluripotency (Tra-1-60 and Nanog)	Genotyping
PRKCG01-1	H36R (exon 1)	Pass	Pass	Pass	Pass	Pass
PRKCG01-10	H36R (exon 1)	Pass	Pass	Pass	Pass	Pass
PRKCG01-17	H36R (exon 1)	Pass	Pass	Pass	Pass	Pass
PRKCG01-18	H36R (exon 1)	Pass	Pass	Pass	Pass	Pass
PRKCG02-3	H36R (exon 1)	Pass	Pass	Pass	Pass	Pass
PRKCG02-7	H36R (exon 1)	Pass	Pass	Pass	Pass	Pass
PRKCG02-12	H36R (exon 1)	Pass	Pass	Pass	Pass	Pass
SCA14-1-1	H101Q (exon4)	Pass	Pass	Pass	Pass	Pass
SCA14-1-10	H101Q (exon4)	Pass	Pass	Pass	Pass	Pass
SCA14-2-3	H101Q (exon4)	Pass	Pass	Pass	Pass	Pass
SCA14-2-14	H101Q (exon4)	Pass	Pass	Pass	Pass	Pass

Chapter 4 Generating isogenic controls for SCA14 iPSCs using CRISPR/Cas9 genome editing

4.1 Introduction

4.1.1 CRISPR/Cas9 system for genome editing

As discussed in the previous chapter, genetic variations in iPSCs might contribute to the phenotypic differences observed between control and patient iPSCs and iPSC-derived models and thereby complicate the interpretation of findings (section 3.4.2-3.4.3). These genetic variations might arise from genomic mutations that accumulate during the process of reprogramming and expansion in addition to the distinct genetic backgrounds between donors. To eliminate the potential variation caused by distinct genetic backgrounds, isogenic controls can be generated from patient iPSC lines by correcting the disease-causing mutations back to the wildtype genotypes. Moreover, the introduction of SCA14 mutations into control iPSC lines would strengthen the conclusion that the observed disease phenotypes are caused by distinct mutations in PKCγ.

Targeted nucleases are powerful tools for precise genome alteration, which is ideal for producing isogenic controls and introducing mutations in stem cell research. The Clustered Regularly Interspaced Short Palindromic Repeat (CRISPR)/Cas9 system is a microbial adaptive immune system that uses RNA-guided nucleases to cleave foreign genetic materials (Ran et al., 2015; Ran et al., 2013b). In brief, a guide RNA (gRNA) directs wildtype Cas9 (WT Cas9) towards the desired DNA region. The gRNA is comprised of two components: a scaffold sequence necessary for Cas9 binding (tracrRNA) and a user-defined 20-nucleotide target sequence, which is complementary to the target sequence (CRISPR RNA; crRNA). Cas9 recognises the species-specific protospacer adjacent motif (PAM) and creates a double-

stranded break (DSB) three bases upstream of the PAM (Fig. 4.1A). A target sequence may have high homology elsewhere in the genome, which can be cut by Cas9 unintentionally, which is also referred to as an off-target effect. To circumvent this problem, approaches have been developed to increase the specificity of the cutting, for example by the use of Cas9 variants such as SpCas9 nickase (SpCas9n) (Ran et al., 2013a). When two sets of gRNAs with the appropriate offset (-2 to 20 bp) and SpCas9n are used, SpCas9n will produce a nick on each strand of the DNA and thus a DSB, increasing the cutting specificity (Fig. 4.1B). The DSB induced by Cas9 can be repaired via non-homologous end joining (NHEJ) or homology-directed repair (HDR). NHEJ is an error-prone process that creates insertions or deletions (indels) and thereby disrupts the target gene. This approach is usually employed to create a gene knockout. On the other hand, HDR takes place when a repair template with homology arms flanking the desired modifications is supplied and therefore allows for precise editing (Ran et al., 2013a) (Fig. 4.1C).

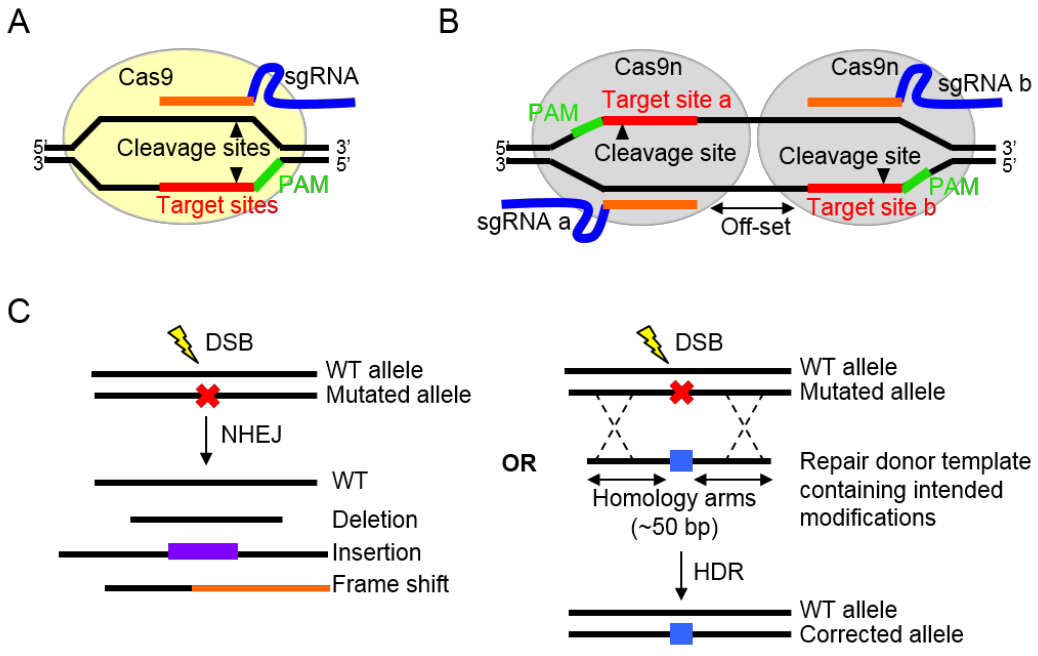


Figure 4.1 Schematic representation of CRISPR/Cas9 genome engineering for generating isogenic controls, selection methods and a flowchart of experiments.

(A) A double-stranded break (DSB) (black arrowheads) is generated by wildtype SpCas9 (WT SpCas9) nuclease (yellow) three bases upstream of the PAM sequence, which immediately follows the 20-nucleotide long target sequence (crRNA) (orange). The sequence in blue represents the scaffold for stabilising the Cas9 (tracrRNA). (B) SpCas9n (grey) contains a D10A mutation that allows it to produce a nick (black arrowheads) on the complementary strand that binds a gRNA (orange lines), also three bases upstream of the PAM. Two sets of gRNAs and SpCas9n with an appropriate offset (-2 to 20 bp) to produce a 5'-overhang for the binding of a repair template if HDR is desired. (C) The DSB induced by Cas9 can be repaired through non-homologous

end joining (NHEJ) (left panel) that produces insertion or deletions (indels). The point mutation (red cross) is corrected (blue box) with the aid of a repair donor by homologous recombination (HDR) (right panel). The donor possesses homology arms (50 bases on each side) flanking the intended modifications.

In addition to SpCas9n, two new Cas9 variants that show low off-target effects achieved by the introduction of rationally designed mutations have been developed. Mutations in enhanced SpCas9 (eSpCas9) reduce the enzyme's helicase activity and thus cleavage at off-target sites without compromising on-target editing (Slaymaker et al., 2016). Another Cas9 variant, SpCas9-HF, harbours engineered mutations to disrupt the interactions between Cas9 and the phosphate backbone of the target DNA strand, resulting in reduced off-target-activity (Kleinstiver et al., 2016).

Moreover, multiple CRISPR nucleases from other bacterial species that recognise distinct PAM sequence from SpCas9 have recently been characterised. This expansion of possible PAM sequences allows scientists to target a wider spectrum of loci in genomes. This will also improve HDR applications as editing efficiency increases when the PAM sequence is closer to the edit site. Table 4.1 shows a list of CRISPR nucleases characterised to-date.

The simple and fast preparation as well as ability to precisely modify human genome has made CRISPR/Cas9 genome editing a good tool for introducing single base pair changes in iPSCs. The aim of this chapter was to generate isogenic controls for SCA14 iPSCs by correcting the patient mutations back to wildtype genotypes. Different CRISPR/Cas9 systems together with a repair donor template were employed. Combinations of gRNAs and Cas9 nucleases that allow for efficient introduction of DSBs in the target regions were first identified using HEK293T cells. Two approaches for introducing gRNAs, Cas9 nuclease and the repair donor template into HEK293T cells and iPSCs were tested. First, co-transfection of gRNAs-Cas9-expressing plasmids and the repair donor were carried out. Subsequently, direct delivery of gRNA, Cas9 protein and repair donor oligos were assessed.

Table 4-1 List of CRISPR nucleases from additional bacterial species and their PAM sequences.

CRISPR nucleases	PAM sequence (5'-3')	References
Streptococcus pyogenes (SpCas9)	NGG or NAG	(Ran et al., 2013b)
SpCas9 D10A variant (SpCas9n)	NGG or NAG	(Ran et al., 2013a)
eSpCas9	NGG	(Slaymaker et al., 2015)
SpCas9-HF	NGG	(Kleinstiver et al., 2016)
SpCas9 D1135E variant	NGG (reduced NAG binding)	(Kleinstiver et al., 2016)
SpCas9 VRER variant	NGCG	(Kleinstiver et al., 2016)
SpCas9 EQR variant	NGAG	(Kleinstiver et al., 2015)
SpCas9 VQR variant	NGAN or NGNG	(Kleinstiver et al., 2015)
Staphylococcus aureus (SaCas9)	NNGRRT or NNGRR(N)	(Ran et al., 2015)
Acidaminococcus sp. (AsCpf1)	TTTV	(Zetsche et al., 2015)
Lachnospiraceae bacterium (LbCpf1)	TTTV	(Zetsche et al., 2015)
AsCpf1 RR variant	TYCV	(Gao et al., 2017)
LbCpf1 RR variant	TYCV	(Gao et al., 2017)
AsCpf1 RVR variant	TATV	(Gao et al., 2017)
Neisseria meningitidis (NM)	TATV	(Hou et al., 2013b)
Streptococcus thermophilus (ST)	NNAGAAW	(Muller et al., 2016)
Treponema denticola (TD)	NAAAAC	(Esvelt et al., 2013)

4.2 Specific Materials and Methods

Experiments for generating isogenic controls for the SCA14 mutations (H36R and H101Q) in the human *PRKCG* gene using the gRNA- and Cas9 nuclease-expressing plasmid approach were conducted in collaboration with Dr. Andrew Bassett, former Head of Genome Engineering Oxford. Experiments for producing an isogenic control for the SCA41 mutation (R762H) in the human *TRPC3* gene using direct transfection of RNPs containing Cas9 proteins, synthetic gRNAs and repair templates were conducted with Dr. Joey Riepsaame, Head of Genome Engineering Oxford, with the assistance of Miss Alexandra Soca, a Masters student at the time. Experiments conducted in human iPSCs were performed with guidance from Dr. Sally Cowley, Head of James Martin Stem Cell Facility, affiliated to the Oxford Stem Cell Institute.

4.2.1 Design of gRNAs and repair donors

The genomic DNA sequences of the regions of interest containing the H36R (exon 1) and H101Q (exon 4) SCA14 mutations, respectively, were determined by Sanger sequencing. Briefly, fragments of 275 nucleotides representing the region of interest in exon 1 and 251 nucleotides for exon 4 of the human *PRKCG* gene were amplified using the Expand High Fidelity PCR System (Roche) and the primers listed in Table 4.2.

The PCR products were purified using the QIAquick PCR Purification Kit (Qiagen) or the Monarch® PCR & DNA Cleanup Kit [(New England BioLabs (NEB)] according to manufacturer's instructions. The purified PCR products were then sent for Sanger sequencing. The resulting DNA sequences were run through the CRISPR design Tool (http://crispr.mit.edu/). gRNA target sites (crRNAs), which are located 20 nucleotides (N_{18}) upstream of the PAM sequences, were searched for in both the sense or antisense strand of the DNA. gRNA target sites were designed for two different species of Cas9 proteins: *Streptococcus pyogenes* (SpCas9) and *Staphylococcus aureus* (SaCas9). In addition to the unmodified wildtype SpCas9 nuclease, crRNAs were also designed for use in combination with

SpCas9 D10A nickase (SpCas9n). PAM sequences for SpCas9 and SpCas9n are 3' NGG or NAG while the PAM sequence for SaCas9 is 3' NNGRRT or NNGRR(N). The best-fitted crRNAs returned by the software were chosen for each species.

Design of the sequencing primers and crRNAs for producing an isogenic control of the *TRPC3* (R762H) mutation was performed by Miss Alexandra Soca with my guidance as described above. Primers listed in Table 4.2 were used to amplify the fragment of 389 nucleotides surrounding the R762H mutation in exon 9 of the human *TRPC3* gene. crRNAs were designed for enhanced SpCas9 nuclease that recognises the PAM sequence 3' NGG (Slaymaker et al., 2016).

Table 4-2 List of primers that were used to amplify fragments of DNA surrounding the target mutations for Sanger sequencing.

Primer name	Sequence 5'-3'	PCR product size [base pair (bp)]
PKCG_EX1F	AGAAAGGCAGGATCCTGGTC	275
PKCG_EX1R	CGGCGTGATAGGAGTCTGCA	
PKCG_EX4F	GCTGACCTAGAGAGCAAGGC	251
PKCG_EX4R	GCTTTGGAAGGGCCCTGGCA	
hTRPC3_1F	GTGGGTACAGGTAGAGGCAT	389
hTRPC3_1R	TCCTTCTGAAGCCTTCTCCTTC	

Off-target effects were checked using Primer BLAST (https://www.ncbi.nlm.nih.gov/tools/primer-blast/) to ensure the specificity of the crRNAs in the human genome. Sequences that perfectly matched the final 12 nucleotides of the target sequence and NGG PAM sequence were discarded (Bassett et al., 2013; Cong et al., 2013). Table 4.3 shows the list of crRNAs designed for *PRKCG:* H36R and H101Q as well as TRPC3 at this stage of the study. crRNAs number 1.1-23.2 were purchased as custom manufactured oligonucleotides from Sigma and subsequently subcloned into nuclease-expressing vectors using restriction enzymes BbsI or BsaI (refer to sections 2.2.2-2.2.3). crRNAs number 24-26 were custom manufactured by Integrated DNA Technologies as synthetic RNA

oligonucleotides. Universal tracrRNA oligonucleotides were purchase from Integrated DNA Technologies.

In addition, a DNA repair template in the form of 100 nucleotides containing two nucleotide changes that introduce the wildtype nucleotide and a silent mutation that create a restriction site was designed for each mutation (Table 4.4). The two nucleotide changes were located at the centre of the sequence and flanked by two homology arms, each around 35-50 nucleotides long. Phosphorothioate chemical modifications were added to both ends of the oligonucleotides to protect them from endo- and exonucleases. All oligonucleotides were custom-manufactured by Integrated DNA Technologies.

Table 4-3 List of crRNAs targeting the SCA14 H36R and H101Q mutations in the human *PRKCG* gene and the SCA41 R762H mutation in the human *TRPC3* gene designed using the CRISPR Design Tool.

Genes	Oligo number	Exon	Mutation	Mutant/ WT	Nuclease	Name	crRNAs
PRKCG	1.1	1	H36R	M	SpCas9	Ex1_M_SpCas9_1T	5'-ACCG**CTTGCGGCTCTTGACTTCG**-3'
	1.2	1	H36R	M	SpCas9	Ex1_M_SpCas9_1B	5'-AAAC**CGAAGTCAAGAGCCGCAAG**C-3'
	2.1	4	H101Q	M	SpCas9	Ex4_M_SpCas9_1T	5'-CACC**GGAACTTCTGTTTGTTCCGG**-3'
	2.2	4	H101Q	M	SpCas9	Ex4_M_SpCas9_1B	5'-AAAC**CCGGAACAAACAGAAGTTCC**-3'
	3.1	1	H36R	M	SpCas9n	Ex1_M_SpCas9n_1T	5'-CACCG**CCACGAAGTCAAGAGCCGC**-3'
	3.2	1	H36R	M	SpCas9n	Ex1_M_SpCas9n_1B	5'-AAAC**GCGGCTCTTGACTTCGTGG**C-3'
	4.1	1	H36R	B	SpCas9n	Ex1_M_SpCas9n_1cT	5'-CACC**GAGCCCCCTTTCTGCAAAAC**-3'
	4.2	1	H36R	B	SpCas9n	Ex1_M_SpCas9n_1cB	5'-AAAC**GTTTTGCAGAAAGGGGGCTC**-3'
	8.1	1	H36R	M	SaCas9	Ex1_M_SaCas9_1T	5'-CACC**GAACTTGCGGCTCTTGACTTC**-3'
	8.2	1	H36R	M	SaCas9	Ex1_M_SaCas9_1B	5'-AAAC**GAAGTCAAGAGCCGCAAGTTC**-3'
	9.1	4	H101Q	M	SaCas9	Ex4_M_SaCas9_2T	5'-CACCG**AGGCGGAACTTCTGTTTGTTC**-3'
	9.2	4	H101Q	M	SaCas9	Ex4_M_SaCas9_2B	5'-AAAC**GAACAAACAGAAGTTCCGCCT**C-3'
	10.1	1	H36R	WT	SpCas9	Ex1_WT_SpCas9_1T	5'-CACCG**CTTGTGGCTCTTGACTTCG**-3'
	10.2	1	H36R	WT	SpCas9	Ex1_WT_SpCas9_1B	5'-AAAC**CGAAGTCAAGAGCCACAAG**C-3'
	11.1	4	H101Q	WT	SpCas9	Ex4_WT_SpCas9_1T	5'-CACC**GGAACTTGTGTTTGTTCCGG**-3'
	11.2	4	H101Q	WT	SpCas9	Ex4_WT_SpCas9_1B	5'-AAAC**CCGGAACAAACACAAGTTCC**-3'
	13.1	1	H36R	WT	SpCas9n	Ex1_WT_SpCas9n_1cT	5'-CACC**GAGCCCCCTTTCTGCAAAAC**-3'
	13.2	1	H36R	WT	SpCas9n	Ex1_WT_SpCas9n_1cB	5'-AAAC**GTTTTGCAGAAAGGGGGCTC**-3'
	17.1	1	H36R	WT	SaCas9	Ex1_WT_SaCas9_1T	5'-CACC**GAACTTGTGGCTCTTGACTTC**-3'
	17.2	1	H36R	WT	SaCas9	Ex1_WT_SaCas9_1B	5'-AAAC**GAAGTCAAGAGCCACAAGTTC**-3'
	18.1	4	H101Q	WT	SaCas9	Ex4_WT_SaCas9_2T	5'-CACCG**AGGCGGAACTTGTGTTTGTTC**-3'
	18.2	4	H101Q	WT	SaCas9	Ex4_WT_SaCas9_2B	5'-AAAC**GAACAAACACAAGTTCCGCCT**C-3'
	19.1	4	H101Q	WT	SpCas9n	Ex4_WT_SpCas9n_1T	5'-CACCG**GGACCCCCGGAACAAACAC**-3'
	19.2	4	H101Q	WT	SpCas9n	Ex4_WT_SpCas9n_1B	5'-AAAC**GTGTTTGTTCCGGGGGTCC**C-3'
	20.1	4	H101Q	B	SpCas9n	Ex4_SpCas9n_1dT	5'-CACC**GCAGAGAAGACTGGCTTAGG**-3'

	20.2	4	H101Q	B	SpCas9n	Ex4_SpCas9n_1dB	5’-AAAC**CCTAAGCCAGTCTTCTCTGC**-3’
	21.1	4	H101Q	B	SpCas9n	Ex4_SpCas9n_1eT	5’-CACCG**AGACTGGCTTAGGGGGCGT**-3’
	21.2	4	H101Q	B	SpCas9n	Ex4_SpCas9n_1eB	5’-AAAC**ACGCCCCCTAAGCCAGTCT**C-3’
	22.1	4	H101Q	M	SpCas9n	Ex4_M_SpCas9n_1T	5’-CACCG**GGACCCCCGGAACAAACA**G-3’
	22.2	4	H101Q	M	SpCas9n	Ex4_M_SpCas9n_1B	5’-AAAC**CTGTTTGTTCCGGGGGTCC**C-3’
	23.1	1	H36R	WT	SpCas9n	Ex1_WT_SpCas9n_1Tcor	5’-CACCG**CCACGAAGTCAAGAGCCAC**-3’
	23.2	1	H36R	WT	SpCas9n	Ex1_WT_SpCas9n_1Bcor	5’-AAAC**GTGGCTCTTGACTTCGTGG**C-3’
TRPC3	24	9	R762H	M	SpCas9	TRPC3_gRNA 1_M	5’-**AGTTTGCTCATTAAAACTT** -3’
	25	9	R762H	WT	SpCas9	TRPC3_gRNA 1_WT	5’-**AGTTTGCTCGTTAAAACTT** -3’
	26	9	R762H	WT	SpCas9	TRPC3_gRNA 2	5’-**TGGTTATCCTATTTTGATGA** -3’
	27	9	R762H	WT	SpCas9	TRPC3_gRNA 3	5’-**AGGATGACAGTGATGTAGAA** -3’

Nucleotides in red denote the mutant nucleotides. Target sequences are indicated in bold. WT: wildtype.

Table 4-4 List of single-stranded DNA repair donor templates used in this study.

Repair donor number	Name of repair donor	Sequences
1	ex1_spCas9_ssOCN donor_ iso_1F	C*TGTTTTGCAGAAAGGGGGCTCTGAGGCAGAAGGTGGTACACGAAGTCAAGAGCCACAAGTTC ACCGCTCGCTTCTTCAAGCAGCCCACCTTCTGCAGC*C
2	ex1_spCas9_ssOCN donor_ iso_1R	G*GCTGCAGAAGGTGGGCTGCTTGAAGAAGCGAGCGGTGAACTTGTGGCTCTTGACTTCGTGTA CCACCTTCTGCCTCAGAGCCCCCTTTCTGCAAAACA*G
3	ex1_spCas9n_ssOCN donor_ iso_1F	G*CAGAAAGGGGGCTCTGAGGCAGAAGGTGGTCCACGAAGTCAAGAGCCACAAATTCACCGCT CGCTTCTTCAAGCAGCCCACCTTCTGCAGCCACTGCA*C
4	ex1_spCas9n_ssOCN donor_ iso_1R	G*TGCAGTGGCTGCAGAAGGTGGGCTGCTTGAAGAAGCGAGCGGTGAATTTGTGGCTCTTGACT TCGTGGACCACCTTCTGCCTCAGAGCCCCCTTTCTG*C
5	ex4_spCas9_ssOCN donor_ iso_1F	t*cccaacgccccctaagccagtcttctctgcccccagGATCCCCGGAACAAACACAAGTTCCGCCTGCATAGCTACA GCAGCCCCACCTTCTGCGACCA*C
6	ex4_spCas9_ssOCN donor_ iso_1R	G*TGGTCGCAGAAGGTGGGGCTGCTGTAGCTATGCAGGCGGAACTTGTGTTTGTTCCGGGGATCc tgggggcagagaagactggcttaggggcgttggg*a
7	ex4_spCas9n_ssOCN donor_ iso_1F	c*gccccctaagccagtcttctctgcccccagGACCCCCGGAACAAACACAAATTCCGCCTGCATAGCTACAGCAG CCCCACCTTCTGCGACCACTGTGG*C
8	ex4_spCas9n_ssOCN donor_ iso_1R	G*CCACAGTGGTCGCAGAAGGTGGGGCTGCTGTAGCTATGCAGGCGGAATTTGTGTTTGTTCCG GGGGTCctgggggcagagaagactggcttagggggc*g
9	TRPC3_R762H_correction donor_old_100mer	C*TATTTTTGTGACACAGGATGACAGTGATGTAGAATGGAAGTTTGCTCGTTCCAAACTTTGGTT ATCCTATTTTGATGATGGAAAAACATTACCTCCAC*C
10	TRPC3_R762H_correction donor_new_70mer_antisense	A*A*T*GTTTTTCCATCATCAAAATAGGATAACCAAAGCTTTGAACGAGCAAACTTCCATTCTAC ATCAC*T*G*T

Asterisks denote a phosphorothioate chemical modification between bases, which protects the single-stranded DNA oligonucleotides from endo- and exonucleases. Introns are indicated in lower case while exons are denoted in uppercase.

4.2.2 Preparation of sgRNAs and Cas9 nuclease-expressing plasmids

All of the restriction digestion enzymes used were purchased from NEB unless stated otherwise. Custom-manufactured oligonucleotides for producing crRNA/tracr RNA targeting the SCA14 mutations (H36R and H101Q) were subcloned into CRISPR vectors as described below.

4.2.2.1 Annealing of oligonucleotides

25 μM of both forward and reverse oligos (denoted as x.1 and x.2 respectively in Table 4.1) were annealed in annealing buffer (10 mM Tris, 1 mM EDTA, 50 mM NaCl, pH8.0) in a PCR machine using the following conditions:

98°C	1 min.
98-18°C	-0.1°C/cycle
18°C	∞

2.5 μM of the annealed oligos were then phosphorylated in 1x T4 DNA ligase buffer (Roche) using 10 units of T4 Polynucleotide Kinase (NEB) at 37°C for 30 minutes. The phosphorylated oligonucleotides were then diluted 10 times in nuclease-free water until used.

4.2.2.2 Preparation of cut vectors

The CRISPR-Cas9 vectors used in this study, pSpCas9(BB)-2A-Puro (pX459) V2.0 (Addgene plasmid # 62988) (Ran et al., 2013b), pSpCas9n(BB)-2A-Puro (pX462) V2.0 (Addgene plasmid # 62987) (Ran et al., 2013a) and pX601-AAV-CMV::NLS-SaCas9-NLS-3xHA-bGHpA;U6::BsaI-sgRNA (pX601) (Addgene plasmid # 61591) were gifts from Feng Zhang (Ran et al., 2015). Vectors pX459, pX462 and pX601 contain cDNAs for the nucleases SpCas9, SpCas9n and SaCas9, respectively. All vectors contain a puromycin selectable marker and an

ampicillin resistance gene. All vectors contain a human U6 RNA polymerase III promoter and a human CMV enhancer, which drive the expression of gRNA and Cas9, respectively (Fig. 4.5). 1 μg of pX459 and pX462 vectors were linearized with BbsI (Fermentas), whereas pX601 was linearized with BsaI at 37ºC for 2 hours. 10 units of calf intestinal alkaline phosphatase (CIP) (NEB) were added to the reaction mix during the last 10 minutes of the reactions to catalyse the dephosphorylation of the 5´ and 3´ ends of the linearized vectors. The linearized vectors were subsequently purified using the QIAquick PCR Purification Kit (Qiagen), resuspended in 50 μl nuclease-free water and stored at -20ºC until used.

4.2.2.3 Ligation of annealed oligonucleotides into CRISPR vectors

2 μl of the phosphorylated and annealed oligonucleotides were ligated into 1 μl of the linearized CRISPR vectors using the Rapid T4 DNA ligase kit (Roche) at 22ºC for 30 minutes. The ligated plasmids were then ready for transformation into competent cells.

4.2.2.4 Transformation and expansion of DH5-α cells

The reaction mix containing 2 μl each of the ligated plasmids and 50 μl DH5-α cells (produced in-house) was incubated on ice for 20 minutes before heatshock for 30 seconds at 42ºC and incubation on ice for 2 minutes. 100 μl 2X YT media were then added to the transformed competent cells and incubated at 37ºC for an hour with shaking. The entire mixture was then plated onto a LB plate containing 100 μg/ml ampicillin and incubated at 37ºC overnight. One colony was picked from each plate and expanded in 5 ml LB media containing 100 μg/ml ampicillin overnight at 37ºC. 1 ml bacteria were mixed with 1 ml of 50% glycerol and stored as glycerol stock at -80ºC. The plasmids in the remaining bacteria were purified using the QIAprep Spin Miniprep Kit (Qiagen). The plasmids were resuspended and diluted to 100 ng/μl in Tris-EDTA (TE) buffer (10 mM Tris pH 8.0 and 1 mM EDTA), and sent for sequencing using the following primer: U6Fseq: 5'-ACTATCATATGCTTACCGTAAC-3'. The

constructs containing the correct sgRNA sequences were expanded in 40 ml LB broth containing 100 μg/ml ampicillin and purified using the GenElute HP Plasmid DNA Midiprep Kit (Sigma). The plasmid concentration was adjusted to 1 μg/μl.

4.2.3 Cell transfection

4.2.3.1 Lipofectamine-based transfection of human HEK293T cells

For the plasmid approach, HEK293T cells were transfected with the constructs prepared above using TransIT-2020 (Mirus Bio LLC). 7.5-8 x 10^5 cells/well were plated 24 hours before transfection onto 24-well plates (Corning). Immediately before transfection, medium was replaced with 0.5ml media supplemented with 10% serum (without P/S). For each transfection, 50 μl of transfection reaction mixture containing 500 ng of the appropriate plasmids, OptiMEM serum-free media (Thermo Fisher Scientific) and TransIT-2020 were incubated at room temperature for 20 minutes. The entire transfection reaction mixture was added dropwise and evenly across the well and incubated at 37ºC with 5% CO_2. Four hours post-transfection, an equal volume of normal media containing 10% serum and P/S was added. The transfected cells were grown for two days prior to harvest. EGFP plasmid was kindly provided by Dr. Andrew Bassett and used as the positive control.

For the direct transfection of Cas9 protein and sgRNAs, HEK293-BFP cells, which are HEK293 cells stably expressing the blue fluorescent protein (BFP) a kindly provided by Dr. Riepsaame, were transfected with Cas9-gRNA ribonucleoprotein (RNP) complexes using Lipofectamine MessengerMAX (Thermo Fisher Scientific). 6 x 10^5 cells/well were plated 24 hours before transfection onto 48-well plates. Immediately before transfection, medium was replaced with 200 μl McCoy's 5A (Lonza) supplemented with 10% serum (without P/S). crRNA and tracrRNA were mixed in equimolar concentrations (5 μM), heated at 95ºC for 5 minutes and then gradually cooled down 0.2ºC/second to 4ºC to form gRNA complexes.

Ribonucleoprotein complexes were prepared by mixing 500 ng gRNAs with 2 μg Cas9 protein in 50 μl OptiMEM and incubated at room temperature for 5 minutes. Three different endonucleases were tested: WT SpCas9 (Integrated DNA Technologies), enhanced SpCas9 (eSpCas9) (Sigma) and HIFI Cas9 (Integrated DNA Technologies). 0.3 μM DNA repair donor template was added to each transfection mixture and incubated at room temperature for 5 minutes. 50 μl transfection reagent Lipofectamine MessengerMAX diluted in OptiMEM was added to the transfection mixture and incubated at room temperature for 15 minutes. The resulting 100 μl transfection mixture was added dropwise and evenly to the corresponding well. gRNA targeting the exogenous BFP gene and repair template for introducing a gene coding for green fluorescent protein (GFP) into the HEK293-BFP cells were kindly provided by Dr. Joey Riepsaame and used as a positive control for HDR. The transfected cells were grown for three days prior to harvest.

4.2.3.2 Nucleofection of iPSC clones

Human SCA14 iPSCs were expanded under feeder-free conditions in mTeSR-1 coated with Matrigel as described previously (section 2.1.6). iPSCs were treated with 10 μM ROCK inhibitor in the absence of P/S to suppress apoptosis for 2 hours prior to transfection. The Neon Transfection System (Life Technologies) was used to transfect gRNAs and Cas9 nuclease-expressing plasmids into iPSCs. 100 μl of the reaction mixture containing $3x10^6$ iPSCs, a total of 15 μg of the appropriate plasmids and repair templates in 150 μl buffer R were transfected using the HiTrans settings (1400V, 20ms, 1 pulse) of the Neon system. A dsRED plasmid was kindly provided by Dr. Sally Cowley and used as transfection control. The transfected iPSCs were then transferred to Matrigel-coated 24-well plates containing 500 μl prewarmed mTeSR supplemented with 10 μM ROCK inhibitor per well. The transfected iPSCs were fed daily and grown for 48 hours prior to puromycin selection.

4.2.4 Transient Puromycin-selection and expansion of iPSC clones

Puromycin was added to the transfected iPSCs at four different concentrations: 0, 0.1, 0.2 and 0.5 μg/ml to determine the optimal concentration of puromycin. Full replacement of mTeSR containing puromycin and P/S was performed daily for three days. $5x10^4$ of the selected iPSCs were plated onto 10-cm dishes the day before with MEFs and maintained in KOSR medium with daily replacement of half of the medium for around one week. The remaining selected iPSCs were pooled and harvested for high resolution melt (HRM) analysis.

Colonies of selected iPSCs grown on MEFs were manually picked and transferred to Matrigel-coated 96-well plates and maintained in mTeSR-1 supplemented with 10 μM ROCK inhibitor and P/S. iPSC clones were expanded onto three 96-well plates for expansion, cryopreservation and genomic DNA analysis.

4.2.5 Screening of modified iPSC clones

4.2.5.1 Extraction of genomic DNA

The transfected HEK293T cells were harvested in 200 μl squishing buffer [10 mM Tris pH=8.0, 1 mM EDTA, 25 mM NaCl and 200 μg/ml Proteinase K (Thermo Fisher Scientific)]. The lysed cells were subsequently incubated at 65 ºC for 30 minutes and then at 95ºC for 2 minutes to inactivate Proteinase K. The crude genomic DNA was used for subsequent HRM analysis and T7 assay.

The transfected HEK293-BFP cells were detached with TrypLE Express, washed once with PBS and lysed in 500 μl lysis buffer [100 mM Tris pH=8.0, 5 mM EDTA, 200 mM NaCl, 0.2% SDS (BioRad) and 100 μg/ml Proteinase K (Roche)]. The lysate was incubated overnight at 55ºC followed by heat inactivation of Proteinase K at 95ºC for 10 minutes. DNA was

precipitated for 20 minutes in 500 µl ice-cold isopropanol (Sigma), washed twice in 1 ml ice-cold ethanol (Sigma) and resuspended in 200 µl Tris-EDTA (Integrated DNA Technologies) at 60ºC for 2 hours with agitation. All centrifugation steps were performed at 2,500 rpm for 5 minutes. The purified DNA was used for Sanger sequencing, TIDE analysis and T7 assay.

The transfected iPSCs in 96-well plates were rinsed once with PBS and lysed in 50 µl lysis buffer [10 mM Tris, pH=7.5, 10 mM EDTA, 10 mM NaCl, 0.25% Triton X-100 and 1 mg/ml Proteinase K (Sigma)] overnight at 55ºC. Genomic DNA was then precipitated in 100 µl ice-cold (-80ºC) precipitation solution (5 M NaCl in 100% ethanol) at room temperature for 2 hours, washed twice with 70% ethanol and air dried. The genomic DNA was subsequently resuspended in 50-100 µl nuclease-free water at 4ºC overnight and used for subsequent HRM analysis and T7 endonuclease assay.

4.2.5.2 High-resolution melt (HRM) analysis

Primers were designed to produce 100-250-nucleotide products spanning the presumed CRISPR cleavage sites (Table 4.5). PCR was performed with either Hotshot Diamond PCR mix (Clent Lifescience) with LCGreen plus dye (BioFire Diagnostics) in RotorGeneQ (Bassett et al., 2013) or Amplitaq Gold 360 Mastermix (Applied Biosystems) with LCGreen Plus (Idaho Technology via Clent Life Sciences) using the StepOnePlus Real-Time PCR System (Applied Biosystems). 2 µl genomic DNA, 5 µl PCR master mix, 1 µl LCGreen Plus, and 200 nM of each forward and reverse primers were mixed and cycled [95ºC 5 min., 45 cycles of (95ºC 20s, 60ºC 30s, 72ºC 30s), 95ºC 30s, 25ºC 30s, 10ºC ∞]. Thermal melt profiles were collected and analysed using the StepOnePlus software (Applied Biosystems).

Table 4-5 List of primers used to amplify fragments surrounding the CRISPR cleavage sites in exon 1 and exon 4 of the human *PRKCG* gene for HRM analysis.

Primer name	Sequence 5'-3'	PCR product size (bp)
Ex1_PRKCG_HRM_1F	TCTCCCTTCCACCTGTTTCC	234
Ex1_PRKCG_HRM_1R	CAGATGAAGTCGGTGCAGTG	
Ex1_PRKCG_HRM_5F	CCTGGTCCCTGCTACGTTTC	209
Ex1_PRKCG_HRM_5R	CCCTTCCCTCACCAGATGAA	
Ex4_PRKCG_HRM_1F	gagcaaggcaggaggaaaag	171
Ex4_PRKCG_HRM_1R	TAGAGGAGGGAGCCACAGT	

Capital letters indicate sequences within the exons while lower case letters represent sequences within the introns. bp: base pairs.

4.2.5.3 T7 endonuclease assays

PCR primers were designed to amplify 400-600 base pairs surrounding the CRISPR cleavage sites (Table 4.6) using the Expand High Fidelity PCR System (Roche). The resulting products were purified using the QIAquick PCR Purification Kit (Qiagen) following the manufacturer's protocol.

Table 4-6 List of primers used to amplify fragments surrounding the CRISPR cleavage sites in exon 1 and exon 4 of the human *PRKCG* and *TRPC3* genes respectively.

Primer name	Sequence 5'-3'	PCR product size (bp)
Ex1_PRKCG_seq_1F	TTCCCTGTGGCTCCTTTGAT	404
Ex1_PRKCG_seq_1R	ttccctggccatcctagaac	
Ex4_PRKCG_seq_1F	agagcacccattaccaacca	575
Ex4_PRKCG_seq_1R	TTCATCTCGCAGCctggag	
hTRPC3_1F	GTGGGTACAGGTAGAGGCAT	389
hTRPC3_1R	TCCTTCTGAAGCCTTCTCCTTC	

Capital letters indicate sequences within the exons while lower case letters represent sequences within the introns. bp: base pairs.

Cutting efficiency was assessed with T7 endonuclease I as follows: 400 ng purified PCR products were denatured and re-annealed to form heteroduplex DNA using a thermocycler (95^{o}C 5 min., 95-85^{o}C -2^{o}C/s, 85-25^{o}C -0.1^{o}C/s, 10^{o}C ∞). The heteroduplex DNA was digested with T7 endonuclease 1 (T7EI) (NEB) for 15 minutes at 37^{o}C followed by the addition of 2 µl

of 0.25 M EDTA to stop the reaction. The reaction products were then analysed on a 2.5% TBE agarose gel.

4.2.5.4 Detection of restriction digestion sites introduced

Purified PCR products prepared above were digested with the restriction enzymes ApoI (SCA14 mutations H36R and H101Q) and PflMI (SCA41 mutation R742H), respectively. The digested products were then analysed by electrophoresis in a 2.5% TBE agarose gel to assess the editing efficiency.

4.2.5.5 Tracking of Indels by Decomposition (TIDE) analysis

Purified PCR products prepared above were sent for Sanger sequencing. The resulting DNA sequences were analysed using Tracking of Indels by DEcomposition (TIDE) software to assess the editing efficiency (Brinkman et al., 2014).

4.3 Results

4.3.1 Producing isogenic controls for SCA14 iPSCs using a CRISPR plasmid approach

SCA14 is caused by point mutations in the human *PRKCG* gene. As described in the previous chapter, at least two iPSC clones were generated for each of the four SCA14 patients carrying two distinct missense mutations (H36R and H101Q) (summarised in Table 3.2). In order to generate isogenic controls for the SCA14 mutations, a DSB or a pair of nicks in the DNA in the proximity of the site where correction of mutation is desired is needed for DNA repair to take place. Therefore, sgRNAs and repair donor templates that target the H36R and H101Q SCA14 mutations in exon 1 and exon 4 respectively were designed and subcloned into CRISPR vectors that contain sequences for Cas9 nuclease expression. Co-transfection of plasmids that contain sequences for the expression of sgRNAs and Cas9 proteins using nucleofection was used to introduce sgRNAs and Cas9 nuclease into SCA14 iPSCs. Since the presence of repair donor templates facilitates DNA repair by HDR, a repair donor in the form of a single-stranded DNA oligonucleotide was designed and co-transfected into iPSCs.

Figure 4.2 Procedures for producing isogenic controls.

1. Obtain the sequence of patient iPSC lines by Sanger sequencing
2. Design gRNAs and repair template
3. Cloning of gRNAs into Cas9-expressing vectors
4. Preliminary test of targeting efficiency of gRNA- and Cas9-expressing vectors in HEK293T cells using HRM analysis and T7assay
5. Nucleofection of gRNAs into gRNA- and Cas9-expressing vectors together with repair template into patient iPSCs
6. Screening of gene correction:
    i. HRM analysis
    ii. PCR & restriction digestion
    iii. Sanger sequencing
7. Expand the edited iPSC clone
8. Quality control tests:
    i. Karyotyping
    ii. Mycoplasma test

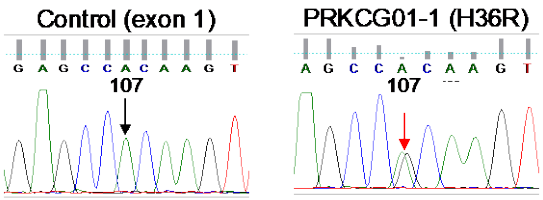
4.3.1.1 Design of gRNAs and repair donor templates for producing isogenic controls for SCA14 iPSCs

The experimental design was based on using the HDR, which is part of the natural DNA damage repair mechanisms after Cas9 endonuclease generates DNA damage sites. Cas9 is guided to the target sequence by a gRNA and cuts the DNA three bases upstream of a PAM sequence, activating the repair machinery. By providing a DNA repair donor template containing the desired edit, the mutation is introduced into the DNA (Ran et al., 2013b). HDR targeting efficiencies drastically reduce as the distance between the DNA break and the desired site of modification increases. Also, the highest targeting frequencies were observed when the mutation is within ten bases of the cleavage site (Byrne et al., 2015; Chen et al., 2013; Yang et al., 2014). The closest possible CRISPR cleavage sites to the intended mutations were therefore chosen in this study. Mismatches between gRNA, repair donor and target sequence would greatly reduce the efficiency and precision of genomic modifications. Thus, knowledge of the DNA sequence of the iPSC line to be edited was required for the design of gRNAs and repair donor templates. Therefore, genomic DNA sequences of around 200-300 bp around the corresponding SCA14 mutations were first obtained by Sanger sequencing of human SCA14 iPSCs (Fig. 3.6, 4.3A & B). In order to correct the SCA14 mutations, a reversal of guanine (mutant) to adenine (wildtype) was intended for H36R while a guanine (mutant) to cytosine (wildtype) change was desired for H101Q (Fig. 4.3C). PAM sequence 3’ NGG around the region of the corresponding mutations were identified because this PAM is better recognised by SpCas9 than 3’ NAG. Although testing of more than one design of gRNA was recommended to search for the most efficient one, due to the limited availability of PAM sequence 3’ NGG within the 20 bp regions around the mutations only one best-fitted gRNA for each SCA14 mutation for wildtype SpCas9 was selected (Fig. 4.4 A & B). Instead, several Cas9 species were tested to compensate for the limited choice of PAM sites for SpCas9 (described below).

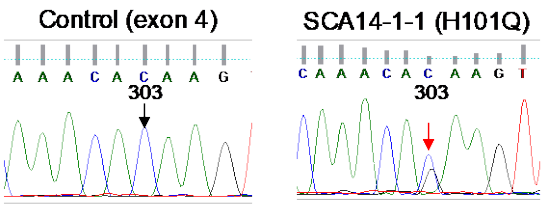
Figure 4.3 The genotypes and the intended corrections of the SCA14 mutations H36R and H101Q.

(A) Sanger sequences of exon 1 showed that the wildtype nucleotide was an A while the H36R was a heterozygous dominant mutation A/G at nucleotide position 107. (B) Sanger sequences of exon 4 showed that control iPSCs contained the wildtype nucleotide C while the H101Q mutant harbours a heterozygous dominant mutation C/G at position 303. (C) In order to correct the mutations back to the wildtype genotypes, a G-to-A change in the mutant allele is intended for H36R whilst a G-to-C change in the mutant allele is desired for H101Q.

A



B



C

Mutations	WT	Mutant	Intended nucleobase change
H36R	A	G	G > A
H101Q	C	G	G > C

Unmodified wildtype Cas9 generates DSBs in DNA when guided to the target site by a single gRNA. However, multiple mismatches between the gRNA and its complementary target DNA sequence can be tolerated using this Cas9, depending on the quantity, position, and base identity of mismatches (Cong et al., 2013; Fu et al., 2013; Hsu et al., 2014; Jiang et al., 2013; Ran et al., 2013a). This may lead to formation of unwanted DSBs and indels, also known as off-target effects. In order to improve the specificity of the modifications, SpCas9n, which only generates site-specific DSBs a pair of nicks when guided by a pair of offset gRNAs complementary to opposite strands of the target site (Cong et al., 2013; Gasiunas et al., 2012; Jinek et al., 2013) was also tested in this study. Two gRNA pairs were designed for each SCA14 mutation surrounding the intended sites of modification for SpCas9n (Fig. 4.4A & B). PAM sequences 3'NGG and NAG were used to maximise the gRNA pairs to test. Both gRNA pairs have offsets of less than 15 bp between ends of gRNA pairs to obtain optimal cutting efficiency of SpCas9n (Ran et al., 2013a).

As the number of potential gRNAs to test was limited by the availability of PAM sequences of SpCas9 around the SCA14 mutations, gRNAs were also designed to use with another species of Cas9, SaCas9. This Cas9 requires the PAM sequences 3' NNGRRT or NNGRR(N) (R=A/G). One gRNA for each SCA14 mutation was selected for SaCas9 (Fig. 4.4 A & B).

A



B



Figure 4.4 Design of gRNAs, DNA repair template and primers for correcting the SCA14 mutations.

(A) CRISPR design for H36R in exon 1 of the *PRKCG* gene. DNA sequence of the patient iPSCs containing the H36R point mutation (red) is shown. gRNAs are designed to cover the mutation. gRNA for SpCas9 is in blue, gRNA pairs for SpCas9n are in green and that for SaCas9 is in black. The forward and reverse DNA repair templates include the wildtype nucleotide A and an additional silent mutation to destroy the PAM sequence at the centre that flanked by two homology arms. The additional silent mutation creates an ApoI restriction site for assessment of successful edit. Primers used for amplification of this region are in orange. (B) CRISPR design for H101Q in exon 4 of the *PRKCG* gene. DNA sequence of the patient iPSCs containing the H101Q point mutation (red) is shown. gRNAs are designed to cover the mutation. gRNA for SpCas9 is in blue, gRNA pairs for SpCas9n are in red and that for SaCas9 is in black. The forward and reverse DNA repair templates include the wildtype nucleotide C and an additional silent mutation to destroy the PAM sequence at the centre that is flanked by two homology arms. The additional silent mutation provides an ApoI restriction site for edit screening. Primers used for amplification of this region are in orange. WT: wildtype allele; M: mutant allele; F: forward; R: reverse; Seq: primers for Sanger sequencing. HRM: primers for HRM analysis.

All crRNA sequences chosen showed less than three mismatches with regions other than the target sequences in the human genome as determined using the CRISPR design tool and Primer BLAST software. Moreover, none of the mismatches was located in the 3' end of the crRNAs,

which might reduce their binding to the target sequences, as calculated by the CRISPR design tool. Table 4.7 summarises the gRNAs designed and tested at this stage of the study.

Table 4-7 List of gRNAs targeting SCA14 mutations designed and tested.

Exon	Mutation	Type	PAM sequence	Target sequence	gRNAs (5'-3') + PAM
1	H36R (A>G)	WT SpCas9	NGG	20nt	ACTTGCGGCTCTTGACTTCGTGG
		SpCas9n	NGG or NAG	20nt	TCCACGAAGTCAAGAGCCGCAAG + GAGCCCCCTTTCTGCAAAACAGG
		WT SaCas9	NNGRR (R=A/G)	21nt	GAACTTGCGGCTCTTGACTTCGTGGA
4	H101Q (C>G)	WT SpCas9	NGG	20nt	GGAACTTCTGTTTGTTCCGGGGG
		SpCas9n	NGG or NAG	20nt	agGACCCCCGGAACAAACACAAG + gcagagaagactggcttagggcg or agGACCCCCGGAACAAACACAAG + aagactggcttagggggcgttgg
		WT SaCas9	NNGRR (R=A/G)	21nt	AGGCGGAACTTCTGTTTGTTCCGGGG

Single stranded DNA oligonucleotides have been shown to be more efficient for HDR of small modifications (less than 50 bp) than a plasmid-based repair donor (Song and Stieger, 2017; Yang et al., 2013a) and were therefore used in this study. Templates of 100 bp in total, with around 50-bp homology arms on either side of the corresponding SCA14 mutation were used. The insertion site was within 20 bp away from all the predicted CRISPR cut sites to enhance HDR efficiency. In order to avoid re-modification of any successful DNA editing, the repair donor templates included an additional nucleotide guanine to adenine change at the PAM sequence that gave rise to a silent mutation. This silent mutation also created a restriction digestion site (R^AATT_Y) recognised by the restriction enzyme ApoI, which was used as a screening method for the successful correction of the mutation (Fig. 4.4 & 4.8).

4.3.1.2 Preparation of constructs

The oligonucelotides listed in Table 4.3 were annealed and inserted into the linearized Cas9 nuclease-expressing vectors (Fig. 4.5). Sanger sequencing confirmed the correct insertion of

the crRNA sequences into the plasmid. The validated constructs were used for the subsequent testing of cutting efficiency in HEK293T cells. Table 4.8 shows a list of constructs prepared at this stage.

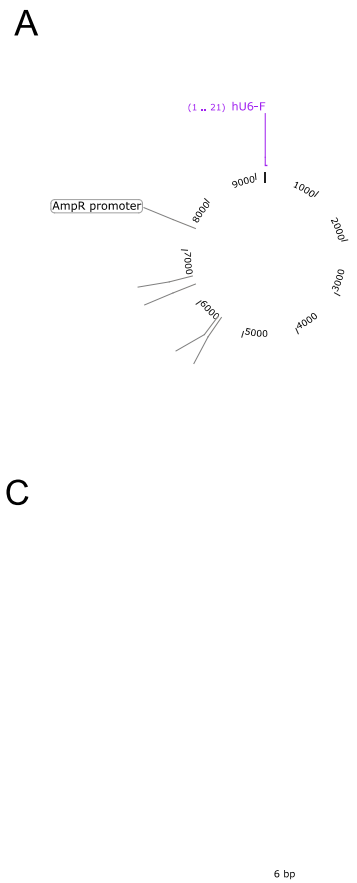


Figure 4.5 Cloning strategy of gRNA- and Cas9-expressing plasmids.

(A) Construct of pX459 expressing WT SpCas9. Annealed oligos were inserted between BbsI restriction sites. (B) Construct of pX462 expressing SpCas9n. Annealed oligos were inserted between BbsI restriction sites. (C) Construct of pX601 expressing SaCas9. Annealed oligos were inserted between BsaI restriction sites. Plasmid maps were generated with SnapGene Viewer software. Sanger sequencing verified the presence of the inserted oligos.

Table 4-8 List of gRNA- and Cas9- expressing constructs that were generated.

Construct number	Name	crRNA sequence (5'-3')
1	Ex1_M_SpCas9_1	CTTGCGGCTCTTGACTTCG
2	Ex4_M_SpCas9_1	GAACTTCTGTTTGTTCCGG
3	Ex1_WT_SpCas9n_1	CCACGAAGTCAAGAGCCAC
4	Ex1_WT_SpCas9n_1c	AGCCCCCTTTCTGCAAAAC
8	Ex1_M_SaCas9_1	AACTTGCGGCTCTTGACTT
9	Ex4_M_SaCas9_2	GGCGGAACTTCTGTTTGTT
10	Ex1_WT_SpCas9_1	CTTGTGGCTCTTGACTTCG
11	Ex4_WT_SpCas9_1	GAACTTGTGTTTGTTCCGG
13	Ex1_M_SpCas9n_1c	AGCCCCCTTTCTGCAAAAC
17	Ex1_WT_SaCas9_1	AACTTGTGGCTCTTGACTT
18	Ex4_WT_SaCas9_2	GGCGGAACTTGTGTTTGTT
19	Ex4_WT_SpCas9n_1T	CGACCCCCGGAACAAACAC
20	Ex4_SpCas9n_1d	CCAGCGCCTGGACACTCGA
21	Ex4_SpCas9n_1e	GGGGGCCCTTCCCAGCGCC
22	Ex4_ M_SpCas9n_1T	CGACCCCCGGAACAAACAG
23	Ex1_M_SpCas9n_1	CCACGAAGTCAAGAGCCGC

4.3.2 Assessing the targeting efficiency of gRNAs in HEK293T cells

Since the HEK293T cells used for assessing the targeting efficiency of gRNAs contain the wildtype genotypes, oligonucelotides targeting the corresponding wildtype nucleotide for each mutation were used in the initial test in HEK293T cells. In contrast, patient iPSCs contain a wildtype and a mutant *PRKCG* allele. To determine whether gRNAs that were supposed to only target the mutation would also target the wildtype allele when expressed in the patient iPSCs, constructs containing gRNAs targeting the mutations were also included in the initial test in HEK293T cells. The constructs prepared were transfected into HEK293T cells. EGFP was used as a transfection control to estimate the transfection efficiency (Fig. 4.6A). Approximately 66.52±5.52% of HEK293T cells were positive for EGFP.

Genomic DNA was extracted from the transfected HEK293T cells three days post transfection. Indels were expected to be present if cells repaired the DSBs in DNA created by Cas9 nuclease using NHEJ. To test for the presence of indels, fragments around the Cas9 cut sites were

amplified and run through HRM analysis to detect the changes of melting temperature resulting from change of sizes in the amplified regions. Untransfected cells and those transfected with the EGFP plasmid were used as unmodified controls and were expected to show no changes in melting temperature. gRNAs designed to be used with SaCas9 did not show changes in melting temperature (data not shown), i.e. no indels were produced, and were therefore omitted from the subsequent analyses and experiments. All gRNAs, targeting the wildtype or mutated alleles, designed for SpCas9 and SpCas9n resulted in a shift of melting curves representing decreases in melting temperature caused by deletions of various sizes (Fig. 4.6B). This suggests that the gRNAs targeting the mutations might also cut the wildtype allele when transfected into patient iPSCs. In order to further quantify the targeting efficiency of the gRNAs, a T7 assay that assessed the proportion of indels present was performed. Fragments surrounding the predicted cut sites were amplified by PCR and re-annealed. The re-annealed products were then incubated with T7EI that recognised and cleaved non-perfectly matched DNA. The DNA fragments corresponding to the non-cleaved and cleaved products were visualised by agarose gels (Fig. 4.6C & D). The intensity of the bands was quantified and the targeting efficiency was calculated. Table 4.9 summarises the conditions of the transfection as well as the results of the HRM analyses and T7 assay. In summary, the gRNAs for both exon 1 and 4 designed to use with either SpCas9 or SpCas9n produced indels efficiently, with targeting efficiencies ranging from 25-47% (Table 4.9). gRNA paired with SpCas9 produced relatively higher off-target effects compared to those used with SpCas9n (Table 4.9). As minimal off-target effect was desired, SpCas9n together with the most specific pair of gRNAs were selected for the generation of iPSC isogenic controls.

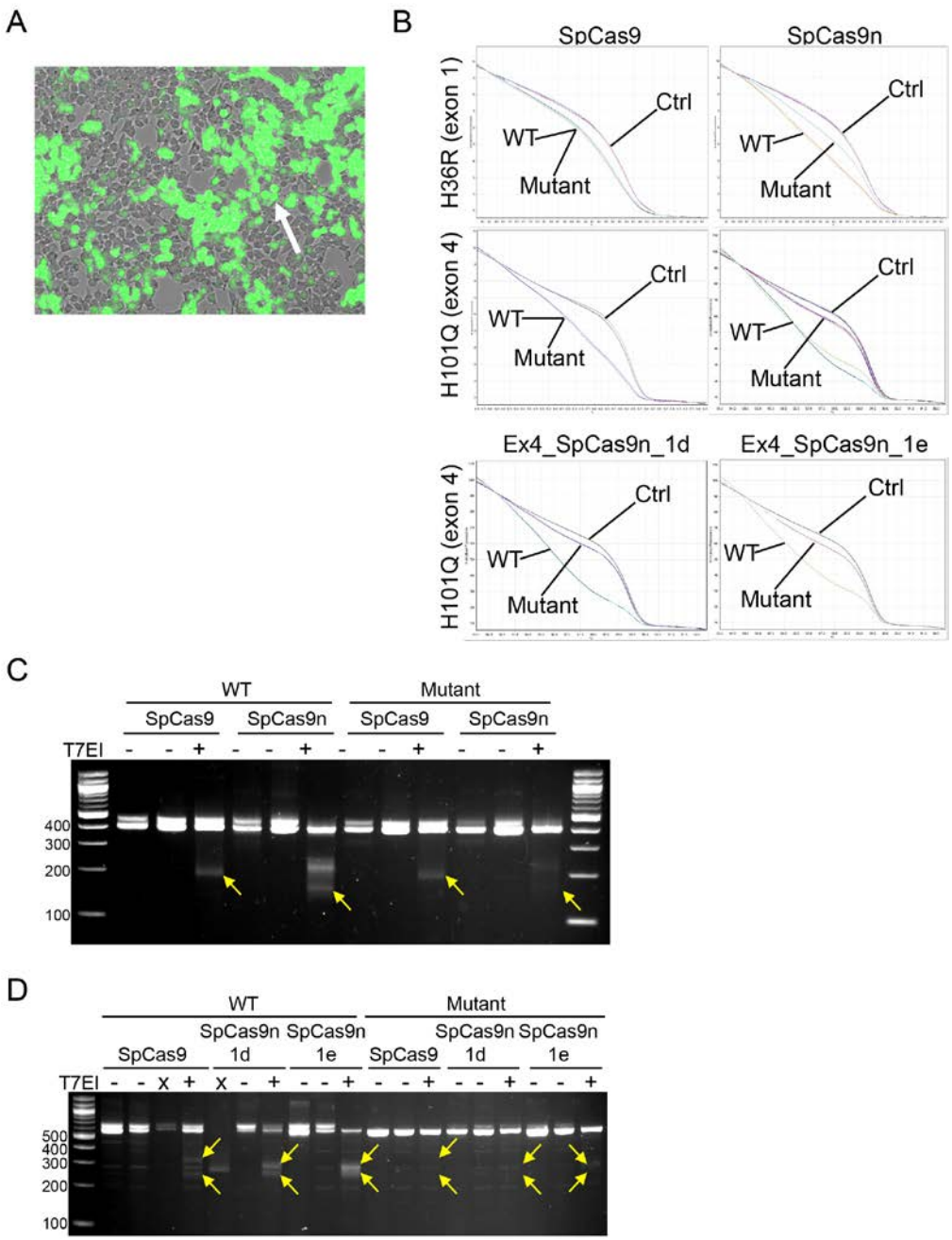


Figure 4.6 Combinations of WT SpCas9, SpCas9n and gRNAs produced indels as detected by HRM analysis and T7 assay.

(A) EGFP transfection control. Transfected HEK293T cells express EGFP (white arrow). (B) HRM analyses of different combinations of gRNAs and Cas9 nucleases targeting H36R and H101Q. All combinations of the gRNAs for SpCas9 and SpCas9n show leftward shift of melt curves compared to untransfected and EGP controls. Both gRNAs containing the wildtype (WT) or mutant (M) nucleotide produced deletions. T7 assay of different combinations of gRNAs and Cas9 nucleases targeting H36R (C) and H101Q (D). For each combination, samples in the absence or presence of T7EI were visualised on agarose gel. In the presence of T7EI, cleaved fragments of various intensities were detected (yellow arrows). gRNAs containing the wildtype nucleotides showed stronger bands that those containing the mutation.

Table 4-9 Summary of the transfection conditions and targeting efficiency of gRNAs tested in HEK293T cells using HRM analysis and T7 assay.

Transfection	Construct	gRNA1	gRNA2	Exon 1 HRM	Exon 4 HRM	Targeting efficiency from T7assay (%)
1	10	Ex1_WT_SpCas9_1		++	-	25.09
2	11	Ex4_WT_SpCas9_1		-	++	30.24
3	23+13	Ex1_WT_SpCas9n_1	Ex1_WT_SpCas9n_1c	+++	-	37.78
4	17	Ex1_WT_SaCas9_1		-	-	-
5	18	Ex4_WT_SaCas9_2		-	-	-
6	19+20	Ex4_WT_SpCas9n_1	Ex4_SpCas9n_1d	-	+++	44.42
7	19+21	Ex4_WT_SpCas9n_1	Ex4_SpCas9n_1e	-	+++	47.52
8	1	Ex1_M_SpCas9_1		++	-	28.36
9	2	Ex4_M_SpCas9_1		-	(+)	30.58
10	3+4	Ex1_M_SpCas9n_1	Ex1_M_SpCas9n_1c	+	-	28.71
11	8	Ex1_M_SaCas9_1		-	-	-
12	9	Ex4_M_SaCas9_2T		-	-	-
13	22+20	Ex4_M_SpCas9n_1T	Ex4_SpCas9n_1dT	-	+	31.35
14	22+21	Ex4_M_SpCas9n_1T	Ex4_SpCas9n_1e	-	+	29.14
15		pCAGG-EGFP		-	-	-
16		No transfection		-	-	0

Different combinations of gRNAs and Cas9 are listed. Results of HRM analyses were displayed as number of "+" positive or "-" negative. More "+" indicates higher targeting efficiency. The final column shows the targeting efficiency determined by the intensity of the bands visualized in Fig. 4.6C & D using this formula: (cleaved fragments)/(cleaved fragments + uncleaved bands)*100.

4.3.3 Producing an isogenic control for SCA14 H36R iPSCs

4.3.3.1 Nucleofection and puromycin selection of SCA14 iPSCs

Having chosen the most efficient pairs of gRNAs and SpCas9n, which showed fewer off-target effects, correction of the SCA14 mutations in patient iPSCs to produce isogenic controls was performed. Patient iPSC line PRKCG01-1 containing the SCA14 mutation (H36R) was used to optimise the genome editing procedures in iPSCs. SCA14 iPSCs were transfected with plasmids expressing the gRNA pair Ex1_M_SpCas9n_1 and Ex1_M_SpCas9n_1c (constructs number 3 and 4 in Table 4.8) as well as nuclease SpCas9n together with a forward or reverse repair donor (repair donor number 3 and 4 in Table 4.3) using nucleofection. A dsRED containing plasmid was used as the transfection control. The transfected iPSCs were plated onto 24-well plates and supplemented with ROCK inhibitor to suppress apoptosis. Patches of iPSCs were visible with some cell death one day post-transfection in all conditions (Fig. 4.7A). Two days after transfection, iPSCs expressed dsRED in the transfection control (Fig. 4.7B). The CRISPR constructs contained a puromycin-resistant gene. Therefore, a concentration gradient of puromycin was used to select for the iPSCs expressing the CRISPR plasmids starting from three days post-transfection for three days. iPSCs transfected with CRISPR plasmids and repair donors showed increasing cell death with increasing puromycin concentration (Fig. 4.7C). Three days after puromycin selection, the surviving cells treated with 0.2 or 0.5 μg/ml puromycin were pooled and replated on mouse feeder cells CF1 at low seeding density to allow colony growth from single cells. The cells transfected with forward or reverse donor were plated separately. The remaining cells were used for an initial estimation of editing. Colonies were visible three days after co-culture with CF1 (Fig. 4.7D) and manually picked when reaching desirable size. The colonies picked were grown in 96-well plates (Fig. 4.7E) for subsequent screening and expansion.

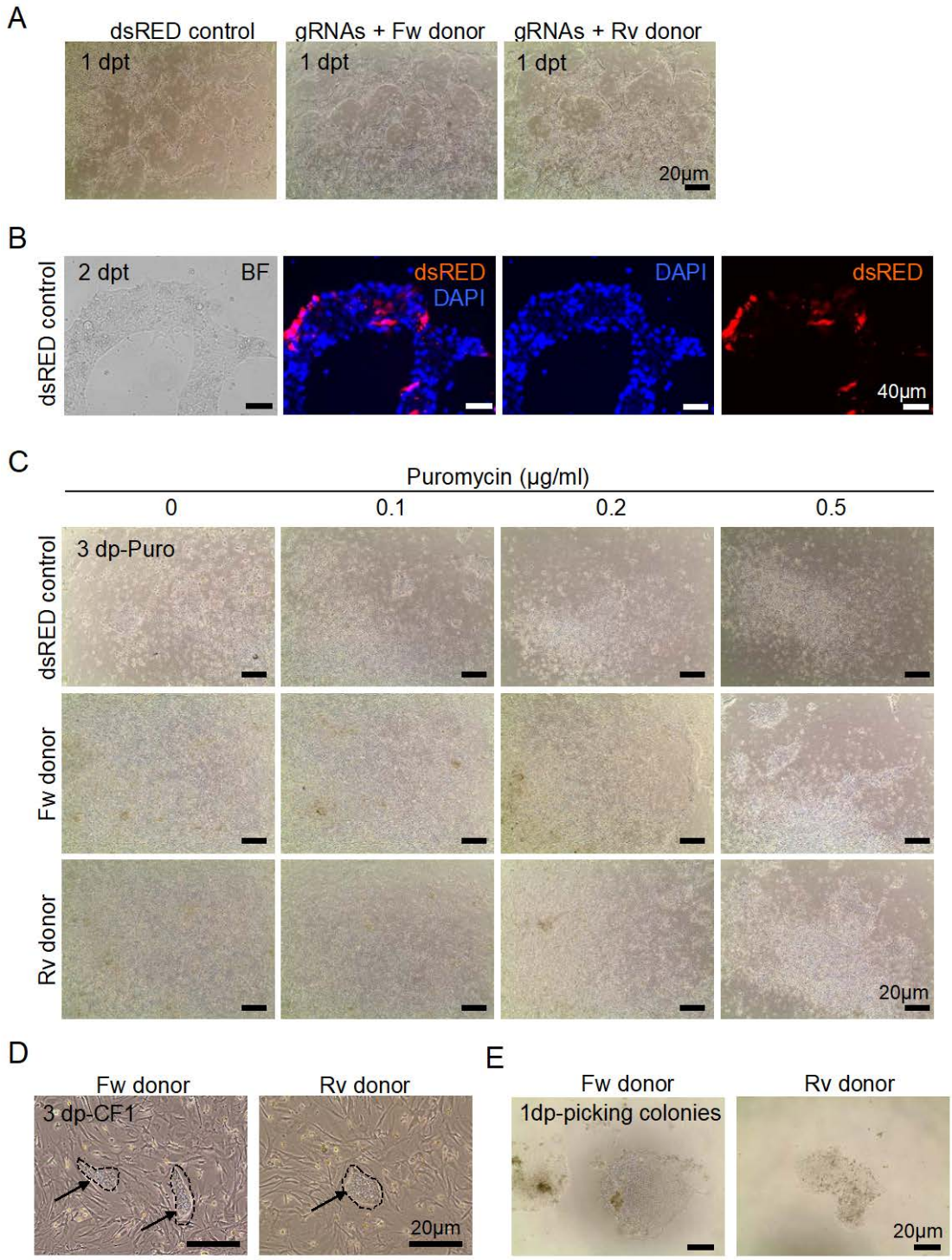


Figure 4.7 PRKCG01-1, a SCA14 iPSC line harbouring the H36R mutation, was transfected with gRNA- and SpCas9n-expressing plasmids using nucleofection and selected for puromycin-resistant cells.

(A) SCA14 iPSCs under different transfection condition showed similar amount of colonies and cell death at one day post transfection. (B) A proportion of SCA14 iPSCs transfected with dsRED as transfection control expressed dsRED two days after transfection. (C) Transfected iPSCs showed increasing cell death with increasing concentration of puromycin after three days of puromycin treatment. Most of the dsRED transfected cells died when treated with 0.2 and 0.5 μg/ml puromycin. iPSCs transfected with forward and reverse donors showed similar degrees of cell death at all concentration of puromycin used. The remaining cells treated with

0.2 and 0.5 μg/ml puromycin were pooled and plated on CF1 feeder cells at low seeding density. The genomic DNA of the unplated remaining cells was used to estimate the overall targeting efficiency using HRM analysis. (D) Colonies of Puromycin-selected iPSCs transfected with forward and reverse donors emerged from single cells after three days of co-culture with CF1 feeder cells (black arrows). Colonies are outlined with black dash lines. (E) Colonies were manually picked and seeded onto Matrigel-coated wells. Colonies at one day after plating on Matrigel are shown.

4.3.3.2 Screening of modified iPSC clones

To estimate the targeting efficiency of gRNAs in iPSCs, an HRM analysis was performed on the pooled cells after puromycin selection (Fig. 4.8A). Five outcomes were possible if Cas9-gRNA-repair donor ribonucleoprotein complexes were expressed, targeted to the target sequence and created DSBs in the transfected iPSCs. These possible outcomes included either correction or indels (Fig. 4.9A). The modifications would result in a change of melting temperature reflected as a shift in melting curves in HRM analysis. As the efficiency of HDR was much lower than NHEJ, the majority of the modifications were predicted to be indels that would lead to large shifts of melting curves. Cells transfected with the forward repair donor showed a larger leftward shift of melting curve than those transfected with the reverse donor, suggesting that the majority of the products in the forward donor-transfected cells were deletions (Fig. 4.8B).

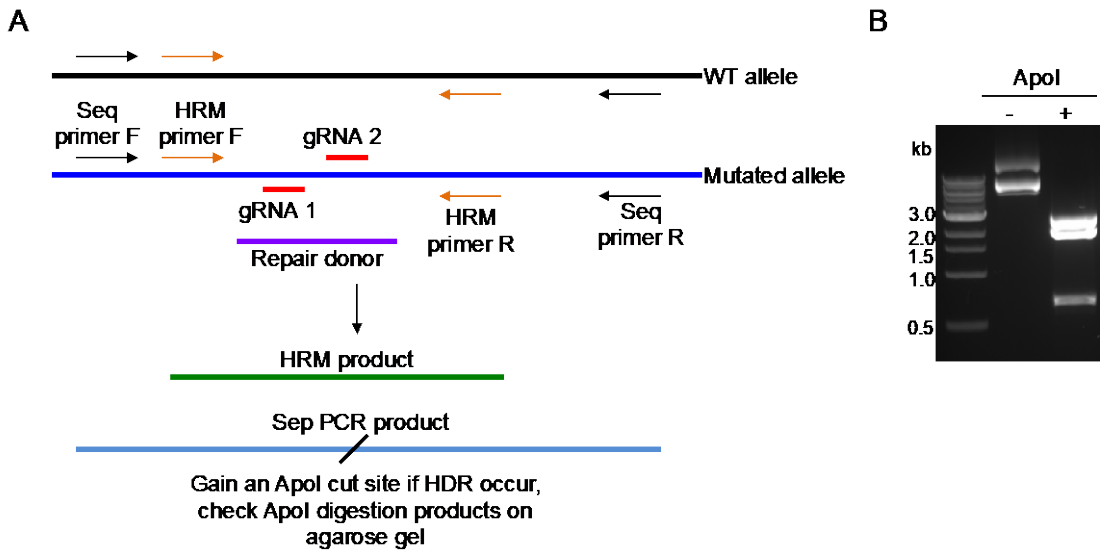
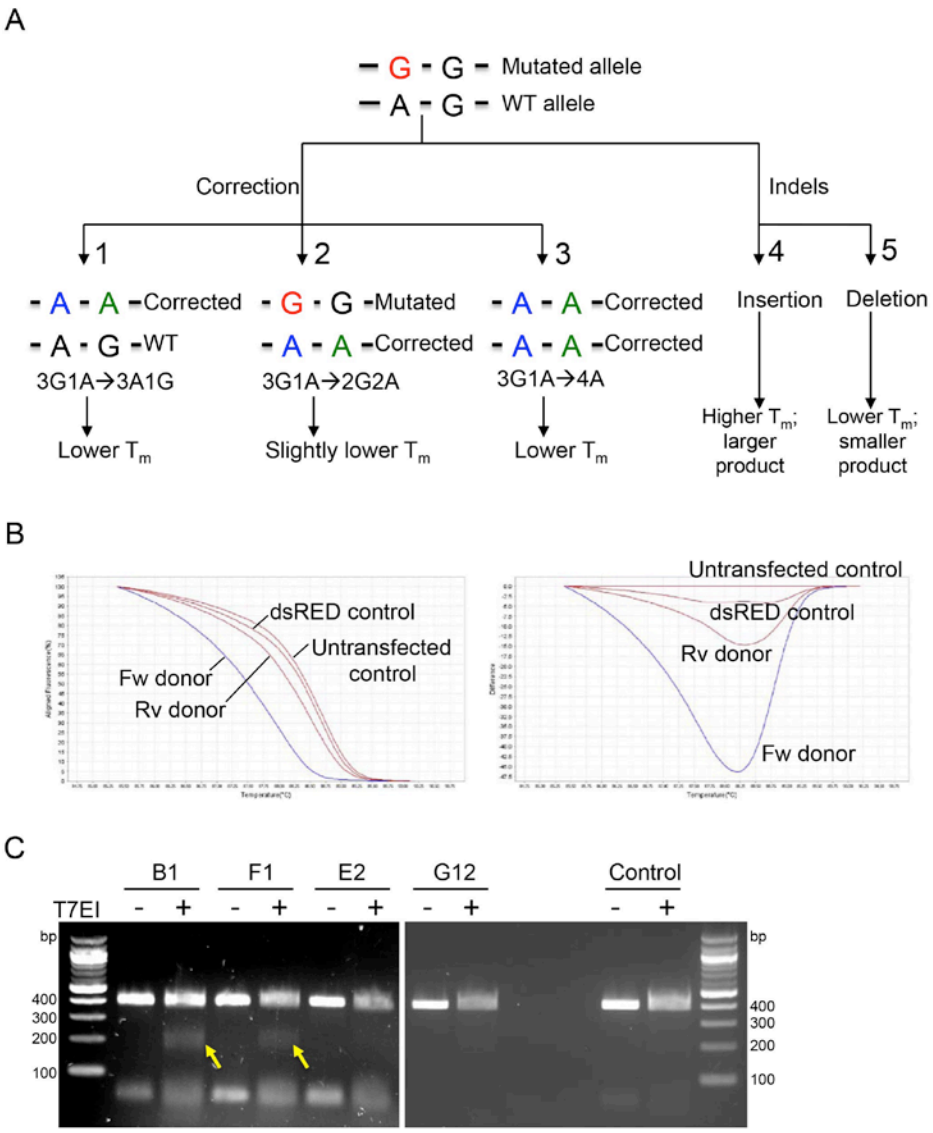


Figure 4.8 Schematic of the screening strategy for edited iPSC clones.

(A) A pair of gRNAs (red) guide SpCas9n to the target sequences in the mutated allele (blue). The double nicks created by the nickase in the DNA will be repaired by NHEJ or HDR if the repair donor is incorporated. This produces indels or point mutations, respectively. The HRM primers (orange) amplify fragments around that region. The melt curve profile is obtained by processing the HRM product (green). The sequencing primers (black) amplify fragments (light blue) for performing Sanger sequencing and ApoI restriction digestion. If edits are present, an ApoI restriction site will be gained and digested fragments of around 200 bp will be visualised by gel electrophoresis. (B) ApoI was confirmed to digest a control plasmid containing ApoI restriction sites in buffer identical to the condition used for digesting DNA extracted from iPSC clones.

HRM analyses were then performed on individual iPSC clones to identify the correction of mutations or the presence of indels. The clones that displayed relatively large leftward shifts were confirmed with T7 assays (Fig. 4.9C). The clones that showed small shifts and a change of shape of the melting curves (Fig. 4.9D) were screened with ApoI digestion to confirm successful editing. The digestion efficiency of the restriction enzyme ApoI in the digestion condition was confirmed beforehand using a plasmid containing ApoI restriction sites (Fig. 4.8B). However, insertion of an ApoI restriction site was not detected in any of the selected clones (Fig. 4.9E). The small change of the melting temperature might be the result of small indels. Sanger sequencing confirmed the small deletions in one of the alleles in those clones (data not shown) but none of the deletions created a frameshift for a heterozygous knockout.



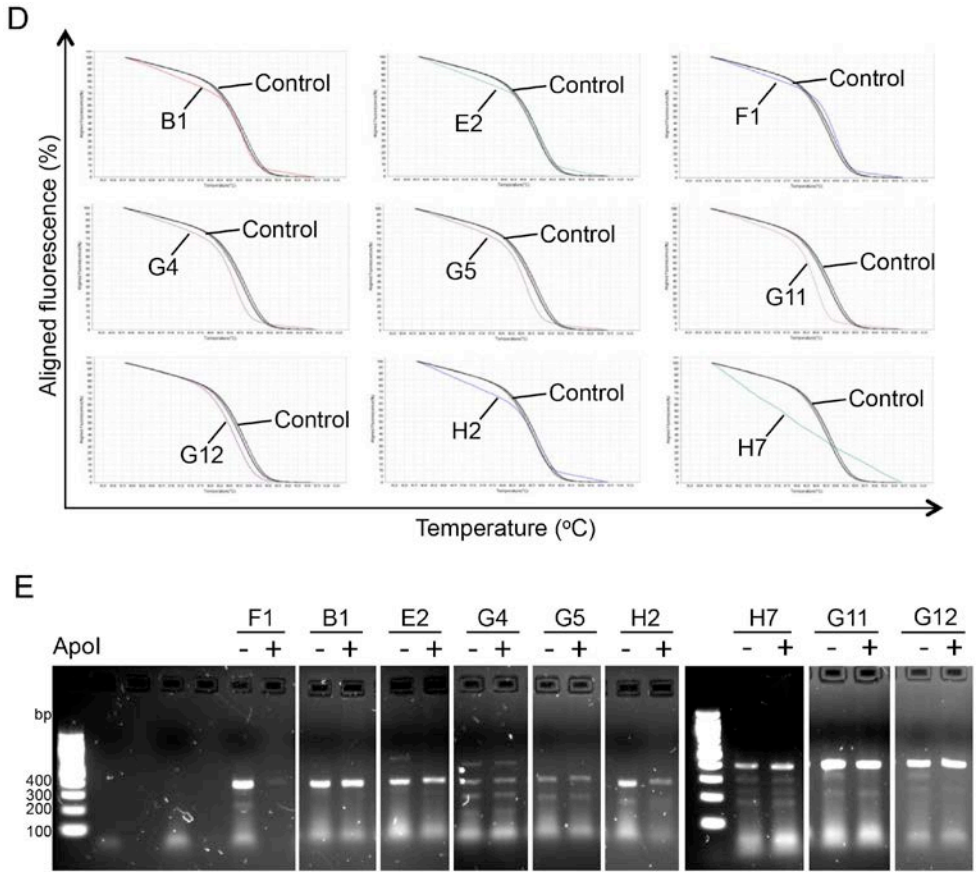


Figure 4.9 Deletions but no single nucleotide edits were detected in iPSCs clones transfected with both forward and reverse donors.

(A) Schematic showing the five possible outcomes detected by HRM analysis if double nicks were generated and repaired in genome DNA of SCA14 iPSCs (H36R). The patient mutation is shown in red, wildtype (WT) nucleotide after correction is in blue and the additional silent point mutation is in green. There would be three possible outcomes if point edits occured as a result of HDR: only the mutant allele was edited (outcome 1), only the WT allele was edited (outcome 2) or both alleles were edited (outcome 3). All three scenarios would result in a lower melting temperature of the PCR products. If NHEJ occured, insertions (outcome 4) or deletions (outcome 5) would lead to a different size of the PCR products and therefore higher or lower melting temperatures. (B) HRM analysis of the genomic DNA extracted from the pool of puromycin-selected iPSCs showed that those transfected with the forward donor led to larger melt curve shift than those transfected with the reverse donor. (C) Representative clones showed cleaved products of T7EI (yellow arrows) as shown by gel electrophoresis. Top bands represent re-annealed PCR products of around 400 bp amplified using the sequencing primers.

4.3.4 Producing isogenic controls for SCA41 R762H iPSCs using direct transfection of ribonucleoprotein complexes

The use of the plasmid approach did not yield a correction of the H36R mutation in SCA14 iPSCs in the previous section. This is consistent with reports in the literature that have described several drawbacks that limit the editing efficiency using plasmid-based editing methods

(Kouranova et al., 2016). Therefore, a different strategy was adopted to produce iPSC isogenic controls. In the past year, researchers have used direct delivery of Cas9-gRNA-repair template ribonucleoprotein (RNP) complexes into cells, which shows significantly increased editing efficiency (Kouranova et al., 2016).

In addition, several new Cas9 mutants have been created to reduce the off-target effects in addition to the previously described Cas9 nickases (Hess et al., 2017). Two Cas9 mutants that improve on-target specificity were developed independently around the same time. eSpCas9 contains a an alanine substitution in the HNH/RuvC groove of the WT SpCas9 that decrease the positive charge in the groove and therefore weakens interactions between the groove and the negatively charged DNA and destabilise basal strand separation (Slaymaker et al., 2016). Another Cas9 variant SpCas9-HF1 contains four mutations that disrupt interactions between Cas9 and the phosphate backbone of the target DNA strand (Kleinstiver et al., 2016).

This part of the study aimed to optimise Cas9 delivery, identify a Cas9 protein with the highest cutting efficiency yet least off-target effects, and compare the targeting efficiency of the gRNAs designed. For this proof-of-principle experiment, a patient iPSC line derived from a SCA41 patient carrying a heterozygous point mutation in the *TRPC3* gene (R762H) was used.

4.3.4.1 Design of the gRNAs and repair donors

The gRNAs and repair donors were designed by Miss Alexandra Soca, a Master student intern from Radboud University in The Netherlands working in our group at the time, with my guidance following the criteria described above. All the designs were then double-checked by Dr. Riepsaame.

To obtain the precise genomic DNA sequences for accurate designs of gRNAs and repair donors, DNA sequences of the region surrounding the R762H mutation in exon 9 of the *TRPC3* gene in the SCA41 patient iPSCs was determined using Sanger sequencing. The heterozygous disease mutation (G-to-A transversion) in exon 9 of the *TRPC3* gene was confirmed in these SCA41 iPSCs. No additional SNPs were identified in this region of the *TRPC3* gene in any of the patient iPSC lines (Fig. 4.9A). To produce an isogenic control, the mutated nucleotide A was intended to revert back to the wildtype G. To do this, three gRNAs were designed for eSpCas9 using the PAM sequence 5'-NGG-3' in the region near the mutation (crRNA number 24, 26 and 27 in Table 4.2) (Fig. 4.9B). One of the three gRNAs covers the mutation (crRNA number 26) and thus should be specific for the mutated allele. The other two gRNAs target regions close to the mutation and will therefore target both mutant and wildtype alleles. The targeting efficiency of the gRNAs designed was tested in HEK293-BFP cells, which contained the wildtype *TRPC3* DNA sequence as confirmed by Sanger sequencing (Fig. 4.10A).

An additional silent mutation (C-to-A) was included in the repair donor to create a PflMI restriction site. The amino acid compositional frequencies of the serine residues in proteins were checked to ensure that the silent mutation would occur at similar frequency as the wildtype sequence. As the additional mutation is in close proximity to the patient mutation, it is very likely that the two changes would be introduced simultaneously. This would allow the assessment of the repair efficiency using a PflMI restriction digest. PflMI digestion would give rise to fragments of approximately 140 and 250 bps in agarose gel electrophoresis if editing occurred (Fig. 4.10B).

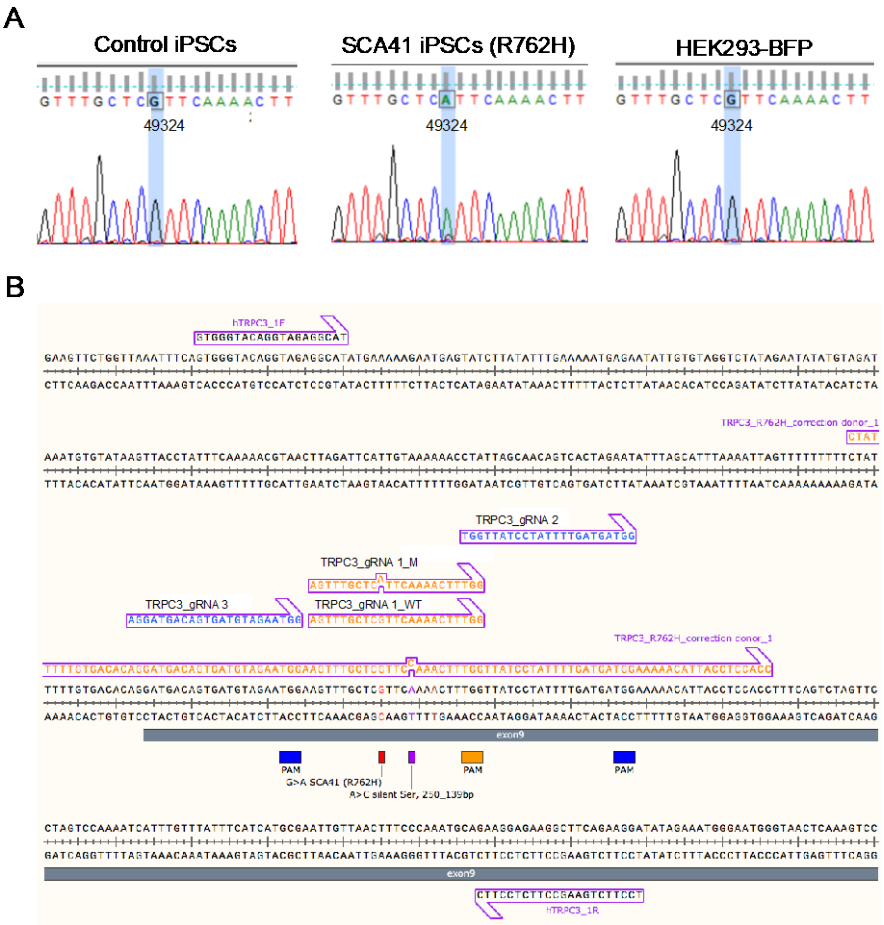


Figure 4.10 Genomic sequences of control iPSCs, SCA41 iPSCs and HEK293-BFP cells were obtained by Sanger sequencing and used for designing CRISPR strategies to correct the R762H mutation in SCA41 iPSCs.

(A) Sanger sequencing showed that control iPSCs and HEK293-BFP contained the WT nucleotide G, whereas all SCA41 iPSC clones were heterozygous (A/G) at position 49324 in the human *TRPC3* gene. (B) Regions of the *TRPC3* genomic DNA sequence close to exon 9 are shown. The WT nucleotide in red is mutated to an A in SCA41 iPSCs. TRPC3_gRNA 1_M and TRPC3_gRNA 1_WT cover sequences comprising the SCA41 (R762H) mutation (orange). TRPC3_gRNA 2 and TRPC3_gRNA 3 (blue) target WT sequences. PAM sequences of the gRNAs are highlighted. A silent mutation (purple) encoding a serine is included in the repair template to create a PflMI restriction site. TRPC3_gRNA 1_WT, TRPC3_gRNA 2 and TRPC3_gRNA 3 were tested in HEK293-BFP cells. Primers hTRPC3_1F & R amplify the region surrounding the SCA41 mutation (389 bp).

4.3.4.2 Testing targeting efficiency of gRNAs in HEK293-BFP cells

The targeting efficiency of gRNAs was first tested in HEK293-BFP cells. To select for the Cas9 protein that provides the highest targeting efficiency, three commercially available Cas9 proteins were tested. These included WT Cas9 and two variants with enhanced specificity: eSpCas9 and HIFI Cas9. Each Cas9 protein was tested with the three different gRNAs designed and therefore nine conditions were tested in total. A T7 assay was used to estimate the targeting efficiency of the different gRNAs. All conditions showed only the original band of the re-annealed PCR products suggesting that no cutting occurred (Fig. 4.11A). In order to confirm that the T7 endonuclease performed normally, the T7 assay were repeated and samples from previous experiments targeting a SCA14 mutation in the *PRKCG* gene, of which cutting was detected in previous T7 assays, were included (Fig. 4.11B). DNA fragments in the absence or presence of T7EI did not differ in the *TRPC3* experiment, whereas fragments cleaved by T7EI were detected in the *PRKCG* experiment. This suggests that the targeting efficiency of all gRNA-Cas9 combinations tested was either too low to be detected by gel electrophoresis or that no targeting had occurred.

Measuring the editing efficiency by PflMI digestion showed only one band with or without PflMI indicating that the restriction site was not inserted (Fig. 4.12A). Furthermore, the Sanger sequences of DNA extracted from cell pools of different conditions were assessed with TIDE software (Brinkman et al., 2014), a rapid method to search for indels and +1 insertions. The results confirmed that the editing was not successful for any of the three gRNAs tested (Fig. 4.12B), which was confirmed by manual checking of the sequences (Fig. 4.12C). Therefore, the gRNA-Cas9 combinations did not show satisfying targeting or editing efficiency.

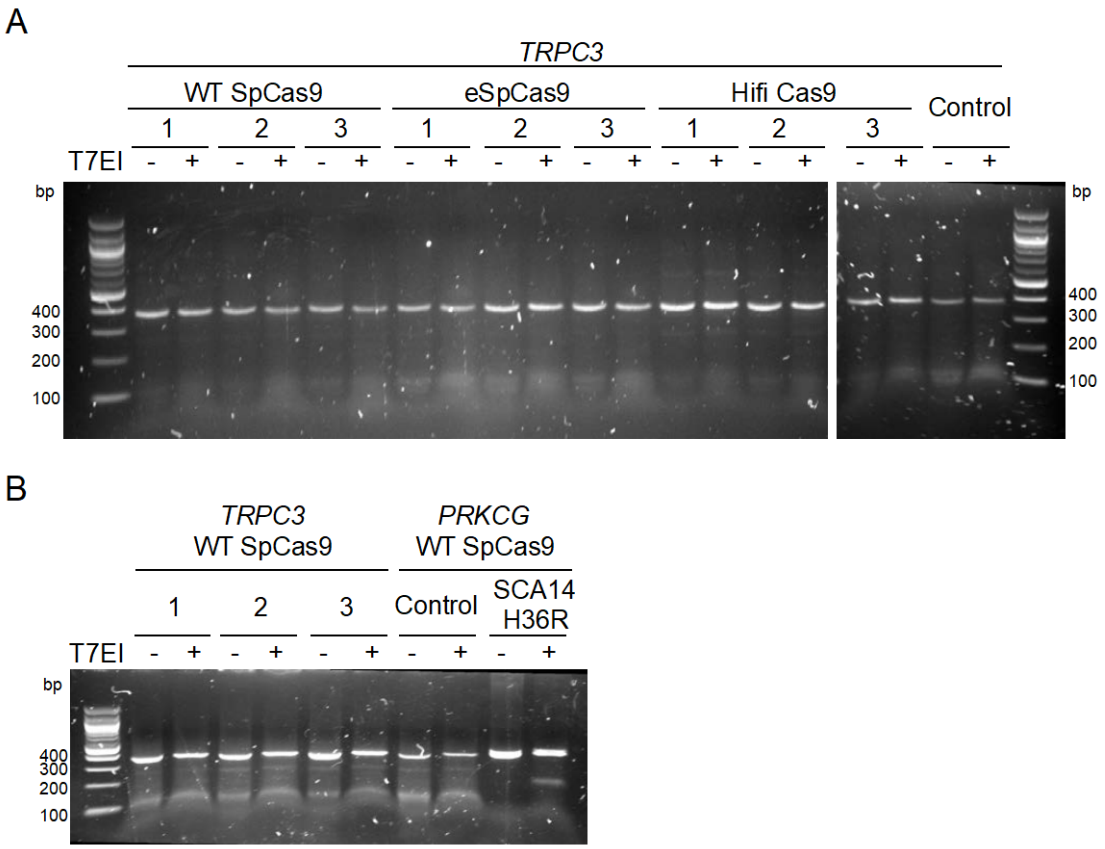


Figure 4.11 T7 assay showed that none of the gRNA-Cas9 combinations successfully produced indels.

(A) All gRNA-Cas9 combinations only showed the re-annealed band around 389 bp but no smaller fragments as a result of T7EI cleavage. (B) Similar results were obtained when the T7 assay was repeated. SCA14 H36R was included as positive control for the T7EI digest (right most lanes).

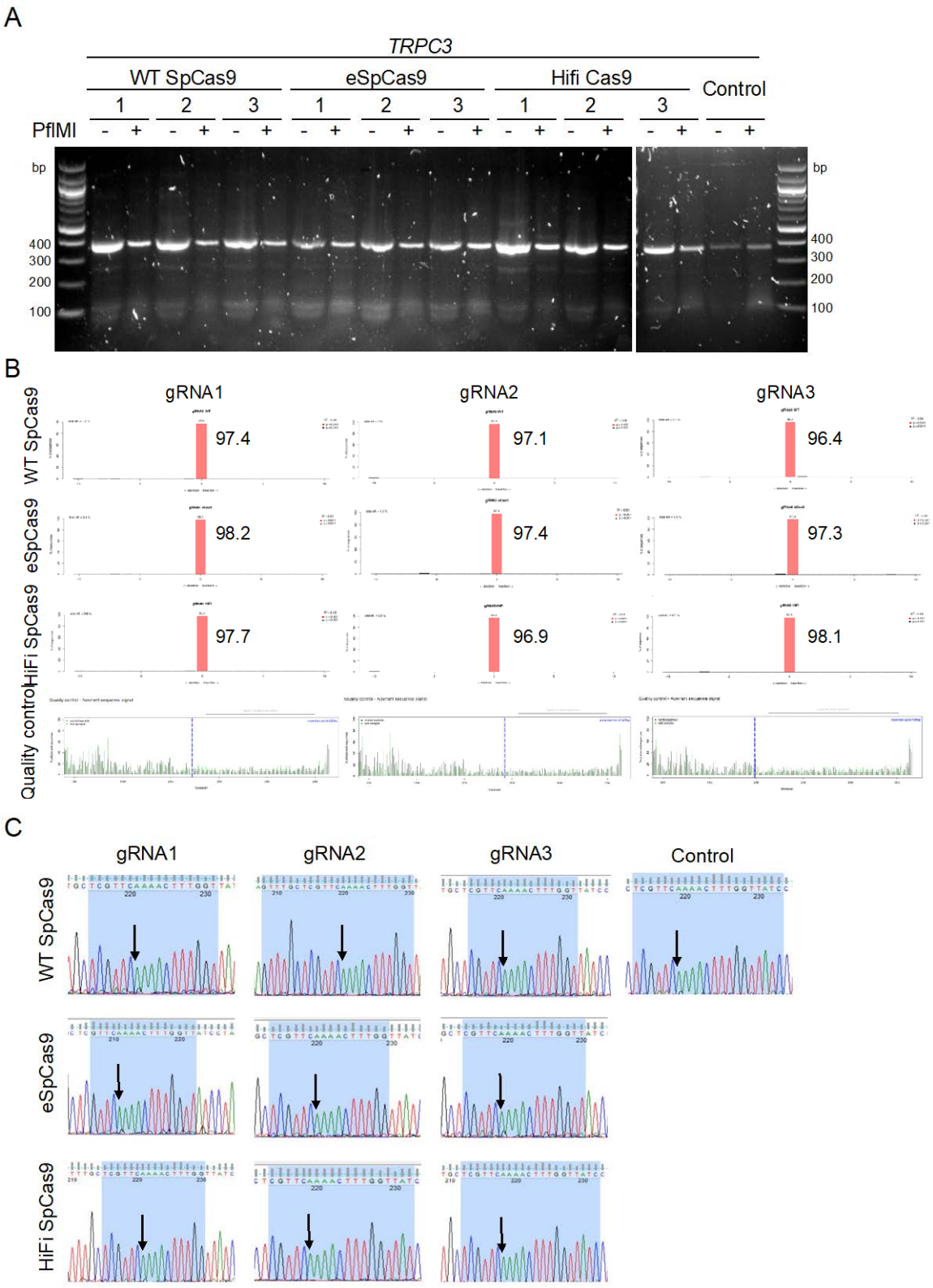


Figure 4.12 PflMI digestion, Sanger sequencing and TIDE analysis showed that none of the gRNA-Cas9 combinations resulted in the desired gene edits.

(A) All gRNA-Cas9 combinations showed only the undigested band around 389 bp but no smaller fragments as a result of PflMI, suggesting that the silent mutation that would have created a PflMI cut site is absent. (B) TIDE analysis confirmed that no indels or edits were generated. (C) Sanger sequencing results confirmed the original, un-edited genotype (black arrows).

4.4 Chapter Discussion

In the first part of this chapter, a plasmid approach was used to produce isogenic controls from patient iPSCs carrying the SCA14 mutations. Although combinations of gRNAs with WT SpCas9 or SpCas9n gave rise to satisfactory targeting efficiency in HEK293T cells, the correction of the patient mutations in SCA14 iPSCs was unsuccessful. Local concentrations of Cas9 protein and gRNAs are critical to nuclease activity (Kouranova et al., 2016). Therefore, the potentially non-simultaneous expression of gRNAs and Cas9 nuclease by separate gNRA-SpCas9n-expressing plasmids in iPSCs might adversely affect the production of double stranded breaks. To overcome this problem, a different approach for the introduction of gRNA, Cas9 protein and repair donor template was tested in the second part of this chapter. The direct delivery of RNPs has yielded increased editing efficiency in other studies compared to the plasmid approach (Kouranova et al., 2016). The targeting and editing efficiency of introducing a point mutation into the genome of HEK293-BFP cells using this method was therefore estimated. However, indels or point mutations were not detected using any of the gRNA-Cas9 combinations. This is likely due to suboptimal delivery conditions of the complexes, as more indels were to be expected if the complexes had entered the nuclei and were guided to the target sequence. Therefore, it would be interesting to test whether the RNP complexes could be delivered into HEK293-BFP or patient iPSCs more efficiently using a different transfection method in future studies. Nucleofection, which is a highly efficient transfection method, could be used.

An alternative explanation could be that the selected gRNAs were not efficiently guiding the complexes to the target sequence. Indeed, the repair template used in the TRPC3 experiments was in the same direction as the targeted strand that could be cleaved by the Cas9 proteins. This might destabilise the RNPs and thus reducing the targeting efficiency. In addition, this would also reduce the repair donor template available for HDR. Therefore, it would be interesting to determine whether an anti-sense single stranded repair template could enhance the efficiency

of editing (Fig. 4.13). At the same time, a more commonly used and better restriction enzyme HindIII could be used to screen edited clones. Moreover, the design of the gRNAs was based on the genomic DNA sequence of the patient iPSCs, which contain a mutation. However, the gRNAs tested in HEK293T cells contain a WT nucleotide and do not necessarily show equivalent efficiency as the gRNA containing a mutation. It might therefore be more appropriate to test the targeting efficiency of the gRNAs directly in patient iPSCs. In addition, efficiencies of HDR by single stranded oligonucelotides in human stem cells are generally low, ranging from 0.5-15% (Gonzalez et al., 2014; Yu et al., 2015), making precise genome editing in these cells challenging. To increase the efficiency of precise editing in iPSCs, small molecules such as STL127705, SCR7, L755507, Brefeldin A, NU7441 and NU7026 that has been shown to enhance HDR or inhibit NHEJ could be used to promote the edit of a point mutation (Greco et al., 2016; Maruyama et al., 2015; Riesenberg and Maricic, 2017; Yu et al., 2015; Zhang et al., 2017a).



Figure 4.13 Schematic of the revised design of CRISPR/Cas9 system for correcting the SCA41 (R762H) mutation in the *TRPC3* gene.

All features are the same as described in Fig. 4.9B except that an additional silent point mutation encoding lysine (brown) could be introduced to create a HindIII restriction site using repair donor 2, which is 70 nucleotide long.

Significant optimization of Cas9-mediated genome editing has allowed for single-nucleotide editing efficiencies reaching 60% or more in cell culture systems (Richardson et al., 2016). However, this strategy generally depends on the induction of a DSB; therefore, small indels are an unintended by-product, which can have major negative functional consequences if parts of targeted gene are deleted. In order to limit DNA damage during editing and eliminate the need to deliver an HDR donor template, a base editor could be used to correct point mutations (Gaudelli et al., 2017; Hess et al., 2017; Komor et al., 2016). The base editor is a fusion protein that contains a catalytically impaired Cas9 protein and a deaminase. Instead of creating a DSB, the cytosine base editor recruits Cas9 variants, cytidine deaminases, while the adenine base editor recruits adenine deaminase to introduce single-base changes. This strategy enables the direct and irreversible conversion of one base pair to another at the desired target site. For example, to correct the R762H SCA41 mutation in the *TRPC3* gene, an A-to-G change is needed. The catalytically impaired Cas9-containing fusion protein (base editor) is guided to the target sequence by a gRNA. The adenine deaminase then removes an amino group from the A in the non-targeted strand to form an inosine (I), which is read as a G by polymerase enzymes. The original A-T pair is then replaced with a G-C base pair at the target site following DNA repair or replication (Gaudelli et al., 2017). This strategy would allow for the generation of point mutations at C and G nucleotides with a low rate of indels, in contrast to HDR-based methods, which often generate more indels than substitutions. However, while it is possible to use baseeditor for C-to-T, A-to-G, T-to-C and G-to-A changes, it is still impossible to perform G-to-C, or A-to-T conversion at the moment. Moreover, the system enables editing at position 4-8 in the non-targeted strand that is around six nucleotides wide. This wide editing window might allow other A bases close to the target A to be edited inadvertently. In addition, off-target

effects might still arise in regions that are highly similar to the target sequence. Therefore, it is necessary to verify the lack of off-target mutations using methods such as deep sequencing and genome-wide, unbiased identification of DSBs enabled by sequencing (GUIDE-seq) no matter which genome editing approaches are used (Heigwer et al., 2014; Hendel et al., 2015; Tsai et al., 2015; Zhang et al., 2015). Nonetheless, the base-editing system promises to be extremely useful when any of these potential problems are addressed and when the remaining nucleotide substitutions will be available.

Once the genome editing conditions are optimised, it should be possible to carry out gene editing in SCA14 iPSCs. In addition, additional SCA14 mutations could be introduced into control iPSC lines, thereby expanding the spectrum of SCA14 mutations that could be tested. This will allow for the comparison of cellular phenotypes caused by various mutations, facilitating the dissection of the underlying pathogenic mechanisms and the development of therapies in a high-throughput fashion.

4.5 Conclusions

In this chapter, two different approaches to produce SCA14 iPSC isogenic controls were tested: plasmid and direct delivery of RNP complexes, respectively. Unfortunately, although gRNAs targeting SCA14 mutations worked efficiently in HEK293T cells, no correction was found in SCA14 iPSCs using the plasmid approach. Optimisation of the conditions for direct delivery of RNP complexes will be required to pursue this strategy in future CRISPR/Cas9 experiments for the generation of isogenic controls.

Chapter 5 SCA14 pathology in patient cerebellum and iPSCs

5.1 Introduction

Spinocerebellar ataxia type 14 (SCA14) is a late-onset autosomal dominant neurodegenerative disorder that is characterised by the progressive dysfunction and degeneration of Purkinje cells in the cerebellum. SCA14 patients usually display gait and limb incoordination, abnormal eye movement and slurred speech, accompanied by a range of other clinical symptoms (refer to section 1.4) (Chen et al., 2012a). Magnetic resonance imaging (MRI) reveals mild to moderate cerebellar atrophy in SCA14 patients (Fig. 1.7B) (Alonso et al., 2005; Hiramoto et al., 2006; Stevanin et al., 2004; Ueda et al., 2013; van de Warrenburg et al., 2003; Wedding et al., 2013). A loss of Purkinje cells was described in patient post-mortem cerebellum (Brkanac et al., 2002; Chen et al., 2003).

SCA14 is caused by mutations in the *PRKCG* gene coding for conventional protein kinase C gamma (PKCγ) (Chen et al., 2003), which is highly expressed in Purkinje cells (Huang, 1989; Kose et al., 1988; Saito et al., 1988). To date, 40 mutations have been identified throughout the coding region of *PRKCG*, of which the majority lie within the regulatory domain (Fig. 1.2) (refer to section 1.3.1). The regulatory domain contains sensors for diacylglycerol (DAG) (C1 domain) and calcium/phospholipid (C2 domain) that respond to second messengers and control the activation and membrane translocation of PKCγ. Similar to other isoforms of conventional PKCs, the regulatory domain of PKCγ is connected to a catalytic domain, connected by a hinge region (Fig. 1.2) (refer to section 1.4.2). The catalytic domain binds ATP and is responsible for the kinase function of PKCγ (Newton, 2003; Newton, 2010; Steinberg, 2008).

Phosphorylation status is central to the maturity, conformation, kinase activity and stability of PKCγ (refer to section 1.4.3) (Callender and Newton, 2017). PKCγ undergoes multiple

phosphorylation events to become mature and responsive to activation (Fig, 1.4). Newly synthesized PKCγ first moves to the plasma membrane in an open conformation, which enables the first phosphorylation at T514 in the activation loop. This is followed by two autophosphorylation events at the turn motif (T655) and the hydrophobic motif (T674). Once phosphorylated, PKCγ adopts a closed conformation. The resulting mature but inactive PKCγ is released from the plasma membrane. Binding of calcium to the C2 domain initiates the activation of PKCγ and induces the rapid translocation of PKCγ from the cytoplasm to the plasma membrane, where it interacts with phospholipids. This leads to the unmasking and exposure of the C1B subdomain, which is hidden when PKCγ is in its inactive state, and allow it to bind to DAG (Farah et al., 2012). PKCγ is further activated by the binding of DAG to the C1B subdomain via surface property changes without conformational changes (Newton, 2001; Zhang et al., 1995), resulting in the release of the pseudo-inhibitory substrate from the catalytic domain and an open (active) conformation (Newton, 2003; Newton, 2010; Steinberg, 2008). The conformation of the regulatory domain (Seki et al., 2005b) and phosphorylation at T655 (Jezierska et al., 2014) and T674 (Jezierska et al., 2014) are therefore important for the regulation of the intrinsic kinase activity and the affinity to the plasma membrane of PKCγ.

The C1 domain is composed of two structurally and functionally similar cysteine (Cys)-rich subdomains, C1A/Cys1 and C1B/Cys2, of which the latter is particularly vulnerable to mutations. Only a few mutations are found in the catalytic domain and C-terminal region of PKCγ (Fig. 1.2). In spite of the numerous gene mutations identified, the molecular disease mechanisms underlying SCA14 remain to be elucidated. The loss of PKCγ in homozygous knockout mice results only in mild ataxia without gross cerebellar degeneration (Abeliovich et al., 1993; Chen et al., 1995) (refer to section 1.3.1). Therefore, the cerebellar degeneration in SCA14 is likely to be caused by a toxic gain-of function effect, rather than loss of function, or a combination of both. Several major pathogenic mechanisms underlying SCA14 have been proposed, including protein aggregation, ubiquitin-proteasomal impairments and altered kinase

function (refer to section 1.6). However, overexpression studies in animals and cell lines often present conflicting cellular disease phenotypes, making a more complete understanding of SCA14 aetiology challenging. Thus, there is an urgent need for better disease models to understand the underlying pathogenic mechanisms. The recent advances in induced pluripotent stem cell (iPSC) technology have enabled the efficient reprogramming of somatic cells from patients into iPSCs (refer to Chapter 2) and thereby allowing the investigation of patient- and disease-specific mechanisms (Watson et al., 2015a; Wong et al., 2017).

The goal of this chapter was to investigate the disease mechanisms underlying SCA14 by employing human SCA14 post-mortem cerebellum and patient-derived iPSCs. A loss of Purkinje cells and dendritic anomaly in the remaining Purkinje cells was observed in the SCA14 cerebellum. These Purkinje cells contained massive cytoplasmic inclusions and displayed reduced membrane staining of PKCγ compared to controls. The molecular impacts of two SCA14 mutations (H36R and H101Q) on PKCγ function in patient iPSCs were investigated. Consistent with the aggregated PKCγ in SCA14 Purkinje cells, massive cytoplasmic aggregates of PKCγ were found in SCA14 iPSCs but not in control iPSCs. The phorbol ester-induced membrane translocation of these aggregated PKCγ was impaired compared to controls. Moreover, the degradation of these aggregates was ineffective leading to their accumulation in the cytoplasm. Finally, mutant PKCγ showed increased kinase activity and resulted in excessive phosphorylation of PKC substrates. Notably, similar autophagy impairments and increased kinase activity of PKCγ was observed in human SCA14 cerebellum. Overall, SCA14 iPSCs faithfully recapitulates patient cerebellar pathology. These results suggest that SCA14 is caused by three interconnected pathogenic mechanisms that include (1) reduced membrane targeting, (2) increased kinase activity and (3) accumulation of mutant PKCγ foci in the cytoplasm. This unique model is therefore an ideal tool to further investigate the molecular pathways underlying SCA14 and to develop effective therapies. Parts of the results presented in this chapter were included in a manuscript submitted to a peer-reviewed journal.

5.2 Specific Materials and Methods

5.2.1 Phorbol 12-myristate 13-acetate (PMA) and Phorbol 12,13-Dibutyrate (PDBu) treatment of iPSCs

Human iPSCs were grown in tissue culture treated 6-well plates coated with Matrigel in mTESR-1 medium as described in section 2.1.6. Human iPSCs were treated with 400nM phorbol 12-myristate 13-acetate (PMA) (R&D) or 200nM phorbol 12,13-dibutyrate (PDBu) (R&D) in PBS for 5, 10 and 15 minutes. Treated iPSCs were processed for immunostaining or SDS-PAGE immunoblotting analysis.

5.2.2 Preparation of cerebellar and cell lysates

40-60 mg of frozen human post-mortem cerebellar tissue from a SCA14 patient and three age-matched healthy donors were lysed in 400-600 µl cold Pierce Radio-Immunoprecipitation Assay (RIPA) buffer [25 mM Tris-HCl pH=7.6, 150 mM NaCl, 1% NP-40, 1% sodium deoxycholate, 0.1% sodium dodecyl sulphate (SDS)] (Thermo Fisher Scientific) containing 1x Complete Protease Inhibitor Cocktail (Roche) and 1x PhosSTOP Phosphatase Inhibitor Cocktail (Roche), and homogenized into suspension using a pre-chilled Dounce homogeniser on ice. The cerebellar lysate was incubated on ice for 10 minutes before centrifugation at maximum speed for 30 minutes at 4 ^{o}C. Human iPSCs grown in six-well plates were washed once with PBS and then lysed in 1 ml cold RIPA buffer on ice. iPSCs were scraped off the plate bottom using a cell scraper and transferred to a pre-cooled Eppendorf tube. iPSC lysate was incubated on ice for 10 minutes and subsequently centrifuged at 16100 x *g* for 20 minutes at 4 ^{o}C in a bench-top centrifuge. The supernatant was transferred to fresh pre-cooled Eppendorf tubes. A Bradford assay (Thermo Fisher Scientific) was performed to determine the protein concentration according to manufacturer's instructions. SDS-sample buffer [188 mM Tris pH=6.8, 30% glycerol, 1.5% SDS, 0.01% bromophenol blue (Sigma)] was added to the lysates,

boiled for 5 minutes and then cooled down to room temperature. The lysates were stored at -20 ^{o}C until further analysis. 50 µg of lysates were used in all polyacrylamide gel electrophoresis (SDS-PAGE) experiments unless specified. Donor information can be found in Fig. 1.8 & 3.2H.

5.2.3 Preparation of Triton-soluble supernatant and --insoluble pellets

Frozen human post-mortem cerebellar tissue was homogenised in 400-600 µl cold lysis buffer [20 mM Tris, pH=7.5, 5 mM ethylene glycol-bis(β-aminoethyl ether)-N,N,N',N'-tetraacetic acid (EGTA), 150 mM NaCl, 1x Complete Protease Inhibitor Cocktail and 1x PhosSTOP Phosphatase Inhibitor Cocktail] containing 1% Triton X-100 using a pre-chilled Dounce homogeniser on ice. PMA-treated iPSCs were harvested in 200 µl cold lysis buffer containing 1% Triton X-100. Tissue and cell lysates were incubated on ice for 10 minutes and then centrifuged for 30 minutes at 16100 x *g* at 4 ^{o}C. The supernatant was collected as Triton-soluble supernatant. The pellet was re-suspended in 50µl cold RIPA buffer (Triton-insoluble pellet) and sonicated at 10 µA for 10-20 seconds (Soniprep 150, MSE). The sonicated lysate was placed on ice immediately following sonication. A Bradford assay was performed on the soluble fraction to determine protein concentration. SDS-sample buffer was added to the lysates, boiled for 5 minutes and then cooled down to room temperature. Equal volumes of soluble and insoluble fractions were loaded for SDS-PAGE.

5.2.4 Dephosphorylation of proteins using Lambda phosphatase

Brain and cell lysates were prepared in RIPA buffer (see above) without phosphatase inhibitor and subsequently incubated with 1200 units of Lambda phosphatase (New England Biolabs) at 30 ^{o}C for 1-2 hours. Mock-treated controls (without phosphatase) were used to determine protein concentration using a Bradford assay. Samples were added with SDS sample buffer,

boiled for 5 minutes and stored at -20 ºC until further analysis. 50 µg of untreated sample and equal volume of phosphatase-treated sample were used for SDS-PAGE as described below.

5.2.5 SDS-PAGE and immunoblotting

Frozen lysates were re-boiled for 2 minutes and cooled down to room temperature. 50µg of lysates were loaded in each lane of 10% or 15% acrylamide gel [for 10% resolving gel: 30% acrylamide mix, 1.5 M Tris pH=8.8, 10% SDS, 10% ammonium sulphate (APS), 1% tetramethylethylenediamine (TEMED); for stacking gel: 30% acrylamide mix, 1 M Tris pH=6.8, 10% SDS, 10% APS, 1% TEMED]. SDS-PAGE was run at 100V for 20 minutes and then 140V for a further 40-60 minutes in SDS-running buffer (247.6 M Tris, 1.918 mM Glycine, 1% SDS). Proteins in the gel were then transferred onto a nitrocellulose or polyvinylidene fluoride (PVDF) membrane (GE Healthcare Life Sciences) at 250 mA for two hours in transfer buffer (247.6 M Tris, 1.918 mM Glycine, 20% methanol).

For separation of phosphorylated and non-phosphorylated proteins, pre-cast SuperSep Phos-tag™ acrylamide gel (Wako Pure Chemical Industries, Ltd) was used. SDS-PAGE was performed at 20 mA for 2 hours in SDS-running buffer. The acrylamide gel was then washed four times in transfer buffer containing 10 mmol/ml ethylenediaminetetraacetic acid (EDTA) for 10 minutes and subsequently rinsed in transfer buffer for 10 minutes before proceeding to wet transfer of proteins onto nitrocellulose membrane.

Blocking was done in TBST buffer [150 mM NaCl, 10 mM Tris pH=8.0, 0.05% Tween-20 (Bio-Rad)] containing 5% skim milk (Sigma) at room temperature for an hour. Membranes were incubated in primary antibodies in 3% BSA (Thermo Fisher Scientific) in TBS containing 0.1-0.5% Tween-20 at 4ºC overnight, and washed three times in TBST for 5 minutes. Membranes were subsequently incubated in horseradish peroxidase (HRP)-conjugated

secondary antibodies in 3%BSA/TBST at room temperature for two hours. Protein bands were visualised using ECL™ Western Blotting Detection Reagents (GE Healthcare Life Sciences) or SuperSignal West Femto Maximum Sensitivity Substrate (Thermo Fisher Scientific) and captured using ImageQuant LAS 4010 (GE Healthcare Life Sciences). Band intensity was quantified using ImageJ software.

Western blot analyses of Triton-X100-soluble supernatant and -insoluble pellets, and kinase activity of PKCγ in lysates of human cerebellar tissues were performed by Prof. Esther Becker.

5.2.6 Immunostaining

Treated iPSCs were fixed in 4% paraformaldehyde (PFA) at room temperature for 20 minutes or ice-cold methanol at -20 ºC for 15 minutes. Fixed cells were washed three times with phosphate buffered saline (PBS) (Sigma) for 5 minutes and stored in PBS containing 0.02% sodium azide at 4 ºC until further analysis or used for immunostaining immediately.

The fixed cells on glass coverslips were permeabilised with 0.4% Triton X-100 in PBS at room temperature for 20 minutes and then blocked for an hour at room temperature in blocking buffer [1% skim milk, 10% serum (Sigma) in TBST (150 mM NaCl, 10 mM Tris pH=8.0 and 0.02% Tween-20)]. The samples were incubated with primary antibodies diluted 3% BSA in TBST at 4 ºC overnight. The next day, samples were washed 3 x 5 minutes in PBS, incubated with secondary antibodies in 3% BSA in TBST for 2 hours at room temperature and then 5 minutes at room temperature in 20 µM Hoechst stain (Thermo Fisher Scientific). The coverslips were mounted onto slides using VECTASHIELD® Mounting medium (VECTOR laboratories). The cells were visualised under a confocal laser-scanned confocal microscope (Leica) using Leica Application Suite X (LAS X) software (Leica). A list of primary and secondary antibodies can be found in Table 2.2.

Immunohistochemistry of human cerebellar sections was performed by Prof. Olaf Ansorge.

5.2.7 Image quantification

Immunostained images were analysed using ImageJ plugins (http://imagej.nih.gov/ij). The size of puncta/foci was measured using Cell Counter plugin (ImageJ). The area of signals was measured using Threshold and Area Measurement. The co-localisation of labelled proteins was quantified using Just Another Colocalization Plugin (JACoP) (Bolte and CordeliÈRes, 2006).

5.2.8 Statistical analysis

For experiments using iPSCs, two clones for each of the four patient lines and two control lines were included (refer to Fig. 3.2H for donor information). All data are expressed as means of three independent experiments, i.e. for untreated iPSCs, three batched of each iPSC clone were harvested for lysate preparation and immunostaining; for PMA treatment, three separate PMA treatment were performed on three separate batches of each clone, unless stated otherwise. Three images were taken from each experiment in each condition and analysed. The results of the corresponding two clones derived from the same patient were pooled and mean of each patient ± S.E.M. were shown. Unpaired Student's t-test or ANOVA with Bonferroni's post-hoc test was performed using GraphPad Prism 7 (GraphPad Software, Inc.) (considered statistically significant at $*p< 0.05$). Results

5.3 Results

5.3.1 SCA14 pathology in patient post-mortem cerebellum

Given the heterogeneous phenotypes caused by SCA14 mutations described in studies using heterologous models, this chapter aimed to investigate the pathological changes in SCA14 post-mortem cerebellum and patient-derived iPSCs. This work focused on two SCA14 mutations,

H36R and H101Q. Both of these mutations are located at the equivalent locations at the C1A and C1B subdomains in the regulatory domain of PKCγ (Fig. 1.8) (Nemeth et al., 2013) and are implicated in zinc coordination and phorbol ester binding (section 1.6.3) (Chen et al., 2003). Although cerebellar atrophy is well described in SCA14 patients in studies showing brain MRI (Fig. 1.7), information regarding the human neuropathology of SCA14 is scarce. Thus far, only one post-mortem cerebellum of a SCA14 patient carrying an H101Y mutation has been reported (Chen et al., 2003). Other than a loss of Purkinje cells, additional pathological details was unavailable, likely due to the substandard quality of the post-mortem material. Remaining Purkinje cells displayed reduced immunoreactivity for PKCγ without any aggregation (Chen et al., 2003). In the present study, post-mortem cerebellar tissue from an affected individual in the SCA14 H101Q family, who died of 'natural causes' at the age of 90 years, was included and pathological changes were examined (Fig. 1.7). Cerebellar tissue from three age-matched healthy donors were also included. Further information of the control cerebellar tissue obtained from can be found in Supplementary Table 5.1 in the Appendix. Brain tissue was examined according to standard protocols for neurodegenerative disease, which included screening for Alzeihmer disease, Lewy body disease and TDP-43 proteinopathy. Braak II/III neurofibrillary Alzeihmer type pathology and mild cereberobascular disease was identified. No Lewy body or TDP-43 proteinopathy was found (data not shonwn). A sequestonsome1/p62 antibody was used as a highly sensitive screening tool for generic protein aggregates (data not shown). To identify Purkinje cells, cerebellar tissue sections were immunolabelled with an anti-Calbindin antibody D28-K. A total loss of Purkinje cells was observed in all lobules of the neocerebellum, associated with Bergmann gliosis. Purkinje cells in the archicerebellum (the flocculonodular lobe) were relatively preserved. Neurons of the deep cerebellar nuclei, pons and inferior olive were not obviously depleted, suggesting a pure Purkinje cell neuronopathy (Fig. 5.1A). This is consistent with the highly restricted expression pattern of PKCγ in Purkinje cells of human cerebellum (Fig. 5.1B). The remaining SCA14 Purkinje cells displayed variable degrees of dendritic and somatic atrophy compared to controls (Fig 5.1C). In age-matched control

cerebellar tissue, PKCγ was localised at the plasma membrane and stained as cytoplasmic puncta in the soma and primary dendrites of Purkinje cells (Fig. 5.1C). In contrast, membrane staining of PKCγ in SCA14 Purkinje cells was lost compared to controls (Fig. 5.1C). Moreover, PKCγ was associated with large cytoplasmic aggregates in the cell bodies (Fig. 5.1C). Foci of misfolded proteins are hallmarks of several neurodegenerative diseases such as Alzheimer's disease, Huntington's disease and polyglutamine SCAs (Ciechanover and Kwon, 2015; Koeppen, 2005; Menzies et al., 2017), and are often detergent-insoluble. To confirm the mislocalisation/insolubility of the PKCγ foci in SCA14 cerebellum, biochemical fractionation of the cerebellar tissue into Triton-soluble supernatant and -insoluble pellets, which has been used to show the insolubility of mutant PKCγ foci in heterologous cell models (Basso et al., 2009; Jezierska et al., 2014; Seki et al., 2005a; Takahashi et al., 2015), was performed. Tissue from one cerebellar region, the archicerebellum, was examined as this region was relatively preserved in the SCA14 case. PKCγ was found in both Triton-soluble supernatant and -insoluble pellets in control cerebellar tissue (Fig. 5.1D & E). In contrast, PKCγ in SCA14 cerebellum was relatively enriched in the Trinton-insoluble pellet compared to controls (Fig. 5.1D & E). Taken together, these results suggest that PKCγ is mislocalised in Triton-insoluble pellet in SCA14 cerebellum.

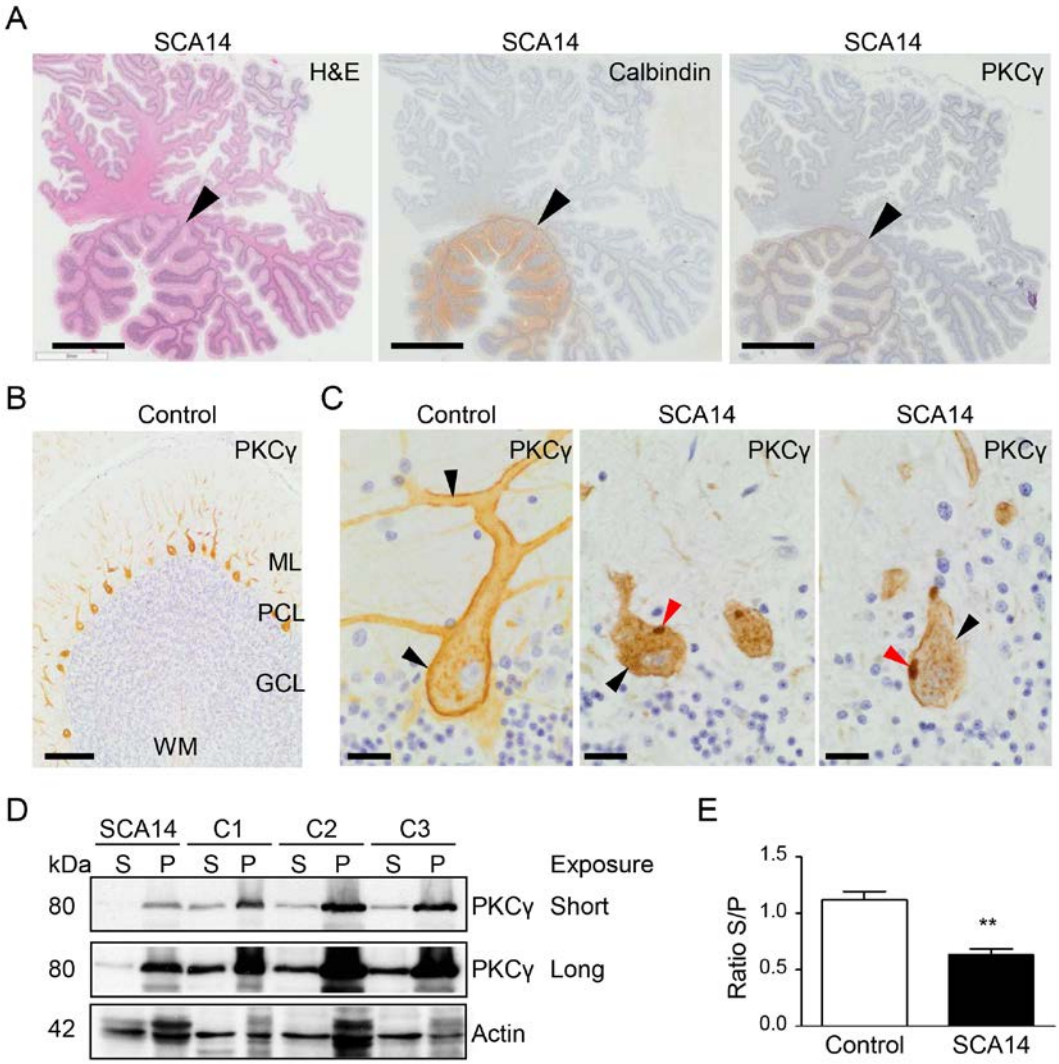


Figure 5.1 Cerebellar pathology in SCA14

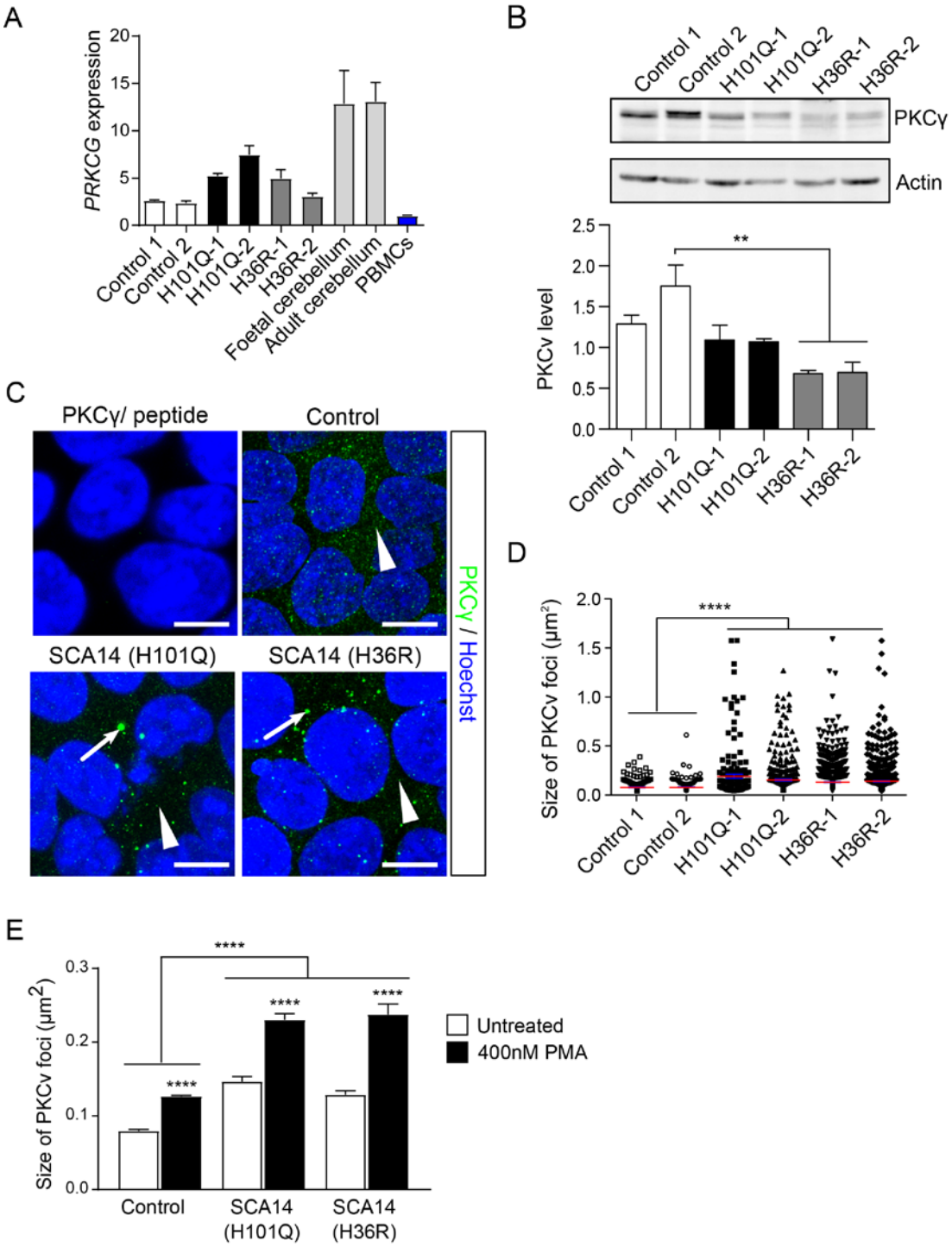
(A) Loss of Purkinje cells in SCA14 cerebellum. A complete loss of Purkinje cells was observed in the neocerebellarm. Purkinje cells in the archicerebellum (flocconodular lobe) were relatively preserved (black arrowheads). Brain sections were stained with hemoatoxylin and eosin (H&E) (left panel), and with antibodies against Calbindin-D28k (centre) and PKCγ (right panel) Scale bars= 5 mm. (B) Normal PKCγ pattern from an age-matched control cerebellum. ML: molecular layer; PCL: Purkinje cell layer; GCL: granule cell layer, WM: white matter. Scale bars= 200 µm. (C) PKCγ staining of control (left) and SCA14 cerebellum (centre and right panels). In control cerebellum, PKCγ showed distinct expression at the plasma membrane, both around the soma, and primary and secondary dendrites (black arrowheads), with minor granular staining in the perinuclear cytoplasm. In SCA14 cerebellum, membrane staining of PKCγ was lost (black arrowheads). Large cytoplasmic foci of PKCγ were found, some foci appeared to be linked to fragments of plasma membrane (red arrowheads). Scale bars= 20 µm. (D) Representative immunoblots showing enrichment of mutant PKCγ in the Triton-insoluble pellets in SCA14 cerebellum compared to controls. Short and long exposure of immunoblots using antibodies detecting PKCγ is shown. Actin: loading control. S: Triton-soluble supernatant; P: Trinton-insoluble pellets. (E) Ratio of PKCγ in Triton-soluble supernatant (S) and Triton-insoluble pellets (P) of human cerebellar tissue was plotted (three lysate preparations of the same cerebellar region of a single SCA14-H101Q case and three age-matched control cerebella, ***p<0.01*, unpaired students' t-test).

5.3.2 PKCγ is endogenously and ubiquitously expressed in the cytoplasm of control and SCA14 iPSCs

It was next investigated whether SCA14 patient-derived iPSCs displayed any pathological changes. In this chapter, at least two clones from each of the four SCA14 patients were included (refer to Chapter 3 for the generation of SCA14 iPSCs). Two age- and sex-matched control iPSC lines, AH017-3 and OX3-7, were also included (Fig. 3.2H). To determine whether iPSCs endogenously expressed PKCγ, RT-qPCR on control and SCA14 iPSC lines was performed to assess the mRNA expression of the *PRKCG* gene. According to data from GTEx, BioGPS, and CGAP SAGE (https://www.genecards.org/cgi-bin/carddisp.pl?gene=PRKCG#expression), human peripheral blood mononuclear cells (PBMCs) do not express PKCγ and were therefore used as a negative control. RNA extracted from human foetal and adult cerebellar tissue was used as positive controls. Although PKCγ is generally considered to be neuron-specific (Saito and Shirai, 2002), *PRKCG* mRNA was expressed at similar levels in control and SCA14 iPSCs (Fig. 5.2A). Furthermore, less PKCγ protein was expressed in patient iPSCs compared to controls (Fig. 5.2B).

Similar to our observations in post-mortem cerebellar tissue, in control iPSCs, wildtype PKCγ was expressed as small cytoplasmic puncta (Fig. 5.2C). In contrast, in SCA14 iPSCs, mutant PKCγ formed significantly larger cytoplasmic foci compared to controls (Fig. 5.2 C & D), in addition to some small dot-like staining in the cytoplasm (Fig 5.2C). To investigate whether formation of PKCγ foci was further enhanced by activation of PKCγ, PKCγ was stimulated in control and SCA14 iPSCs with 400 nM phorbol 12-myristate 13-acetate (PMA), which is a commonly used PKCγ activator, for 15 minutes. The sizes of both wildtype and mutant PKCγ puncta significantly increased following 15 minutes of PMA treatment (Fig. 5.2E). Importantly, mutant PKCγ formed significantly larger cytoplasmic foci in the presence or absence of PMA, compared to controls (Fig. 5.2E). DMSO vehicle controls did not affect the size of PKCγ puncta

(Fig. 5.3A). Prolonged activation of PKC results in its accumulation in the Triton-insoluble pellets, where it is subjected to dephosphorylation and degradation (Antal and Newton, 2014; Curnutte et al., 1994; Nixon and McPhail, 1999). To determine whether the PKCγ foci in SCA14 iPSCs were also Triton-insoluble similar to those in the SCA14 cerebellum, lysates of iPSCs were separated into Triton-soluble supernatant and -insoluble pellets before and after 15, 30 or 60 minutes of stimulation with 400 nM PMA. However, preliminary results showed that transient PKCγ activation did not facilitate the accumulation of mutant PKCγ in the Triton-insoluble pellets (Fig. 5.2F-H). Taken together, these findings suggest that SCA14 mutations (H36R and H101Q) promote the formation of PKCγ foci in the cytoplasm of iPSCs, which is further enhanced by PKCγ activation. However, preliminary results suggest that the cytoplasmic mutant PKCγ foci do not appear to be particularly Triton-insoluble following transient PKCγ activation.


A
PRKCG expression
20
15
10
5
0
Control 1
Control 2
H101Q-1
H101Q-2
H36R-1
H36R-2
Foetal cerebellum
Adult cerebellum
PBMCs
B
Control 1
Control 2
H101Q-1
H101Q-2
H36R-1
H36R-2
PKCγ
Actin
PKCv level
2.5
2.0
1.5
1.0
0.5
0.0
**
C
PKCγ/ peptide
Control
SCA14 (H101Q)
SCA14 (H36R)
PKCγ / Hoechst
D
Size of PKCv foci (μm²)
2.0
1.5
1.0
0.5
0.0
****
E
Size of PKCv foci (μm²)
0.3
0.2
0.1
0.0
****
Untreated
400nM PMA
Control
SCA14 (H101Q)
SCA14 (H36R)

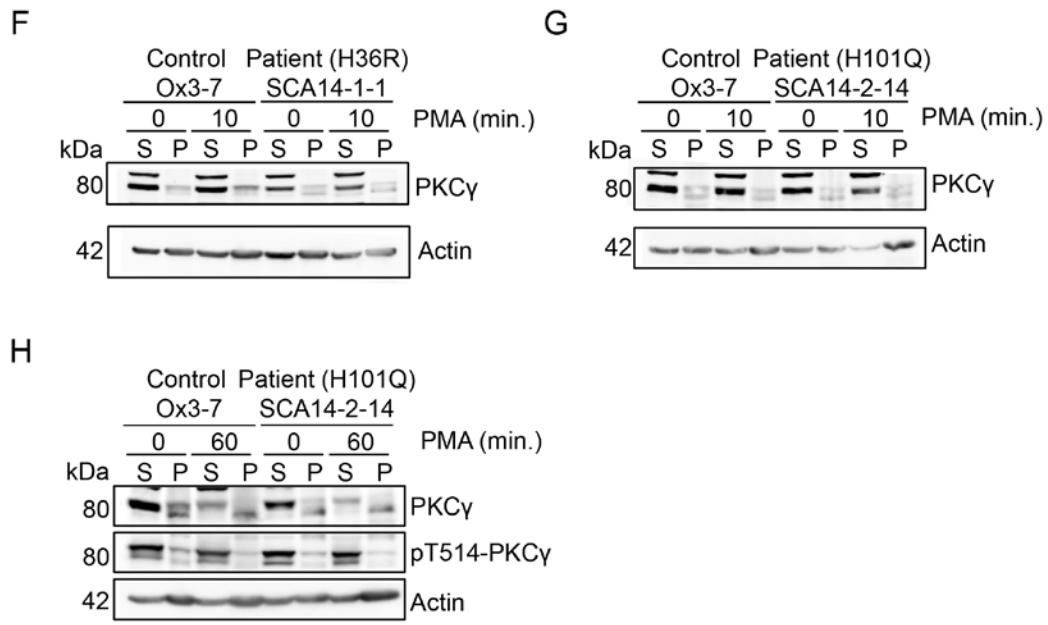


Figure 5.2 Mutant PKCγ forms cytoplasmic foci in iPSCs.

(A) *PRKCG* mRNA expression in control and SCA14 iPSCs, human cerebellum (positive controls) and peripheral blood mononuclear cells (PBMCs) (negative control). *PRKCG* gene expression levels shown are normalised to housekeeping gene β-actin, and relative to negative control. RNA was extracted from two clones each derived from four SCA14 patients and two control iPSC lines. cDNA synthesis and qPCR were performed. The experiment was repeated for three times. Results from the corresponding clones derived from the same patient were pooled and presented (*p>0.5,* one-way ANOVA followed by Bonferroni's post-hoc test for iPSCs). (B) Upper panel: representative immunoblots of PKCγ protein expression in controls and SCA14 iPSCs, representative iPSC clones were shown. Actin: loading control. Lower panel: Normalised PKCγ levels in untreated iPSCs. Actin: loading control. Intensity of bands representating PKCγ in three immunoblots from three lysate preprations of each untreated iPSC lines were analysed (***p<0.001,* one-way ANOVA followed by Bonferroni's post-hoc test). (C) Immunostaining of iPSC lines for PKCγ. Specificity of the anti-PKCγ antibody was confirmed by peptide absorption assay (top left panel). Small punctate staining of PKCγ (white solid arrowheads) was observed in the cytoplasm of control and SCA14 iPSCs, while large cytoplasmic foci (white arrows) were only present in SCA14 iPSCs. Hoechst stain was used for nuclear staining of iPSCs. Scale bars = 10 μm. (D) PKCγ formed significantly larger foci in SCA14 iPSCs compared to control iPSCs. Immunostaining were performed on three batches of each iPSC lines, each dot represents one data entry for the visualisation of the distribution of PKCγ foci size, *****p<0.00001,* one-way ANOVA followed by Bonferroni's post-hoc test. (E) Following treatment with 400 nM PMA, a potent PKCγ activator, both wildtype and mutant PKCγ increased in size. Compared to control, PKCγ formed significantly larger puncta in SCA14 iPSCs following PMA treatment. Three independent PMA treatment and immunostaining was performed on each iPSC clones. Size of PKCγ puncta were analysed. Results from different control iPSC lines and patient iPSCs with the same mutation behaved similarly and were therefore pooled and shown. *****p<0.00001,* two-way ANOVA followed by Bonferroni's post-hoc test. Short-term PKCγ activation with 10- (F, G) or 60-minute (H) of PMA treatment did not facilitate the accumulation of PKCγ in the Triton-insoluble pellets in SCA14 iPSCs compared to controls. (F, G) Two independent PKCγ activation with 400nM PMA for 10 min. was performed on each SCA14 iPSC clone (SCA14-1-1 and SCA14-2-14) and control iPSC line Ox3-7. Representative immunoblots are shown. Actin: loading control. (H) PKCγ activation with 100nM PMA for 60 min was performed twice in control iPSC line Ox3-7 and SCA14 iPSC clone SCA14-2-14. Representative immunoblot is shown. Actin: loading control. S: Triton-soluble supernatant, I: Triton-insoluble pellets.

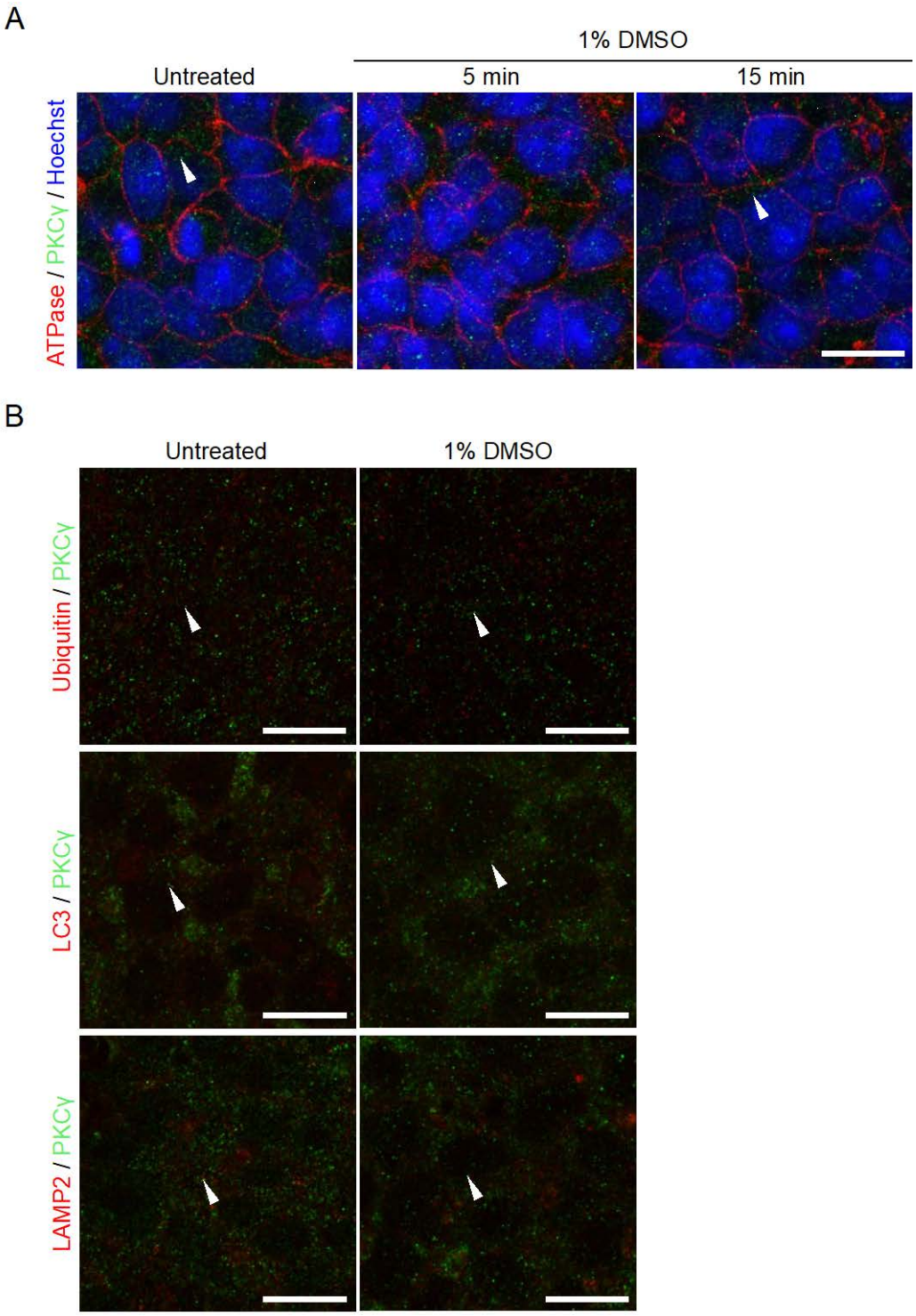


Figure 5.3 DMSO treatment does not affect iPSC cellular phenotypes.

Representative images of control iPSCs co-stained with PKCγ (white solid arrowheads) and plasma membrane marker sodium potassium ATPase (A), ubiquitin, lysosome marker LAMP2 or autophagosome marker LC3 (B), in the absence or presence of 1% DMSO. Hoechst stain was used for nuclear staining. Scale bars = 10 μm.

5.3.3 SCA14 mutations reduce membrane targeting of mutant PKCγ

The C1 domain regulates binding of PKCγ to DAG and phospholipids at the plasma membrane (sections 1.4.2 and 1.4.3.2). Upon activation, PKC rapidly translocates from the cytoplasm to the plasma membrane and interacts with its substrates (Newton, 2003; Newton, 2010). Modelling and mutational studies have shown that mutations in the C1B domain of PKCδ abolish phorbol-ester binding to the C1B domain (Kazanietz et al., 1995; Quest et al., 1994; Xu et al., 1997). As both of the SCA14 mutations included in this study are located at the C1 domain, it was therefore investigated whether the membrane targeting of SCA14 mutants would be affected. Interestingly, as described above, PKCγ staining at the plasma membrane of Purkinje cells was markedly reduced in the SCA14 post-mortem cerebellar tissue (Fig. 5.1B). To determine whether the membrane translocation of mutant PKCγ was affected in SCA14 iPSCs, cells were treated with 400 nM PMA to activate PKCγ, and the subcellular localisation of PKCγ was examined. In control iPSCs, the co-localisation of PKCγ and sodium potassium ATPase at the plasma membrane significantly increased after 5 minutes of PMA treatment (Fig. 5.4A & B). After 15 minutes of PMA treatment, PKCγ was found in the cytoplasm again (Fig. 5.4A & B). In contrast, in SCA14 iPSCs, large PKCγ foci remained in the cytoplasm and did not translocate to the plasma membrane in response to PMA treatment (Fig. 5.4 A & B). Similar results were obtained following treatment with 200 nM phorbol 12,13-dibutyrate (PDBu), another PKCγ-activating phorbol ester (Fig. 5.4C). DMSO vehicle control did not affect the translocation of PKCγ (Fig. 5.3A). Together, these findings indicate that mutant PKCγ is mislocalised in the cytoplasm following phorbol ester-activation.

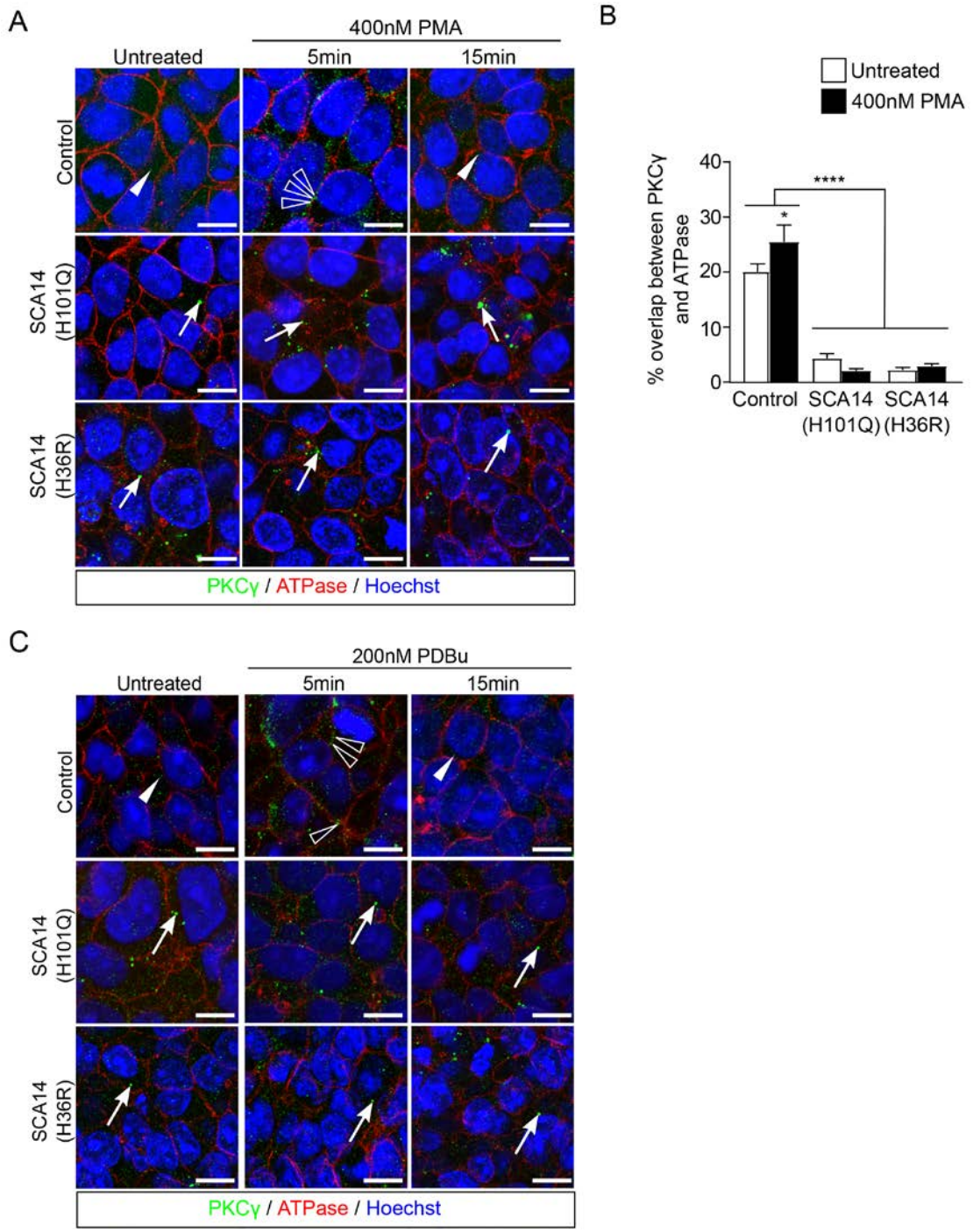


Figure 5.4 SCA14 mutations reduce membrane association of PKCγ.

(A) Control and SCA14 iPSCs were immunostained for PKCγ before or after treatment with 400 nM PMA. The cell membrane was stained with an antibody against sodium potassium ATPase. Hoechst stain was used for nuclear staining. In unstimulated control iPSCs, PKCγ was expressed as small puncta in the cytoplasm (white solid arrowheads). After 5 minutes of PMA treatment, PKCγ was found at the plasma membrane (white hollow arrowheads), and returned to the cytoplasm after 15 minutes of PMA treatment (white solid arrowhead). In unstimulated SCA14 iPSCs, large foci (white arrows) of PKCγ were found in the cytoplasm. PKCγ foci remained in the cytoplasm throughout the treatment with PMA. Scale bars = 10 μm. (B) PKCγ in SCA14 iPSCs showed significantly less membrane association than that in controls iPSCs in response to PMA stimulation. Three independent PMA treatment and immunostaining was performed on each iPSC clone. Colocalisation between PKCγ and plasma membrane markers were analysed. Results from the corresponding clones derived from the same patient were pooled and shown. *$p<0.05$, ****$p<0.0001$, two-way ANOVA

followed by Bonferroni's post-hoc test. (C) Control and patient iPSCs were immunostained for PKCγ before or after treatment with 200 nM PDBu. The cell membrane was stained with an antibody against sodium potassium ATPase. Cell nuclei are visualized by Hoechst staining. In unstimulated control iPSCs, PKCγ was expressed as small dots in the cytoplasm (white solid arrowhead). After 5 minutes of PDBu treatment, PKCγ was found at the plasma membrane (white hollow arrowheads), and returned to the cytoplasm after 15 minutes of PDBu treatment (white solid arrowhead). In unstimulated SCA14 iPSCs, large foci (white arrows) of PKCγ were present in the cytoplasm. PKCγ foci remained in the cytoplasm (white arrows) throughout the treatment with PDBu. Scale bars = 10 μm.

5.3.4 Degradation of mutant PKCγ foci

5.3.4.1 Mutant PKCγ foci do not co-localise with ubiquitin

The function and survival of neurons heavily depend on the efficient removal of misfolded proteins, as they cannot dilute cytotoxic proteins by cell division (Ciechanover and Kwon, 2017; Menzies et al., 2017). Due to the late-onset nature of SCA14, age-related decline of the protein degradation system is likely to contribute to the accumulation of mutant PKCγ foci (Ciechanover and Kwon, 2015; Seki et al., 2007). Cells operate two major protein degradation machineries: the ubiquitin-proteasome system (UPS) and autophagy (Ciechanover and Kwon, 2015, 2017). Impairments of protein degradation systems have been associated with several neurodegenerative diseases including Alzheimer's disease, Parkinson's disease, Huntington's disease and polyglutamine SCAs (Ciechanover and Kwon, 2015, 2017; Dantuma and Bott, 2014; VerPlank et al., 2017; Zheng et al., 2016). Misfolded and aggregated proteins are first tagged by ubiquitin and transported to proteasomes or autophagosomes for their subsequent degradation (Kwon and Ciechanover, 2017; Zheng et al., 2016). Therefore, it was first assessed whether mutant PKCγ foci colocalised with ubiquitin. Control and patient iPSCs were immunostained with antibodies against PKCγ or ubiquitin in the presence or absence of PMA or PDBu. In all conditions, mutant PKCγ foci were negative for ubiquitin (Fig. 5.5). DMSO vehicle treatment did not affect the co-localisation of PKCγ and ubiquitin (Fig. 5.3B). Consistent with the iPSC results, no co-localisation of PKCγ and ubiquitin was detected in Purkinje cells in SCA14 cerebellum (data not shown). These results suggest that mutant PKCγ foci do not colocalise with ubiquitin.

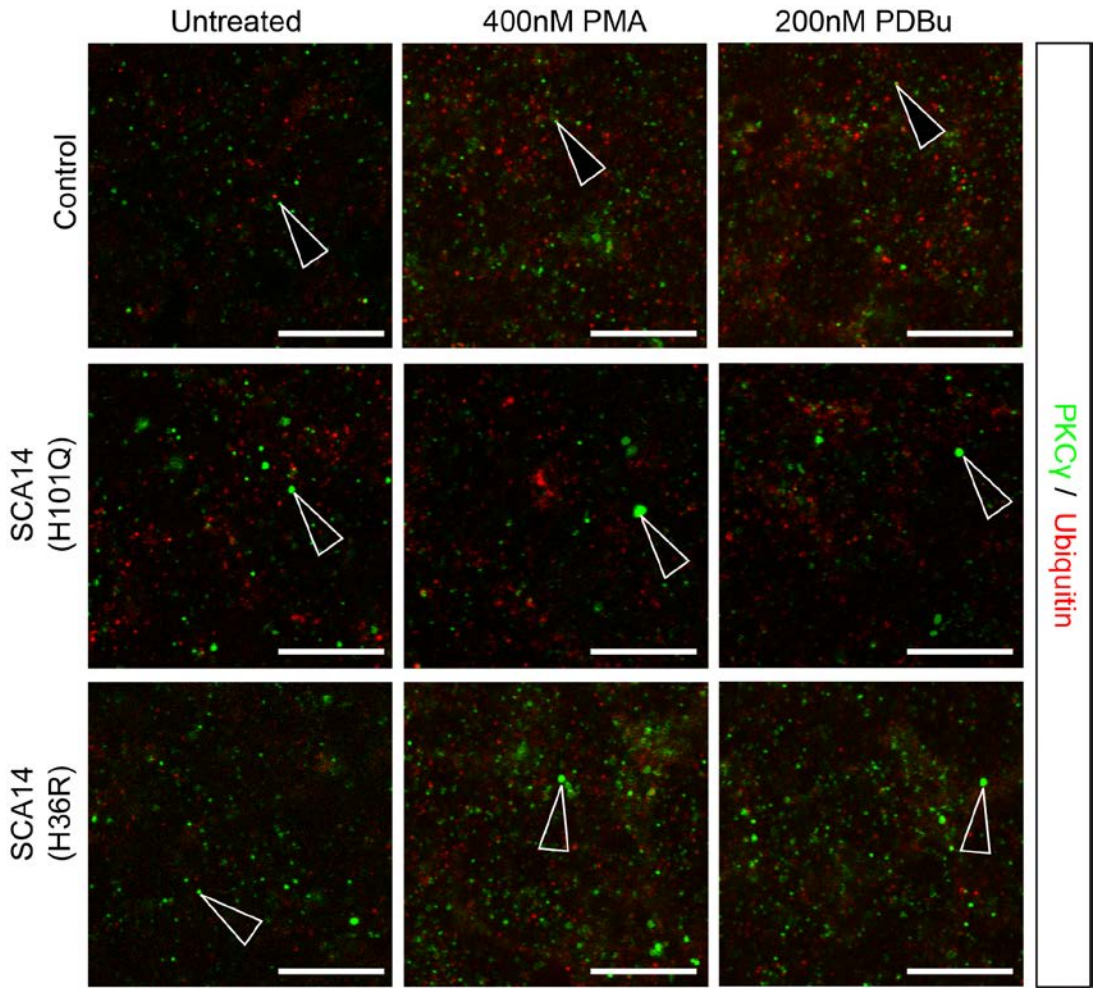


Figure 5.5 Mutant PKCγ foci do not colocalise with ubiquitin.

Control and patient iPSCs were immunostained for PKCγ and ubiquitin following PMA or PDBu treatment. Wildtype and mutant PKCγ in control and SCA14 iPSCs was negative for ubiquitin staining (white hollow arrowheads) before and after 15 minutes of PMA (A) or PDBu (B) treatment. Scale bars = 10 μm.

5.3.4.2 Mutant PKCγ foci are not removed by autophagy

It was next investigated whether mutant PKCγ foci was degraded via other cellular pathways. Ubiquitination of misfolded or aggregated proteins is also required for their recruitment into the autophagosomes (Menzies et al., 2017). The lack of aossociation of ubiquitin and mutant PKCγ foci might therefore affect its degradation by autophagy. When healthy cells are under cellular stress, the formation of autophagosomes is induced; phagophores elongate to enclose misfolded or partially unfolded proteins. Autophagosomes are formed when the two ends of the double-layered membrane of phagophore fuse together. Autophagosomes then fuse with

lysosomes to form autolysosomes, which eventually become lysosomes where unwanted proteins are digested by its acidic environment (Menzies et al., 2017; Ryter et al., 2013; Schwake et al., 2013). In addition, PKC has been shown to regulate autophgy (Jiang et al., 2010; Li and Zhang, 2017; Sakaki et al., 2008; Wang et al., 2017). Autophagosome formation in control and patient iPSCs was therefore first examined through immunostaining of microtubule-associated protein 1 light chain 3 (LC3), a central protein in the autophagy pathway. In untreated control iPSCs, PKCγ showed little co-localisation with LC3, and their co-localisation significantly increased following PMA treatment (Fig. 5.6A & B). In contrast, in SCA14 iPSCs, PKCγ and LC3 already showed significantly more co-localisation compared to controls in the absence of PMA (Fig. 5.6A & B). However, this overlap did not increase following PMA treatment (Fig. 5.6A & B), despite the significant increase of size of PKCγ foci (Fig. 5.2E). Similar results were obtained from cells treated with PDBu (Fig. 5.6C). DMSO vehicle control did not affect autophagosome formation and co-localisation with PKCγ (Fig. 5.3C). Autophagosome formation in control and patient iPSCs was then assessed by the level of LC3 before and after PMA treatment. LC3I represents the free cytosolic LC3, while LC3II represents the LC3 that is anchored to the inner membrane of autophagosomes and thus correlates with auphagosome load (Ashkenazi et al., 2017; Mizushima et al., 2010). Consistent with the immunostaining results, the ratio of LC3II/total LC3 did not change in either control or SCA14 iPSCs following PMA treatment (Fig. 5.6D & E). This suggests that autophagosome formation is not induced in response to PKCγ activation despite the increased formation of PKCγ foci.

Autophagy selectively degrades target proteins via p62 labelling. p62, also known as Sequestosome-1 (SQSTM1), is a factor that recruits ubiquitinated proteins into autophagosomes (Menzies et al., 2017; Mizushima et al., 2010; Ryter et al., 2013). The absence of association of ubiquitin and PKCγ foci might therefore affect p62 labelling and the subsequent recruitment of PKCγ foci into autophagosomes. The levels of p62 protein in control

and SCA14 iPSCs were monitored before or after PMA treatment. In unstimulated SCA14 iPSCs with the H101Q mutation, p62 level was significantly lower compared to controls while unstimulated SCA14 H36R iPSCs only showed a slight reduction of p62 levels (Fig. 5.6F & G). After 10 minutes of PMA treatment, all SCA14 iPSCs showed comparable p62 levels to control iPSCs (Fig. 5.6F & G). These results suggest that in SCA14 iPSCs, the basal level of p62 was already low despite the presence of mutant PKCγ foci. Moreover, when the size of mutant PKCγ foci significantly increased in the presence of PMA, p62 level only slightly increased (H101Q) or remained unchanged (H36R). This might lead to insufficient labeling of mutant PKCγ foci. Consistent with the results obtained from iPSCs, no changes in LC3 levels and reduced p62 levels were detected in human SCA14 and control cerebellar tissue (Fig. 5.6H). Preliminary results showed that following treatment with Bafilomycin A1, an inhibitor of the autophgosome and lysosome fusion, PKCγ protein levels remained constant in both control and SCA14 iPSCs (Supplementary figure 5.1). This suggests that PKCγ appears not to be removed via autophagosomes in control and SCA14 iPSCs.

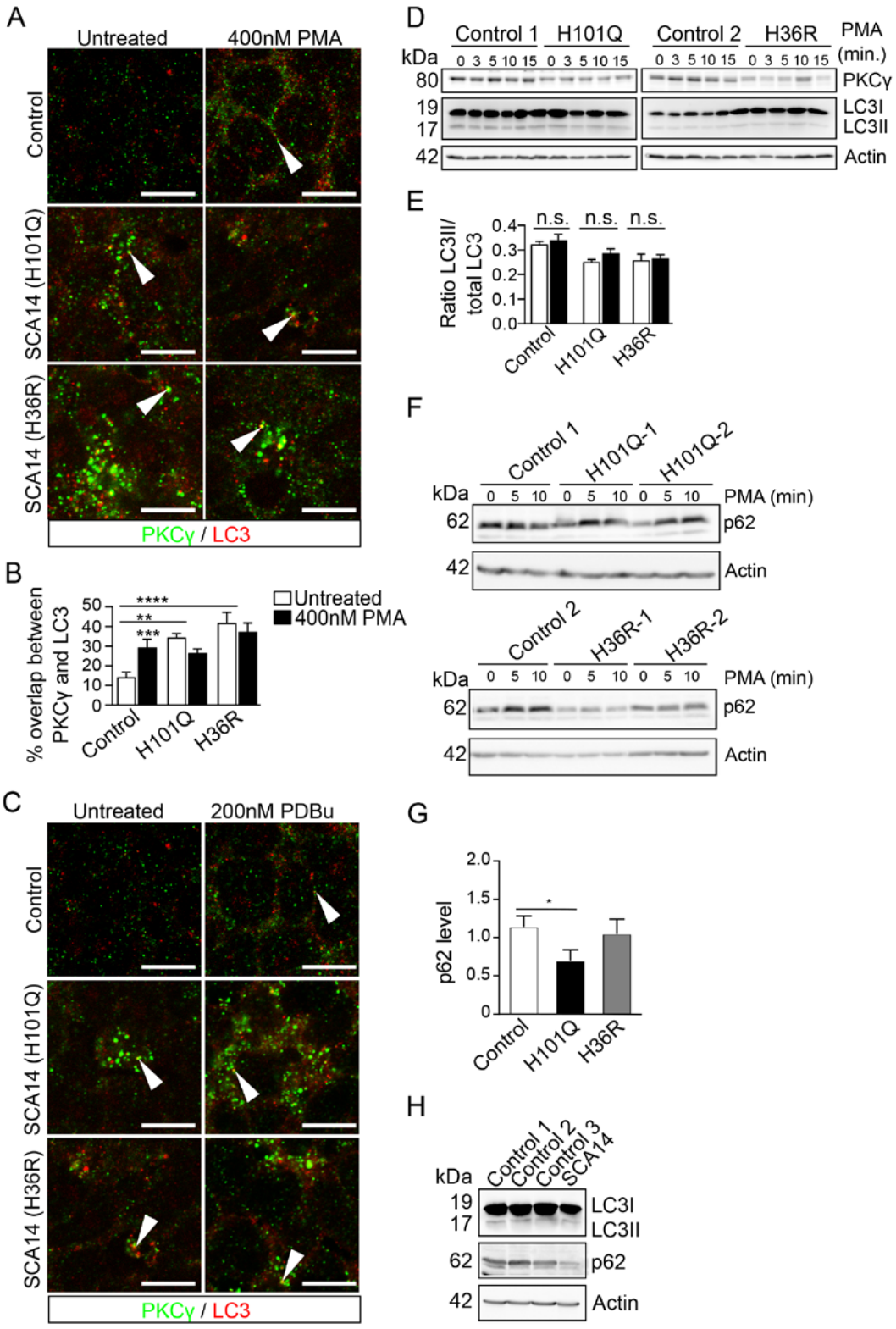


Figure 5.6 Mutant PKCγ foci do not colocalise with LC3II-positive autophgosomes and autophagosome formation is not induced following PKCγ activation.

(A, B) Two iPSC clones for each mutation was used in each experiment, i.e. PMA treatment. The experiment was repeated for three times and cells were fixed and then subject to immunostaining. Control and patient iPSCs were immunostained for PKCγ and the autophagosomal marker LC3 before or after treatment with PMA for 15 minutes. Results of control iPSCs and patient iPSCs with the same mutation were pooled

respectively and shown. In control iPSCs, PKCγ co-localised with LC3 (white solid arrowheads) increased following treatment with PMA. In untreated SCA14 iPSCs, there was already a significant overlap with LC3 (white solid arrowheads), which did not further increase with PKCγ activation (**$p<0.01$, ***$p<0.001$, ****$p<0.0001$, two-way ANOVA followed by Bonferroni's post-hoc test). Scale bars = 10 μm. (C) Control and patient iPSCs were immunostained for PKCγ and the autophagosomal marker LC3 before or after treatment with PDBu for 15 minutes. In control iPSCs, PKCγ co-localised with LC3 (white solid arrowheads) increased following treatment with PMA. In untreated SCA14 iPSCs, there was already a significant overlap with LC3 (white solid arrowheads), which did not further increase with PKCγ activation. Scale bars = 10 μm. (D) Two iPSC clones for each mutation was used in each experiment, i.e. PMA treatment. The experiment was repeated for three times and cell lysates were prepared. Lysates of iPSCs were subjected to immunoblotting for PKCγ and LC3. LC3I represents free cytosolic cleaved LC3. LC3II represents LC3 that is anchored to the autophagosome membrane and indicates autophagosome load. Actin: loading control. (E) Ratio of LC3II/total LC3 levels at 15 min. post-PMA treatment was quantified and was shown to remain constant in control and SCA14 iPSCs. (F) Two iPSC clones for each mutation was used in each experiment, i.e. PMA treatment. The experiment was repeated for three times and cell lysates were prepared. Lysates of iPSCs were subjected to immunoblotting for p62. Representative immunoblots were shown. (G) SCA14 H101Q, but not H36R, iPSCs showed lower p62 level compared to control iPSCs under basal condition. Quantification of p62 protein levels in untreated iPSCs (t= 0 min. in F) was shown. *$p<0.05$, one-way ANOVA followed by Bonferroni's post-hoc test. Actin: loading control. (H) Human SCA14 cerebellum showed no changes in LC3I and LC3II levels but lower p62 expression compared to controls. Representative immunoblot of three immunoblotting experiments that included two lysate preparation from the same cerebellar region of a single SCA14 case and three age-matched controls was shown. Actin: loading control.

5.3.4.3 Reduced co-localisation of mutant PKCγ foci with lysosomes despite increased lysosomal formation

Proteins that are engulfed by autophagosomes are subsequently degraded through the fusion with lysosomes (Menzies et al., 2017). To determine whether mutant PKCγ foci that are particularly abundant in SCA14 iPSCs following PMA treatment are effectively targeted to lysosomes, immunostaining for PKCγ and lysosomal marker lysosome-associated membrane protein 2 (LAMP2) was performed. In control iPSCs, a small proportion of wildtype PKCγ co-localised with LAMP2 in the absence of PMA treatment (Fig. 5.7A & C). Following 10 minutes of PMA treatment in control iPSCs, both LAMP2 area, which is indicative of lysosome formation, and co-localisation of PKCγ and LAMP2 were significantly increased (Fig. 5.7A-C). In SCA14 iPSCs, a significantly higher co-localisation of PKCγ and LAMP2 as well as enlargement of lysosomes was already observed before PMA treatment (Fig. 5.7A-C). After treatment with PMA for 15 minutes, lysosomes fused together to form larger vesicles (Fig. 5.7A & C). A subset of PKCγ foci co-localised with or were surrounded by these enlarged lysosome vesicles (Fig. 5.7A & B). However, the majority of the PKCγ foci did not co-localise with LAMP2 (Fig. 5.7A & B). Furthermore, compared to control iPSCs, less PKCγ co-localised

with LAMP2 following PMA treatment in SCA14 iPSCs. Similar results were obtained with cells treated with PDBu (Fig. 5.7D). DMSO vehicle control did not affect lysosome formation and co-localisation with PKCγ (Fig. 5.3B). Importantly, human SCA14 cerebellum also showed higher LAMP2 level compared to controls (Fig. 5.7E). Together, these findings suggest that only a subset of mutant PKCγ foci colocalise with lysosomes despite significant increase in lysosomal formation, and therefore accumulate in the cytoplasm in SCA14 cells.

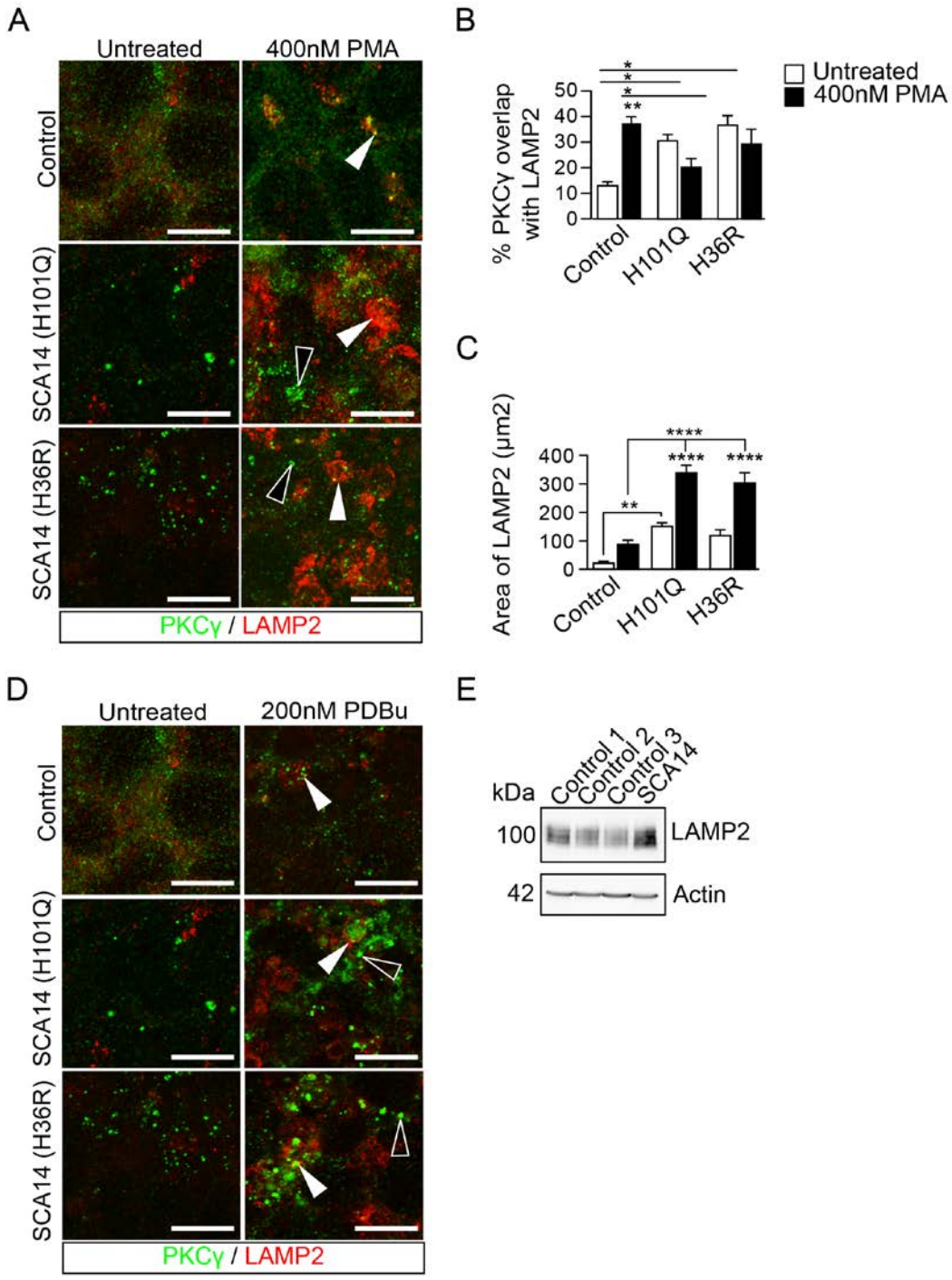


Figure 5.7 SCA14 PKCγ foci only partially colocalise with lysosomes despite significant lysosome enlargement.

(A, B) Two control iPSCs and two iPSC clones for derived from the four SCA14 patients were used in each experiment, i.e. PMA treatment. The experiment was repeated for three times and cells were fixed and then subject to immunostaining. Control and SCA14 iPSCs were immunostained for PKCγ and the lysosomal marker LAMP2 before or after 15 minutes of PMA treatment. In control iPSCs, co-localisation of PKCγ and LAMP2 (white solid arrowhead) increased upon PKCγ activation. In contrast, in SCA14 iPSCs, lysosomes fused together to form larger vesicles enclosing PKCγ foci (white solid arrowheads) in the presence of PMA. However, the majority of PKCγ foci did not co-localise with LAMP2-positive lysosomes (white hollow arrowheads) (*$p<0.05$, two-way ANOVA followed by Bonferroni's post-hoc test). (C) Two control iPSCs and two iPSC clones for derived from the four SCA14 patients were used in each experiment, i.e. PMA treatment.

The experiment was repeated for three times and cells were fixed and then subject to immunostaining. Results from control iPSCs and patient iPSCs with the same mutation were pooled respetively and shown. The area of LAMP2 signal, representing the formation of lysosomes, significantly increased in both control and SCA14 iPSCs following PMA treatment. The lysosomal area was significantly larger in patient iPSCs compared to control iPSCs (***p<0.01*, *****p<0.*0001, two-way ANOVA followed by Bonferroni's post-hoc test). (D) Control and SCA14 iPSCs were immunostained for PKCγ and the lysosomal marker LAMP2 before or after 15 minutes of PDBu treatment. In control iPSCs, co-localisation of PKCγ and LAMP2 (white solid arrowhead) increased upon PKCγ activation. In contrast, in SCA14 iPSCs, lysosomes fused together to form larger vesicles enclosing PKCγ foci (white solid arrowheads) in the presence of PDBu. However, the majority of PKCγ foci did not co-localise with LAMP2-positive lysosomes. (E) Human SCA14 cerebellum showed higher level of LAMP2 compared to controls. Representative immunoblot of three lysate preparation from a single SCA14 case and three age-matched controls was shown. Actin: loading control.

5.3.5 SCA14 mutations increase kinase activity of mutant PKCγ

Phosphorylation is known to play an important role in regulating PKCγ, stabilising PKCγ in a catalytically competent conformation, and protecting it from degradation (Newton, 2003; Newton, 2010; Seki et al., 2005b). PKCγ is first phosphorylated at T514 by PDK1. This is followed by two autophosphorylation events at T655 and T674 that allows PKCγ to become mature and capable of responding to activation by DAG and calcium (Newton, 2003; Newton, 2010). Altered phosphorylation status of PKCγ might affect its stability and kinase activity. Therefore, it was next determined whether mutations in the regulatory domain affected phosphorylation of PKCγ in SCA14 iPSCs using phospho-specific antibodies. Although the total PKCγ level was lower in SCA14 iPSCs compared to control iPSCs, PKCγ was highly phosphorylated at T514 and T674 in SCA14 iPSCs (Fig. 5.9A & B). Consistent with the results obtained in iPSCs, there was a reduced level of total PKCγ in SCA14 cerebellar tissue compared to controls (Fig. 5.9C & D). A reduction in Calbindin levels in the SCA14 cerebellum, which is consistent with the loss of Purkinje cells shown in histopathology, was also observed (Fig. 5.1A). Although there was less PKCγ present in SCA14 cerebellar tissue compared to controls, PKCγ was highly phosphorylated at the activation loop (T514) in SCA14 cerebellum (Fig. 5.9C & D). These results suggest that SCA14 mutations (H36R and H101Q) promote the aberrant maturation of PKCγ into a stable and catalytically competent conformation.

The increased phosphorylation of mutant PKCγ might promote its kinase activity and affect signalling downstream of PKCγ. The phosphorylation status of PKC substrates was therefore assessed using a phospho (Ser)-PKC substrate antibody that recognises cellular proteins phosphorylated at the PKC consensus motif. PKC substrate phosphorylation was markedly elevated in SCA14 iPSCs compared to controls (Fig. 5.9A). PKC substrates in SCA14 H101Q cerebellum were also more highly phosphorylated (Fig. 5.9E). The phosphorylation status of myristoylated alanine-rich C-kinase substrate (MARCKS), which is a known intracellular substrate of PKCγ (Bubb et al., 1999; Hartwig et al., 1992; Hussain et al., 2006; Larsson, 2006; Verbeek et al., 2008), was also assessed. Increased phosphorylation of MARCKS was detected in the SCA14 cerebellum compared to controls using a phospho-specific antibody (Fig. 5.9E). Taken together, these results suggest that SCA14 mutations (H36R and H101Q) result in increased kinase activity of PKCγ in SCA14 iPSCs and post-mortem cerebellum.

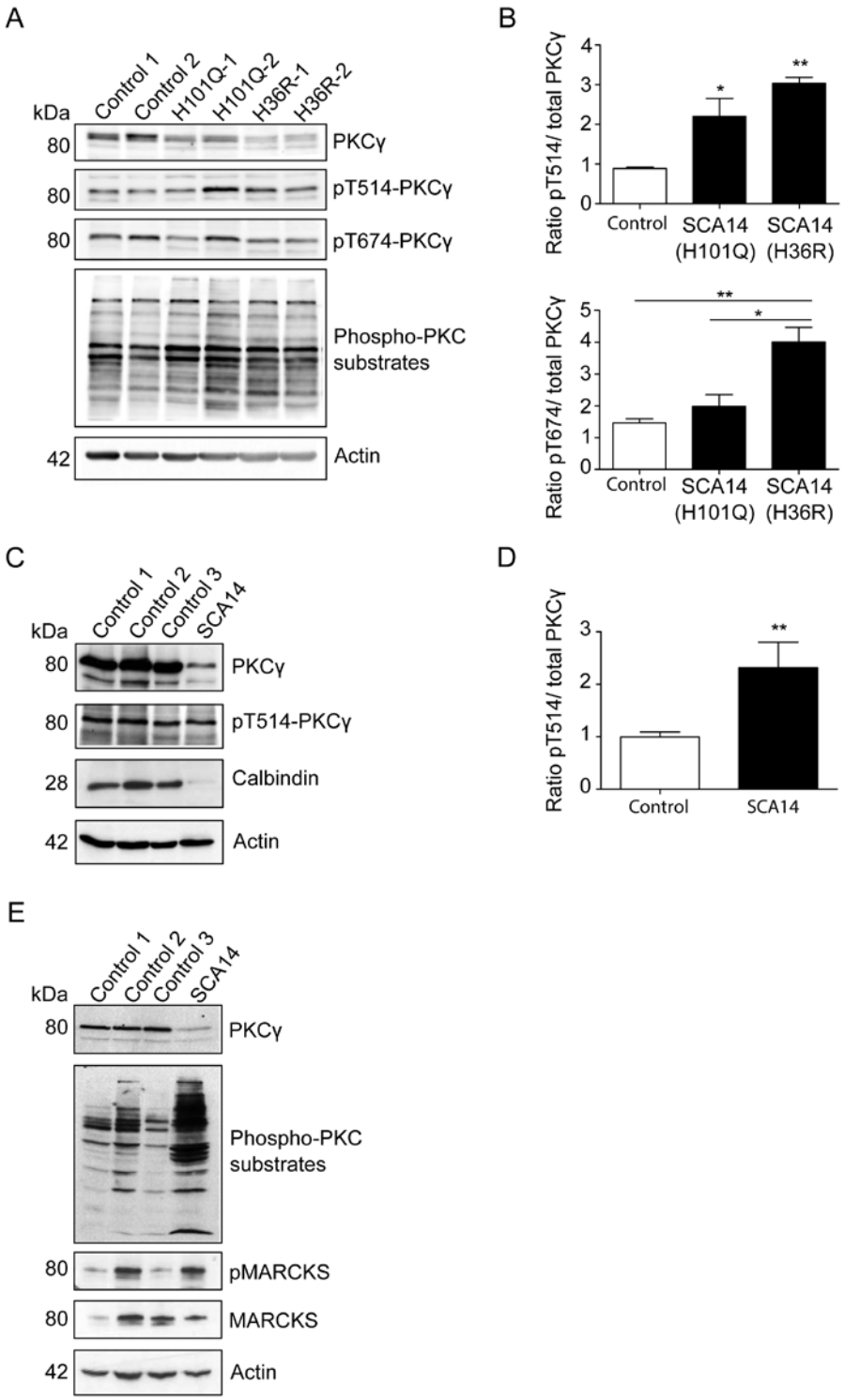


Figure 5.8 SCA14 mutations enhance kinase activity of PKCγ.

(A) Cell lysates were prepared from three batches of two control iPSC lines and two clones each of four patients. Lysates of iPSCs were subjected to immunoblotting for PKCγ, T514- and T674-phosphorylated PKCγ and phosphor-PKC substrates. Representitive immunoblots are shown. Actin: loading control. (B) Quantification of PKCγ phosphorylation at T514 (upper panel) and T674 (lower panel) versus total PKCγ. Results from the two control iPSC lines and patient iPSCs carrying the same mutation were pooled respectively and shown. Phosphorylation of PKCγ was significantly increased in SCA14 iPSCs compared to controls (*$p<0.05$, **$p<0.01$, one-way ANOVA followed by Bonferroni's post-hoc test). (C) Three lysate preparation of the same cerebellar region of a SCA14 case and three age-matched controls was performed. Cerebellar

lysates were subjected to immunoblotting for PKCγ, T514-phosphorylated PKCγ, Calbindin and Actin. (D) Quantification of PKCγ phosphorylation at T514 versus total PKCγ. Phosphorylation of PKCγ at T514 was significantly in SCA14 cerebellum was significantly higher compared to controls (three lysate preparation of the same cerebellar region of a SCA14 case and three age-matched controls, $**p<0.01$, unpaired students' t-test). (E) Cerebellar lysates were subjected to immunoblotting for PKCγ, phospho-PKC substrates, phosphorylated MARCKS, MARCKS and Actin (loading control).

5.3.6 SCA14 mutations in PKCγ increase phosphorylation of its substrate TRPC3 in iPSCs

A number of proteins have been identified as PKCγ substrates (section 1.6.4). However, it remains unclear whether interactions with these substrates are pathological and how these interactions cause dysfunction and death of Purkinje cells in SCA14 patients. C3-type transient receptor potential channel (TRPC3) is one of the known substrates of PKCγ (Trebak et al., 2005; Venkatachalam et al., 2003). TRPC3 is a non-selective cation channel that controls intracellular calcium balance. Mutations in TRPC3 affect channel gating and cause cerebellar ataxia in SCA41 patients (Fogel et al., 2015) and mice (Becker et al., 2009; Hartmann et al., 2008). Interestingly, both PKCγ and TRPC3 are highly expressed in Purkinje cells during development and are important for metabotropic glutamate receptor 1 (mGluR1) signalling in Purkinje cells (Adachi et al., 2008; Becker, 2015; Dulneva et al., 2015; Hartmann et al., 2008; Metzger and Kapfhammer, 2000). PKCγ-mediated phosphorylation of TRPC3 has been shown to act as a negative feedback mechanism that inhibits TRPC3 and blocks further calcium influx in overexpression systems (Trebak et al., 2005; Venkatachalam et al., 2003). Having identified that mutant PKCγ showed increased kinase activity, it was hypothesized that phosphorylation of membrane proteins such as TRPC3 might be altered. The resulting calcium imbalance and aberrant downstream calcium signalling might thereby cause dysfunction of Purkinje cells and SCA14.

To test this hypothesis, it was investigated whether TRPC3 might show a different phosphorylation status in SCA14 iPSCs compared to control iPSCs. *TRPC3* RNA (Fig. 5.10A)

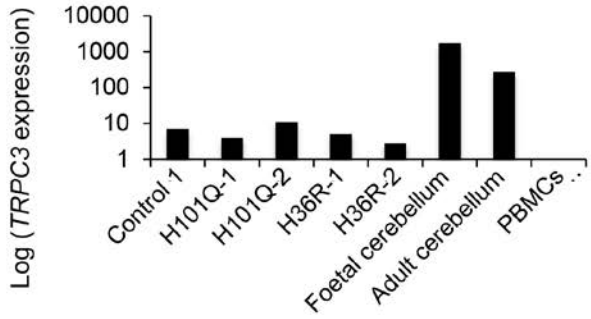
and TRPC3 protein (Fig. 5.10B & C) were expressed in control and SCA14 iPSCs. In the presence or absence of PMA, TRPC3 protein levels remained constant in control and SCA14 iPSCs. Moreover, protein level of wildtype PKCγ largely increased and that of mutant PKCγ only slightly elevated following PMA treatment (Fig. 5.10D & E). PhosTag acrylamide gel, which contains molecules that could attach to and slow down the migration of phosphorylated proteins (Kinoshita-Kikuta et al., 2007; Kinoshita et al., 2006), was used to separate phosphorylated and non-phosphorylated proteins extracted from control and SCA14 iPSCs. The membrane was then subjected to immunoblotting for TRPC3. To identify the bands that represent phosphorylated TRPC3, control iPSCs were first treated with 400 nM PMA for 10 minutes to maximise PKCγ kinase activity. Lambda phosphatase was used to remove phosphate groups on proteins. In the presence of phosphatase, multiple bands of TRPC3 shifted downwards compared to untreated control, indicating that the top band represented phosphorylated TRPC3 and the bands below were partially or fully dephosphorylated TRPC3 (Fig. 5.10F). After treated with PMA for 5 and 10 minutes, phosphorylation of TRPC3 increased in both control and SCA14 iPSCs (Fig. 5.10G & H). Interestingly, TRPC3 was more phosphorylated in SCA14 iPSCs compared to controls in the absence or presence of PMA treatment (Fig. 5.10 G & H). This suggests that SCA14 mutations in the C1 domain promote phosphorylation of TRPC3 in iPSCs.

It was next examined whether phosphorylation of TRPC3 might also be altered in human SCA14 cerebellum. TRPC3 was expressed at a similar level in the SCA14 cerebellum compared to controls (Fig. 5.10I). To distinguish phosphorylated and non-phosphorylated TRPC3, brain lysates with or without phosphatase treatment were compared using a PhosTag acrylamide gel. There was no difference detected between phosphatase-treated and -untreated samples in the SCA14 and control cerebellar tissue (Fig. 5.10J). In addition, the top bands that represent phosphorylated protein were very weak even though 50μg of protein was loaded.

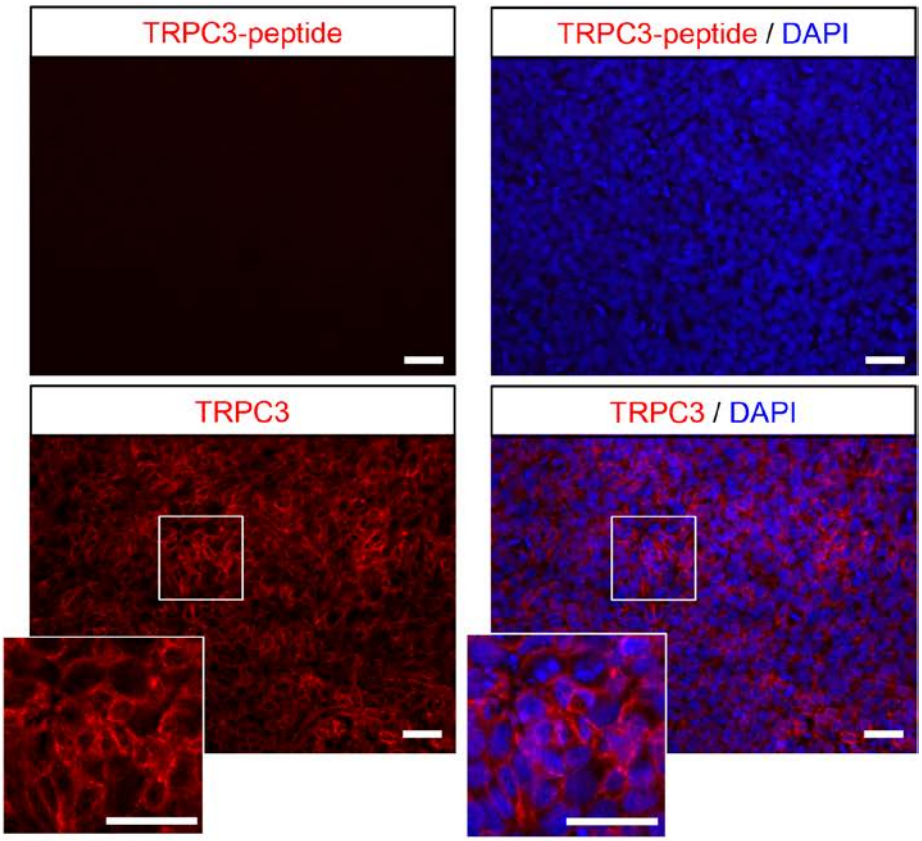
Therefore, it remains inconclusive whether TRPC3 phosphorylation differs in SCA14 cerebellum compared to controls.

Taken together, mutant PKCγ enhances phosphorylation of TRPC3 in iPSCs. This could result in inhibition of TRPC3 and thus altered calcium homeostasis and subsequent cellular dysfunction in SCA14. Nonetheless, it remains to be elucidated whether TRPC3 phosphorylation is also altered in patient cerebellum.

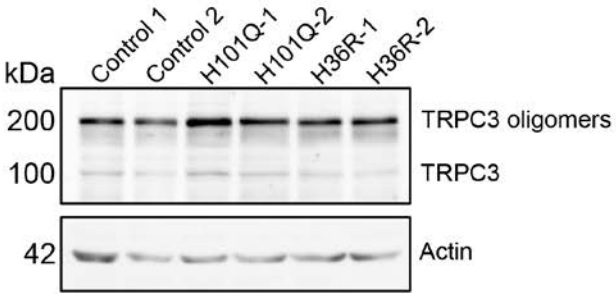
A


Log (TRPC3 expression)
10000
1000
100
10
1
Control 1
H101Q-1
H101Q-2
H36R-1
H36R-2
Foetal cerebellum
Adult cerebellum
PBMCs

B


TRPC3-peptide
TRPC3-peptide / DAPI
TRPC3
TRPC3 / DAPI

C


kDa
Control 1
Control 2
H101Q-1
H101Q-2
H36R-1
H36R-2
200
100
TRPC3 oligomers
TRPC3
42
Actin

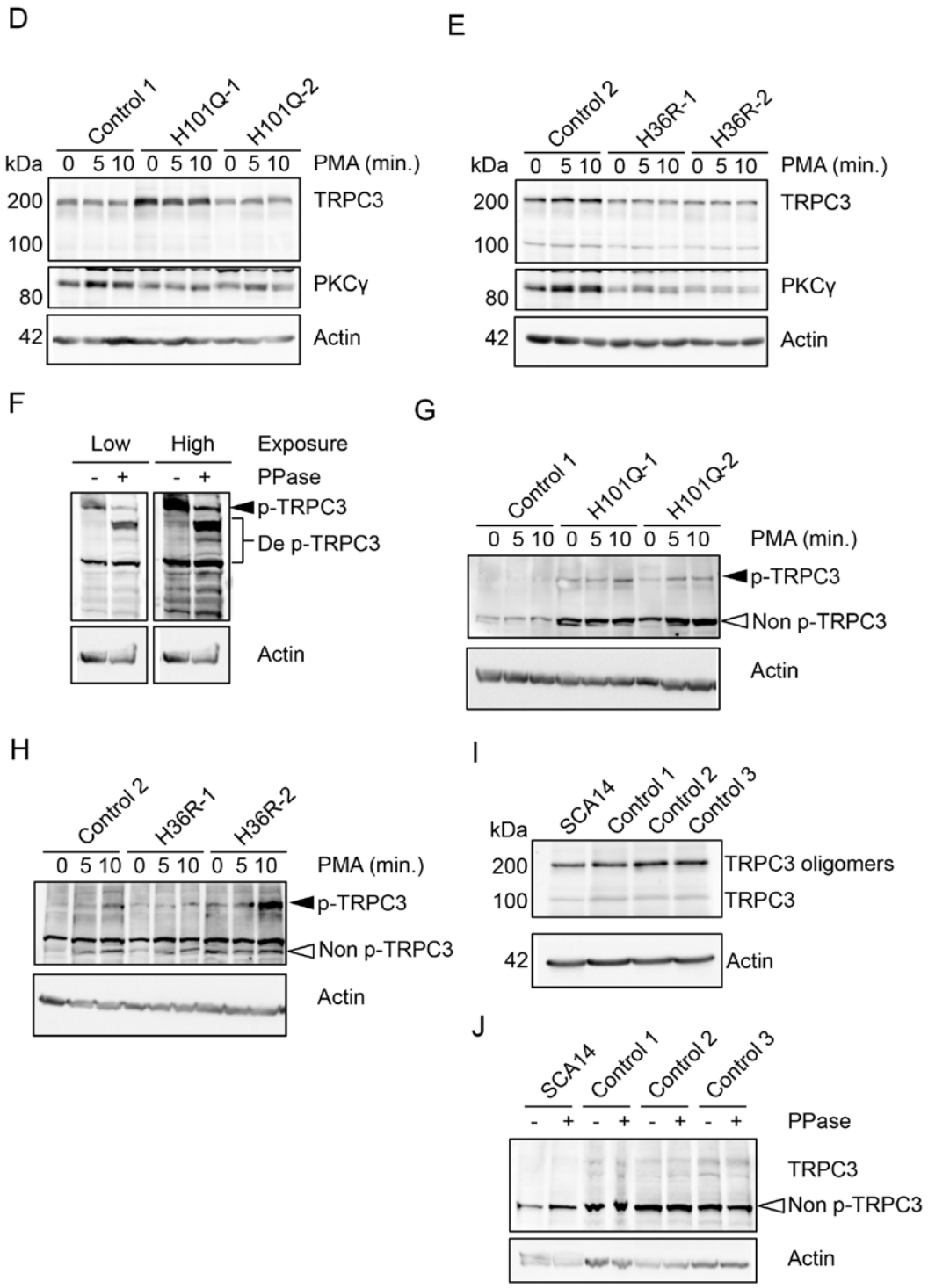

D
Control 1
H101Q-1
H101Q-2
kDa
0 5 10 0 5 10 0 5 10
PMA (min.)
200
100
TRPC3
80
PKCγ
42
Actin
E
Control 2
H36R-1
H36R-2
kDa
0 5 10 0 5 10 0 5 10
PMA (min.)
200
100
TRPC3
80
PKCγ
42
Actin
F
Low
High
Exposure
- + - +
PPase
p-TRPC3
De p-TRPC3
Actin
G
Control 1
H101Q-1
H101Q-2
0 5 10 0 5 10 0 5 10
PMA (min.)
p-TRPC3
Non p-TRPC3
Actin
H
Control 2
H36R-1
H36R-2
0 5 10 0 5 10 0 5 10
PMA (min.)
p-TRPC3
Non p-TRPC3
Actin
I
kDa
SCA14
Control 1
Control 2
Control 3
200
100
TRPC3 oligomers
TRPC3
42
Actin
J
SCA14
Control 1
Control 2
Control 3
- + - + - + - +
PPase
TRPC3
Non p-TRPC3
Actin

Figure 5.9 Phosphorylation of TRPC3, a known substrate of PKCγ, is increased in SCA14 iPSCs.

(A) *TRPC3* mRNA expression in control and SCA14 iPSCs, human cerebellum (positive controls) and peripheral blood mononuclear cells (PBMCs) (negative control). *TRPC3* gene expression levels shown are normalised to housekeeping gene β-actin, and relative to negative control. (B) Immunostaining of iPSCs for TRPC3. Specificity of the anti-TRPC3 antibody was confirmed by peptide absorption assay (top left panel). TRPC3 protein was expressed in control iPSCs. Hoechst stain was used for nuclear staining of iPSCs. Scale bars = 10 μm. (C) Lysates of iPSCs were subjected to immunoblotting for TRPC3 and Actin (loading control). (D, E) Lysates of iPSCs were subjected to immunoblotting for TRPC3, PKCγ and Actin before or after 5 and 10 minutes of PMA treatment. Protein levels of TRPC3 in control and SCA14 iPSCs were not affected by PKCγ activation. (F) Proteins treated with or without 1200 units of Lambda phosphatase (PPase) were separated in PhosTag acrylamide gel and subjected to immunoblotting for TRPC3 and Actin. The migration of phosphorylated proteins in PhosTag acrylamide gel do not correspond to the protein size according to manufacturer's protocol. In the presence of PPase, bands probed for TRPC3 shifted downwards indicating that the top band represents phosphorylated TRPC3 and those below are partially dephosphorylated TRPC3. (G, H) Lysates of iPSCs were separated in PhosTag acrylamide gel and subjected to immunoblotting for TRPC3 and Actin before or after 5 and 10 minutes of PMA treatment. SCA14 iPSCs containing the H101Q (G) and H36R (H) mutations showed higher levels of phosphorylated TRPC3 (top bands) than control iPSCs. (I) Cerebellar lysates were subjected to immunoblotting for TRPC3 and Actin. TRPC3 was expressed at similar levels in human SCA14 and control cerebellar tissue. (J) Cerebellar lysates with or without PPase treatment were separated in PhosTag acrylamide gel and subjected to immunoblotting for TRPC3 and Actin. Bands that represent phosphorylated TRPC3 were weak. No changes in phosphorylation status of TRPC3 were detected with or without PPase treatment in SCA14 and control cerebellar tissue. Experiments in this part were repeated for three times and representative images and immunoblots are shown.

5.4 Chapter Discussion

In this chapter, an *in vitro* disease model was generated using iPSCs derived from SCA14 patients carrying two distinct mutations (H36R and H101Q) that faithfully recapitulates the pathological findings observed in human SCA14 cerebellum. These results suggest that SCA14 is caused by three interconnected pathogenic mechanisms. First, SCA14 mutations in the C1 domain promote formation of PKCγ foci in the cytoplasm, which is further enhanced by PKCγ activation and accumulate in the cytoplasm. Second, the reduction of mutant PKCγ at the plasma membrane is likely to reduce its interactions with substrates at the membrane. Third, the extended cytoplasmic retention of the hyperactive mutant PKCγ results in the aberrant phosphorylation of its substrates in the cytoplasm. Together, this unique model is an ideal tool for further investigation of the molecular pathogenic mechanisms underlying SCA14 and for development of therapies.

5.4.1 SCA14 mutations promote formation of PKCγ foci

This study sheds light on the importance of how mutant PKCγ causes SCA14 aetiology. Although cerebellar atrophy has been observed in MRI images of SCA14 patients in clinical cases, information regarding human neuropathology is limited as brain tissue of SCA14 patients is scarce. In this chapter, a loss of Purkinje cells in the SCA14-H101Q patient cerebellum was identified, in which the surviving Purkinje cells showed dendritic abnormalities (Fig. 5.1). Moreover, both mutations investigated in this study enhanced the formation of PKCγ foci in the cytoplasm in iPSCs (Fig. 5.2) and Purkinje cells of SCA14 H101Q cerebellum (Fig. 5.1). This clustering of PKCγ was further facilitated by PKCγ activation in SCA14 iPSCs (Fig. 5.2). PKCγ foci formation has also been described in overexpression of PKCγ in heterologous cell lines (Doran et al., 2008; Nemeth et al., 2013; Ogawa et al., 2013; Seki et al., 2005a; Seki et al., 2007) and in Purkinje cells *in vivo* (Shuvaev et al., 2011). These foci are often Triton-insoluble. Mutant PKCγ was more enriched in the Triton-insoluble pellets in SCA14-H101Q

cerebellum (Fig. 5.1C & D). A considerable portion of PKCγ localised in the Triton-insoluble pellet in control cerebellar tissue, which is consistent with the results obtained in overexpression models (Huang et al., 1989; Jezierska et al., 2014). Similarly, prolonged activation of PKC results in its accumulation in the Triton-insoluble fraction, where it is subjected to dephosphorylation and degradation (Antal and Newton, 2014; Curnutte et al., 1994; Nixon and McPhail, 1999). This shows that it is plausible that the repeated/chronic activation of PKCγ *in vivo* under normal physiological condition lead to its localisation in the Triton-soluble supernatant while SCA14 mutations facilitate this process in patient cerebellum. However, preliminary results showed that mutant PKCγ in SCA14 iPSCs did not appear to be particularly Triton-insoluble in the absence or presence of transient PMA treatment (10 and 60 minutes) (Fig. 5.2F-H). A possible explanation is that mutant PKCγ in SCA14 iPSCs forms oligomers prior to forming insoluble inclusions, as described in several other neurodegenerative diseases (Glabe and Kayed, 2006; Haass and Selkoe, 2007; Takahashi et al., 2015). This is consistent with the Triton-soluble oligomers formed by another SCA14 mutation (V138E) in the C1B subdomain in COS-7 cells (Takahashi et al., 2015). This suggests that prolonged PKCγ activation might be required for the accumulation of PKCγ in Triton-insoluble pellets. However, prolonged treatment (4 hours) of iPSCs with 400 nM PMA caused cell death (data not shown). In the future, it would be interesting to examine whether longer incubation of SCA14 iPSCs using a lower dosage of PMA will promote the accumulation of mutant PKCγ in Triton-insoluble pellets. Alternatively, the formation of mutant PKCγ oligomers that is Triton-soluble in SCA14 iPSCs may be a result of the gel-like phase separation, which acts as an adaptive cellular response against short-term cellular stress (Riback et al.). It has been shown that *in vitro*, under physiological stress condition, proteins form gel-like structures that are microscopically visible under stress conditions (Riback et al.). A transient formation and gradual disappearance of small mutant PKCγ foci was observed in primary cultured mouse Purkinje cells overexpressing a SCA14-S119P mutation in C1B subdomain (Seki et al., 2009). This disappearance of remaining small foci was more evident when overexpression of mutant

PKCγ was shut down (Seki et al., 2009). While the observations in iPSCs are likely to reflect the early stages of pathogenesis, chronic activation of PKCγ might be needed for the formation and accumulation of insoluble and dysfunctional foci in SCA14 cells, which might explain the late-onset nature of SCA14. In the future, to assess the presence of PKCγ inclusions in SCA14 cerebellum, 1% SDS extraction of control and diseased cerebellum and ultracentrifugation at 100000 x *g* could be performed (Peng et al., 2018; Tofaris et al., 2003).

Owing to their post-mitotic nature, neurons are particularly vulnerable to misfolded proteins, as they cannot dilute toxic substances by division (Menzies et al., 2017). Foci formation of three SCA14 mutants (H101Y, S119P and G128G) has been shown to induce ER stress and apoptosis in mammalian cell lines and neuronal cells (Lin et al., 2007; Lin and Takemoto, 2007; Seki et al., 2007). Gap junctions have been suggested to propagate the cell death signals to neighbouring cells (Lin et al., 2007; Lin and Takemoto, 2007; Nguyen et al., 2004). However, no significant cell death in SCA14 iPSC culture was observed in the absence or presence of phorbol ester activation, potentially due to the short-term activation of mutant PKCγ. Consistently, co-localisation of mutant PKCγ foci and the apoptotic cell death marker cleaved caspase 3 was not detected in the remaining Purkinje cells in the SCA14 cerebellum (data not shown). This suggests that the loss of Purkinje cells in SCA14 patients might be caused by cell death mechanisms other than apoptosis (Jellinger, 2001). Interestingly, lysosomes participate in cell death signalling mediated by cathepsins in a caspase-independent manner (Appelqvist et al., 2013). In the future, it would be interesting to perform cell death assays to determine if the accumulation of mutant PKCγ foci induces other cell death mechanisms following PKCγ activation in SCA14 iPSCs.

5.4.2 Accumulation of PKCγ foci in the cytoplasm

Misfolded proteins are primarily degraded via the UPS, and age-decline of the UPS has been shown to be an important pathogenic mechanism underlying neurodegeneration (Ciechanover and Kwon, 2015, 2017; Dantuma and Bott, 2014; Kwon and Ciechanover, 2017; VerPlank et al., 2017). However, co-localisation of mutant PKCγ foci and ubiquitin was not observed in SCA14 iPSCs (Fig. 5.5) and Purkinje cells (data not shown), which is consistent with the lack of co-localisation of ubiquitin and PKCγ foci in cell models reported in another study (Doran et al., 2008). Importantly, ubiquitination of misfolded proteins is also required for their recruitment into autophagosomes for subsequent degradation. The lack of association between ubiquitin and PKCγ foci might therefore also affect their degradation via autophagy. Indeed, autophagosome formation was not induced and p62 protein expression was reduced in SCA14 iPSCs and post-mortem cerebellar tissue (Fig. 5.6). Moreover, the majority of PKCγ foci did not localise with autophagosomes following PMA treatment and PKCγ levels were not affected in the presence of autophagy inhibitor BafA1 (Supplementary figure 5.1), suggesting that mutant PKCγ is not degraded by autophagosome-mediated pathways. These results thus bring a plausible hypothesis that PKCγ might be involved in autophagy regulation in the cerebellum and the pathways might be dysregulated by mutant PKCγ. Indeed, PKCs has been shown to inhibit autophagy and phosphorylate LC3 following PKC activation by PMA treatment *in vitro* (Jiang et al., 2010) and in cellular models (Jiang et al., 2010; Li and Zhang, 2017). Furthermore, PKCα supressed the formation of LCII-positive autophagosomes via miR-129-2 that repressed the expression of peroxisome proliferator-activaated receptor c coactivator 1alpha (PGC-1α) in mouse embryonic brain (Wang et al., 2017). Although the reduced p62 basal levels and the lack of autophagosome formation appear to be conflicting, PKC has also been shown to regulate autohpahy through a mechanism independent of LC3 phosphorylation (Jiang et al., 2010). Therefore, it is plausible that PKCγ might be involved in regulating p62 expression. It would be interesting to study whether and how autophagy regulation is affected by mutant PKCγ in SCA14 in future studies.

Since ubiquitination is central to the degradation of misfolded proteins via the proteasome and autophagosome pathways, it would be interesting to investigate why PKCγ foci do not associate with ubiquitin in future studies. Dephosphorylation of PKC is a prerequisite of the subsequent ubiquitination and degradation via a proteasome pathway (Lu et al., 1998). The hyper-phosphorylation state of mutant PKCγ detected in SCA14 iPSCs and cerebellum (Fig. 5.9) might result in its resistance to ubiquitination. Moreover, degradation of misfolded proteins is initiated when chaperones and ubiquitin ligases recognize abnormalities in folding, such as hydrophobic residues exposed on the surface and improper disulphide bonds (Ciechanover and Kwon, 2015). Interestingly, mammalian heat shock protein 70 (Hsp70) interacts with an E3 ligase CHIP and promotes the proteasome degradation of cytosolic misfolded proteins (Ciechanover and Kwon, 2015, 2017). HSP70 has been reported to be upregulated and co-localise with mutant PKCγ foci in SH-SY5Y cells and primary mouse Purkinje cells overexpressing the S119P mutant (Ogawa et al., 2013). It is possible that the recognition of mutant PKCγ foci by ubiquitin ligases is impaired and therefore cannot be degraded. To confirm that PKCγ aggregates are not degraded by proteasomes, aggregation of mutant PKCγ could be monitored in the presence of proteasome inhibitor e.g. MG132. In addition, immunoprecipitation of PKCγ and immunoblotting for ubiquitin could be performed to examine whether PKCγ is ubiquitinated. Impairments in the ubiquitination processes could be identified using antibodies against linkage- and length-specific ubiquitin. The levels and the interactions of the three enzymes regulating ubiquitination (E1, E2 and E3) with mutant PKCγ could also be monitored.

Interestingly, although PKCγ does not appear to be degraded via autophagy and its association with ubiquitin and lysosomes is limited, lower protein levels of PKCγ was detected (Fig. 5.2). This might be a result of aberrant mRNA translation. To test this hypothesis, protein

biosynthesis can be halted by cyclohexamide and the levels of PKCγ can be determined via immunoblotting.

The enhanced formation of lysosomes in SCA14 iPSCs and cerebellum (Fig. 5.7) suggests that PKCγ aggregates might enter the lysosomal pathway via autophagosome-independent routes. Mutant PKCγ has been shown to localise within endosomes in an overexpression system (Doran et al., 2008). PKCγ foci might enter the lysosomes via alternative mechanisms such as chaperone-mediated-autophagy (CMA). Misfolded proteins carrying a KFERQ peptide sequence are sort out by molecular chaperones, unfolded and directly delivered to the lysosomes for degradation through LAMP2A (Ciechanover and Kwon, 2015, 2017). As CMA can be activated to compensate for impaired macroautophagy in degenerating neurons (Ciechanover and Kwon, 2015), it would be interesting to investigate whether levels of chaperones involved in CMA such as heat shock cognate 70 (HSC70), heat shock proteins 40 (HSP40) and 90 (HSP90) (Chiang et al., 1989; Ciechanover and Kwon, 2017) as well as LAMP2A are altered in SCA14 iPSCs and cerebellum. Overall, the results presented here suggest that PKCγ is not degraded by autophagy and its association with ubiquitin and lysosomes is limited, which results in the accumulation of PKCγ foci in the cytoplasm in SCA14 iPSCs. Future studies into the mechanisms of ubiquitination and degradation of mutant PKCγ will be crucial to understanding the disease pathways of SCA14.

5.4.3 SCA14 mutations reduce membrane association of mutant PKCγ

The mobility and the resulting subcellular localisation of PKCγ could be affected by SCA14 mutations via the disruption of its binding to regulators (Jezierska et al., 2014; Seki et al., 2005b). Several SCA14 mutations in C1B domains have been predicted to disrupt the zinc-finger regions and phorbol ester-binding sites (Chen et al., 2003; Lin et al., 2007; Verbeek et

al., 2008). In the present study, reduced staining of PKCγ at the plasma membrane of Purkinje cells in SCA14 cerebellum was observed (Fig. 5.1B). Moreover, mutant PKCγ foci remained in the cytoplasm following phorbol ester treatment in SCA14 iPSCs (Fig. 5.4). Consistent with our results, membrane translocation of mutant PKCγ was retarded in cell models following phorbol ester stimulation (Nibbeling et al., 2017; Verbeek et al., 2008) and in Purkinje cell dendrites when stimulated with potassium chloride (Seki et al., 2009). Single-molecule microscopy of SCA14 mutants also showed a reduction of their residence time at the membrane (Adachi et al., 2008). Although C1A and C1B were thought to be functionally redundant due to their comparable affinity to DAG (Ananthanarayanan et al., 2003), these findings indicated that SCA14 mutations in either C1 subdomain alone reduced PKCγ membrane translocation, which was not compensated by the other intact C1 subdomain (Fig. 5.4). This observed attenuated membrane translocation of mutant PKCγ is in contrast to a report that two SCA14 mutations (G118D and C150F) did not affect phorbol ester-induced membrane targeting (Verbeek et al., 2005). This difference could be due to the nature of distinct mutations and explained by different experimental designs. In this study, the overall effect of SCA14 mutations on cell populations in fixed iPSCs was studied at selected time-points following PMA treatment. On the other hand, Verbeek et al. (2005) performed time-lapse experiments to capture real-time translocation of mutant PKCγ co-expressed with fluorescence reporters in individual cells. These two approaches have different advantages and limitations. To address this limitation of the current method, time-lapse experiments of GFP-tagged PKCγ in gemone-modified iPSC lines could be used to verify that whether mutant PKCγ did not interact with plasma membrane at all or only briefly that would be difficult to capture using fixed time-point experiments.

Membrane translocation of PKCγ appears to be stimulus-dependent. The membrane translocation of SCA14 mutants has been shown to differ in response to different stimulation such as phorbol ester, calcium and purinergic receptors in heterologous cell lines (Adachi et al.,

2008; Seki et al., 2005a; Seki et al., 2005b; Verbeek et al., 2005; Yagi et al., 2004). It would be interesting to investigate whether mutant PKCγ in SCA14 iPSCs responds differently to other cellular stress or to stimuli that interact with domains other than C1 domains. In fact, studies have reported that the C1 domain of PKCγ is masked in the inactive form by the C2 domain and is inaccessible to DAG (Farah et al., 2012). The region immediately upstream of the C1 domain contains an inhibitory pseudosubstrate, which acts as a clamp to keep C1 domain inaccessible to DAG and is released when C2 domain binds to membrane (Newton, 2003; Newton, 2010; Oancea and Meyer, 1998). SCA14 mutations on C1 domains might weaken the C1 clamp making C2 domain more accessible to calcium. This might explain the enhanced membrane retention of SCA14 mutants when stimulated by calcium ionophores. Overall, my results suggest that SCA14 mutations significantly reduce phorbol ester-induced membrane association of PKCγ.

5.4.4 Increased kinase activity of PKCγ and excessive downstream signalling

The phosphorylation status of PKCγ closely regulates its maturity and kinase activity (Callender and Newton, 2017). In this chapter, the phosphorylation levels of mutant PKCγ at different sites were investigated. Although kinase activity of mutant PKCγ has been shown to be higher than wildtype PKCγ in *in vitro* cell models (Adachi et al., 2008; Asai et al., 2009; Shimobayashi and Kapfhammer, 2017; Verbeek et al., 2005) and implicated in one study using SCA14 transgenic mice (Ji et al., 2014), it remains unclear whether increased kinase activity directly cause abnormal development, function and loss of Purkinje cells in SCA14. This work demonstrated that SCA14 mutations promoted the phosphorylation and a catalytically competent state of mutant PKCγ in both human SCA14 patient cerebellum and iPSCs (Fig. 5.9). The open conformation caused by SCA14 mutations in C1 domains (Jezierska et al., 2014; Verbeek et al., 2008) might make mutant PKCγ more accessible to PDK-1, resulting in high

phosphorylation at T514 and possibly enhanced subsequent autophosphorylation events. The robust elevation of phosphorylated-PKC substrates in the patient cerebellum, which showed Purkinje cell loss and dendritic atrophy, further indicates that increased kinase activity of mutant PKCγ is a major pathogenic mechanism underlying SCA14. Notably, SCA14 mutants led to enhanced phosphorylation of PKC substrates even under basal condition suggesting that the constitutive kinase activity of mutant PKCγ is indeed higher (Fig. 5.9). A number of SCA14 mutations in the C1 domains including H101Q have been reported to show higher kinase activity using *in vitro* kinase activity assays in COS-7 and CHO cells, before and after PMA treatment (Adachi et al., 2008; Asai et al., 2009; Verbeek et al., 2005).

SCA14 mutations such as V138E that sit at the C1B clamp for maintaining proper PKCγ conformation are reported to show reduced kinase activity (Verbeek et al., 2008). This is in line with the hypothesis that differential results obtained from different SCA14 mutants are likely due to the distinctive impact of these mutations on the overall structure and activity of PKCγ. A recent study comparing dendritic development of mouse Purkinje cells overexpressing mutant PKCγ suggests that mutations in different domains affect dendritic development differentially (Shimobayashi and Kapfhammer, 2017). The authors reported that although the tested mutations showed increased kinase activity in *in vitro* cell models and biochemical analyses, some of the SCA14 mutants did not affect dendritic growth in primary cultured mouse Purkinje cells. They therefore concluded that increased biological activity of mutant PKCγ is not required for SCA14 pathogenesis. However, the molecular pathways by which PKCγ affects dendritic development of Purkinje cells remain incompletely understood. It is still unclear whether there is a direct link between PKCγ kinase activity and Purkinje cell dendritic development. Therefore, overall area of Purkinje cell dendritic trees might not be the ideal measurement and should not be the only parameter for evaluating the impact of mutant PKCγ on dendritic development of Purkinje cells. In addition, thickness, length and degree of branching of dendrites, which are widely used parameters, should be taken into consideration

as demonstrated in other studies (Gundlfinger et al., 2003; Ji et al., 2014; Metzger and Kapfhammer, 2000; Schrenk et al., 2002). Overall, mutations in different domains of PKCγ are likely to effect PKCγ kinase activity in different ways. Nonetheless, regardless of upregulation or downregulation of kinase activity, changes in mutant PKCγ function ultimately lead to dysfunction and degeneration of Purkinje cells in SCA14. This suggests that maintaining the homeostasis of signalling downstream of PKCγ is key to treating SCA14.

It is noteworthy that, although PKCγ is broadly expressed in the brain, Purkinje cells are particularly vulnerable to altered functions of mutant PKCγ. One possible explanation is that mutant PKCγ reacts with substrates that are only or highly expressed in Purkinje cells. However, substrates of PKCγ remain largely unknown. PKC has long been implicated in the regulation of neurotransmission and synaptic plasticity by phosphorylating membrane receptors and ion channels (Callender and Newton, 2017) (section 1.4.4). Mutant PKCγ might affect membrane excitability in Purkinje cells either indirectly through altering the membrane kinetics of PKCα (Shuvaev et al., 2011), or directly via phosphorylation of receptors. The reduction of PKCγ at the plasma membrane might affect its interactions with substrates. One possible membrane-associated substrate of PKCγ is the cation channel TRPC3, which is highly expressed in Purkinje cells (section 1.4.4). PKCγ has been shown to negatively regulate calcium entry via the phosphorylation of TRPC3 (Trebak et al., 2005; Venkatachalam et al., 2003). Surprisingly, increased phosphorylation of TRPC3 was detected in SCA14 iPSCs despite the reduction of mutant PKCγ at the plasma membrane (Fig. 5.10G & H). This suggests that the enhanced kinase activity of mutant PKCγ might be sufficient to increase TRPC3 phosphorylation in spite of the reduced membrane retention of mutant PKCγ. Indeed, weak staining of small PKCγ puncta, which might be wildtype or non-aggregated soluble mutant PKCγ, was observed at the plasma membrane of SCA14 iPSCs (data not shown). Therefore, an excessive phosphorylation and inhibition of TRPC3 might lead to aberrant calcium homeostasis and thereby contribute to Purkinje cell dysfunction and cell death. The altered signalling

downstream of TRPC3 is likely to affect Purkinje cell development and functions. C1 domain mutants of PKCγ cause sustained calcium influx while other SCA14 mutants with an intact C1 domain inhibit calcium entry (Adachi et al., 2008). This suggests that SCA14 might be caused by calcium imbalance through either increased or decreased calcium signalling. It is therefore important to examine whether calcium transients are affected in SCA14 iPSCs using calcium imaging in a combination with pharmaceutical enhancers and blockers of different calcium-permeable channels in future studies.

Moreover, the cytoplasmic retention of hyperactive mutant PKCγ might increase the interactions with its substrates in the cytoplasm. In this chapter, an increase of phosphorylation of PKC substrates and MARCKS, a known PKCγ substrate, was shown in the SCA14 cerebellum (Fig. 5.9E). This observed increase in phosphorylation of PKC substrates and MARCKS in the SCA14 cerebellum is in contrast to another study reporting reduced phosphorylated MARCKS in PMA-treated HeLa cells that were overexpressing mutant PKCγ (Verbeek et al., 2008). This suggests that the interactions detected in the SCA14 cerebellum are likely to be specific to Purkinje cells and might not be detected in heterologous cell lines, further highlighting the need of a reliable disease model of SCA14. MARCKS is a multifunctional protein that regulates actin cytoskeleton and endocytosis, and has been suggested to be involved in brain development (Bubb et al., 1999; Hartwig et al., 1992; Hussain et al., 2006; Larsson, 2006). Interestingly, PKCγ triggers actin reorganisation and activates endocytosis in response to PMA possibly via the perinuclear translocation of phosphorylated MARCKS (Yamamoto et al., 2014). This actin-dependent endocytotic pathway is important for the morphological changes of the cells by incorporating membrane proteins and contributes to growth cone collapse in repulsive axonal guidance (Kabayama et al., 2009; Kolpak et al., 2009; Lim and Gleeson, 2011). The PKCγ-mediated phosphorylation of MARCKS might serve to activate the endocytosis of membrane proteins and F-actin, which might be important for the retraction of excessive dendritic arborisation of Purkinje cells during development. The excessive

phosphorylation of MARCKS caused by mutant PKCγ might therefore lead to over retraction of dendrites and ultimately atrophy observed in Purkinje cells of the post-mortem cerebellum.

Taken together, these results suggest that SCA14 mutations lead to increased kinase activity of PKCγ in patient iPSCs and cerebellum, confirming the importance of altered kinase activity of mutant PKCγ in SCA14 pathogenesis. Moreover, the increased phosphorylation of TRPC3 in SCA14 iPSCs suggests that abnormal signalling downstream of PKCγ is likely to involve convergent pathways linking different SCA subtypes (Becker, 2017; Meera et al., 2016), and therefore a pathological role of PKCγ beyond SCA14. To gain a better understanding of the pathogenic mechanism in SCA14 and other ataxias, it would be important to identify the aberrantly phosphorylated proteins in SCA14 using a proteomics approach.

Overall, SCA14 appears to be caused by a combination of gain and loss of function of PKCγ. The reduced membrane association of mutant PKCγ is likely to affect the phosphosphorylation of its membrane substrates, which is a loss of PKCγ function. The extended cytoplasmic retention of hyperactive mutant PKCγ might increase its substrate phosphorylation in the cytoplasm, which represents a gain of function. However, it remains unclear whether and how these impairments affect the development and function of human Purkinje cells, which are important to be addressed in future studies.

5.5 Conclusions

In this chapter, a faithful and reliable *in vitro* model of SCA14 that reflects cerebellar pathology using human patient-derived iPSCs is presented. The findings reported in this chapter indicate that SCA14 appears to be caused by a combination of gain and loss of function of PKCγ (Fig. 5.11). (1) SCA14 mutations enhanced the formation of PKCγ foci and its accumulation in the cytoplasm. (2) While the reduced membrane association (loss of function) of the hyperactive

(gain of function) mutant PKCγ might alter its interactions with substrates at the membrane, (3) the extended cytoplasmic retention might increase phosphorylation of its substrates in the cytoplasm (gain of function). The identification of mutant PKCγ substrates will enable the further elucidation of the underlying pathological pathways. Moreover, the generated patient iPSCs could be differentiated into human Purkinje cells to investigate the pathogenic pathways that cause their dysfunction and degeneration *in vitro*. Ultimately, these findings will be extremely valuable to identify novel therapeutic targets for SCA14 and related SCAs.

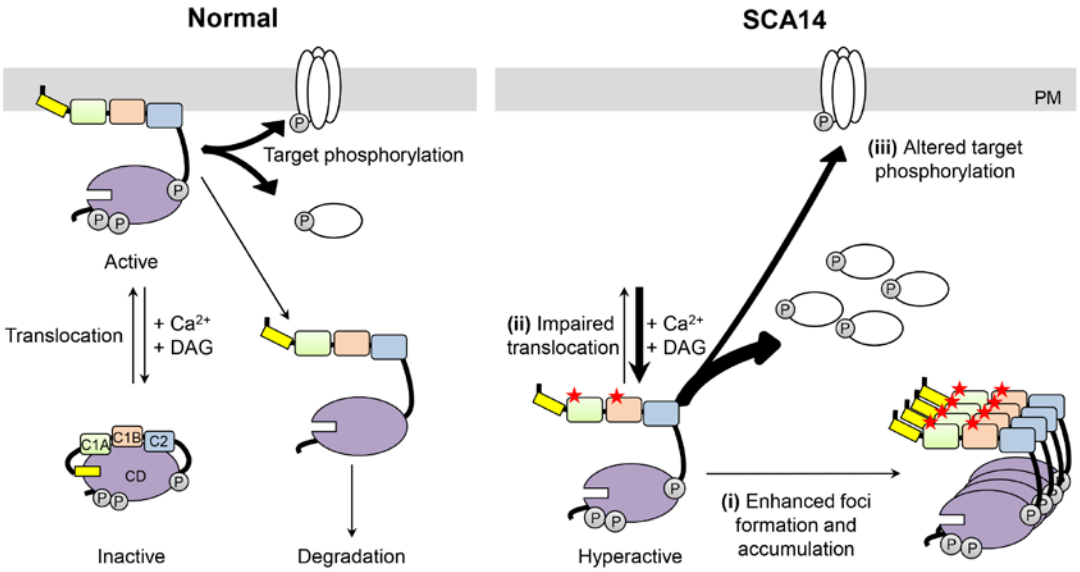


Figure 5.10 Model of the functional effect of PKCγ mutations.

In normal cells, mature wildtype PKCγ resides in the cytoplasm in an autoinhibited conformation (inactive). Binding of second messengers such as DAG/phorbol ester and calcium ions (Ca^{2+}) to PKCγ promotes its translocation to the plasma membrane. The pseudosubstrate is then released from the substrate-binding cavity of the catalytic domain. This active PKCγ phosphorylates its substrates at the membrane. PKCγ returns to the autoinhibited conformation following the decay of its second messengers. The membrane-bound confirmation of PKCγ is sensitive to dephosphorylation by phosphatases PHLPP and PP2A producing a dephosphorylated PKCγ that is subjected to degradation. In contrast, in SCA14, PKCγ forms foci, which accumulate in the cytoplasm. (1) The membrane association of mutant PKCγ is reduced. The reduction of PKCγ at the membrane is likely to alter the phosphorylation of its membrane substrates. In addition, (3) the extended cytoplasmic retention of the hyperactive mutant PKCγ might increase the phosphorylation of PKCγ substrates in the cytoplasm.

Chapter 6 Understanding the pathogenic mechanisms underlying SCA14 using human iPSC-derived Purkinje cells

6.1 Introduction

6.1.1 The role of SCA14 mutations in Purkinje cell development

Protein kinase C gamma (PKCγ) plays important roles in the development and function of Purkinje cells (refer to section 1.4.4). The expression of PKCγ peaks in the third postnatal week in mice (Crepel, 1982), which is the period of extensive dendritic growth in Purkinje cells, and remains high throughout life. PKCγ is involved in the regulation of size and complexity of Purkinje cell dendritic arbours (Fujishima et al., 2012; Metzger and Kapfhammer, 2000; Schrenk et al., 2002). In addition, PKCγ regulates the elimination of redundant synapses and innervation from climbing fibres (Chen et al., 1995; Kano et al., 1995). The loss of PKCγ in knockout mice results in mild ataxia (Abeliovich et al., 1993; Chen et al., 1995). Moreover, abnormal, persistent and multiple climbing fibre innervations of Purkinje cells *in vivo* were found (Kano et al., 1995), but gross cerebellar atrophy was absent (Abeliovich et al., 1993; Chen et al., 1995). Moreover, Purkinje cell dendritic trees were enlarged and had an increased number of branching points in slice cultures from PKCγ-deficient mice (Schrenk et al., 2002). Consistent with the knockout studies, pharmacological inhibition of PKC resulted in overgrown dendritic trees and excessive branching points of Purkinje cells, whereas pharmacological activation of PKC caused dendritic atrophy (Metzger and Kapfhammer, 2003; Schrenk et al., 2002). However, the effect of SCA14 mutations on human Purkinje cell development remains to be elucidated. In the previous chapter, SCA14 mutations were shown to alter PKCγ function in iPSCs. This raises the interesting hypothesis that in Purkinje cells, altered functions of PKCγ might disrupt signalling downstream of PKCγ, and impair the development and dysfunction of Purkinje cells. Two transgenic mice overexpressing distinct SCA14 (H101Y, S361G)

mutations have been generated. However, inconsistent disease phenotypes have been reported for these (Ji et al., 2014; Zhang et al., 2009). Although both PKCγ-H101Y and PKCγ-S361G transgenic mice displayed mild cerebellar ataxia, only PKCγ-H101Y transgenic mice, but not PKCγ-S361G mice, showed a loss of Purkinje cells (Ji et al., 2014; Zhang et al., 2009). Purkinje cells from PKCγ-S361G mice showed impairments in length, thickness and complexity of dendritic trees in slice culture experiments (Ji et al., 2014). However, the molecular mechanisms by which PKCγ controls these processes and how mutant PKCγ ultimately results in the dysfunction and degeneration of human Purkinje cells remain to be elucidated.

Previous studies of SCA14 pathogenesis have predominantly relied on heterologous cell lines and two transgenic mouse models (out of 40 known SCA14 mutations) (Ji et al., 2014; Seki et al., 2009; Zhang et al., 2009). Thus far, no patient-derived induced pluripotent stem cells (iPSCs) or iPSC-derived neurons have been reported. In this chapter, a protocol for the differentiation of Purkinje cells from human iPSCs was developed in order to study the developmental changes in human Purkinje cells. Using this protocol, human control and patient iPSCs were differentiated into Purkinje cells. Finally, the *in vitro* developmental changes of human iPSC-derived Purkinje cells caused by SCA14 mutations were investigated.

6.1.2 Cerebellar development

The *in vitro* generation of Purkinje cells from human iPSCs relies on the recapitulation of the key molecular events that control cerebellar development *in vivo*. However, the molecular pathways underlying human cerebellar development remain incompletely understood. Our understanding of human cerebellar development is predominantly obtained through studies of the mammalian cerebellum, in particular that of rodents, of which cerebellar structure and genetic programmes are highly conserved. The development of the mammalian cerebellum is orchestrated by both cell-autonomous programmes and inductive environmental cues (Leto et

al., 2016). Cerebellar development is divided into three phases: (1) specification of cerebellar anlage during early hindbrain development, (2) allocation of cerebellar cell types along the dorsoventral axis, and (3) amplification and migration of granule cell precursors from the external granule layer (EGL) over the cerebellar surface to form the internal granule layer (IGL) (Andreu et al., 2014; Butts et al., 2014).

Mammalian embryos establish three cell germ layers including ectoderm, mesoderm and endoderm that give rise to distinct cell lineages during embryonic development. The neural plate of the ectoderm is a key structure that develops into the nervous system. During neurulation, the edges of the neural plate thicken and roll up to form the neural tube (Andreu et al., 2014). The anterior part of the neural tube is progressively regionalised into three primary brain vesicles: forebrain, midbrain and hindbrain, with defined boundaries (Andreu et al., 2014). These processes are under the control of temporally and spatially coordinated gradients of gene expression (Andreu et al., 2014).

6.1.2.1 Early cerebellar specification

The specification of the cerebellar territory starts as early as embryonic day (E) 8.5 in mice (Fig. 6.1A & B). The reciprocal inhibition of the transcription factors orthodenticle homeobox 2 (Otx2) in the rostral neuroepithelium and gastrulation brain homeobox 2 (Gbx2) in the caudal neuroepithelium broadly marks and maintains the position of midbrain-hindbrain boundary (MHB) in the neural tube (Andreu et al., 2014; Butts et al., 2014; Leto et al., 2016; Martinez-Barbera et al., 2001). The isthmus/isthmic organiser located at the MHB expresses different transcription factors that further refine neural regions along the anterior-posterior or dorsal-ventral axis. One of the major signalling molecules in the isthmus is Fgf8, which is a member of the fibroblast growth factor (Fgf) family (Hidalgo-Sanchez et al., 1999). Fgf8 is expressed from E8.5 at the interface of Otx2 and Gbx2 expression and further stabilises the MHB. Ectopic

expression of Fgf8 is sufficient to induce the formation of isthmus-like tissue (Crossley et al., 1996; Garda et al., 2001; Martinez et al., 1999). A decreasing gradient of Fgf8 protein concentration in the alar plate of the isthmus and rhombomere 1 of the hindbrain is essential for cell survival and differential development of cerebellar regions (Basson et al., 2008; Chi et al., 2003; Nakamura et al., 2005). Fgf8 induces the expression of wingless homologue 1 (Wnt1) through LIM homeobox transcription factor 1-beta (Lmx1b) (Adams et al., 2000; Reifers et al., 1998). Wnt1 and Lmx1b are expressed as in a thin band confined to the caudal-most Otx2 expression domain next to the Fgf8-expressing isthmus (Danielian and McMahon, 1996). Wnt1 maintains the expression of engrailed-1 (En1), which in turns positively regulates Fgf8 expression, completing the feedback regulatory loop (Danielian and McMahon, 1996; Simeone, 2000). Engrailed-2 (En2), a paralogue of En1, is shortly expressed after En1 across the MHB with a maximum expression level at the isthmus (Joyner, 1996). Gradients of En1 and En2 are oriented towards the rostral and caudal ends of the neural tube. Importantly, En2 contributes to the specification of all cerebellar cell types (Andreu et al., 2014; Leto et al., 2016).

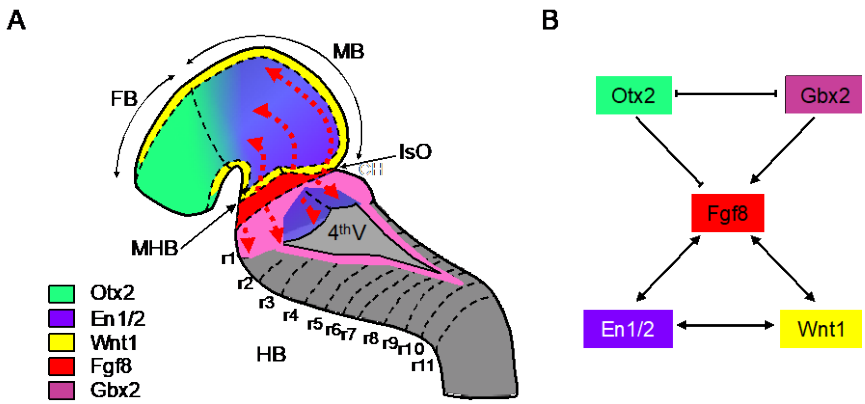


Figure 6.1 Schematic representation of the specification of the cerebellar territory.

(A) Distribution of the major gene expression gradients within the mouse neural tube at E11.5. The spatio-temporal interactions between the gradients define the boundaries between the forebrain (FB), midbrain (MB) and hindbrain (HB). The reciprocal inhibition between Otx2 and Gbx2 positions the isthmic organizer (IsO) at the midbrain–hindbrain boundary (MHB). The IsO is critical for the induction of the cerebellum from rhombomeres r0 and r1 via the expression of Fgf8. Red dotted arrows indicate the rostral and caudal gradients of Fgf8 expression. Modified from (Andreu et al., 2014; Leto et al., 2016; Watson et al., 2015b). (B) Interactions between the main genes that are required for the specification of the midbrain/hindbrain region. Adapted from (Watson et al., 2015b).

6.1.2.2 Specification of cerebellar progenitors

Following early cerebellar patterning and closure of the neural tube, cell fate specification of cerebellar progenitors begins at E10.5-12.5 in mice. All cerebellar neurons are produced in the two germinal zones in the alar plate of rhombomere 1: the rhombic lip and the cerebellar ventricular zone (Alder et al., 1996; Wingate and Hatten, 1999). The rhombic lip generates glutamatergic neurons including granule cells, unipolar brush cells and projection neurons of the deep cerebellar nuclei. The cerebellar ventricular zone gives rise to GABAergic neurons including Purkinje, Lugaro, Golgi, basket and stellate cells, and Bergmann glia (Andreu et al., 2014; Leto et al., 2016; Muguruma et al., 2015; Muguruma et al., 2010).

The generation of cerebellar cells is spatially and temporally regulated by two tissue-specific basic helix-loop-helix transcription factors: Atoh1/Math1 and Ptf1α at E10.5-12.5 in mice. The expression of Atoh1 in the rostral rhombic lip is induced by bone morphogenetic protein (BMP) from the roof plate and is regulated by TGFβ and Delta-Notch signalling (Alder et al., 1996). Targeted disruption of the *Atoh1* gene led to the loss of glutamatergic neurons in the cerebellum (Ben-Arie et al., 1997; Englund et al., 2006; Machold and Fishell, 2005; Wang et al., 2005). Ptf1α is one of the earliest markers of the cerebellar ventricular zone and its expression is influenced by Shh signals (Huang et al., 2010). The expression of Ptf1α is essential to the genesis of Purkinje cells and other GABAergic neurons. Deletion of the *Ptf1α* gene caused the loss of GABAergic neurons in the cerebellum (Hoshino et al., 2005; Pascual et al., 2007). Moreover, the expression of Atoh1 and Ptf1α are mutually exclusive. Misexpression of Atoh1 and Ptf1α caused ectopic generation of glutamatergic and GABAergic neurons (Pascual et al., 2007; Yamada et al., 2014), suggesting that progenitors might have the potential to contribute to any lineage within the cerebellum.

6.1.2.3 Migration and maturation of Purkinje cells

Purkinje cells are generated by Ptf1α-positive progenitors in the ventricular zone at E10.5-12.5 in mice (Leto et al., 2016; Sotelo and Rossi, 2013). This Purkinje cell precursor-containing region is characterised by the transient strong expression of E-cadherin and downstream targets of Ptf1α such as Kirrel2/Neph3, neurogenin 1 and 2, and Nephrin (Hoshino, 2012; Mizuhara et al., 2010). Neurogenin 1 and 2 are transiently expressed in restricted regions during Purkinje cell genesis, suggesting their involvement in the specification of heterogeneous Purkinje cell subsets (Florio et al., 2012; Hoshino, 2012; Mizuhara et al., 2010; Zordan et al., 2008). These precursors in the ventricular zone continue to mature and express early Purkinje cell markers Lhx1, Lhx5 and Corl2 as development proceeds (Chizhikov et al., 2006; Minaki et al., 2008; Morales and Hatten, 2006; Zhao et al., 2007). Subtype specification of Purkinje cells likely occurs when Purkinje cells undergo terminal mitosis between E10.5 and E13.5 (Miale and Sidman, 1961). Birth dating studies show that early born Purkinje cells (E10.5-11.5), which are negative for Neurogenins 1 and 2, and early B-cell factor 2 (Ebf2), become zebrin II-positive. In contrary, Purkinje cells born between E11.5 and E13 express Neurogenins 1 and 2, and Ebf2 but not zebrin II (Chung et al., 2008; Hashimoto and Mikoshiba, 2003; Karam et al., 2000; Larouche et al., 2006; Namba et al., 2011).

Migration of Purkinje cells follows after their genesis in the ventricular zone. Newborn Purkinje cells at the posterior edge of the ventricular zone migrate tangentially from E10.5 and then anteriorly between E12.5 and E14.5 in mice (Croci et al., 2011; Miyata et al., 2004). These Purkinje cells are characterised by long leading processes and a shorter trailing process containing the Golgi apparatus. By contrast, Purkinje cells born more anteriorly display radial orientation and migration along the processes of radial glia from the ventricular neuroepithelium to the pial surface between E14.5 and E17.5 (Miyata et al., 2010). Granule cells are important for the proper migration and maturation of Purkinje cells. From E13.5, granule cell precursors migrate tangentially along the pial surface and form a transient

superficial layer of proliferating cells, the EGL. The proliferating granule cell precursors in the EGL secret the glycoprotein Reelin, which mediates the radial migration of Purkinje cells (D'Arcangelo et al., 1995; D'Arcangelo et al., 1997; Tissir and Goffinet, 2003). Purkinje cells subsequently accumulate and form the Purkinje cell plate underneath the EGL (Goffinet, 1983; Yuasa et al., 1991). Disruption of Reelin signalling in *reeler* mice led to clustering of Purkinje cells close to the region of the cerebellar nuclei instead of normal cortical allocation (D'Arcangelo et al., 1995; Mariani et al., 1977; Rice and Curran, 2001). Secreted Reelin binds two surface receptors on Purkinje cells: apolipoprotein E receptor 2 (ApoER2) and the very-low-density-lipoprotein receptor (VLDLR) (Larouche and Hawkes, 2006; Trommsdorff et al., 1999). This binding induces receptor clustering (Strasser et al., 2004) and activates two Src-family kinases Fyn and Src (Bock and Herz, 2003). Activated Fyn and Src phosphorylate the intracellular adaptor docking protein Disabled1 (DAB1) that promotes neuronal migration (Hiesberger et al., 1999). The Reelin-signalling directs the slow radial migration of Purkinje cells and at the same time, restrain this movement to maintain the correct alignment. Purkinje cells are continuously attracted toward the pial surface of the expanding cortex and arranged into the final monolayer by the end of the first postnatal week (Altman, 1972a; Altman and Bayer, 1985; Altman and Bayer, 1997). In parallel, during the first two postnatal weeks in mice, postmitotic granule cell precursors continue to differentiate and migrate radially along Bergmann glia through the molecular layer. Finally, granule cell precursors migrate through Purkinje cell layer to form the final internal granule layer leaving their bifurcated axons in the molecular layer where the dendritic trees of Purkinje cells reside.

6.1.2.4 Maturation and dendritic development of Purkinje cells

The establishment of Purkinje cell dendritic trees is highly dynamic and tightly controlled by growth factors and synaptic inputs (Metzger, 2010). This dynamic process can be divided into two stages: 1) the initial extension and retraction of dendritic branches, followed by 2) the

stabilisation of existing dendrites and synaptic connections (Kapfhammer, 2004; Metzger, 2010; Sotelo and Rossi, 2013).

During the last phase of radial migration in rodents, Purkinje cells display a fusiform elongated morphology, i.e. having unbranched apical dendrites growing from one side of the cell body and the axon leaving from the other side (Armengol and Sotelo, 1991; Ramon y Cajal, 1911). In the first postnatal days, primitive apical dendrites of fusiform Purkinje cells retract while side branches develop. At the same time, multiple new and thinner processes radiate from the soma. In the first postnatal week, Purkinje cells become aligned in a monolayer. Throughout the initial dendritic development, Purkinje cell bodies receive synapses from climbing fibres as early as E19.5 in mice (Mason et al., 1990). Parallel fibres at this time are just starting to develop and only make few immature synapses onto the Purkinje cell dendrites (Altman, 1972b), which show little electrophysiological responses (Woodward et al., 1971). At the end of the first postnatal week, a fast and intense pruning of all or most of Purkinje cell dendritic processes take place and marks the beginning of the ultimate dendritic arborisation.

The early phase of the dendritic formation of fusiform Purkinje cells is controlled by intrinsic factors. The molecular mechanisms of these processes remain to be elucidated. Nuclear receptors RORα is the first to be known to promote dendritic arborisation of Purkinje cells (Rakic and Sidman, 1973). *Staggerer* mice that contained a mutation in RORα and RORα-deficient mice showed cerebellar atrophy as well as a loss of Purkinje and granule cells (Hamilton et al., 1996; Steinmayr et al., 1998). The surviving Purkinje cells displayed a wide range of morphology, including smaller dendrites that were not confined to a single plane and impaired regression of early somatic protrusions (Hamilton et al., 1996; Steinmayr et al., 1998). In contrast, overexpression of RORα1 in fusiform Purkinje cells in slice cultures accelerated dendritic differentiation (Boukhtouche et al., 2006), suggesting that RORα is crucial for dendritic regression. Several growth hormones and trophic factors have been suggested to

modulate dendritic growth of Purkinje cells. Thyroid hormone L-3,3',5-triiodothyronine (T3) increased branching of Purkinje cell dendrites (Lindholm et al., 1993) and number of synapses with parallel fibres in a dose- and time-dependent manner (Heuer and Mason, 2003). Recent studies revealed that T3 acted, independent of neurotrophins (Heuer and Mason, 2003), via the activation of RORα (Boukhtouche et al., 2010), thyroid hormone receptor α1 (TRα1), inhibition of Trk signalling (Heuer and Mason, 2003) and peroxisome proliferator-activated receptor gamma co-activator 1α (PGC-1α) signalling in developing Purkinje cells (Hatsukano et al., 2017). Moreover, the activation of the p75 neurotrophin receptor (p75NTR) (Mount, 1998), neurotrophins 3 and 4 (NT3, NT4) (Heuer and Mason, 2003; Mount et al., 1994), ciliary neurotrophic factor (CNTF) (Larkfors et al., 1994) and insulin-like growth factor IGF1 (Torres-Aleman et al., 1994; Torres-Aleman et al., 1992) were shown to promote Purkinje cell survival and dendritic outgrowth in dissociated cultures. However, their role during normal Purkinje cell development *in vivo* is unclear.

During the later stage of dendritic development, when Purkinje cell bodies acquire their monolayer position, perisomatic protrusions emerge in all directions. Subsequently, lateral and basal processes are withdrawn leaving one to three primary apical segments. Meanwhile, the apical side of the cell body grow and form an apical cone from which a thick primary dendrite emerges. This primary dendrite extensively grows and develops branches. The climbing fibre synapses gradually shift from perisomatic to close to dendrites. In addition, parallel fibres form synaptic contacts with dendritic spines on the outgrowing processes of Purkinje cells. The typical flattened apical dendritic tree emerges by postnatal (P) 6-10. The flat dendritic tree grows laterally to reach the adult size between P10-15. Finally, Purkinje cells reorient from transverse to vertical position from P15 to P30 [reviewed in (Kapfhammer, 2004; Sotelo and Rossi, 2013)]. Synaptogenesis continues throughout the dendritic enlargement until the end of the fourth postnatal week (Altman, 1972a).

These processes are controlled by a combination of intrinsic and extrinsic factors including afferent inputs, trophic factors and hormones (Kapfhammer, 2004; Sotelo and Rossi, 2013). Dissociated Purkinje cells grown in culture in the presence of tetrodotoxin (TTX) or high concentration of magnesium ions, which blocked neuronal action potentials, showed significant reduction in dendritic branching (Schilling et al., 2008). Moreover, granule cell inputs were shown to promote the survival and maturation of Purkinje cells (Baptista et al., 1994) via the modulation of NMDA receptors and brain-derived neurotrophic factor (BDNF) secretion (Hirai and Launey, 2000). Migrating granule cells express the NR2B subunit and subsequently the NR2C subunit of NMDA receptors. Granule cell migration and parallel fibre synapse formation was disrupted when subunit exchange from NR2C to NR2B in transgenic mice was defective (Metzger et al., 2005; Tarnok et al., 2008). The diminishing parallel fibre synaptic inputs led to reduced complexity of Purkinje cell dendritic trees, which was rescued by NMDA treatment in slice cultures (Metzger et al., 2005; Tarnok et al., 2008). This suggests that stronger activation of the fewer parallel fibre inputs might overcome the deficit (Metzger et al., 2005; Schlett et al., 2004) The lack of granule cells and the resulting absence of parallel fibres led to abnormal dendritic development of Purkinje cells as shown in rat cerebellum exposed to X-irradiation (Anderson and Altman, 1972), in the *weaver* and the *reeler* mice (Hirano and Dembitzer, 1973; Mariani et al., 1977; Rakic and Sidman, 1973; Sotelo, 1973, 1975; Sotelo and Changeux, 1974). These mice all had smaller dendritic trees without planar disposition. Furthermore, the dendritic complexity of Purkinje cells grown in slice cultures was significantly reduced resulting from the lack of extrinsic excitatory inputs from mossy and climbing fibres, and diminished parallel fibre inputs. These studies show that the final dendritic arborisation and correct orientation of Purkinje cells require adequate and proper inputs from afferent innervation.

Trophic factors such as BDNF are important for Purkinje cell dendritic development. However, the molecular pathways by which BDNF regulates these processes remain elusive. Conflicting results have been reported. Dendritic development of Purkinje cells was severely reduced in

generic BDNF-deficient mice (Schwartz et al., 1997). Purkinje cell dendritic growth was found strongly reduced after blockade of the BDNF receptor TrkB in dissociated co-cultures with granule cells (Hirai and Launey, 2000). In contrast, Purkinje cell dendritic differentiation was normal in a mouse model with cerebellar-specific TrkB ablation (Rico et al., 2002) and in slice cultures (Adcock et al., 2004). Furthermore, BDNF only affected spine density but not major dendritic growth parameters in dissociated Purkinje cell cultures (Shimada et al., 1998). Such conflicting results might suggest that differential nutritional requirements are required for different culture conditions. Overall, the molecular pathways that execute and modulate Purkinje cell dendritic growth downstream to neuronal input remains incompletely understood.

6.1.3 Existing protocols for generating cerebellar neurons using human iPSCs

Human Purkinje cells are particularly vulnerable in cerebellar ataxia but difficult to differentiate *in vitro*. The incomplete understanding of the key molecular events that control Purkinje cell development has hampered the generation of human Purkinje cells *in vitro*. Early protocols that mimic the *in vivo* signals involved in early cerebellar development by introducing growth factors in a step-wise fashion throughout the differentiation processes were inefficient and predominantly produced granule cells from mouse and human ESCs (Erceg et al., 2012; Erceg et al., 2010).

Muguruma *et al.* adopted a different approach, which aimed to induce endogenous signals mimicking early patterning of cerebellum by adding a combination of three factors to mouse or human ESCs in suspension culture (Muguruma et al., 2015; Muguruma et al., 2010). Fluorescence-activated cell sorting (FACS) for KIRREL2-positive Purkinje cell precursors, followed by co-culture with primary mouse rhombic lip-derived granule cell precursors resulted in a much higher efficiency in the generation of Purkinje cells. The generated Purkinje cells

expressed mature markers including L7/PCP2 and GRID2, possessed a characteristic morphology and distinctive firing pattern, suggesting that they were functionally mature.

Wang *et al.* used a similar self-inductive approach to produce Purkinje cells from human iPSCs co-cultured with human foetal cerebellar slices. Although these cells appeared to display Purkinje cell-specific markers and were electrically active, they did not possess the characteristic morphology of mature Purkinje cells. Moreover, the use of human foetal materials is likely to limit the applications of this protocol. At the time this study was designed, these were the only reported cerebellar differentiation protocols from human pluripotent stem cells.

More recently, the Mugumura group used a very similar approach to their original method to generate Purkinje cells from human iPSCs, with the supplementation of two addition growth factors that have been shown to enhance dendritic development of Purkinje cells (Ishida et al., 2016). After co-culture with mouse primary granule cell precursors for 75 days, the human cells expressed later markers and had extensively branched dendritic trees with a thick stem, characteristic of mature Purkinje cells. However, none of these studies have been reproduced by other research groups, likely due to the complexity and long differentiation time.

Therefore, this chapter aims: (1) to optimise the differentiation of Purkinje cells from human iPSCs; (2) to generate human Purkinje cells from control- and patient-derived iPSCs and (3) to elucidate the development changes caused by SCA14 mutations. Human control and SCA14 iPSCs were first differentiated into Purkinje cells using a modified differentiation protocol. The morphologies and marker expression of human control and SCA14 Purkinje cells were examined. Part of the results presented in this chapter were published in a peer-reviewed journal article (Watson et al., 2018).

6.2 Specific Materials and Methods

6.1.1 Differentiation of human iPSCs into Purkinje cells

6.1.1.1 Dissociation of human iPSCs

Reagents were purchased from Thermo Fisher Scientific, unless otherwise stated. Human iPSCs were grown in tissue culture-treated 6-well plates coated with Matrigel in mTESR-1 medium as described in section 2.1.6. On day 0, iPSCs were dissociated into single cells for 5 minutes at 37 °C in pre-warmed TrypLE Express. iPSCs dissociated in TrypLE Express were diluted 1:10 in 1 x Dulbecco's phosphate-buffered saline (DPBS) and then centrifuged for 5 minutes at 228 x *g* (1000 rpm) at room temperature.

6.1.1.2 Formation and culture of embryoid bodies

The cell pellet was re-suspended in induction medium [Iscove's modified Dulbecco's medium/Ham's F12 1:1, 7 μg/ml insulin (Sigma), 5 mg/ml crystallisation-purified bovine serum albumin (BSA, Sigma), 1% chemically defined lipid concentrate, 450 μM monothioglycerol (Sigma), 15 μg/ml apo-transferrin (Sigma) and 1% penicillin/streptomycin (P/S)], supplemented with 50 μM Y-27632 (Sigma) and 10 μM SB431542 (R&D). 10,000-12,000 cells/well were transferred to low-adhesion V-bottomed 96-well PrimeSurface culture plates (Sumitomo Bakelite) in this supplemented induction medium, and incubated for 48 hours at 37 °C, 5% CO2. 50 ng/ml recombinant fibroblast growth factor 2 (FGF2, R&D) was added to the culture on day 2.

One-third of the medium was replaced on day 7 by fresh induction medium without Y-27632 or SB431542. Medium was fully replaced on day 14. On day 21, neural progenitors were transferred from 96-well plates to ultra-low-adhesion 24-well plates (Corning) (four to six embryoid bodies per 24-well) and incubated in differentiation medium (neurobasal medium,

1% GlutaMAX, 1% N2 and 1% P/S). On day 28, medium was fully replaced with fresh differentiation medium and further incubated for seven days.

6.1.1.3 Dissociation and co-culture of Purkinje cells

On day 35, approximately ten embryoid bodies were transferred into Eppendorf tubes. Aggregates were washed twice with HHGN [HBSS, 2.5 mM HEPES pH=7.3-7.5, 35 mM glucose and 4 mM sodium bicarbonate ($NaHCO_3$)] and then incubated in 200 µl Neuronal Isolation Enzyme with Papain for 20-30 minutes at 37 °C, with periodic agitation. After removing the enzyme solution, embryoid bodies were washed gently three times with HHGN. The embryoid bodies were then triturated for 20-25 times into single cell suspension in 500 µl seeding medium [DMEM/F12 with L-glutamine, 1% N2, 1.4 mM additional L-glutamine, 5 µg/ml additional insulin (Sigma), 10% HyClone US-defined heat-inactivated foetal bovine serum (FBS, GE Healthcare Life Sciences) and 1% P/S]. Air bubble formation should be avoided during the process. Cells were then pooled in a 15-ml Falcon tube, topped up to 5 ml seeding medium and centrifuged at 185 x *g* (900 rpm) for 5 minutes. The pellet was first re-suspended in 250 µl seeding medium and then adjusted to $5.0x10^6$ or $8.0x10^6$ cells/ml in seeding medium.

Three different approaches were tested for the optimal conditions for the survival and maturation of human iPSC-derived Purkinje cells: human-cell-only cultures, mixed co-cultures and physically separated co-cultures.

For human-cell-only cultures, 55 µl of the cell suspension containing human iPSC-derived neural progenitors was seeded as a small droplet on Cell Desk LF plastic coverslips (Sumitomo Bakelite), previously coated with 0.5 mg/ml poly-L-ornithine (PLO, Sigma- Aldrich) and 10 mg/ml natural mouse laminin.

For mixed co-cultures and physically separated co-cultures, primary mouse cerebellar cells were prepared in parallel. Pregnant dams (C57BL/6) at 18 days of gestation were sacrificed. Cerebella were dissected from the pups and the meninges were removed carefully. Approximately one litter was used for each iPSC line. Cerebella were washed twice with HHGN, and incubated in TrypLE Express for 10 minutes at 37 °C with periodic agitation. The dissociated cerebella were washed three times with HHGN before dissociated by trituration in seeding medium, centrifugation and re-suspension at $5.0x10^6$ or $8.0x10^6$ cells/ml, as described above. For mixed co-cultures, human and mouse cells were mixed at a ratio of 1:10. 55 µl of the mixed cell suspension was seeded as a small droplet on the PLO-laminin-coated plastic coverslips. For physically separated co-cultures, 55 µl of human cells were seeded as a small bubble on the plastic coverslips while 35 µl of mouse cells were transferred to either BRANDplates® Insert System (polyester/PET or polycarbonate/PC membrane) (Brand), or 6.5-mm Transwell -COL collagen-coated 0.4-µm pore membrane inserts (Polytetrafluoroethylene/PTFE or PET membrane) (Corning). The inserts were placed in wells above the human cells cultured on coverslips to keep the cell bodies of human and mouse cells physically separated. All surfaces were additionally coated with PLO and laminin as described above.

For all three culture conditions, after incubation for 4 hours at 37 °C, 5% CO2, 500-800 µl of culture medium [DMEM/F12 with L-glutamine, 1% N2, 1.4 mM additional L-glutamine, 5 µg/ml additional insulin, 0.5 ng/ml tri-iodothyronine (T3, Sigma), 100 µg/ml BSA (Sigma) and 1% P/S] was gently added to each well to reduce the final serum concentration. Half volume of medium was replaced once a week with fresh feeding medium [culture medium supplemented with 4 µM cytosine β-D-arabinofuranoside (AraC) (Sigma), a glial proliferation inhibitor, and 5-10 µg/ml laminin].

6.1.2 Immunocytochemistry

Embryoid bodies were harvested for immunocytochemistry at days 21 and 35 of differentiation. In both cases, four to six aggregates were fixed for 15-20 minutes at 4°C in 4% paraformaldehyde and subjected to processing for cryosectioning (Lancaster and Knoblich, 2014). Fixed embryoid bodies were washed three times for 5 minutes in PBS at room temperature and incubated in 20% sucrose at 4°C overnight. The embryoid bodies were transferred to plastic molds and frozen on dry ice for 30 minutes before storing at -80°C until needed. 10-µm cryosections were subjected to immunocytochemistry as previously described (Muguruma et al., 2010). Briefly, the frozen cryosections were rested to room temperature and washed twice for 15 minutes in PBS. The cryosections was permeabilised three times for 10 minutes in 0.3% Triton X-100 in PBS at room temperature. The sections were incubated in blocking solution (2% skim milk in 0.3% Triton X-100 in PBS) for one hour at room temperature and subsequently in primary antibodies in blocking solution at 4°C overnight. Three 0.05% Tween20/PBS 10-minute washes were followed by a 2-hour incubation in secondary antibodies at room temperature. The immunostained sections were mounted onto slides in mounting medium VECTASHIELD® Mounting medium containing DAPI (VECTOR laboratories).

For cells in dissociated cultures, immunostaining was performed at selected time points that were grouped into four stages: days 50-60, days 70-85, days 100-115 and days 120-125, as described in section 5.2.6. The cells were visualised under an upright fluorescence Axioplan2 Imaging Universal Microscope with Axiovision software (Carl Zeiss). A list of primary and secondary antibodies can be found in Table 2.2.

6.1.3 Image quantification

Immunostained images were analyzed using ImageJ plugins (http://imagej.nih.gov/ij). Analysis of cell morphology and differentiation was performed across at least six separate differentiation experiments, using at least 20 images per experiment.

6.1.4 Statistical analysis

One clone for each of the patient lines carrying the H36R mutations (clones PRKCG01-1 and PRKCG02-12) and two control lines (AH017-3 and SFC841-03-01) were included (Fig. 3.2H). One clone differentiation is defined as one experiment, i.e. n. Mean ± S.E.M. were shown. Unpaired students' t-test or ANOVA with Bonferroni's post-hoc test was performed using GraphPad Prism 7 (GraphPad Software, Inc.). Results were considered statistically significant at $*p < 0.05$.

6.3 Results

6.3.1 Generation of Purkinje cells from human iPSCs

Differentiation of Purkinje cells from human iPSCs has been proven particularly challenging, owing to its large size, long period of maturation and many interacting factors involved in the differentiation process (Watson et al., 2015b; Wong et al., 2017). Existing protocols have yet been reproduced due to the complex and challenging procedures (Watson et al., 2015b; Wong et al., 2017). Therefore, the first part of this chapter aimed to develop a simplified yet reproducible protocol for the differentiation of Purkinje cells from human iPSCs. In this simplified protocol (Fig. 6.2), the self-induction approach that mimics the *in vivo* cerebellar development was modified (Muguruma et al., 2015). To identify the key factors and procedures that enable robust differentiation of cerebellar progenitors and Purkinje cells, different approaches were tested. One iPSC clone for each of the SCA14 patients carrying the H36R mutation (PRKCG01-1 and PRKCG02-12) and two control iPSC lines (AH017-3 and SFC841-03-01) were used for Purkinje cell differentiation. On day 0, the initial seeding number was increased from 6,000 cells/well to 10,000-12,000 cells/well and the concentration of ROCK inhibitor Y-27632 was increased from 10 μM to 50 μM. These modifications significantly increased cell survival and efficiency of aggregate formation during the early stage of the differentiation (Watson et al., 2018).

A combination of three factors, insulin, SB431542 and FGF2, enables robust and reproducible generation of cerebellar progenitors from human iPSCs (Ishida et al., 2016; Watson et al., 2018). Insulin was shown to inhibit the expression of forebrain markers Six3 and Rx and increased Wnt1, Fgf8 and En2 markers expressed at the MHB (Muguruma et al., 2015; Muguruma et al., 2010). Insulin was therefore included from day 0 to induce neural patterning and inhibit differentiation into forebrain identity (casualisation). The transforming growth factor β (TGFβ)-receptor blocker SB431542, which inhibits SMAD-signalling by blocking

phosphorylation of ALK4, ALK5, ALK7 receptors (Smith et al., 2008), was included from day 0 to inhibit mesenchymal- and promote neuroectodermal differentiation (Chambers et al., 2009; Muguruma et al., 2015). FGF2 has been shown to induce the expression of MHB markers FGF8, GBX2 and WNT1, and supress expression of forebrain markers OTX2 and SIX3 in human ESCs (Muguruma et al., 2015; Muguruma et al., 2010). In particular, insulin and Fgf2 showed synergistic effect at inducing the expression of isthmic organizer factors En2 and Fgf8 in mouse ESCs (Muguruma et al., 2010). Thus, FGF2 was added from day 2 to induce rhombic lip formation in rhombomere 1 in the presence of insulin (Irving and Mason, 2000; Muguruma et al., 2015; Muguruma et al., 2010; Ye et al., 1998).

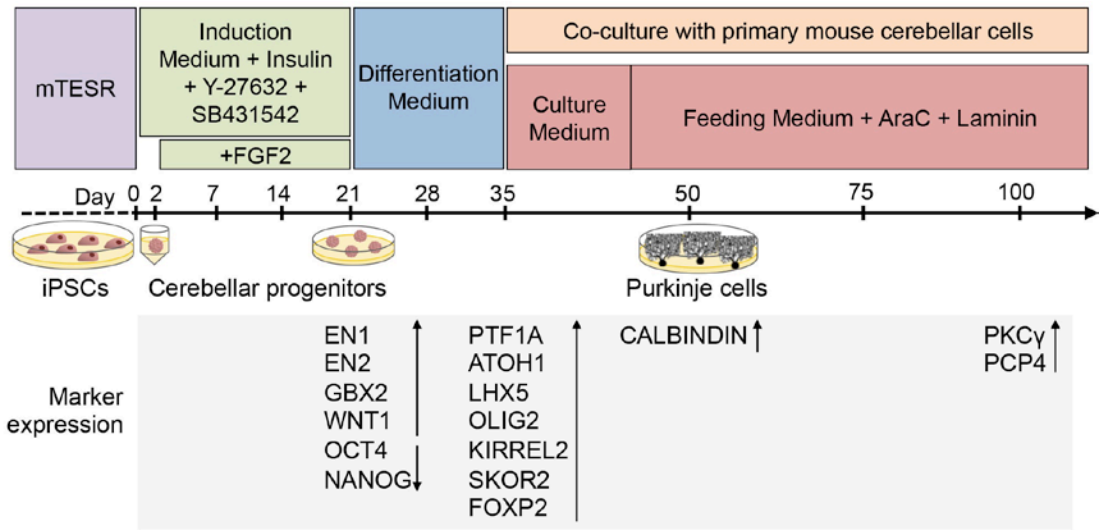


Figure 6.2 Overview of cerebellar neuronal differentiation protocol.

Human iPSCs were seeded at 10,000-12,000 cells/well in ultra-low attachment plates and cultured in suspension for 35 days. iPSC-derived embryoid bodies containing cerebellar progenitors were dissociated and co-cultured with E18.5 primary mouse cerebellar cells. Gene and protein expression was assessed at various time points by means of qPCR and immunofluorescence. Modified from (Watson et al., 2018). 4V: fourth ventricle; CH, cerebellar hemisphere; CV, cerebellar vermis.

6.3.2 Populations of progenitors within control and SCA14 embryoid bodies express early midbrain-hindbrain markers on day 21

To examine the developmental changes of human Purkinje cells caused by SCA14 mutations, human control and SCA14 iPSCs were differentiated into Purkinje cells. Patient iPSCs carrying the H36R mutation were used as a proof of principle. During early cerebellar development, En1 and En2 are strongly expressed mainly in the MHB and its neighbouring regions including the isthmic organiser, rhombomere 1 region and the caudal most-midbrain region at E12.5 in mice (Fig. 6.1A). Therefore, it was first examined whether the embryoid bodies expressed *EN1* and *EN2*. On day 21, both control and SCA14 embryoid bodies showed downregulation of pluripotency markers *OCT4* and *NANOG* (Fig. 6.3A). Moreover, expression of *EN1* and *EN2* mRNA in control and SCA14 embryoid bodies were similar (Fig. 6.3A). The proportion of cells within the embryoid bodies that were positive for EN1 and EN2 were counted (Fig.6.2B-C). Approximately 55.05±5.27% of cells within control iPSC-derived embryoid bodies were stained for EN1 (46.84±6.42% for AH017-3 and 69.40±1.52% for SFC843-03-01) (Fig. 6.3B). Within the SCA14 iPSC-derived embryoid bodies, 62.51±7.90% of cells were EN1-positive (58.18±12.00% for PRKCG01-1 and 70.08±6.21% for PRKCG02-12) (Fig. 6.3B). Moreover, these neural progenitors derived from control and SCA14 iPSCs expressed comparable levels of early midbrain marker *WNT1* (Fig. 6.3A) and early hindbrain marker GBX2 (Fig. 6.3C). Notably, the expression of *WNT1* and *GBX2* are important for the reinforced expression of *FGF8*, *EN1* and *EN2* for further cerebellar development (Fig. 6.1B). These results suggest that both control and SCA14 iPSC-derived embryoid bodies contain midbrain-hindbrain neuronal precursors. Expression of early midbrain-hindbrain markers of neural progenitors derived from individual iPSC clones can be found in Supplementary Figure 6.1A in Appendix.

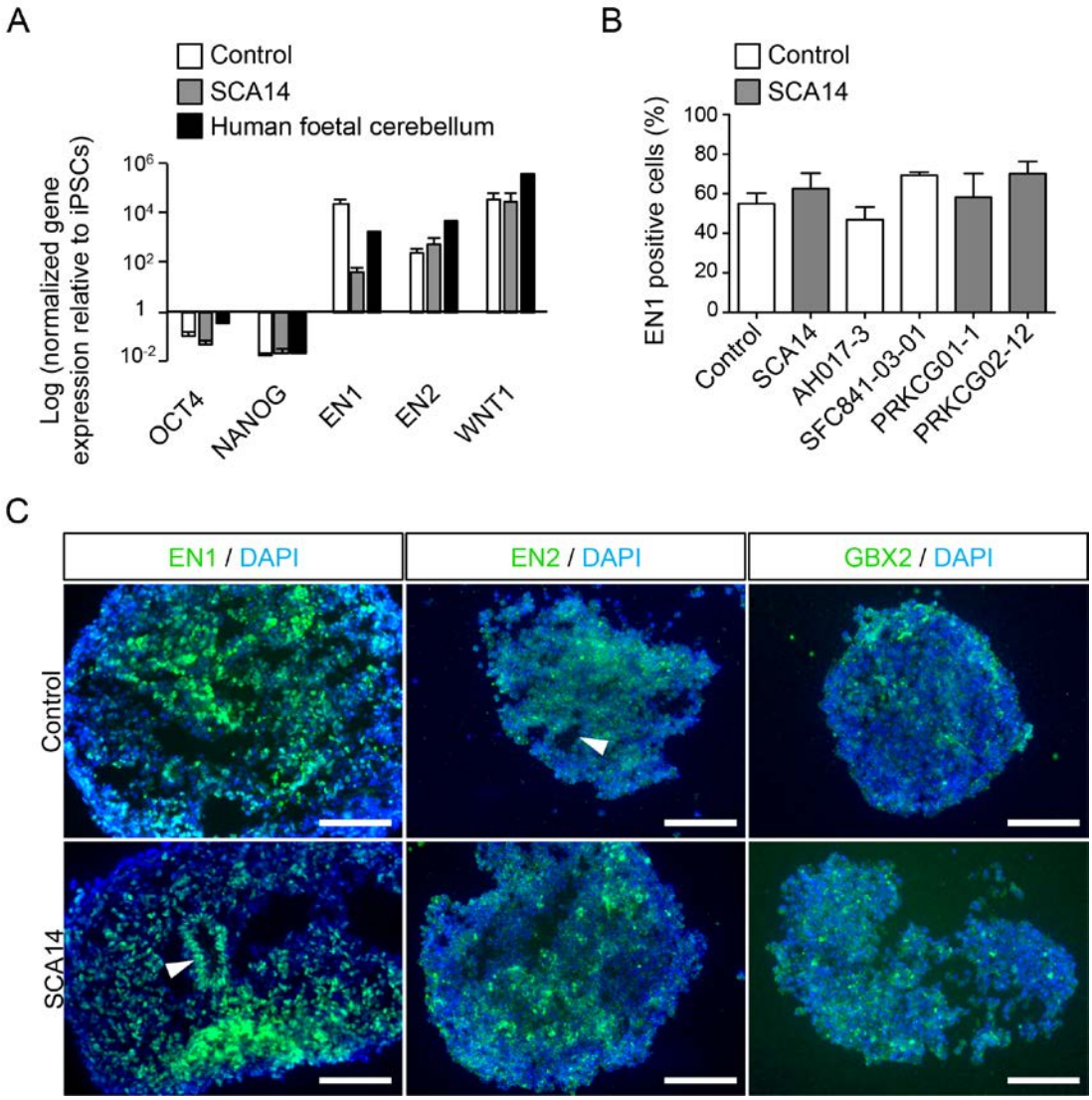


Figure 6.3 Control- and SCA14 iPSC-derived neural progenitors express similar levels of early midbrain-hindbrain markers on day 21

(A) Gene expression of cerebellar progenitors after 21 days in suspension culture. The expression of pluripotency markers *OCT4* and *NANOG* were downregulated while early markers of midbrain-hindbrain proximity regions *EN1*, *EN2* and *WNT1* were upregulated. Control and SCA14 cerebellar progenitors showed similar expression levels of all markers assessed and were comparable to human foetal cerebellum. Gene expression is shown normalised to β-actin and relative to iPSCs (set to one) (n=6, ANOVA followed by Bonferroni's post-hoc test, $p>0.05$). (B) Control and SCA14 cerebellar progenitors contained similar proportion of EN1-positive cells. Proportion of EN1-positive cells in cerebellar progenitors of individual iPSC clones are also shown (n=6, ANOVA followed by Bonferroni's post-hoc test, $p>0.05$). (C) Immunostaining of cryosections of embryoid bodies after 21 days in suspension culture. Protein expression of early midbrain markers EN1 and EN2 as well as hindbrain marker GBX2 were detected in both control and SCA14 embryoid bodies. Neural rosettes representing cerebellar ventricular zones are indicated by white solid arrowheads. DAPI was used for nuclear staining of cells. Scale bars= 20 μm.

6.3.3 Control and SCA14 iPSC-derived neural progenitors express markers of Purkinje cell precursors on day 35

As early as E11-12, mouse cerebellar neuroepithelium starts to express tissue-specific markers. Transcription factors Atoh1 and Ptf1α are one of the earliest markers of the rhombic lip and the cerebellar ventricular zone, respectively. Subsequently, specific markers for Purkinje cell progenitors such as Kirrel2, which is a target gene of Ptf1α, as well as Olig2 and Lhx5 are expressed (Andreu et al., 2014; Leto et al., 2016; Muguruma et al., 2015; Muguruma et al., 2010). To determine the developmental stages of the embryoid bodies, the marker expression of cerebellar neuronal progenitors were examined. The expression of these markers in control- and patient-derived progenitors was compared.

On day 35, subpopulations of cells within the embryoid bodies expressed the ventricular zone marker *PTF1A* (Fig. 6.4A) and the rhombic lip marker *ATOH1* (Fink et al., 2006; Muguruma et al., 2010) (Fig. 6.4A & B). This indicates the presence of precursors of both cerebellar GABAergic and glutametergic neurons. Furthermore, subsets of cells within the embryoid bodies expressed specific markers of Purkinje cell precursors including KIRREL2, LHX5 and OLIG2 (Ishida et al., 2016; Mizuhara et al., 2010; Morales and Hatten, 2006; Muguruma et al., 2015; Muguruma et al., 2010; Seto et al., 2014; Watson et al., 2018) (Fig. 6.4A & C). These cell aggregates contained hollow rosettes resembling neuroepithelium that were positive for cell surface KIRREL2 (Fig. 6.4C), which is one of the earliest specific markers of Purkinje cells. Interestingly, most of the KIRREL2-positive neurons were located at the inner side of the hollow rosettes (Fig. 6.4C), while the ATOH1-positive cells were situated within and around the rosettes (Fig. 6.4B). Control and SCA14 embryoid bodies showed similar mRNA expression of *ATOH1*, *PTF1A*, *KIRREL2*, *LHX5* and *OLIG2* (Fig. 6.4A). Expression of cerebellar progenitor markers in embryoid bodies derived from individual iPSC clones on day 35 is included in supplementary figure 6.1B. Taken together, these results suggest that both

control and SCA14 iPSCs are capable of developing into more mature cerebellar neuronal progenitors. Thus, cellular commitment of cerebellar progenitors is not affected by the SCA14 mutation (H36R).

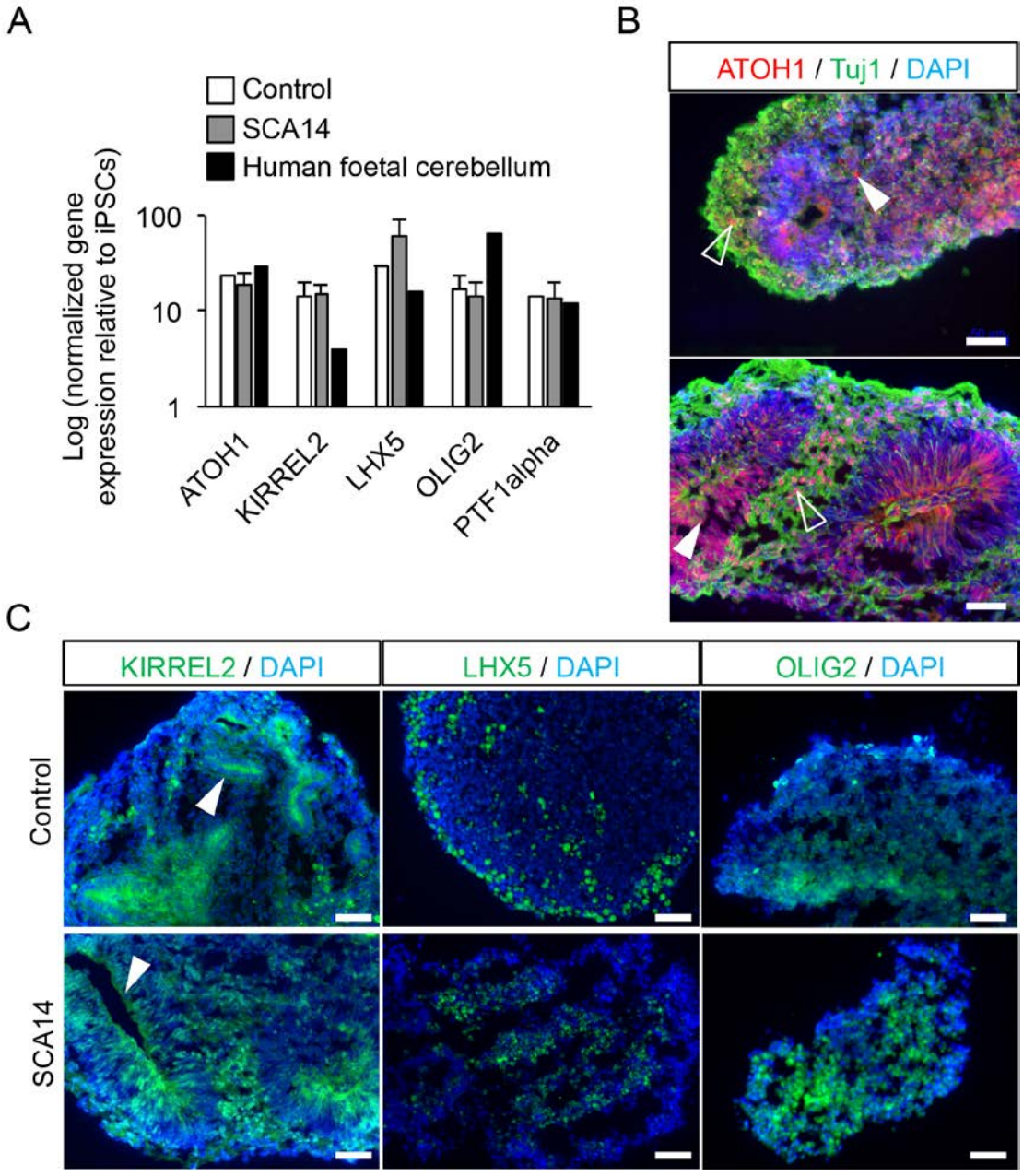


Figure 6.4 Control and SCA14 iPSC-derived neural progenitors express early specific markers of Purkinje cell precursors on day 35

(A) Gene expression of cerebellar progenitors after 35 days in suspension culture. Control and SCA14 embryoid bodies showed similar expression of the ventricular zone (GABAergic) marker *PTF1A*, and the rhombic lip (glutamatergic) marker *ATOH1*, as well as additional Purkinje cell markers *KIRREL2*, *LHX5* and *OLIG2*. Gene expression is shown normalised to β-actin and relative to iPSCs (set to one) (n=6, ANOVA followed by Bonferroni's post-hoc test, $p>0.05$). (B) Subpopulations of cells within embryoid bodies

expressed an early neuronal marker Tuj1 (βIII-tubulin) and a granule cell marker ATOH1. ATOH1-postive cells were found within (white solid arrowheads) and around neural rosettes (white hollow arrowheads). DAPI was used for nuclear staining of cells. Scale bars= 20 μm. (C) Purkinje cell precursor markers KIRREL2, LHX5 and OLIG2 were also expressed by subsets of cells within embryoid bodies. KIRREL2 were mainly expressed at the inner side of neural rosettes (white solid arrowheads). DAPI was used for nuclear staining of cells. Scale bars= 20 μm.

6.3.4 Human cells express specific markers and show distinctive features of Purkinje cells from day 50 onwards

To optimise the culture condition and to promote survival and maturation of Purkinje cells during the later stage of differentiation, three different approaches were tested (Fig. 6.5A). The survival and maturation of dissociated mouse Purkinje cells have been shown to be promoted upon co-culture with mouse cerebellar cells. Moreover, co-culture of primary mouse external granular layer (EGL) cells derived from embryonic rhombic lip has been shown to promote maturation of FACS-purified mouse Purkinje cells (Muguruma et al., 2010) and human ES cell-derived Purkinje progenitors (Muguruma et al., 2015). However, mouse rhombic lip cultures are technically challenging and result in low cell yield. Therefore, to increase the number of cells available for co-culture, dissociated cells from the whole E18.5 mouse cerebellum were used in this study. These have been shown previously to support the development of cultured mouse Purkinje cells (Baptista et al., 1994). In contrast to the existing protocols (Ishida et al., 2016; Muguruma et al., 2015), live cell sorting for dissociated KIRREL2-postive progenitors prior to co-culture with mouse cerebellar cells was found to be unnecessary for generating human Purkinje cells. Moreover, 5-10 μg/ml of laminin was added to the feeding medium from day 42 to provide additional structural support to maturing cultures. T3 promotes arborisation and spine formation a dose- and time-dependent manner. This process has been shown to act via the activation of TRα1 (Heuer and Mason, 2003), nuclear receptor Retinoic acid receptor-related orphan receptor alpha (RORα) (Boukhtouche et al., 2010) and peroxisome proliferator-activated receptor gamma co-activator 1α (PGC-1α) (Hatsukano et al., 2017). Therefore, to aid

Purkinje cell dendritic maturation, T3 was supplemented to the cultures from day 35 onwards throughout the course of terminal differentiation.

To examine the presence of developing Purkinje cells in the cultures, immunostaining for an early Purkinje cell marker Calbindin D-28k was performed at selected time points. An antibody against human nuclear antigen was used to identify human cells in the mixed co-cultures. On day 50, in mixed co-culture ($5x10^6$ cells/ml), neurons that were positive for both Calbindin and human nuclear antigen were present (Fig. 6.5B-D), indicating that these neurons were human Purkinje cells derived from iPSCs. At this stage, almost 20% of cells in the mixed co-cultures were human Purkinje cells. These human Purkinje cells displayed diverse morphologies resembling the developing Purkinje cells in *in vitro* cultures (Baptista et al., 1994). This suggests that these co-cultures contain Purkinje cells of varying maturity. The presence and abundance of mature mouse Purkinje cells, which were negative for human nuclear antigen, were dependent on the age of embryonic mice used. Cerebellar cultures from E18.5 mice resulted in the least amount of mouse Purkinje cells in the co-culture (day 50, Fig. 6.5E), which were usually undetectable after 25-30 days in culture, and were therefore used in this study.

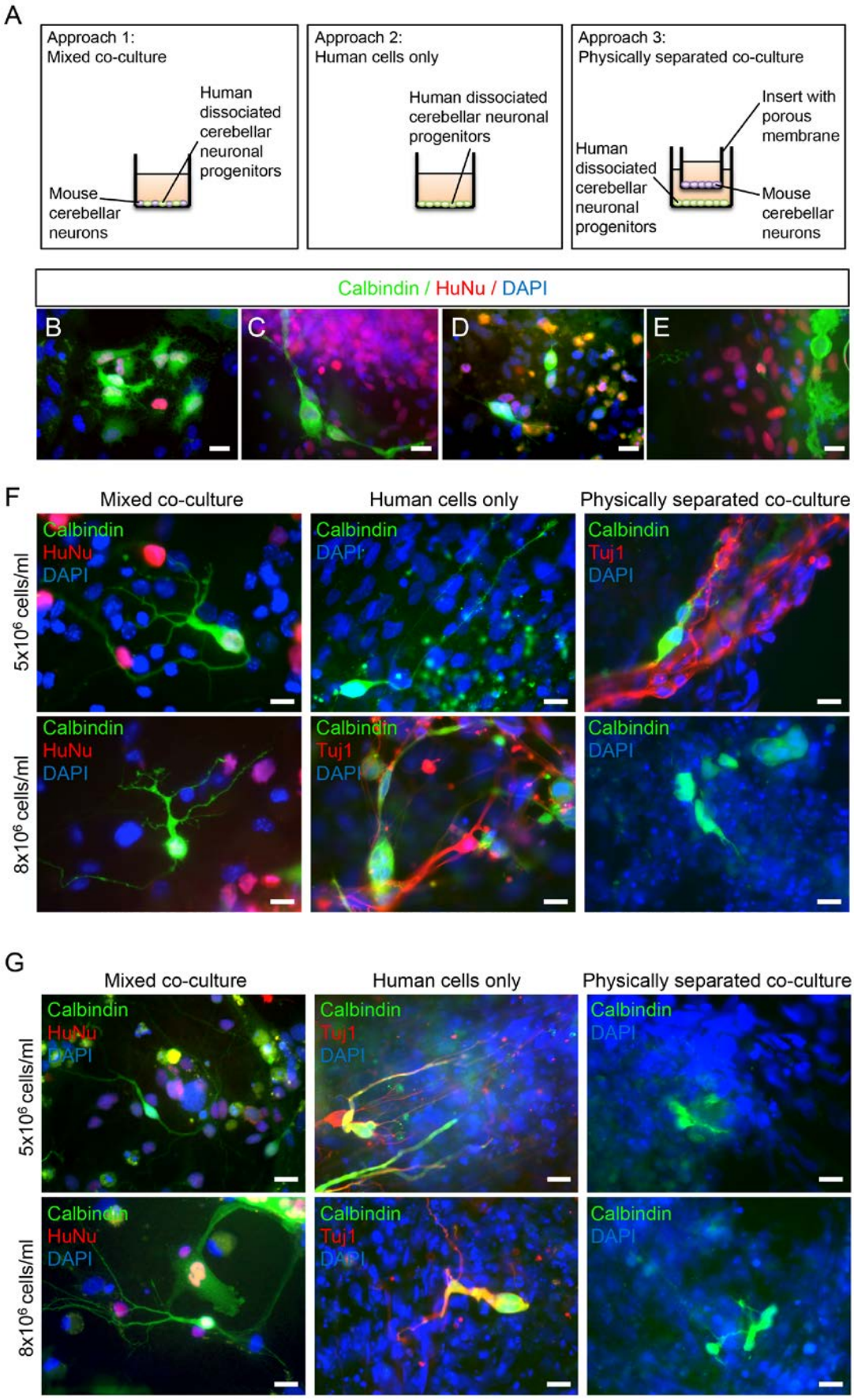
The presence of mouse cells in mixed co-culture limited the downstream analyses. Hence, to determine if intrinsic factors of human Purkinje cells are sufficient to support their maturation, human dissociated cerebellar progenitors were also cultured in the absence of co-cultures (approach 2, Fig. 6.5A). In addition, to test whether the physical contact between mouse cerebellar cells and human Purkinje cells was essential to their development and survival, mouse cerebellar cells were cultured in porous inserts, which were put above the human dissociated cerebellar progenitors cultured on PLO-laminin-coated coverslips at the well bottom (approach 3, Fig. 6.5A). In this way, the cell bodies of the human and mouse cells were not in physical contact, whereas the growth factors secreted by the mouse cells were allowed to diffuse in medium and nurture the human cells. Finally, as initial cell seeding density might

also affect the survival and growth of Purkinje cells, two seeding densities $5.0x10^6$ or $8.0x10^6$ cells/ml ($2.75x10^5$ or $4.4x10^5$ cells/well) were also tested for each approach.

On day 50, human Calbindin-positive Purkinje cells were observed in all three approaches with both seeding densities (Fig. 6.5F). These Purkinje cells showed various morphologies. In mixed co-cultures of both seeding densities, the majority of Purkinje cells showed a polarised morphology. Several thin processes were present on a short dendritic stem that grew from one side of the smooth cell bodies (Fig. 6.5F). In human cell-only cultures and physically separated co-cultures, less than 5% of the human cells were positively for Calbindin (Fig. 6.5F). The majority of the Calbindin-positive cells in human cell-only cultures possessed a single long and thin process stemming from a smooth cell body (Fig. 6.5F). In physically separated co-cultures, the Calbindin-positive human cells had a large, smooth and oval-shaped cell body with several primitive processes. Moreover, most of these human Purkinje cells were aligned with bundles of long Tuj1-positive axons, the origin of which could not be traced. These bundles of axons therefore were likely to be axons of mouse cerebellar neurons that crossed the pores of the inserts and reached the human cells cultured underneath (Fig. 6.5F). Furthermore, increased cell death was observed in human cell-only cultures whilst survival of human cells was enhanced in physically separated co-cultures. This suggests that structural support and physical interactions between Purkinje cells and other cerebellar neurons are required for the survival of human Purkinje cells *in vitro*.

On day 70, in mixed co-cultures of both seeding densities, the proportion of human cells remained constant, almost 60% of the total cells and around 16 % of the human cells were positive for Calbindin. These human Purkinje cells developed more complex dendritic arbours from a single dendritic stem (Fig. 6.5G). Approaches 2 and 3 showed similar results at both seeding densities on day 70 of differentiation. In both human cell-only cultures and physically separated co-cultures, only around 1% of human cells were Calbindin-positive (Fig. 6.5F). In

cultures with human cells alone, cells positive for both Calbindin and Tuj1 had a single long and thin process without branching (Fig. 6.5F). In contrast, the Calbindin-positive cells in physically separated co-cultures remained in immature form and had short, thin and unbranched processes (Fig. 6.5F). Moreover, both human cell-only cultures and physically separated co-cultures displayed significant cell death and did not survive beyond day 85. Finally, no Calbindin-positive cells were found in mixed co-culture of $5.0x10^6$ cells/ml ($2.75x10^5$ cells/ well) beyond day 120. Only mixed co-culture of the density $8.0x10^6$ cells/ml ($4.4x10^5$ cells/ well) routinely gave rise to human Purkinje cells with complex dendritic arbours branching from a thick stem beyond days 100-115 (Fig. 6.5H-I) and 120-125 (Fig. 6.4J). Immunoreactivity for Purkinje cell protein 4 (PCP4), which is a more mature Purkinje cell marker, was also detected (Fig. 6.5K). Therefore, mixed co-cultures with a seeding density of density $8.0x10^6$ cells/ml ($4.4x10^5$ cells/ well) were used in subsequent experiments.


A
Approach 1:
Mixed co-culture
Human dissociated cerebellar neuronal progenitors
Mouse cerebellar neurons
Approach 2:
Human cells only
Human dissociated cerebellar neuronal progenitors
Approach 3:
Physically separated co-culture
Insert with porous membrane
Human dissociated cerebellar neuronal progenitors
Mouse cerebellar neurons
Calbindin / HuNu / DAPI
B
C
D
E
F
Mixed co-culture
Human cells only
Physically separated co-culture
5x10^6 cells/ml
8x10^6 cells/ml
Calbindin
HuNu
DAPI
Tuj1
G

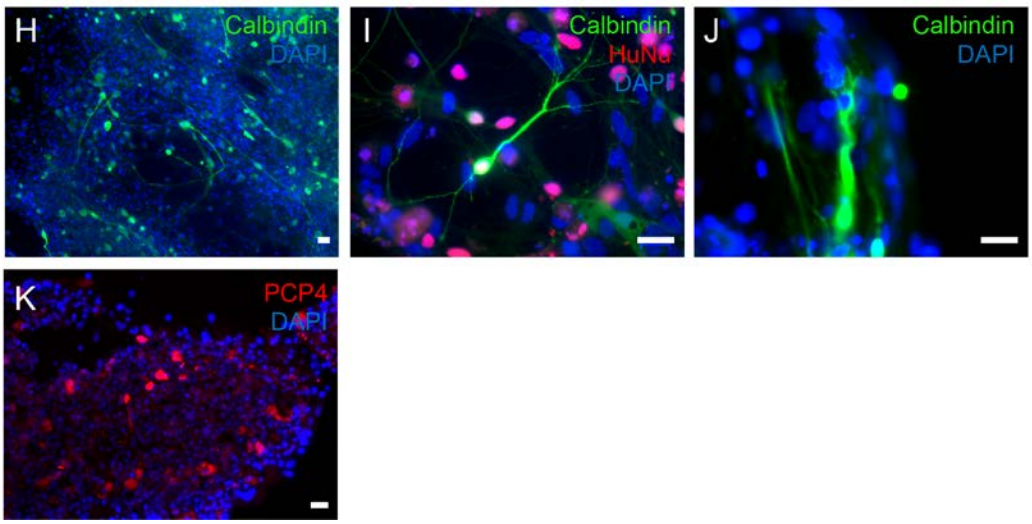


Figure 6.5 Optimisation of terminal differentiation of human iPSC-derived cerebellar Purkinje cells from day 35 onwards.

(A) On day 35, human control iPSC-derived embryoid bodies were dissociated and cultured in three different approaches for terminal differentiation. Schematic representation of approach 1: human dissociated cerebellar progenitors co-cultured with whole mouse cerebellar cells; approach 2: human dissociated cerebellar progenitors cultured alone; and approach 3: human dissociated cerebellar progenitors were grown on coverslips while mouse cerebellar cells grown in porous inserts above. On day 50, human cells (positive for human nuclear antigen, HuNu) in mixed co-cultures were stained for Calbindin and possessed primitive dendritic processes on smooth cell bodies (B-D). Mouse Purkinje cells that were negative for HuNu were also observed in mixed co-cultures (E). (F) On day 50, Calbindin-positive neurons were observed in cultures of all three approaches of both seeding densities. Purkinje cells showed rudimentary dendrites on smooth cell bodies in mixed co-cultures (left column). When human cells were cultured alone, Purkinje cell neurons possessed a single long thin process and were also stained for neuronal marker Tuj1 (middle column). In physically separated co-cultures, Calbindin-positive neurons had short processes and were associated with bundles of long Tuj1-positive axons (right column). (G) By day 70 of differentiation, Calbindin-positive cells showed characteristic morphology of Purkinje cells with branched dendrites growing from one side of the smooth cell bodies in mixed co-cultures (left column). In both cultures with human cells only (middle column) and physically separated co-cultures (right column), cells positive for Calbindin remained in immature morphologies. Only mixed co-cultures of $8.0x10^5$ cells/ml (approach 1) gave rise to Purkinje cells (Calbindin-positive) with elaborate dendritic arbours on days 100 (H & I) and 125 (J). A subpopulation of cells in mixed co-cultures was positive for a more mature marker of Purkinje cell PCP4 (K). DAPI was used for nuclear staining. Scale bars= 20 μm.

6.3.5 The development and survival of human SCA14 Purkinje cells are compromised

To investigate how SCA14 mutations might affect the development of human Purkinje cells, control and SCA14 iPSCs carrying the H36R mutation were differentiated into Purkinje cells using the above-described optimised protocol. Gene expression and morphologies of Purkinje cells were assessed at selected time points. To compare the abundance of Purkinje cells in the control and SCA14 cultures, *CALB1* mRNA expression was first assessed. As mouse cerebellar

cells were present in the mixed co-culture, which might affect the detection of *PRKCG* mRNA, human cell-only cultures were used to avoid the detection of mouse cells. In control cultures, *CALB1* mRNA expression steadily rose throughout the differentiation and peaked at day 60, which is comparable to the expression in human foetal cerebellum (Fig. 6.6A). In contrast, in SCA14 cultures, expression of *CALB1* remained low (Fig. 6.6A).

The survival and maturation of human cerebellar progenitors was significantly enhanced when co-cultured with primary mouse cerebellar cells as shown in the previous section. Therefore, on day 35, control- and SCA14 iPSC-derived embryoid bodies were dissociated into single-cell suspensions and co-cultured with cerebellar cells derived from E18.5 mouse embryos. On days 50-60, approximately 60% of the total cells were positive for human nuclear antigen, indicating the presence of human cells, in both control and SCA14 cultures (Fig. 6.6A). In control cultures, 18.06±1.85% of the human cells were positive for Calbindin. In contrast, in SCA14 cultures, significantly fewer human cells were positive for Calbindin (Fig. 6.6B). Notably, the difference of the proportion of human Purkinje cells present in the co-cultures further increased on days 110-115 (control: 13.56±1.26%; SCA14: 4.19±0.57%) and days 120-125 (control: 9.44±1.19%; SCA14: 1.92±0.45%) (Fig. 6.6B). These results suggest that SCA14 cells were less capable of developing into Purkinje cells and survived poorly in long-term culture compared to controls.

To compare the morphologies of the control and SCA14 Purkinje cells, area of soma as well as the number, length, degree of branching and thickness of the dendrites were measured (Fig. 6.6E). On days 50-60, in both control and SCA14 cultures, developing human Purkinje cells (positive for human nuclear antigen and Calbindin) displayed a rudimentary dendritic arbour growing from one side of the smooth cell bodies (Fig. 6.6D). Interestingly, developing SCA14 Purkinje cells had smaller cell bodies compared to control Purkinje cells at days 50-60 (Fig. 6.6F). This difference disappeared in long-term cultures. On days 110-125, SCA14 Purkinje

cells showed excessive dendritic branching compared to controls (Fig. 6.6D & G). By days 120-125, the majority of control Purkinje cells had a single thick dendritic stem without branches while SCA14 Purkinje cells possessed multiple thin dendrites (Fig. 6.6D, H & I). Finally, no difference in dendritic length was detected between control and SCA14 Purkinje cells (Fig. 6.6J). Taken together, these results suggest that the dendritic development and the survival of human SCA14 iPSC-derived Purkinje cells were compromised.

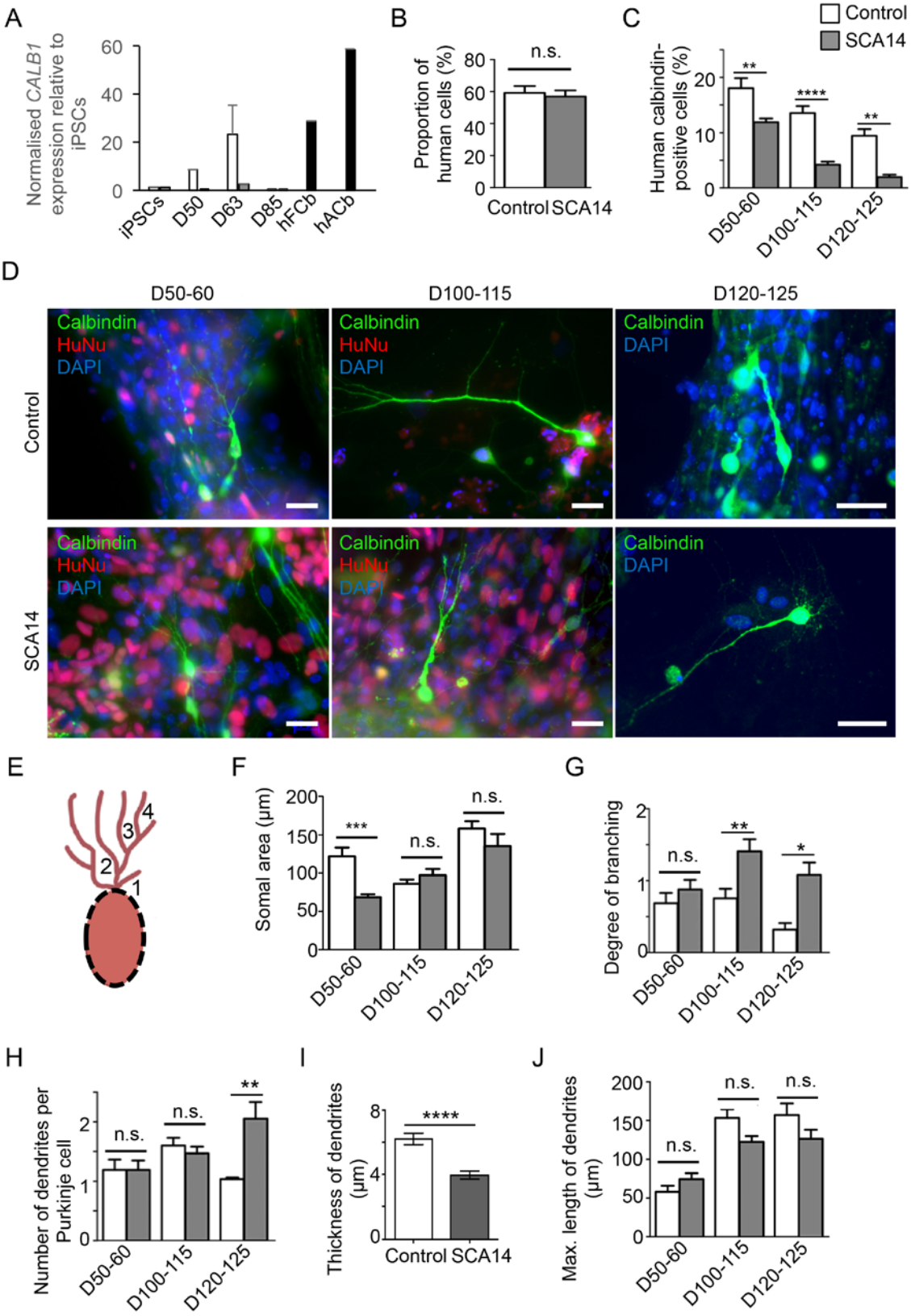

A
Normalised CALB1 expression relative to iPSCs
60
40
20
0
iPSCs
D50
D63
D85
hFCb
hACb
B
Proportion of human cells (%)
80
60
40
20
0
n.s.
Control
SCA14
C
Control
SCA14
Human calbindin-positive cells (%)
20
10
0
**
****
**
D50-60
D100-115
D120-125
D
D50-60
D100-115
D120-125
Control
SCA14
Calbindin
HuNu
DAPI
E
1
2
3
4
F
Somal area (µm)
200
150
100
50
0
***
n.s.
n.s.
D50-60
D100-115
D120-125
G
Degree of branching
2
1
0
n.s.
**
*
D50-60
D100-115
D120-125
H
Number of dendrites per Purkinje cell
2
1
0
n.s.
n.s.
**
D50-60
D100-115
D120-125
I
Thickness of dendrites (µm)
8
4
0
****
Control
SCA14
J
Max. length of dendrites (µm)
200
150
100
50
0
n.s.
n.s.
n.s.
D50-60
D100-115
D120-125

Figure 6.6 The development and survival of SCA14 Purkinje cells were compromised in long-term culture.

(A) Gene expression of *CALB1* in control and SCA14 cultures at days 0, 50, 63 and 85. Expression of *CALB1* in control cultures steadily increased from day 50 while that in SCA14 cultures remained low. *CALB1* expression of human foetal (hFCb) and adult (hACb) cerebella was also shown. Gene expression is shown normalised to β-actin and relative to iPSCs (set to one) (n=6). (B) Quantification of number of cells stained positive for human nuclear antigen, i.e. human cells. Approximately 60% of the total cells in the control and SCA14 cultures on day 50 were human cells (n=6, unpaired students' t-test, $p>0.05$). (C) SCA14 cultures contained significantly fewer cells positive for human nuclear antigen and Calbindin than control cultures throughout the differentiation (n=6, one-way ANOVA followed by Bonferroni's post-hoc test, $^{**}p>0.01$, $^{****}p>0.0001$). (D) Immunostaining of cells in control and SCA14 cultures for Calbindin and human nuclear antigen on days 50-60, days 100-115 and days 120-125. Human control and SCA14 Purkinje cells showed different morphologies throughout differentiation. DAPI was used for nuclear staining. Scale bars= 20 μm. (E) Parameters of neural properties including somal area, degree of branching, number, thickness and maximum length of dendrites were measured. (F) SCA14 Purkinje cells had smaller soma than control Purkinje cells on days 50-60 but not days 100-125. SCA14 Purkinje cells showed excessive dendritic branching from day 100 onwards (G), more (H) and thicker (I) dendrites on days 120-125, while the length of dendrites were unaffected (J) (n=6, unpaired students' t-test, one-way ANOVA followed by Bonferroni's post-hoc test, $^{*}p < 0.05$; $^{**}p < 0.01$; $^{***}p < 0.001$; $^{****}p < 0.0001$).

6.3.6 Differential expression of PKCγ in control and SCA14 Purkinje cells on day 100

To compare the abundance of PKCγ in control and SCA14 iPSC-derived cerebellar neurons, *PRKCG* mRNA expression were assessed on days 0 (iPSCs), 21, 35, 50, 63 and 85. The presence of mouse cerebellar cells in the mixed co-cultures might affect the detection of *PRKCG* mRNA. Therefore, on days 50, 63 and 85, human cell-only cultures were used. *PRKCG* mRNA expression in control and SCA14 cerebellar progenitors increased on day 21 and slightly decreased on day 35 (Fig. 6.7A). No difference in *PRKCG* expression was detected between control and SCA14 cerebellar progenitors on days 21 and 35 (Fig. 6.7A). *PRKCG* expression in both control and SCA14 cultures was almost undetectable on day 50. Notably, on day 63, *PRKCG* was highly expressed in control cultures (Fig. 6.7A). In contrast, *PRKCG* expression in SCA14 cultures was significantly lower compared to controls (Fig. 6.7A).

To examine the subcellular localisation of PKCγ in cerebellar progenitors, immunostaining for PKCγ and neuronal marker Tuj1 was performed in cryosections of embryoid bodies on days 21 and 35. On day 21, PKCγ was expressed ubiquitously as small dots in the cytoplasm of both control and SCA14 iPSC-derived early cerebellar progenitors (Fig. 6.7B). On day 35, PKCγ

was expressed in fibre-like structures in a subset of cells within control and SCA14 cerebellar progenitors (Fig. 6.7C). Interestingly, PKCγ was highly co-localised with neuron-specific Class III β-tubulin Tuj1, which is a structural protein that that contributes to microtubule stability in neuronal cell bodies and axons. The co-localisation was detected particularly around rosettes-like structures in control and SCA14 cerebellar progenitors on both days 21 and 35 (Fig. 6.7B-D). This suggests that PKCγ might be associated with microtubule function during early cerebellar development. Quantification of co-localisation of PKCγ and Tuj1 in cerebellar progenitors derived from each iPSC clones are shown in Supplementary Figure 6.1C.

On days 100-115, human cells that showed neuronal morphology in mixed co-cultures expressed PKCγ ubiquitously in the cytoplasm of cell bodies and throughout their processes (Fig. 6.7E). Moreover, these PKCγ-positive cells were also positive for Calbindin suggesting that human control Purkinje cells expressed PKCγ (Fig. 6.7F). In contrast, SCA14 Purkinje cells were negative for PKCγ (Fig. 6.7F). A few PKCγ-expressing neurons that were negative for Calbindin were present in SCA14 cultures (data not shown). Of note, thread-like structures of PKCγ were present in SCA14 cultures (Fig. 6.7F). Taken together, these results suggest that PKCγ is not expressed in SCA14 Purkinje cells.

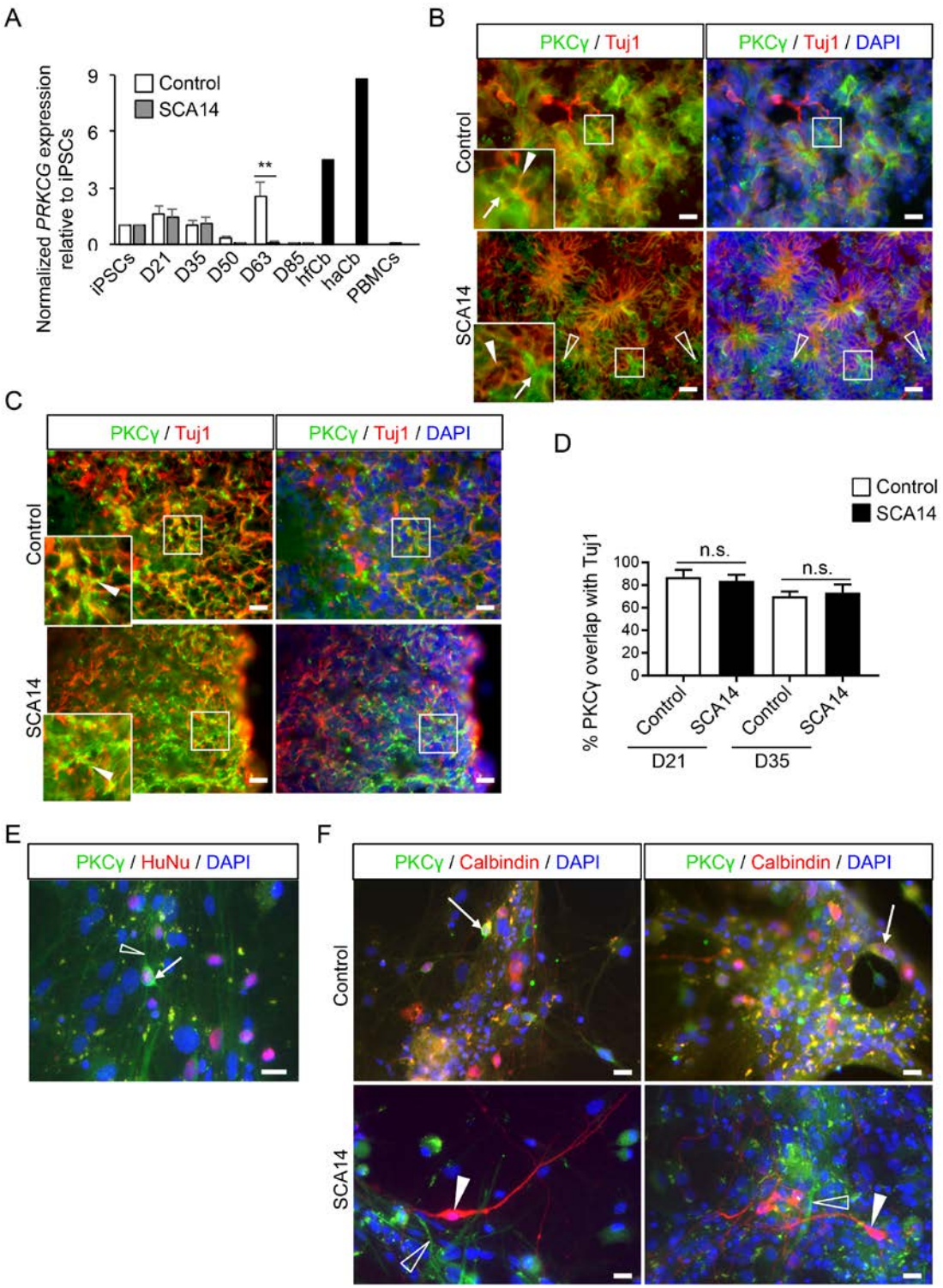


Figure 6.7 Control and SCA14 cerebellar progenitors showed similar expression pattern of PKCγ on days 21 and 35 but not during terminal differentiation.

(A) *PRKCG* expression of in human cell-only cerebellar cultures derived from control and SCA14 iPSCs. Human control and SCA14 cells expressed similar level of *PRKCG* mRNA on days 21 and 35. *PRKCG* mRNA expression was significantly higher in SCA14 cultures compared controls on day 63. RNA extracted from human foetal (hFCb) and adult (hACb) cerebellar tissue was used as positive controls. RNA extracted from human peripheral bone mononuclear cells (hPBMCs) was used as the negative control (n=5, one-way ANOVA followed by Bonferroni's post-hoc test, $**p<0.01$). (B) Immunostaining of embryoid bodies for PKCγ and

neuronal marker Tuj1. Punctate staining of PKCγ was observed in the cytoplasm of a subset of cells within the embryoid bodies (white arrows). PKCγ partially co-localised with βIII-tubulin Tuj1 (white solid arrowheads) in control and SCA14 cerebellar progenitors on day 21. DAPI was used for nuclear staining. Scale bars= 20 μm. (C) Immunostaining of embryoid bodies for PKCγ and Tuj1 on day 35. PKCγ was expressed as thread-like structures and highly co-localised with Tuj1 within the embryoid bodies (white solid arrowheads). DAPI was used for nuclear staining. Scale bars= 20 μm. (D) Quantification of co-localisation of PKCγ and Tuj1 in control and SCA14 cerebellar progenitors on days 21 and 35 (n=6, two-way ANOVA followed by ANOVA followed by Bonferroni's post-hoc test, $p>0.05$). (E) Immunostaining of Purkinje cell cultures for PKCγ and human nuclear antigen. PKCγ was expressed in cytoplasm of cell bodies (white arrow) and throughout the neuronal processes (white hollow arrowheads) of human nuclear antigen (HuNu)-positive cells derived from control iPSCs in mixed co-cultures. (F) Immunostaining of Purkinje cell cultures for PKCγ and Purkinje cell marker Calbindin. On day 100, only control cultures, but not SCA14 cultures, contained Purkinje cells expressing cytoplasmic PKCγ (white arrows). In SCA14 cultures, PKCγ was expressed as thread-like structures (white hollow arrowheads) outside Purkinje cells (white solid arrowheads). DAPI was used for nuclear staining. Scale bars= 20 μm.

6.4 Chapter Discussion

6.4.1 A simplified protocol for the reproducible generation of cerebellar Purkinje cells *in vitro*

The lack of reliable disease models has hindered our understanding of the underlying pathogenic mechanisms of, and the development of effective therapies for SCA14 and related SCAs (Lukovic et al., 2016; Watson et al., 2015b; Wong et al., 2017). There is thus an urgent need to develop a robust and reproducible method for generating human Purkinje cells *in vitro*. However, existing protocols are lengthy and challenging to reproduce (Muguruma et al., 2015; Muguruma et al., 2010; Wang et al., 2015b). Therefore, in the first part of this study, approaches were tested to simplify and enhance the survival and maturation of human Purkinje cells, particularly in the later stages of differentiation *in vitro*. Several key modifications that were designed to enhance cell survival and maturation were incorporated. At the early stage of differentiation, cells were seeded at a higher density at day 0 and higher concentration of apoptosis inhibitor was supplemented to the suspension culture to enhance cell survival (Fig. 6.2-3). Treatment of human iPSC aggregates with insulin and the caudalising factor FGF2 resulted in drastic induction of endogenous expression of isthmic organiser factors EN1, EN2 and WNT1 as well as hindbrain marker GBX2 on day 21, resembling the gene expression at the midbrain-hindbrain boundary during development (Fig. 6.2). Progenitor-containing neural rosettes, which are highly organized structures resembling the ventricular zone (Ziv et al., 2015), emerged on day 21. By day 35, subpopulations of cells within the embryoid bodies differentiated into GABAergic and glutamatergic precursors, which could be further expanded and matured (Fig. 6.3). Of note, ATOH1- and KIRREL2 positive neural progenitors displayed differential spatial distribution around the neural rosettes. ATOH1-postive rhombic lip precursors were located within and around the neural rosettes while KIRREL2-expressing cells were located at the inner side of the rosettes. This suggests that these regions around neural rosettes display strong apicobasal cell polarity (Elkabetz et al., 2008), and recapitulate the *in*

vivo development of cerebellar ventricular zones. Importantly, FACS for KIRREL2 prior to terminal differentiation was unnecessary to produce Purkinje cells *in vitro.* At the later stage of differentiation, instead of the technically challenging E14.5 rhombic lip preparation that resulted in limited cell number for co-cultures, co-culture with E18.5 whole cerebellar cells also robustly produced human Purkinje cells. Furthermore, the mixed co-cultures at increased cell seeding density at day 35 reproducibly generated human Purkinje cells that displayed characteristic morphology and expressed markers specific for Purkinje cells (Fig. 6.4). The addition of laminin into the feeding medium provided additional structural support that enhanced adhesion of cells and neuronal processes during maturation. With these modifications, approximately 15-20% human Purkinje cells were reproducibly generated on days 50-100. These Purkinje cells resembled, by morphology and marker expression, those in embryonic mice. Moreover, 10% Purkinje cells that morphologically resembled those in neonatal mice (P0-P3) were produced by days 120-125 (Fig. 6.4) (Leto et al., 2016). Taken together, a simplified protocol for the reproducible generation of cerebellar cells from human iPSCs *in vitro* is presented.

6.4.2 Further improvements to the Purkinje cell differentiation protocol

Despite significant progress, a number of challenges remain to be addressed before researchers can fully exploit iPSC-based cerebellar models. The survival and maturation of the above-described dissociated cultures of Purkinje cells is still limited. To further increase the efficiency of Purkinje cell generation and facilitate cell maturation during terminal differentiation, several modifications to this differentiation protocol could be included. Cerebellar ventricular zones give rise to Purkinje cells and other GABAergic neurons in a temporal distinct manner. Purkinje cells are predominantly produced on E11.5-13.5 from the cerebellar plate neuroepithelium. These cells that give rise to Purkinje cells express E-cadherin, Ptf1α and Kirrel2 while those

that develop into other GABAergic neurons express only Ptf1α and Kirrel2 but not E-cadherin at E13.5-15.5 (Leto et al., 2016; Mizuhara et al., 2010; Morales and Hatten, 2006; Muguruma et al., 2010; Seto et al., 2014). Therefore, ways to increase co-expression of E-cadherin, PTFIα and KIRREL2 such as transient overexpression of E-cadherin and PTF1α in embryoid bodies could enhance the differentiation efficiency of Purkinje cells during early stage of differentiation. Likewise, suppression of E-cadherin and induction of PAX2 and SHH signalling would theoretically facilitate the production of other GABAergic neurons as well as astrocytes.

Interactions with cerebellar granule cells are essential for dendritic maturation of Purkinje cells but might reduce their survival (Baptista et al., 1994; Seil, 1987) via a delicate balance between neurotrophin and glutamate signalling (Morrison and Mason, 1998). Although BDNF was not required for basic dendritic growth and differentiation in dissociated Purkinje cell cultures (Shimada et al., 1998) or slice cultures (Adcock et al., 2004), it was shown to increase spine density of Purkinje cell dendrites (Morrison and Mason, 1998; Schwartz et al., 1997; Shimada et al., 1998). Moreover, the combination of BDNF and NT3 enhanced the survival of Purkinje cells in pure cultures (Morrison and Mason, 1998). Recently, BDNF and NT3 were shown to enhance human iPSC-derived Purkinje cell maturation in co-culture with mouse whole cerebellar cells (Watson et al., 2018) or granule cells (Ishida et al., 2016).

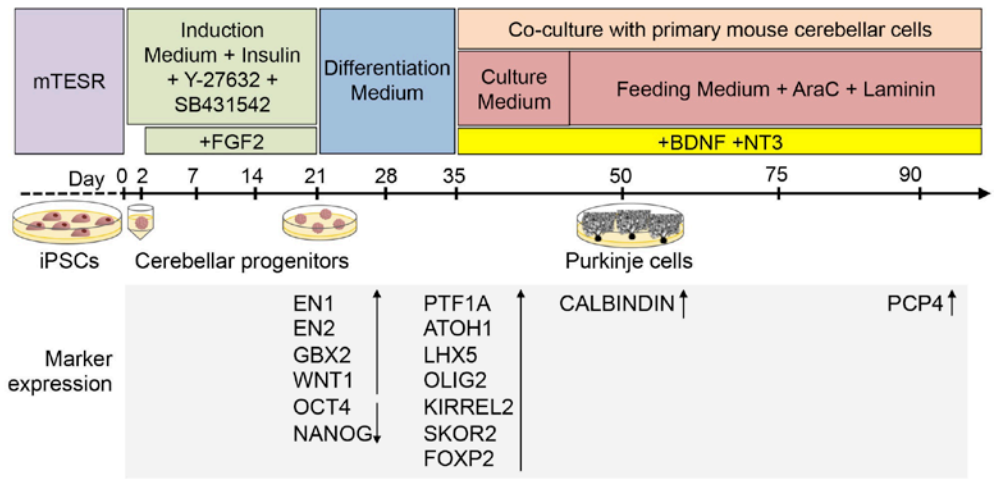


Figure 6.8 Overview of improved cerebellar neuronal differentiation protocol.

Similar to the simplified protocol used in this study, human iPSCs are seeded at 10,000-12,000 cells/well in ultra-low attachment plates and cultures in suspension for 35 days before dissociation and co-culture with E18.5 mouse cerebellar cells. The cultures are supplemented by two additional growth factors BDNF and NT3 to promote the survival and maturation of human Purkinje cells *in vitro*. Up- and downregulated expression of markers for neural precursors and Purkinje cells are indicated. Adapted from (Watson et al., 2018).

NT3 was shown to reduce survival of Purkinje cells when they are isolated (Morrison and Mason, 1998). This is consistent with the reduced survival of human cells cultured alone when supplemented with BDNF and NT3 (Becker group, unpublished data). Moreover, human cells co-cultured with mouse cerebellar cells in porous inserts showed severe cell death and the remaining Purkinje cells displayed abnormal morphologies (Fig. 6.4). Furthermore, human Calbindin-positive cells co-cultured with mouse cells in inserts often associated with bundles of Tuj1-positive axons of which cell bodies could not be traced. These results suggest that in addition to neuotrophins secreted by granule cells (Morrison and Mason, 1998), physical interaction between axons of granule cells and Purkinje cells is also essential to Purkinje cell development. Moreover, human cells cultured alone showed severe cell death and remained in immature form, resembling the long and thin dendrites observed in isolated mouse Purkinje cells (Baptista et al., 1994). This is likely due to the lack of synaptic input and local growth factors that promote dendritic maturation (Metzger, 2010; Schilling et al., 2008).

In contrast, mixed co-cultures of human cerebellar progenitors with primary mouse cerebellar cells provide an initial boost for Purkinje cell maturation and phenotypic differentiation. However, Pax6-positive granule cell precursors derived from primary mouse whole cerebella did not survive beyond 30 days in culture (Becker group, unpublished data). As reported previously, in co-culture with astrocytes only, mouse Purkinje cells showed aberrant morphology without spine formation although dendritic branching was present in dissociated cultures (Baptista et al., 1994). The persistence of GFAP-positive astrocytes after granule cell death in mixed co-culture might therefore lead to abnormal dendritic development of human Purkinje cells in long-term culture. To address this problem, primary mouse cerebellar cells

could be replenished in mixed co-cultures regularly to aid the maturation of Purkinje cells. BDNF and NT3 were also shown to reduce Purkinje cell survival in the presence of granule cells (Morrison and Mason, 1998). Most recently, only BDNF, but not NT3, was included in another differentiation protocol to enhance the maturation of human Purkinje cells in the presence of primary granule cells from P6 mice (Sundberg et al., 2018). The loss of Purkinje cells in dissociated cultures resulting from BDNF or neurotrophin 4 (NT4) supplementation could be overcome by the addition of CNQX, a non-NMDA glutamate receptor antagonist, in the presence of granule cells (Morrison and Mason, 1998). Hence, the addition of CNQX to mixed co-cultures might enhance the survival of human Purkinje cells. Moreover, early postnatal developmental changes in NMDA receptor subunits regulate cerebellar granule cell maturation and potentially Purkinje cell development. NMDA supplementation of the mixed-co-culture that mimics activation of parallel fibre inputs (Metzger et al., 2005) might enhance Purkinje cell dendritic arborisation.

Finally, the resemblance of human iPSC-derived Purkinje cells to human Purkinje cells *in vivo* remains to be elucidated. To assess the maturity of the human Purkinje cells generated, further assessment of more mature Purkinje cell markers and spine formation including PCP2/L7, TRPC3, IP3R1 and GRID2 would be crucial. In addition, it would be important to examine the transcriptomic profiles of purified Purkinje cells to further determine their variability and maturity when compared to existing data of mouse and human cerebella. Furthermore, to assess the functionality of the Purkinje cells, it would be necessary to perform electrophysiological studies. Indeed, transcriptomic analysis of other iPSC-derived neuronal models has shown that the generated neurons are still in an embryonic state, despite the fact the individual neurons express mature markers and show spontaneous firing patterns (reviewed in (Ardhanareeswaran et al., 2017)). To further improve the differentiation protocol, it would be beneficial to determine the overall cell composition of the cultures using a single cell transcriptomic approach, so that ways to adjust the cell composition could be developed accordingly.

6.4.3 Developing a differentiation protocol for three-dimensional cerebellar organoids from human iPSCs

Intrinsic programs control the basal dendrite outgrowth and patterning of Purkinje cells when isolated in culture. However, complete dendritic maturation requires inputs from connecting neuronal partners (Baptista et al., 1994; Metzger, 2010). Mouse Purkinje cells at P20 *in vivo* had a more complex and arborized dendritic tree compared to those *in vitro* at P8 after 12 days in slice culture (Metzger, 2010). This suggests that the lack of cell composition and cell-cell interaction in two-dimensional dissociated cultures of Purkinje cells is likely to limit their maturation. Specific disease phenotypes affecting synapse formation, dendritic retraction and neural migration, which might only emerge from interactions between cells and their environment, might be lost in these two-dimensional cultures (Wong et al., 2017). In particular, a recent study showed that climbing fibre innervation of Purkinje cell dendrites and expression of synaptic actitivity markers were disturbed in the lobule 7 of the cerebellum of SCA14-S361 transgenic mice (Trzesniewski et al., 2018). To overcome these hurdles, three-dimensional cultures of self-organising organoids, which include multiple cell types and mimic the *in vivo* architecture of an organ (Dutta et al., 2017), could be used. Thus far, only one study has reported the generation of immature cerebellar organoids from human ESCs (Muguruma et al., 2015). The Muguruma group showed that the supplementation of FGF19 and stromal cell-derived factor (SDF1) promoted the self-organisation of human ESCs into polarised three-layer structures similar to the human embryonic cerebellum (Muguruma et al., 2015). Attempts have been made to generate cerebellar organoids from human iPSCs through the addition of FGF2 and FGF8B, retinoic acid, BDNF, glial derived neurotrophic factor (GDNF), smoothened agonist (SAG) and NT3 (Holmes and Heine, 2017). However, these human iPSC-derived aggregates lack polarisation of cell layers despite the expression of cerebellar markers, and are therefore spheroids, rather than organoids.

Furthermore, the question remains whether self-induction alone is sufficient to generate a functionally mature human cerebellum *in vitro.* While long-term culture is needed for the maturation of multiple cell types that form active neuronal networks in spatially organised manner, the lack of mechanical support, as well as nutrient and gas limit culture duration and maturity (Kelava and Lancaster, 2016). To overcome this, cerebellar organoids could be grown on orbital shakers to improve nutrient and gas exchange and therefore their viability (Lancaster and Knoblich, 2014). Alternatively, the self-induction approach could be used to generate progenitors of various cerebellar subtypes, which could subsequently be plated onto biodegradable scaffolds to support their organisation into a layered three-dimensional structure (Wong et al., 2017) and at the same time promote terminal differentiation and neuronal circuit formation (Birey et al., 2017). An on-chip approach, which enables development of human brain organoids to millimetre diameter and efficient nutrient exchange by diffusion, has been developed (Karzbrun et al., 2018). This approach allows for whole-organ fluorescent live imaging, which is impossible in three-dimensional organoids as limited by the tissue thickness, in the expense of overall architecture of organoids. This might be beneficial for modelling of early cerebellar development but might not be ideal for the later stage when Purkinje cells obtain a spatially distinct orientation. Alternatively, slice culture of organoids can be used for live imaging to visualise cell maturation and migration (Lancaster et al., 2017) as well as for electrophysiological studies to determine the firing properties and functionality of cerebellar circuitry (Watanabe et al., 2017). Overall, the generation of cerebellar organoids from human iPSCs remains a challenge.

6.4.4 Effect of SCA14 mutations on the development and survival of human Purkinje cells

In this study, the first SCA14 disease model using human Purkinje cells derived from iPSCs was reported. PKCγ is highly expressed in developing Purkinje cells and is important for their

development in rodents (Kano et al., 1995; Metzger, 2010). No obvious differences were observed between control and SCA14 cerebellar progenitors at the early stage of the differentiation (at days 21 and 35), which was consistent with the normal cerebellar specification in PKCγ-knockout (Abeliovich et al., 1993; Kano et al., 1995) and SCA14 transgenic mice (Ji et al., 2014; Zhang et al., 2009). However, at later stages, human SCA14 Purkinje cells demonstrated developmental abnormalities and reduced survival.

Importantly, PKCγ was expressed on days 21 and 35 in both control and SCA14 iPSC-derived cerebellar progenitors. On day 21, iPSC-derived cerebellar progenitors recapitulated gene and protein expression of cells at the midbrain-hindbrain boundary during early cerebellar specification. At this stage, subpopulations of cells within the aggregates expressed PKCγ ubiquitously in the cytoplasm, many of which are Tuj1-postive neural progenitors. Interestingly, punctate staining of PKCγ was highly co-localised with neuronal βIII-tubulin, a structural component of cytoskeletal microtubules, particularly within the neural rosettes (Fig. 6.6B & D). At day 35, PKCγ formed thread-like structures in both control and SC14 iPSC-derived cerebellar progenitors rather than cytoplasmic punctae (Fig. 6.6C). This is consistent with the observation of PKCγ-fibrils *in vitro* and in neuronal cell lines. In the same study, SCA14 mutations accelerated the fibril formation *in vitro* (Takahashi et al., 2015). However, the nature and role of these amyloid-like fibrils remain unclear. Of note, the thread-like structures of PKCγ in iPSCs were highly co-localised with neuronal βIII-tubulin (Fig. 6.6C & D). This further suggests that PKCγ might be involved in organisation and stabilisation of microtubules during early cerebellar development. No obvious difference in gene expression or localisation of PKCγ was observed on days 21 or 35. This would explain the similar gene and protein expression of markers of cerebellar precursors in control and SCA14 cerebellar progenitors at days 21 and 35. Further experiments including immunoblotting for PKCγ and cerebellar precursor markers would be important to determine their protein expression. PKC has long been implicated in interacting with the cytoskeleton (Larsson, 2006). It would be

interesting to determine whether PKCγ physically interacts with neuronal microtubules and if this interaction was altered in the presence of SCA14 mutations. Also, immunoblotting for components of signalling pathways in microtubule organisation and dendritic development in control and SCA14 cerebellar progenitors would provide insights into how mutant PKCγ affects dendritic development via the cytoskeleton.

The expression of PKCγ is restricted to Purkinje cells in the cerebellum (Kano et al., 1995; Schrenk et al., 2002). It would therefore be important to determine whether PKCγ is localised in specific types of cerebellar progenitors such as Purkinje cell precursors in the embryoid bodies. Therefore, further experiments such as co-staining of PKCγ with markers of Purkinje cell progenitors PTF1α, KIRREL2, LHX5 as well as granule cell precursors ATOH1 and PAX6 could be performed. It would also be interesting to determine if the thread-like structures are expressed predominantly in particular cell types or in extracellular space.

Although no obvious difference was observed in progenitors undergoing early cerebellar specification, the effect of mutant PKCγ could be apparent and affect Purkinje cell development at later stages of differentiation. Indeed, SCA14 iPSC-derived cerebellar progenitors in mixed co-cultures were less capable of developing into Purkinje cells than controls from day 50 onwards during terminal differentiation. This was independent of overall survival of human cells, when expression of PKCγ was not detected until day 100 by immunocytochemistry (Fig. 6.5A-B, 6.6E-F). This reduced survival of SCA14 Purkinje cells is consistent with the loss of Purkinje cells observed in SCA14 patients (Fig. 5.1) (Chen et al., 2003) and transgenic mice (Zhang et al., 2009). Furthermore, SCA14 Purkinje cells had smaller cell bodies on day 50, further suggesting that the effect of mutant PKCγ on development and survival of SCA14 cells was delayed. This result is in line with the altered soma morphology of Purkinje cells in PKCγ-H101Y transgenic mice at P28 (Zhang et al., 2009). However, dendritic morphologies of Purkinje cells in these mice was not characterised and the effect of the H101Y mutation on

Purkinje cell dendritic development therefore remains unclear (Zhang et al., 2009). *PRKCG* mRNA expression was significantly lower on day 63 in SCA14 iPSC-derived cultures (human cell-only cultures) compared to controls. However, *PRKCG* mRNA expression was completely lost on day 85 in both control and SCA14 cultures (Fig. 6.7A). This loss of *PRKCG* mRNA expression is likely to be an artifact as there was significant cell death in these human cell-only cultures on day 85. To address this limitation, mixed co-cultures, which contain adequate Purkinje cells, could be used together with human-specific primers to detect *PRKCG* mRNA expression in future studies.

From day 100 onwards, SCA14 Purkinje cells showed abnormal dendritic development with higher degree of branching, increased number of thinner dendrites (Fig. 6.5G-I). These results are in contrast to the reduction in dendritic branching of Purkinje cells observed in human SCA14 patients (Fig. 5.2E). This could be because Purkinje cells in adult patients' post-mortem brain tissues only captured the end point of the disease but could not reflect the earlier events. This further highlights the importance of an *in vitro* model that allows the visualisation of development changes of diseased Purkinje cells. Previous studies performed in primary mouse Purkinje cells expressing different mutant PKCγ showed inconsistent results. Contrary to abnormal development in SCA14 iPSC-derived Purkinje cells (H36R) shown in this study, cultured mouse Purkinje cells overexpressing mutant PKCγ-S119P and PKCγ-G128D had leaner dendrites with reduced branches *in vitro* (Seki et al., 2009) while transgenic mice harbouring PKCγ-S119P had developing Purkinje cells with normal dendritic differentiation *in vivo* (Shuvaev et al., 2011). On the other hand, the dendritic tree of Purkinje cells in lobule 7 of the cerebellum in PKCγ-S361G transgenic mice was drastically reduced in size and complexity as well as thicker primary dendritic branches and short secondary side branches (Ji et al., 2014; Trzesniewski et al., 2018). These differences could be a result of the distinct functions and activities of PKCγ caused by mutations in different protein domains, which led to inconsistent results in heterologous cell lines. For example, Purkinje cells overexpressing mutant PKCγ with

mutations in the catalytic domain and C-terminus but not in the C1 or C2 domain showed abnormal dendritic development (Shimobayashi and Kapfhammer, 2017).

On days 100-125, PKCγ was expressed in the cell bodies and neuronal processes of control Purkinje cells in mixed co-cultures, but not in SCA14 Purkinje cells (Fig. 6.6E-F). This suggests that PKCγ expression in SCA14 Purkinje cells could be delayed. Instead, PKCγ was expressed as thread-like structure outside of Purkinje cells in SCA14 cultures, potentially secreted into extracellular space or expressed in other cell types, for example, glia (Fig. 6.6F) or Calbindin-negative neurons (data not shown). In the future, it would be interesting to determine the identity of PKCγ-expressing cells by means of immunostaining. Alternatively, the abnormalities of SCA14 Purkinje cells could result from the absence of PKCγ expression. The dendritic anormalies of the SCA14 iPSC-derived Purkinje cells was similar to the disease phenotypes of Purkinje cells in PKCγ-knockout mice as well as with pharmaceutical inhibition of PKC *in vitro* and *in vivo* but not PKC activation (Metzger and Kapfhammer, 2000; Schrenk et al., 2002). As dendritic maturation is driven by calcium-dependent signalling involving PKC to limit overgrowth at a later stage (Metzger, 2010), the period between days 100-115 and 120-125 in control mixed co-cultures might reflect the retraction of Purkinje cell dendrites, which is a critical period of dendritic overgrowth inhibition.

The supplementation of trophic factors might advance the expression of PKCγ in iPSC-derived Purkinje cells. It would be important to determine whether SCA14 Purkinje cells might show similar disease phenotypes as shown in iPSCs in Chapter 5 including accumulation of mutant PKCγ foci, reduced membrane association and excessive signalling. Furthermore, it would be important to study calcium homeostasis, which has been shown to be impaired in heterologous SCA14 cell models. Expression windows of key indicators of Purkinje cell generation, maturation and synaptogenesis should be further investigated to reveal any subtle developmental disease phenotypes in SCA14 Purkinje cells. Moreover, it would be interesting

to determine whether synapse elimination, long-term depression and spine formation are impaired in human SCA14 Purkinje cells, as shown in SCA14-S119P transgenic mice (Shuvaev et al., 2011) and primary cultured mouse Purkinje cells overexpressing mutant PKCγ (S119P and G128D) (Seki et al., 2009). Finally, it would be of importance to show whether these observed disease phenotypes could be reversed. Taken together, these results suggest that the abnormal dendritic development of Purkinje cells might also contribute to the pathogenesis of SCA14, in addition to degeneration and loss of Purkinje cells that is observed in patients at the end stage of the disease.

6.5 Conclusions

In conclusion, a simplified differentiation protocol that robustly and reproducibly produces 10-20% of cerebellar Purkinje cells from human iPSCs was developed. Moreover, Purkinje cells were generated from human control and SCA14 iPSCs. Finally, development and survival of Purkinje cells were impaired in *in vitro* cultures, which was likely due to delayed expression of mutant PKCγ in cerebellar progenitors. Overall, this is the first report that demonstrates developmental abnormalities in human Purkinje cells in SCAs. These iPSC-derived Purkinje cells are therefore ideal tools for further investigation of pathogenic mechanisms underlying SCA14 and related SCAs, and for the development of therapies.

Chapter 7 Discussion

7.1 Summary and significance

The cerebellar ataxias are a group of heterogeneous disorders that is characterised by cerebellar atrophy and progressive Purkinje cell degeneration. In the past decades, with the advancement of next generation sequencing technology, many novel genes that cause ataxia when mutated have been identified. Yet, the pathogenic mechanisms underlying this complex group of disorders remain incompletely understood and therefore no cure or effective treatment is available. This is largely due to the limited source of human brain tissue and the lack of reliable disease models of cerebellar ataxia. Although studies performed using heterologous cell lines and animal models has provided important insights into the understanding the pathogenic mechanisms underlying cerebellar ataxia, the results obtained are often inconsistent. Moreover, there is not yet a disease model that can faithfully recapitulate the pathological findings observed in human patients. Therefore, a reliable disease model is urgently needed. Human induced pluripotent stem cells (iPSCs), which can be differentiated into any cell types that are affected in ataxia, are therefore an ideal tool for the investigation of underlying disease mechanisms.

Major questions that remain unresolved include why Purkinje cells are particularly vulnerable to genetic insults and how distinct genetic mutations cause Purkinje cell degeneration and cerebellar ataxia. Interestingly, accumulating evidence has suggested that subtypes of the autosomal dominant ataxias or spinocerebellar ataxias (SCAs) are likely to be caused by shared pathogenic pathways. Focused on spinocerebellar ataxia type 14 (SCA14), a subtype of SCAs, this work aimed to understand the disease mechanisms underlying SCA14 and related SCAs using novel disease models derived from human iPSCs. SCA14 is caused by mutations in PKCγ, a central molecule in signalling pathways that are important for Purkinje cell development and function. Interestingly, the PKCγ-encoding gene *PRKCG* was identified as a

hub gene in ataxia-linked gene networks in a transcriptomic co-expression analysis in human cerebellar tissue (Bettencourt et al., 2014), as well as in mouse models of other SCAs such as SCA1 (Ingram et al., 2016) and SCA2 (Pflieger et al., 2017). Therefore, in addition to the selective Purkinje cell degeneration observed in SCA14 patients, the central role of PKCγ in Purkinje cell development and function has made PKCγ and SCA14 an excellent entry point to understand the shared pathogenic pathways underlying SCAs.

In this thesis, a unique *in vitro* model of SCA14 using human patient-derived iPSCs carrying two distinct SCA14 mutations, H36R and H101Q, respectively is presented. To our knowledge, this is the first study reporting the generation of SCA14 iPSCs. The equivalent positions of these mutations in the C1A and C1B subdomains have provided a unique opportunity for the direct comparison of the functional consequences of PKCγ caused by alterations in the two apparently complementary subdomains. This work has shown that these two SCA14 mutations behave consistently in iPSC models. The results presented in Chapter 5 indicate that SCA14 is caused by three interconnected pathogenic mechanisms (Fig. 5.11). SCA14 mutations enhance the formation and accumulation of PKCγ foci in the cytoplasm. Moreover, reduced residence of PKCγ at the plasma membrane is likely to decrease its interaction with target substrates. Extended cytoplasmic retention of hyperactive PKCγ leads to abnormal phosphorylation of substrates in the cytoplasm. Importantly, this model faithfully recapitulates the pathological findings observed in human SCA14 cerebellum. To determine the developmental changes of Purkinje cells caused by SCA14 mutations, control and SCA14 iPSCs were successfully differentiated into human Purkinje cells using a simplified differentiation protocol in Chapter 6. Notably, this is the first report that demonstrates developmental anomalies and reduced survival of human Purkinje cells carrying a SCA14 mutation. Taken together, SCA14 iPSCs and iPSC-derived Purkinje cells are reliable models of SCA14. It is noteworthy that human iPSC models are applicable to all types of hereditary ataxias when incorporated with genome editing technology. In the future, these cells could be used as a platform to further investigate

the shared pathogenic mechanisms underlying SCAs and to screen therapeutic approaches in a high-throughput manner prior to clinical trials. Finally, the developed model could also allow for a personalised medicine approach in the future, when simple administration and derivation of patient cells, bioassays for disease phenotypes and patient-specific drugs are available as a streamline.

7.2 Shared disease mechanisms and potential therapies of SCAs

7.2.1 Accumulation of protein foci

Protein misfolding and aggregation is one of the consensus disease mechanisms in polyglutamine SCAs. In this work, PKCγ foci were found in the surviving Purkinje cells in human cerebellum and in iPSCs from patients with SCA14, a non-polyglutamine SCA. Mutant PKCγ foci formation was enhanced and accumulate in the cytoplasm. These findings provide evidence that clustering of PKCγ might be an early and crucial event in SCA14. Furthermore, these results connect the pathogenic mechanisms underlying SCAs caused by conventional mutations and repeat expansions. Importantly, this suggests that these SCAs could be treated with similar therapeutic approaches, i.e. inhibiting protein foci formation and/or enhancing the clearance of protein degradation. In addition, drugs that were shown effective in other aggregation-prone diseases might also be used to treat SCA14. Overexpression of chaperones PDK-1 was shown to reduce accumulation of mutant PKCγ in Triton-insoluble fractions (Jezierska et al., 2014). Furthermore, inhibitors of protein oligomerisation and aggregation such as Congo Red, which were found to alleviate aggregation of mutant proteins, inhibit cell death and reverse improper dendritic development in primary mouse Purkinje cells (Seki et al., 2010a; Seki et al., 2010b), might be used to treat SCA14. It would therefore be interesting to determine whether overexpression of chaperones or drugs could lessen the accumulation of PKCγ foci.

Alternatively, methods that promote clearance of protein foci might be used as potential therapeutic approaches. Enhanced autophagy was shown to promote degradation whereas inhibition of autophagy increased formation of mutant PKCγ (S119P) foci with the same mutation of which effect was not compensated by the UPS, in SH-SY5Y cells (Yamamoto et al., 2010). As autophagic processes appear to capture small oligomers but not massive inclusions (Menzies et al., 2017), the decreased massive inclusion is likely a result of reduced input of small foci. Therefore, autophagy inducers such as rapamycin, Rilmenidine, trehalose and protein phosphatase 2A agonists, which have been shown to alleviate disease phenotypes in animal models of other neurodegenerative diseases including SCA17 (Chen et al., 2015; Ciechanover and Kwon, 2015; Menzies et al., 2017), might be used to treat SCA14 by facilitating the clearance of PKCγ foci. However, the molecular mechanisms of how these drugs alleviate the disease phenotypes are incompletely understood. It would thus be important to investigate the detailed mechanisms. Finally, it remains unclear why mutant PKCγ foci were not ubiquitinated, which is an important step for clearance for unwanted proteins. One possibility is that components of the ubiquitin pathways might be substrates of PKCγ and the interactions are deregulated in SCA14. This might provide novel links between SCA14 and other neurodegenerative diseases in which ubiquitin-mediated pathways are also impaired. Indeed, genes involved in the ubiquitin-proteasome pathway were enriched in the human cerebellum and are associated with several SCA genes (Bettencourt et al., 2014). Therefore, it would be important to delineate the ubiquitin-mediated pathways that are impaired to identify novel targets for treating SCA14 and related disorders.

7.2.2 Aberrant phosphorylation of substrates in Purkinje cell-enriched pathways

The answer to the vulnerability of Purkinje cells may lay in their unique structure, physiology and functions in the cerebellum. Purkinje cells are the centres of the cerebellar network.

Purkinje cells posses a dendritic tree with elaborate arborisation, which receive excitatory inputs from climbing and parallel fibres. The axons are connected to the deep cerebellar nuclei (DCN) to convey the sole output of the cerebellar cortex. To support the development of such a unique structure and function, components of different pathways, potentially enriched in Purkinje cells, need to be highly orchestrated. Many of the genes affected in SCAs including *ITPR1*, *AFG3L2*, *TRPC3* and *CACNA1G* are exclusively or highly expressed in Purkinje cells (Doyle et al., 2008; Huang and Verbeek, 2018). Several of these genes converge onto pathways that regulate intracellular neuronal calcium homeostasis, which is critical for the development and function of Purkinje cells including neurotransmission and synaptic plasticity. One of these pathways is the mGluR1-signalling pathway. Glutamate released from granule cell terminal binds to the mGluR1 receptor at the Purkinje cell postsynaptic terminals, resulting in activation of phospholipase C (PLC), the enzyme that hydrolyses phosphatidylinositol 4,5-bisphosphate (PIP_2) to generate membrane-bound DAG and inositol trisphosphate (IP_3). IP_3 then binds to IP_3R1 in the endoplasmic reticulum (ER) leading to intracellular release of calcium into the cytosol (Steinberg, 2008). Meanwhile, the produced DAG activates TRPC3 causing calcium influx (Trebak et al., 2005). PKCγ is activated by calcium and translocates to the plasma membrane, where it phosphorylates TRPC3 among other substrates. The PKCγ-mediated phosphorylation, acting as a negative feedback mechanism (Trebak et al., 2005; Venkatachalam et al., 2003), inhibits TRPC3, blocks further calcium influx and as a result, the cytoplasmic homeostasis is maintained. Mutations in the components of the mGluR1-signalling pathway such as PKCγ, TRPC3, mGluR1 and IP_3R1 all result in SCAs (Chen et al., 2003; Fogel et al., 2015; Huang et al., 2012; Iwaki et al., 2008; van de Leemput et al., 2007; Watson et al., 2017) (Table 1.1), suggesting that these ataxia genes are crucial to cerebellar function. Notably, this work has shown that PKCγ-mediated phosphorylation of TRPC3 was increased in SCA14 iPSCs compared to controls. This suggests that mutant PKCγ might affect Purkinje cell dendritic development and cause their dysfunction in SCA14 via altered function of TRPC3. Interestingly, TRPC3 function was found to be impaired in ataxic *Moonwalker* (*Mwk*) mice

(Becker et al., 2009) and in an ataxia patient carrying a mutation in the *TRPC3* gene (Fogel et al., 2015). The gain-of-function *Mwk* mutation was shown to result in aberrant calcium signalling in Purkinje cells and gene expression changes that resulted in altered lipid homeostasis and, ultimately, impairments in dendritic arborisation and synapse formation during Purkinje cell development (Becker et al., 2009; Dulneva et al., 2015). These findings therefore raise the intriguing hypothesis that the excessive phosphorylation of TRPC3 caused by hyperactive mutant PKCγ might impair Purkinje cell dendritic development and function via disrupted lipid homeostasis.

Lipid homeostasis and trafficking is important for the dendritic development and maintenance of Purkinje cells. Notably, mutations in genes involved in fatty acid synthesis such as *ELOVL5, ELOVL4, FAT1 and FAT2* cause SCAs (Di Gregorio et al., 2014; Nibbeling et al., 2017; Ozaki et al., 2015). Furthermore, deletion of *Acer3* and mutations in *Laa1,* both of which affect ceramide biosynthesis, led to abnormal development and premature degeneration of Purkinje cells and ataxia in mice (Wang et al., 2015a; Zhao et al., 2011). During dendritic tree expansion, large amount of lipid and membrane receptors are transported and incorporated to plasma membrane of Purkinje cells. PKCγ has been shown to be involved in the trafficking and insertion of membrane receptors (Patten and Ali, 2009). Mutant PKCγ might affect the abundance and stability of neurotransmitter receptors at the synapse, which could in turn impair the membrane excitability and long-term survival of Purkinje cells. Indeed, increased PKC activity was shown to reduce Purkinje cell membrane excitability (Chopra et al., 2018). Interestingly, the aberrant enlargement of lysosomes observed in SCA14 iPSCs might be a result of the impaired membrane trafficking and lipid metabolism. Recently, deletion of the Golgin protein of the Golgi apparatus, of which morphology and activity are crucial to secretory trafficking in cells, was shown to cause cerebellar ataxia in mice (Liu et al., 2017). Deletion of GM130 did not affect early growth of Purkinje cell dendrites but was required for maintenance of dendritic trees (Liu et al., 2017). This suggests that PKCγ might disrupt membrane

trafficking via multiple interconnected pathways and ultimately cause SCA14. In addition, the phosphorylation of MARCKS, which is important for cell motility and membrane trafficking, was elevated in SCA14 iPSCs and patient cerebellum. This further indicates that PKCγ are likely to be involved in multiple pathways that are crucial to Purkinje cell development and function, and disruption of PKCγ function might be associated to other SCAs. Indeed, the level of PKCγ, but not PKCα, both are important for membrane excitability of Purkinje cells (Hirai, 2017; Metzger and Kapfhammer, 2000, 2003), decreased in mouse models of SCA1 and SCA2 (Chopra et al., 2018; Skinner et al., 2001). This reduction might result from the altered functions of ataxin-1 as a transcription repressor (Tsai et al., 2004), and ataxin-2, which is involved in RNA regulation (Ostrowski et al., 2017). However, the activity of PKC was increased due to the reduced DAG metabolism and the resulting increased PKC activation. Therefore, aberrant PKCγ activity is likely to show a pathological role beyond SCA14 and PKCγ might be an attractive therapeutic target of more than one subtype of SCAs.

7.3 Conclusion

In conclusion, this work has highlighted the value of human patient materials to investigate the novel pathogenic mechanisms underlying cerebellar ataxias. This thesis has also demonstrated how human iPSCs and iPSC-derived Purkinje cells can successfully be used to model the disease and understand the molecular pathways involved in SCA14. The results obtained are deemed invaluable to develop, in the long run, potential therapies for SCA14 and other SCAs.

References

Abeliovich, A., Chen, C., Goda, Y., Silva, A.J., Stevens, C.F., and Tonegawa, S. (1993). Modified hippocampal long-term potentiation in PKCγ-mutant mice. Cell *75*, 1253-1262.

Abrahamsen, H., O'Neill, A.K., Kannan, N., Kruse, N., Taylor, S.S., Jennings, P.A., and Newton, A.C. (2012). Peptidyl-prolyl isomerase Pin1 controls down-regulation of conventional protein kinase C isozymes. The Journal of biological chemistry *287*, 13262-13278.

Adachi, N., Kobayashi, T., Takahashi, H., Kawasaki, T., Shirai, Y., Ueyama, T., Matsuda, T., Seki, T., Sakai, N., and Saito, N. (2008). Enzymological analysis of mutant protein kinase Cgamma causing spinocerebellar ataxia type 14 and dysfunction in Ca2+ homeostasis. The Journal of biological chemistry *283*, 19854-19863.

Adams, K.A., Maida, J.M., Golden, J.A., and Riddle, R.D. (2000). The transcription factor Lmx1b maintains Wnt1 expression within the isthmic organizer. Development *127*, 1857-1867.

Adcock, K.H., Metzger, F., and Kapfhammer, J.P. (2004). Purkinje cell dendritic tree development in the absence of excitatory neurotransmission and of brain-derived neurotrophic factor in organotypic slice cultures. Neuroscience *127*, 137-145.

Alder, J., Cho, N.K., and Hatten, M.E. (1996). Embryonic precursor cells from the rhombic lip are specified to a cerebellar granule neuron identity. Neuron *17*, 389-399.

Alonso, I., Costa, C., Gomes, A., Ferro, A., Seixas, A.I., Silva, S., Cruz, V.T., Coutinho, P., Sequeiros, J., and Silveira, I. (2005). A novel H101Q mutation causes PKCgamma loss in spinocerebellar ataxia type 14. Journal of human genetics *50*, 523-529.

Altman, J. (1972a). Postnatal development of the cerebellar cortex in the rat. I. The external germinal layer and the transitional molecular layer. The Journal of comparative neurology *145*, 353-397.

Altman, J. (1972b). Postnatal development of the cerebellar cortex in the rat. II. Phases in the maturation of Purkinje cells and of the molecular layer. The Journal of comparative neurology *145*, 399-463.

Altman, J., and Bayer, S.A. (1985). Embryonic development of the rat cerebellum. II. Translocation and regional distribution of the deep neurons. The Journal of comparative neurology *231*, 27-41.

Altman, J., and Bayer, S.A. (1997). Development of the cerebellar system: in relation to its evolution, structure, and functions (CRC Press).

Ananthanarayanan, B., Stahelin, R.V., Digman, M.A., and Cho, W. (2003). Activation mechanisms of conventional protein kinase C isoforms are determined by the ligand affinity and conformational flexibility of their C1 domains. The Journal of biological chemistry *278*, 46886-46894.

Anderson, W.J., and Altman, J. (1972). Retardation of cerebellar and motor development in rats by focal X-irradiation beginning at four days. Physiology & behavior *8*, 57-67.

Andreu, A., Crespo-Enriquez, I., and Echevarria, D. (2014). Molecular events directing the patterning and specification of the cerebellum. Eur J Anat *18*, 245-252.

Antal, C.E., and Newton, A.C. (2014). Tuning the signalling output of protein kinase C. Biochemical Society transactions *42*, 1477-1483.

Antal, C.E., Violin, J.D., Kunkel, M.T., Skovso, S., and Newton, A.C. (2014). Intramolecular conformational changes optimize protein kinase C signaling. Chemistry & biology *21*, 459-469.

Appelqvist, H., Waster, P., Kagedal, K., and Ollinger, K. (2013). The lysosome: from waste bag to potential therapeutic target. Journal of molecular cell biology *5*, 214-226.

Ardhanareeswaran, K., Mariani, J., Coppola, G., Abyzov, A., and Vaccarino, F.M. (2017). Human induced pluripotent stem cells for modelling neurodevelopmental disorders. Nature reviews Neurology *13*, 265-278.

Armengol, J.A., and Sotelo, C. (1991). Early dendritic development of Purkinje cells in the rat cerebellum. A light and electron microscopic study using axonal tracing in 'in vitro' slices. Brain research Developmental brain research *64*, 95-114.

Asai, H., Hirano, M., Shimada, K., Kiriyama, T., Furiya, Y., Ikeda, M., Iwamoto, T., Mori, T., Nishinaka, K., Konishi, N., *et al.* (2009). Protein kinase C gamma, a protein causative for dominant ataxia, negatively regulates nuclear import of recessive-ataxia-related aprataxin. Human molecular genetics *18*, 3533-3543.
Ase, K., Saito, N., Shearman, M.S., Kikkawa, U., Ono, Y., Igarashi, K., Tanaka, C., and Nishizuka, Y. (1988). Distinct cellular expression of beta I- and beta II-subspecies of protein kinase C in rat cerebellum. The Journal of neuroscience : the official journal of the Society for Neuroscience *8*, 3850-3856.
Ashkenazi, A., Bento, C.F., Ricketts, T., Vicinanza, M., Siddiqi, F., Pavel, M., Squitieri, F., Hardenberg, M.C., Imarisio, S., Menzies, F.M., *et al.* (2017). Polyglutamine tracts regulate beclin 1-dependent autophagy. Nature *545*, 108-111.
Avior, Y., Sagi, I., and Benvenisty, N. (2016). Pluripotent stem cells in disease modelling and drug discovery. Nature reviews Molecular cell biology *17*, 170-182.
Bakalkin, G., Watanabe, H., Jezierska, J., Depoorter, C., Verschuuren-Bemelmans, C., Bazov, I., Artemenko, K.A., Yakovleva, T., Dooijes, D., Van de Warrenburg, B.P., *et al.* (2010). Prodynorphin mutations cause the neurodegenerative disorder spinocerebellar ataxia type 23. American journal of human genetics *87*, 593-603.
Baptista, C.A., Hatten, M.E., Blazeski, R., and Mason, C.A. (1994). Cell-cell interactions influence survival and differentiation of purified Purkinje cells in vitro. Neuron *12*, 243-260.
Bareggi, R., Narducci, P., Grill, V., Lach, S., and Martelli, A.M. (1996). Selective distribution of multiple protein kinase C isoforms in mouse cerebellar cortex. Biology of the cell *87*, 55-63.
Barmack, N.H., Qian, Z., and Yoshimura, J. (2000). Regional and cellular distribution of protein kinase C in rat cerebellar Purkinje cells. The Journal of comparative neurology *427*, 235-254.
Bassett, A.R., Tibbit, C., Ponting, C.P., and Liu, J.L. (2013). Highly efficient targeted mutagenesis of Drosophila with the CRISPR/Cas9 system. Cell reports *4*, 220-228.
Basso, M., Samengo, G., Nardo, G., Massignan, T., D'Alessandro, G., Tartari, S., Cantoni, L., Marino, M., Cheroni, C., De Biasi, S., *et al.* (2009). Characterization of detergent-insoluble proteins in ALS indicates a causal link between nitrative stress and aggregation in pathogenesis. PloS one *4*, e8130.
Basson, M.A., Echevarria, D., Ahn, C.P., Sudarov, A., Joyner, A.L., Mason, I.J., Martinez, S., and Martin, G.R. (2008). Specific regions within the embryonic midbrain and cerebellum require different levels of FGF signaling during development. Development *135*, 889-898.
Becker, E.B. (2015). From Mice to Men: TRPC3 in Cerebellar Ataxia. Cerebellum.
Becker, E.B., Oliver, P.L., Glitsch, M.D., Banks, G.T., Achilli, F., Hardy, A., Nolan, P.M., Fisher, E.M., and Davies, K.E. (2009). A point mutation in TRPC3 causes abnormal Purkinje cell development and cerebellar ataxia in moonwalker mice. Proceedings of the National Academy of Sciences of the United States of America *106*, 6706-6711.
Becker, E.B., and Stoodley, C.J. (2013). Autism spectrum disorder and the cerebellum. International review of neurobiology *113*, 1-34.
Becker, E.B.E. (2017). From Mice to Men: TRPC3 in Cerebellar Ataxia. Cerebellum *16*, 877-879.
Beckinghausen, J., and Sillitoe, R.V. (2018). Insights into cerebellar development and connectivity. Neuroscience letters.
Beers, J., Gulbranson, D.R., George, N., Siniscalchi, L.I., Jones, J., Thomson, J.A., and Chen, G. (2012). Passaging and colony expansion of human pluripotent stem cells by enzyme-free dissociation in chemically defined culture conditions. Nature protocols *7*, 2029-2040.
Behn-Krappa, A., and Newton, A.C. (1999). The hydrophobic phosphorylation motif of conventional protein kinase C is regulated by autophosphorylation. Current biology : CB *9*, 728-737.
Ben-Arie, N., Bellen, H.J., Armstrong, D.L., McCall, A.E., Gordadze, P.R., Guo, Q., Matzuk, M.M., and Zoghbi, H.Y. (1997). Math1 is essential for genesis of cerebellar granule neurons. Nature *390*, 169-172.

Ben-David, U., and Benvenisty, N. (2008). Analyzing the genomic integrity of stem cells. In StemBook (Cambridge (MA): Harvard Stem Cell Institute
Copyright: (c) 2012 Uri Ben-Davi and Nissim Benvenisty.).
Bettencourt, C., Ryten, M., Forabosco, P., Schorge, S., Hersheson, J., Hardy, J., and Houlden, H. (2014). Insights from cerebellar transcriptomic analysis into the pathogenesis of ataxia. JAMA neurology *71*, 831-839.
Bilic, J., and Izpisua Belmonte, J.C. (2012). Concise review: Induced pluripotent stem cells versus embryonic stem cells: close enough or yet too far apart? Stem Cells *30*, 33-41.
Birey, F., Andersen, J., Makinson, C.D., Islam, S., Wei, W., Huber, N., Fan, H.C., Metzler, K.R.C., Panagiotakos, G., Thom, N., *et al.* (2017). Assembly of functionally integrated human forebrain spheroids. Nature *545*, 54-59.
Bock, H.H., and Herz, J. (2003). Reelin activates SRC family tyrosine kinases in neurons. Current biology : CB *13*, 18-26.
Bolte, S., and CordeliÈRes, F.P. (2006). A guided tour into subcellular colocalization analysis in light microscopy. Journal of Microscopy *224*, 213-232.
Bornancin, F., and Parker, P.J. (1997). Phosphorylation of protein kinase C-alpha on serine 657 controls the accumulation of active enzyme and contributes to its phosphatase-resistant state. The Journal of biological chemistry *272*, 3544-3549.
Bostan, A.C., Dum, R.P., and Strick, P.L. (2010). The basal ganglia communicate with the cerebellum. Proceedings of the National Academy of Sciences of the United States of America *107*, 8452-8456.
Boukhtouche, F., Brugg, B., Wehrle, R., Bois-Joyeux, B., Danan, J.L., Dusart, I., and Mariani, J. (2010). Induction of early Purkinje cell dendritic differentiation by thyroid hormone requires RORalpha. Neural development *5*, 18.
Boukhtouche, F., Janmaat, S., Vodjdani, G., Gautheron, V., Mallet, J., Dusart, I., and Mariani, J. (2006). Retinoid-related orphan receptor alpha controls the early steps of Purkinje cell dendritic differentiation. The Journal of neuroscience : the official journal of the Society for Neuroscience *26*, 1531-1538.
Brinkman, E.K., Chen, T., Amendola, M., and van Steensel, B. (2014). Easy quantitative assessment of genome editing by sequence trace decomposition. Nucleic acids research *42*, e168-e168.
Brix, J., Zhou, Y., and Luo, Y. (2015). The Epigenetic Reprogramming Roadmap in Generation of iPSCs from Somatic Cells. Journal of genetics and genomics = Yi chuan xue bao *42*, 661-670.
Brkanac, Z., Bylenok, L., Fernandez, M., Matsushita, M., Lipe, H., Wolff, J., Nochlin, D., Raskind, W.H., and Bird, T.D. (2002). A new dominant spinocerebellar ataxia linked to chromosome 19q13.4-qter. Archives of neurology *59*, 1291-1295.
Brkanac, Z., Spencer, D., Shendure, J., Robertson, P.D., Matsushita, M., Vu, T., Bird, T.D., Olson, M.V., and Raskind, W.H. (2009). IFRD1 is a candidate gene for SMNA on chromosome 7q22-q23. American journal of human genetics *84*, 692-697.
Bubb, M.R., Lenox, R.H., and Edison, A.S. (1999). Phosphorylation-dependent conformational changes induce a switch in the actin-binding function of MARCKS. The Journal of biological chemistry *274*, 36472-36478.
Buganim, Y., Faddah, D.A., Cheng, A.W., Itskovich, E., Markoulaki, S., Ganz, K., Klemm, S.L., van Oudenaarden, A., and Jaenisch, R. (2012). Single-cell expression analyses during cellular reprogramming reveal an early stochastic and a late hierarchic phase. Cell *150*, 1209-1222.
Buisseret-Delmas, C., and Angaut, P. (1993). The cerebellar olivo-corticonuclear connections in the rat. Progress in neurobiology *40*, 63-87.
Bushart, D.D., Murphy, G.G., and Shakkottai, V.G. (2016). Precision medicine in spinocerebellar ataxias: treatment based on common mechanisms of disease. Ann Transl Med *4*, 25.

Button, R.W., Roberts, S.L., Willis, T.L., Hanemann, C.O., and Luo, S. (2017). Accumulation of autophagosomes confers cytotoxicity. Journal of Biological Chemistry.
Butts, T., Green, M.J., and Wingate, R.J. (2014). Development of the cerebellum: simple steps to make a 'little brain'. Development *141*, 4031-4041.
Byrne, S.M., Ortiz, L., Mali, P., Aach, J., and Church, G.M. (2015). Multi-kilobase homozygous targeted gene replacement in human induced pluripotent stem cells. Nucleic acids research *43*, e21.
Cadieux-Dion, M., Turcotte-Gauthier, M., Noreau, A., Martin, C., Meloche, C., Gravel, M., Drouin, C.A., Rouleau, G.A., Nguyen, D.K., and Cossette, P. (2014). Expanding the clinical phenotype associated with ELOVL4 mutation: study of a large French-Canadian family with autosomal dominant spinocerebellar ataxia and erythrokeratodermia. JAMA neurology *71*, 470-475.
Calabrese, V., Lodi, R., Tonon, C., D'Agata, V., Sapienza, M., Scapagnini, G., Mangiameli, A., Pennisi, G., Stella, A.M., and Butterfield, D.A. (2005). Oxidative stress, mitochondrial dysfunction and cellular stress response in Friedreich's ataxia. Journal of the neurological sciences *233*, 145-162.
Caligiore, D., Pezzulo, G., Baldassarre, G., Bostan, A.C., Strick, P.L., Doya, K., Helmich, R.C., Dirkx, M., Houk, J., Jörntell, H., *et al.* (2017). Consensus Paper: Towards a Systems-Level View of Cerebellar Function: the Interplay Between Cerebellum, Basal Ganglia, and Cortex. Cerebellum (London, England) *16*, 203-229.
Callender, Julia A., and Newton, Alexandra C. (2017). Conventional protein kinase C in the brain: 40 years later. Neuronal Signaling *1*.
Cameron, A.J., Linch, M.D., Saurin, A.T., Escribano, C., and Parker, P.J. (2011). mTORC2 targets AGC kinases through Sin1-dependent recruitment. The Biochemical journal *439*, 287-297.
Cantone, I., and Fisher, A.G. (2013). Epigenetic programming and reprogramming during development. Nat Struct Mol Biol *20*, 282-289.
Cardell, M., Landsend, A.S., Eidet, J., Wieloch, T., Blackstad, T.W., and Ottersen, O.P. (1997). High resolution immunogold analysis reveals distinct subcellular compartmentation of protein kinase Cγ and δ in rat Purkinje cells. Neuroscience *82*, 709-725.
Carlson, K.M., Andresen, J.M., and Orr, H.T. (2009). Emerging pathogenic pathways in the spinocerebellar ataxias. Current opinion in genetics & development *19*, 247-253.
Cerminara, N.L., Lang, E.J., Sillitoe, R.V., and Apps, R. (2015). Redefining the cerebellar cortex as an assembly of non-uniform Purkinje cell microcircuits. Nat Rev Neurosci *16*, 79-93.
Chai, Y., Wu, L., Griffin, J.D., and Paulson, H.L. (2001). The role of protein composition in specifying nuclear inclusion formation in polyglutamine disease. The Journal of biological chemistry *276*, 44889-44897.
Chambers, S.M., Fasano, C.A., Papapetrou, E.P., Tomishima, M., Sadelain, M., and Studer, L. (2009). Highly efficient neural conversion of human ES and iPS cells by dual inhibition of SMAD signaling. Nature biotechnology *27*, 275-280.
Chelban, V., Wiethoff, S., Fabian-Jessing, B.K., Haridy, N.A., Khan, A., Efthymiou, S., Becker, E.B.E., O'Connor, E., Hersheson, J., Newland, K., *et al.* (2018). Genotype-phenotype correlations, dystonia and disease progression in spinocerebellar ataxia type 14. Movement disorders : official journal of the Movement Disorder Society.
Chen, B., Gilbert, L.A., Cimini, B.A., Schnitzbauer, J., Zhang, W., Li, G.W., Park, J., Blackburn, E.H., Weissman, J.S., Qi, L.S., *et al.* (2013). Dynamic imaging of genomic loci in living human cells by an optimized CRISPR/Cas system. Cell *155*, 1479-1491.
Chen, C., Kano, M., Abeliovich, A., Chen, L., Bao, S., Kim, J.J., Hashimoto, K., Thompson, R.F., and Tonegawa, S. (1995). Impaired motor coordination correlates with persistent multiple climbing fiber innervation in PKC gamma mutant mice. Cell *83*, 1233-1242.
Chen, D.H., Brkanac, Z., Verlinde, C.L., Tan, X.J., Bylenok, L., Nochlin, D., Matsushita, M., Lipe, H., Wolff, J., Fernandez, M., *et al.* (2003). Missense mutations in the regulatory domain

of PKC gamma: a new mechanism for dominant nonepisodic cerebellar ataxia. American journal of human genetics *72*, 839-849.
Chen, D.H., Cimino, P.J., Ranum, L.P., Zoghbi, H.Y., Yabe, I., Schut, L., Margolis, R.L., Lipe, H.P., Feleke, A., Matsushita, M., *et al.* (2005). The clinical and genetic spectrum of spinocerebellar ataxia 14. Neurology *64*, 1258-1260.
Chen, D.H., Raskind, W.H., and Bird, T.D. (2012a). Spinocerebellar ataxia type 14. Handbook of clinical neurology *103*, 555-559.
Chen, X., Guo, C., and Kong, J. (2012b). Oxidative stress in neurodegenerative diseases. Neural Regeneration Research *7*, 376-385.
Chen, X., Tang, T.S., Tu, H., Nelson, O., Pook, M., Hammer, R., Nukina, N., and Bezprozvanny, I. (2008). Deranged calcium signaling and neurodegeneration in spinocerebellar ataxia type 3. The Journal of neuroscience : the official journal of the Society for Neuroscience *28*, 12713-12724.
Chen, Z.Z., Wang, C.M., Lee, G.C., Hsu, H.C., Wu, T.L., Lin, C.W., Ma, C.K., Lee-Chen, G.J., Huang, H.J., and Hsieh-Li, H.M. (2015). Trehalose attenuates the gait ataxia and gliosis of spinocerebellar ataxia type 17 mice. Neurochemical research *40*, 800-810.
Chi, C.L., Martinez, S., Wurst, W., and Martin, G.R. (2003). The isthmic organizer signal FGF8 is required for cell survival in the prospective midbrain and cerebellum. Development *130*, 2633-2644.
Chiang, H.L., Terlecky, S.R., Plant, C.P., and Dice, J.F. (1989). A role for a 70-kilodalton heat shock protein in lysosomal degradation of intracellular proteins. Science *246*, 382-385.
Chizhikov, V.V., Lindgren, A.G., Currle, D.S., Rose, M.F., Monuki, E.S., and Millen, K.J. (2006). The roof plate regulates cerebellar cell-type specification and proliferation. Development *133*, 2793-2804.
Chopra, R., Wasserman, A.H., Pulst, S.M., De Zeeuw, C.I., and Shakkottai, V.G. (2018). Protein kinase C activity is a protective modifier of Purkinje neuron degeneration in cerebellar ataxia. Human molecular genetics *27*, 1396-1410.
Chung, H.J., Steinberg, J.P., Huganir, R.L., and Linden, D.J. (2003). Requirement of AMPA receptor GluR2 phosphorylation for cerebellar long-term depression. Science *300*, 1751-1755.
Chung, H.J., Xia, J., Scannevin, R.H., Zhang, X., and Huganir, R.L. (2000). Phosphorylation of the AMPA receptor subunit GluR2 differentially regulates its interaction with PDZ domain-containing proteins. The Journal of neuroscience : the official journal of the Society for Neuroscience *20*, 7258-7267.
Chung, S.H., Marzban, H., Croci, L., Consalez, G.G., and Hawkes, R. (2008). Purkinje cell subtype specification in the cerebellar cortex: early B-cell factor 2 acts to repress the zebrin II-positive Purkinje cell phenotype. Neuroscience *153*, 721-732.
Ciechanover, A., and Kwon, Y.T. (2015). Degradation of misfolded proteins in neurodegenerative diseases: therapeutic targets and strategies. Experimental & molecular medicine *47*, e147.
Ciechanover, A., and Kwon, Y.T. (2017). Protein Quality Control by Molecular Chaperones in Neurodegeneration. Frontiers in neuroscience *11*, 185.
Cong, L., Ran, F.A., Cox, D., Lin, S., Barretto, R., Habib, N., Hsu, P.D., Wu, X., Jiang, W., Marraffini, L.A., *et al.* (2013). Multiplex genome engineering using CRISPR/Cas systems. Science *339*, 819-823.
Correia, S.S., Duarte, C.B., Faro, C.J., Pires, E.V., and Carvalho, A.L.s. (2003). Protein Kinase Cγ Associates Directly with the GluR4 α-Amino-3-hydroxy-5-methyl-4-isoxazole Propionate Receptor Subunit: EFFECT ON RECEPTOR PHOSPHORYLATION. Journal of Biological Chemistry *278*, 6307-6313.
Coutelier, M., Blesneac, I., Monteil, A., Monin, M.L., Ando, K., Mundwiller, E., Brusco, A., Le Ber, I., Anheim, M., Castrioto, A., *et al.* (2015). A Recurrent Mutation in CACNA1G Alters Cav3.1 T-Type Calcium-Channel Conduction and Causes Autosomal-Dominant Cerebellar Ataxia. American journal of human genetics *97*, 726-737.

Craig, N.J., Durán Alonso, M.B., Hawker, K.L., Shiels, P., Glencorse, T.A., Campbell, J.M., Bennett, N.K., Canham, M., Donald, D., Gardiner, M., *et al.* (2001). A candidate gene for human neurodegenerative disorders: a rat PKCγ mutation causes a Parkinsonian syndrome. Nature Neuroscience *4*, 1061.
Crepel, F. (1982). Regression of functional synapses in the immature mammalian cerebellum. Trends in Neurosciences *5*, 266-269.
Croci, L., Barili, V., Chia, D., Massimino, L., van Vugt, R., Masserdotti, G., Longhi, R., Rotwein, P., and Consalez, G.G. (2011). Local insulin-like growth factor I expression is essential for Purkinje neuron survival at birth. Cell death and differentiation *18*, 48-59.
Crossley, P.H., Minowada, G., MacArthur, C.A., and Martin, G.R. (1996). Roles for FGF8 in the induction, initiation, and maintenance of chick limb development. Cell *84*, 127-136.
Cumming, R.C., Andon, N.L., Haynes, P.A., Park, M., Fischer, W.H., and Schubert, D. (2004). Protein disulfide bond formation in the cytoplasm during oxidative stress. The Journal of biological chemistry *279*, 21749-21758.
Cummings, C.J., Sun, Y., Opal, P., Antalffy, B., Mestril, R., Orr, H.T., Dillmann, W.H., and Zoghbi, H.Y. (2001). Over-expression of inducible HSP70 chaperone suppresses neuropathology and improves motor function in SCA1 mice. Human molecular genetics *10*, 1511-1518.
Curnutte, J.T., Erickson, R.W., Ding, J., and Badwey, J.A. (1994). Reciprocal interactions between protein kinase C and components of the NADPH oxidase complex may regulate superoxide production by neutrophils stimulated with a phorbol ester. The Journal of biological chemistry *269*, 10813-10819.
D'Arcangelo, G., Miao, G.G., Chen, S.C., Soares, H.D., Morgan, J.I., and Curran, T. (1995). A protein related to extracellular matrix proteins deleted in the mouse mutant reeler. Nature *374*, 719-723.
D'Arcangelo, G., Nakajima, K., Miyata, T., Ogawa, M., Mikoshiba, K., and Curran, T. (1997). Reelin is a secreted glycoprotein recognized by the CR-50 monoclonal antibody. The Journal of neuroscience : the official journal of the Society for Neuroscience *17*, 23-31.
Dafinca, R., Scaber, J., Ababneh, N., Lalic, T., Weir, G., Christian, H., Vowles, J., Douglas, A.G., Fletcher-Jones, A., Browne, C., *et al.* (2016). C9orf72 Hexanucleotide Expansions Are Associated with Altered Endoplasmic Reticulum Calcium Homeostasis and Stress Granule Formation in Induced Pluripotent Stem Cell-Derived Neurons from Patients with Amyotrophic Lateral Sclerosis and Frontotemporal Dementia. Stem Cells *34*, 2063-2078.
Dalski, A., Mitulla, B., Burk, K., Schattenfroh, C., Schwinger, E., and Zuhlke, C. (2006). Mutation of the highly conserved cysteine residue 131 of the SCA14 associated PRKCG gene in a family with slow progressive cerebellar ataxia. Journal of neurology *253*, 1111-1112.
Danielian, P.S., and McMahon, A.P. (1996). Engrailed-1 as a target of the Wnt-1 signalling pathway in vertebrate midbrain development. Nature *383*, 332-334.
Dantuma, N.P., and Bott, L.C. (2014). The ubiquitin-proteasome system in neurodegenerative diseases: precipitating factor, yet part of the solution. Frontiers in molecular neuroscience *7*, 70.
David, G., Abbas, N., Stevanin, G., Durr, A., Yvert, G., Cancel, G., Weber, C., Imbert, G., Saudou, F., Antoniou, E., *et al.* (1997). Cloning of the SCA7 gene reveals a highly unstable CAG repeat expansion. Nat Genet *17*, 65-70.
De Zeeuw, C.I., Hansel, C., Bian, F., Koekkoek, S.K., van Alphen, A.M., Linden, D.J., and Oberdick, J. (1998). Expression of a protein kinase C inhibitor in Purkinje cells blocks cerebellar LTD and adaptation of the vestibulo-ocular reflex. Neuron *20*, 495-508.
Delplanque, J., Devos, D., Huin, V., Genet, A., Sand, O., Moreau, C., Goizet, C., Charles, P., Anheim, M., Monin, M.L., *et al.* (2014). TMEM240 mutations cause spinocerebellar ataxia 21 with mental retardation and severe cognitive impairment. Brain : a journal of neurology *137*, 2657-2663.

Depondt, C., Donatello, S., Rai, M., Wang, F.C., Manto, M., Simonis, N., and Pandolfo, M. (2016). MME mutation in dominant spinocerebellar ataxia with neuropathy (SCA43). Neurology Genetics *2*, e94.
Di Bella, D., Lazzaro, F., Brusco, A., Plumari, M., Battaglia, G., Pastore, A., Finardi, A., Cagnoli, C., Tempia, F., Frontali, M., *et al.* (2010). Mutations in the mitochondrial protease gene AFG3L2 cause dominant hereditary ataxia SCA28. Nat Genet *42*, 313-321.
Di Gregorio, E., Borroni, B., Giorgio, E., Lacerenza, D., Ferrero, M., Lo Buono, N., Ragusa, N., Mancini, C., Gaussen, M., Calcia, A., *et al.* (2014). ELOVL5 mutations cause spinocerebellar ataxia 38. American journal of human genetics *95*, 209-217.
Didonna, A., and Opal, P. (2016). Advances in Sequencing Technologies for Understanding Hereditary Ataxias: A Review. JAMA neurology *73*, 1485-1490.
Ding, Y.Q., Xiang, C.X., and Chen, Z.F. (2005). Generation and characterization of the PKC gamma-Cre mouse line. Genesis (New York, NY : 2000) *43*, 28-33.
Dong, H., O'Brien, R.J., Fung, E.T., Lanahan, A.A., Worley, P.F., and Huganir, R.L. (1997). GRIP: a synaptic PDZ domain-containing protein that interacts with AMPA receptors. Nature *386*, 279-284.
Doran, G., Davies, K.E., and Talbot, K. (2008). Activation of mutant protein kinase Cgamma leads to aberrant sequestration and impairment of its cellular function. Biochemical and biophysical research communications *372*, 447-453.
Doron, K.W., Funk, C.M., and Glickstein, M. (2010). Fronto-cerebellar circuits and eye movement control: A diffusion imaging tractography study of human cortico-pontine projections. Brain research *1307*, 63-71.
Doyle, J.P., Dougherty, J.D., Heiman, M., Schmidt, E.F., Stevens, T.R., Ma, G., Bupp, S., Shrestha, P., Shah, R.D., Doughty, M.L., *et al.* (2008). Application of a translational profiling approach for the comparative analysis of CNS cell types. Cell *135*, 749-762.
Dries, D.R., Gallegos, L.L., and Newton, A.C. (2007). A single residue in the C1 domain sensitizes novel protein kinase C isoforms to cellular diacylglycerol production. The Journal of biological chemistry *282*, 826-830.
Duarri, A., Jezierska, J., Fokkens, M., Meijer, M., Schelhaas, H.J., den Dunnen, W.F., van Dijk, F., Verschuuren-Bemelmans, C., Hageman, G., van de Vlies, P., *et al.* (2012). Mutations in potassium channel kcnd3 cause spinocerebellar ataxia type 19. Annals of neurology *72*, 870-880.
Dulneva, A., Lee, S., Oliver, P.L., Di Gleria, K., Kessler, B.M., Davies, K.E., and Becker, E.B. (2015). The mutant Moonwalker TRPC3 channel links calcium signaling to lipid metabolism in the developing cerebellum. Human molecular genetics.
Dutil, E.M., Keranen, L.M., DePaoli-Roach, A.A., and Newton, A.C. (1994). In vivo regulation of protein kinase C by trans-phosphorylation followed by autophosphorylation. The Journal of biological chemistry *269*, 29359-29362.
Dutta, D., Heo, I., and Clevers, H. (2017). Disease Modeling in Stem Cell-Derived 3D Organoid Systems. Trends in molecular medicine *23*, 393-410.
Eccles, J.C. (1973). The cerebellum as a computer: patterns in space and time. The Journal of physiology *229*, 1-32.
Eccles, J.C., Ito, M. and Szentágothai, J. (1967). The cerebellum as a neuronal machine (New York: Springer-Verlag).
Edwards, A.S., and Newton, A.C. (1997). Phosphorylation at conserved carboxyl-terminal hydrophobic motif regulates the catalytic and regulatory domains of protein kinase C. The Journal of biological chemistry *272*, 18382-18390.
Elkabetz, Y., Panagiotakos, G., Al Shamy, G., Socci, N.D., Tabar, V., and Studer, L. (2008). Human ES cell-derived neural rosettes reveal a functionally distinct early neural stem cell stage. Genes & development *22*, 152-165.
Englund, C., Kowalczyk, T., Daza, R.A., Dagan, A., Lau, C., Rose, M.F., and Hevner, R.F. (2006). Unipolar brush cells of the cerebellum are produced in the rhombic lip and migrate

through developing white matter. The Journal of neuroscience : the official journal of the Society for Neuroscience *26*, 9184-9195.
Erceg, S., Lukovic, D., Moreno-Manzano, V., Stojkovic, M., and Bhattacharya, S.S. (2012). Derivation of cerebellar neurons from human pluripotent stem cells. Current protocols in stem cell biology *Chapter 1*, Unit 1H.5.
Erceg, S., Ronaghi, M., Zipancic, I., Lainez, S., Rosello, M.G., Xiong, C., Moreno-Manzano, V., Rodriguez-Jimenez, F.J., Planells, R., Alvarez-Dolado, M., *et al.* (2010). Efficient differentiation of human embryonic stem cells into functional cerebellar-like cells. Stem cells and development *19*, 1745-1756.
Esvelt, K.M., Mali, P., Braff, J.L., Moosburner, M., Yaung, S.J., and Church, G.M. (2013). Orthogonal Cas9 proteins for RNA-guided gene regulation and editing. Nature methods *10*, 1116-1121.
Evans, J.H., Murray, D., Leslie, C.C., and Falke, J.J. (2006). Specific translocation of protein kinase Calpha to the plasma membrane requires both Ca2+ and PIP2 recognition by its C2 domain. Molecular biology of the cell *17*, 56-66.
Fahey, M.C., Knight, M.A., Shaw, J.H., Gardner, R.J., du Sart, D., Lockhart, P.J., Delatycki, M.B., Gates, P.C., and Storey, E. (2005). Spinocerebellar ataxia type 14: study of a family with an exon 5 mutation in the PRKCG gene. Journal of neurology, neurosurgery, and psychiatry *76*, 1720-1722.
Farah, C.A., Lindeman, A.A., Siu, V., Gupta, M.D., and Sossin, W.S. (2012). Autophosphorylation of the C2 domain inhibits translocation of the novel protein kinase C (nPKC) Apl II. Journal of Neurochemistry *123*, 360-372.
Farah, C.A., and Sossin, W.S. (2012). The role of C2 domains in PKC signaling. Advances in experimental medicine and biology *740*, 663-683.
Federico, A., Cardaioli, E., Da Pozzo, P., Formichi, P., Gallus, G.N., and Radi, E. (2012). Mitochondria, oxidative stress and neurodegeneration. Journal of the neurological sciences *322*, 254-262.
Fink, A.J., Englund, C., Daza, R.A., Pham, D., Lau, C., Nivison, M., Kowalczyk, T., and Hevner, R.F. (2006). Development of the deep cerebellar nuclei: transcription factors and cell migration from the rhombic lip. The Journal of neuroscience : the official journal of the Society for Neuroscience *26*, 3066-3076.
Fletcher, C.F., Tottene, A., Lennon, V.A., Wilson, S.M., Dubel, S.J., Paylor, R., Hosford, D.A., Tessarollo, L., McEnery, M.W., Pietrobon, D., *et al.* (2001). Dystonia and cerebellar atrophy in Cacna1a null mice lacking P/Q calcium channel activity. FASEB journal : official publication of the Federation of American Societies for Experimental Biology *15*, 1288-1290.
Florio, M., Leto, K., Muzio, L., Tinterri, A., Badaloni, A., Croci, L., Zordan, P., Barili, V., Albieri, I., Guillemot, F., *et al.* (2012). Neurogenin 2 regulates progenitor cell-cycle progression and Purkinje cell dendritogenesis in cerebellar development. Development *139*, 2308-2320.
Fogel, B.L., Hanson, S.M., and Becker, E.B. (2015). Do mutations in the murine ataxia gene TRPC3 cause cerebellar ataxia in humans? Movement disorders : official journal of the Movement Disorder Society *30*, 284-286.
Fu, Y., Foden, J.A., Khayter, C., Maeder, M.L., Reyon, D., Joung, J.K., and Sander, J.D. (2013). High-frequency off-target mutagenesis induced by CRISPR-Cas nucleases in human cells. Nature biotechnology *31*, 822-826.
Fujigasaki, H., Martin, J.J., De Deyn, P.P., Camuzat, A., Deffond, D., Stevanin, G., Dermaut, B., Van Broeckhoven, C., Durr, A., and Brice, A. (2001). CAG repeat expansion in the TATA box-binding protein gene causes autosomal dominant cerebellar ataxia. Brain : a journal of neurology *124*, 1939-1947.
Fujishima, K., Horie, R., Mochizuki, A., and Kengaku, M. (2012). Principles of branch dynamics governing shape characteristics of cerebellar Purkinje cell dendrites. Development *139*, 3442-3455.

Gallegos, L.L., and Newton, A.C. (2008). Spatiotemporal dynamics of lipid signaling: protein kinase C as a paradigm. IUBMB Life *60*, 782-789.
Ganos, C., Zittel, S., Minnerop, M., Schunke, O., Heinbokel, C., Gerloff, C., Zuhlke, C., Bauer, P., Klockgether, T., Munchau, A., *et al.* (2014). Clinical and neurophysiological profile of four German families with spinocerebellar ataxia type 14. Cerebellum *13*, 89-96.
Gao, L., Cox, D.B.T., Yan, W.X., Manteiga, J.C., Schneider, M.W., Yamano, T., Nishimasu, H., Nureki, O., Crosetto, N., and Zhang, F. (2017). Engineered Cpf1 variants with altered PAM specificities. Nature biotechnology *35*, 789-792.
Gao, T., Brognard, J., and Newton, A.C. (2008). The phosphatase PHLPP controls the cellular levels of protein kinase C. The Journal of biological chemistry *283*, 6300-6311.
Gao, T., and Newton, A.C. (2006). Invariant Leu preceding turn motif phosphorylation site controls the interaction of protein kinase C with Hsp70. The Journal of biological chemistry *281*, 32461-32468.
Gao, T., Toker, A., and Newton, A.C. (2001). The carboxyl terminus of protein kinase c provides a switch to regulate its interaction with the phosphoinositide-dependent kinase, PDK-1. The Journal of biological chemistry *276*, 19588-19596.
Garda, A.L., Echevarria, D., and Martinez, S. (2001). Neuroepithelial co-expression of Gbx2 and Otx2 precedes Fgf8 expression in the isthmic organizer. Mech Dev *101*, 111-118.
Gasiunas, G., Barrangou, R., Horvath, P., and Siksnys, V. (2012). Cas9-crRNA ribonucleoprotein complex mediates specific DNA cleavage for adaptive immunity in bacteria. Proceedings of the National Academy of Sciences of the United States of America *109*, E2579-2586.
Gaudelli, N.M., Komor, A.C., Rees, H.A., Packer, M.S., Badran, A.H., Bryson, D.I., and Liu, D.R. (2017). Programmable base editing of A•T to G•C in genomic DNA without DNA cleavage. Nature.
Gerrow, K., and Triller, A. (2010). Synaptic stability and plasticity in a floating world. Current opinion in neurobiology *20*, 631-639.
Glabe, C.G., and Kayed, R. (2006). Common structure and toxic function of amyloid oligomers implies a common mechanism of pathogenesis. Neurology *66*, S74-78.
Goffinet, A.M. (1983). The embryonic development of the cerebellum in normal and reeler mutant mice. Anatomy and embryology *168*, 73-86.
Goldowitz, D., and Hamre, K. (1998). The cells and molecules that make a cerebellum. Trends Neurosci *21*, 375-382.
Golipour, A., David, L., Liu, Y., Jayakumaran, G., Hirsch, C.L., Trcka, D., and Wrana, J.L. (2012). A late transition in somatic cell reprogramming requires regulators distinct from the pluripotency network. Cell stem cell *11*, 769-782.
Gonzalez, F., Zhu, Z., Shi, Z.D., Lelli, K., Verma, N., Li, Q.V., and Huangfu, D. (2014). An iCRISPR platform for rapid, multiplexable, and inducible genome editing in human pluripotent stem cells. Cell stem cell *15*, 215-226.
Goossens, J., Daniel, H., Rancillac, A., van der Steen, J., Oberdick, J., Crepel, F., De Zeeuw, C.I., and Frens, M.A. (2001). Expression of protein kinase C inhibitor blocks cerebellar long-term depression without affecting Purkinje cell excitability in alert mice. The Journal of neuroscience : the official journal of the Society for Neuroscience *21*, 5813-5823.
Gore, A., Li, Z., Fung, H.L., Young, J.E., Agarwal, S., Antosiewicz-Bourget, J., Canto, I., Giorgetti, A., Israel, M.A., Kiskinis, E., *et al.* (2011). Somatic coding mutations in human induced pluripotent stem cells. Nature *471*, 63-67.
Greco, G.E., Matsumoto, Y., Brooks, R.C., Lu, Z., Lieber, M.R., and Tomkinson, A.E. (2016). SCR7 is neither a selective nor a potent inhibitor of human DNA ligase IV. DNA repair *43*, 18-23.
Grodsky, N., Li, Y., Bouzida, D., Love, R., Jensen, J., Nodes, B., Nonomiya, J., and Grant, S. (2006). Structure of the catalytic domain of human protein kinase C beta II complexed with a bisindolylmaleimide inhibitor. Biochemistry *45*, 13970-13981.

Gundlfinger, A., Kapfhammer, J.P., Kruse, F., Leitges, M., and Metzger, F. (2003). Different regulation of Purkinje cell dendritic development in cerebellar slice cultures by protein kinase Calpha and -beta. J Neurobiol *57*, 95-109.
Haass, C., and Selkoe, D.J. (2007). Soluble protein oligomers in neurodegeneration: lessons from the Alzheimer's amyloid beta-peptide. Nature reviews Molecular cell biology *8*, 101-112.
Hamilton, B.A., Frankel, W.N., Kerrebrock, A.W., Hawkins, T.L., FitzHugh, W., Kusumi, K., Russell, L.B., Mueller, K.L., van Berkel, V., Birren, B.W., *et al.* (1996). Disruption of the nuclear hormone receptor RORalpha in staggerer mice. Nature *379*, 736-739.
Hanley, J.G. (2008). PICK1: a multi-talented modulator of AMPA receptor trafficking. Pharmacology & therapeutics *118*, 152-160.
Hansel, C., de Jeu, M., Belmeguenai, A., Houtman, S.H., Buitendijk, G.H., Andreev, D., De Zeeuw, C.I., and Elgersma, Y. (2006). alphaCaMKII Is essential for cerebellar LTD and motor learning. Neuron *51*, 835-843.
Hansra, G., Bornancin, F., Whelan, R., Hemmings, B.A., and Parker, P.J. (1996). 12-O-Tetradecanoylphorbol-13-acetate-induced dephosphorylation of protein kinase Calpha correlates with the presence of a membrane-associated protein phosphatase 2A heterotrimer. The Journal of biological chemistry *271*, 32785-32788.
Hansra, G., Garcia-Paramio, P., Prevostel, C., Whelan, R.D., Bornancin, F., and Parker, P.J. (1999). Multisite dephosphorylation and desensitization of conventional protein kinase C isotypes. The Biochemical journal *342 (Pt 2)*, 337-344.
Hartmann, J., Dragicevic, E., Adelsberger, H., Henning, H.A., Sumser, M., Abramowitz, J., Blum, R., Dietrich, A., Freichel, M., Flockerzi, V., *et al.* (2008). TRPC3 channels are required for synaptic transmission and motor coordination. Neuron *59*, 392-398.
Hartwig, J.H., Thelen, M., Rosen, A., Janmey, P.A., Nairn, A.C., and Aderem, A. (1992). MARCKS is an actin filament crosslinking protein regulated by protein kinase C and calcium-calmodulin. Nature *356*, 618-622.
Hashimoto, K., Ichikawa, R., Kitamura, K., Watanabe, M., and Kano, M. (2009). Translocation of a "winner" climbing fiber to the Purkinje cell dendrite and subsequent elimination of "losers" from the soma in developing cerebellum. Neuron *63*, 106-118.
Hashimoto, K., Watanabe, M., Kurihara, H., Offermanns, S., Jiang, H., Wu, Y., Jun, K., Shin, H.S., Inoue, Y., Wu, D., *et al.* (2000). Climbing fiber synapse elimination during postnatal cerebellar development requires signal transduction involving G alpha q and phospholipase C beta 4. Progress in brain research *124*, 31-48.
Hashimoto, M., and Mikoshiba, K. (2003). Mediolateral compartmentalization of the cerebellum is determined on the "birth date" of Purkinje cells. The Journal of neuroscience : the official journal of the Society for Neuroscience *23*, 11342-11351.
Hashimoto, T., Ase, K., Sawamura, S., Kikkawa, U., Saito, N., Tanaka, C., and Nishizuka, Y. (1988). Postnatal development of a brain-specific subspecies of protein kinase C in rat. The Journal of neuroscience : the official journal of the Society for Neuroscience *8*, 1678-1683.
Hatsukano, T., Kurisu, J., Fukumitsu, K., Fujishima, K., and Kengaku, M. (2017). Thyroid Hormone Induces PGC-1alpha during Dendritic Outgrowth in Mouse Cerebellar Purkinje Cells. Front Cell Neurosci *11*, 133.
Heigwer, F., Kerr, G., and Boutros, M. (2014). E-CRISP: fast CRISPR target site identification. Nature methods *11*, 122-123.
Hekman, K.E., Yu, G.Y., Brown, C.D., Zhu, H., Du, X., Gervin, K., Undlien, D.E., Peterson, A., Stevanin, G., Clark, H.B., *et al.* (2012). A conserved eEF2 coding variant in SCA26 leads to loss of translational fidelity and increased susceptibility to proteostatic insult. Human molecular genetics *21*, 5472-5483.
Hendel, A., Fine, E.J., Bao, G., and Porteus, M.H. (2015). Quantifying on- and off-target genome editing. Trends in biotechnology *33*, 132-140.
Herculano-Houzel, S. (2009). The human brain in numbers: a linearly scaled-up primate brain. Frontiers in human neuroscience *3*, 31.

Hess, G.T., Tycko, J., Yao, D., and Bassik, M.C. (2017). Methods and Applications of CRISPR-Mediated Base Editing in Eukaryotic Genomes. Molecular cell *68*, 26-43.
Heuer, H., and Mason, C.A. (2003). Thyroid hormone induces cerebellar Purkinje cell dendritic development via the thyroid hormone receptor alpha1. The Journal of neuroscience : the official journal of the Society for Neuroscience *23*, 10604-10612.
Hidalgo-Sanchez, M., Millet, S., Simeone, A., and Alvarado-Mallart, R.M. (1999). Comparative analysis of Otx2, Gbx2, Pax2, Fgf8 and Wnt1 gene expressions during the formation of the chick midbrain/hindbrain domain. Mech Dev *81*, 175-178.
Hiesberger, T., Trommsdorff, M., Howell, B.W., Goffinet, A., Mumby, M.C., Cooper, J.A., and Herz, J. (1999). Direct binding of Reelin to VLDL receptor and ApoE receptor 2 induces tyrosine phosphorylation of disabled-1 and modulates tau phosphorylation. Neuron *24*, 481-489.
Hirai, H. (2001). Modification of AMPA receptor clustering regulates cerebellar synaptic plasticity. Neuroscience research *39*, 261-267.
Hirai, H. (2017). Protein Kinase C in the Cerebellum: Its Significance and Remaining Conundrums. Cerebellum.
Hirai, H., and Launey, T. (2000). The regulatory connection between the activity of granule cell NMDA receptors and dendritic differentiation of cerebellar Purkinje cells. The Journal of neuroscience : the official journal of the Society for Neuroscience *20*, 5217-5224.
Hiramoto, K., Kawakami, H., Inoue, K., Seki, T., Maruyama, H., Morino, H., Matsumoto, M., Kurisu, K., and Sakai, N. (2006). Identification of a new family of spinocerebellar ataxia type 14 in the japanese spinocerebellar ataxia population by the screening of PRKCG exon 4. Movement Disorders *21*, 1355-1360.
Hirano, A., and Dembitzer, H.M. (1973). Cerebellar alterations in the weaver mouse. The Journal of cell biology *56*, 478-486.
Hirono, M., Sugiyama, T., Kishimoto, Y., Sakai, I., Miyazawa, T., Kishio, M., Inoue, H., Nakao, K., Ikeda, M., Kawahara, S., *et al.* (2001). Phospholipase Cbeta4 and protein kinase Calpha and/or protein kinase CbetaI are involved in the induction of long term depression in cerebellar Purkinje cells. The Journal of biological chemistry *276*, 45236-45242.
Holmes, D.B., and Heine, V.M. (2017). Streamlined 3D Cerebellar Differentiation Protocol with Optional 2D Modification. J Vis Exp.
Holmes, S.E., O'Hearn, E.E., McInnis, M.G., Gorelick-Feldman, D.A., Kleiderlein, J.J., Callahan, C., Kwak, N.G., Ingersoll-Ashworth, R.G., Sherr, M., Sumner, A.J., *et al.* (1999). Expansion of a novel CAG trinucleotide repeat in the 5' region of PPP2R2B is associated with SCA12. Nat Genet *23*, 391-392.
Hoshi, E., Tremblay, L., Feger, J., Carras, P.L., and Strick, P.L. (2005). The cerebellum communicates with the basal ganglia. Nat Neurosci *8*, 1491-1493.
Hoshino, M. (2012). Neuronal subtype specification in the cerebellum and dorsal hindbrain. Development, growth & differentiation *54*, 317-326.
Hoshino, M., Nakamura, S., Mori, K., Kawauchi, T., Terao, M., Nishimura, Y.V., Fukuda, A., Fuse, T., Matsuo, N., Sone, M., *et al.* (2005). Ptf1a, a bHLH transcriptional gene, defines GABAergic neuronal fates in cerebellum. Neuron *47*, 201-213.
Hou, P., Li, Y., Zhang, X., Liu, C., Guan, J., Li, H., Zhao, T., Ye, J., Yang, W., Liu, K., *et al.* (2013a). Pluripotent stem cells induced from mouse somatic cells by small-molecule compounds. Science *341*, 651-654.
Hou, Z., Zhang, Y., Propson, N.E., Howden, S.E., Chu, L.F., Sontheimer, E.J., and Thomson, J.A. (2013b). Efficient genome engineering in human pluripotent stem cells using Cas9 from Neisseria meningitidis. Proceedings of the National Academy of Sciences of the United States of America *110*, 15644-15649.
Houlden, H., Johnson, J., Gardner-Thorpe, C., Lashley, T., Hernandez, D., Worth, P., Singleton, A.B., Hilton, D.A., Holton, J., Revesz, T., *et al.* (2007). Mutations in TTBK2, encoding a kinase implicated in tau phosphorylation, segregate with spinocerebellar ataxia type 11. Nat Genet *39*, 1434-1436.

House, C., and Kemp, B.E. (1990). Protein kinase C pseudosubstrate prototope: structure-function relationships. Cellular signalling *2*, 187-190.
Hsu, P.D., Lander, E.S., and Zhang, F. (2014). Development and applications of CRISPR-Cas9 for genome engineering. Cell *157*, 1262-1278.
Hu, G.Y., Hvalby, O., Walaas, S.I., Albert, K.A., Skjeflo, P., Andersen, P., and Greengard, P. (1987). Protein kinase C injection into hippocampal pyramidal cells elicits features of long term potentiation. Nature *328*, 426-429.
Hu, Y.-B., Dammer, E.B., Ren, R.-J., and Wang, G. (2015). The endosomal-lysosomal system: from acidification and cargo sorting to neurodegeneration. Translational Neurodegeneration *4*, 18.
Huang, F.L., Yoshida, Y., Cunha-Melo, J.R., Beaven, M.A., and Huang, K.P. (1989). Differential down-regulation of protein kinase C isozymes. The Journal of biological chemistry *264*, 4238-4243.
Huang, F.L., Yoshida, Y., Nakabayashi, H., Young, W.S., 3rd, and Huang, K.P. (1988). Immunocytochemical localization of protein kinase C isozymes in rat brain. The Journal of neuroscience : the official journal of the Society for Neuroscience *8*, 4734-4744.
Huang, K.-P. (1989). The mechanism of protein kinase C activation. Trends in Neurosciences *12*, 425-432.
Huang, L., Chardon, J.W., Carter, M.T., Friend, K.L., Dudding, T.E., Schwartzentruber, J., Zou, R., Schofield, P.W., Douglas, S., Bulman, D.E., *et al.* (2012). Missense mutations in ITPR1 cause autosomal dominant congenital nonprogressive spinocerebellar ataxia. Orphanet journal of rare diseases *7*, 67.
Huang, M., and Verbeek, D.S. (2018). Why do so many genetic insults lead to Purkinje Cell degeneration and spinocerebellar ataxia? Neuroscience letters.
Huang, X., Liu, J., Ketova, T., Fleming, J.T., Grover, V.K., Cooper, M.K., Litingtung, Y., and Chiang, C. (2010). Transventricular delivery of Sonic hedgehog is essential to cerebellar ventricular zone development. Proceedings of the National Academy of Sciences of the United States of America *107*, 8422-8427.
Hussain, R.J., Stumpo, D.J., Blackshear, P.J., Lenox, R.H., Abel, T., and McNamara, R.K. (2006). Myristoylated alanine rich C kinase substrate (MARCKS) heterozygous mutant mice exhibit deficits in hippocampal mossy fiber-CA3 long-term potentiation. Hippocampus *16*, 495-503.
Hussein, S.M., Batada, N.N., Vuoristo, S., Ching, R.W., Autio, R., Narva, E., Ng, S., Sourour, M., Hamalainen, R., Olsson, C., *et al.* (2011). Copy number variation and selection during reprogramming to pluripotency. Nature *471*, 58-62.
Ichise, T., Kano, M., Hashimoto, K., Yanagihara, D., Nakao, K., Shigemoto, R., Katsuki, M., and Aiba, A. (2000). mGluR1 in cerebellar Purkinje cells essential for long-term depression, synapse elimination, and motor coordination. Science *288*, 1832-1835.
Ikeda, Y., Dick, K.A., Weatherspoon, M.R., Gincel, D., Armbrust, K.R., Dalton, J.C., Stevanin, G., Durr, A., Zuhlke, C., Burk, K., *et al.* (2006). Spectrin mutations cause spinocerebellar ataxia type 5. Nat Genet *38*, 184-190.
Ikenoue, T., Inoki, K., Yang, Q., Zhou, X., and Guan, K.L. (2008). Essential function of TORC2 in PKC and Akt turn motif phosphorylation, maturation and signalling. The EMBO journal *27*, 1919-1931.
Ingram, M., Wozniak, E.A.L., Duvick, L., Yang, R., Bergmann, P., Carson, R., O'Callaghan, B., Zoghbi, H.Y., Henzler, C., and Orr, H.T. (2016). Cerebellar Transcriptome Profiles of ATXN1 Transgenic Mice Reveal SCA1 Disease Progression and Protection Pathways. Neuron *89*, 1194-1207.
Irving, C., and Mason, I. (2000). Signalling by FGF8 from the isthmus patterns anterior hindbrain and establishes the anterior limit of Hox gene expression. Development *127*, 177-186.

Ishida, Y., Kawakami, H., Kitajima, H., Nishiyama, A., Sasai, Y., Inoue, H., and Muguruma, K. (2016). Vulnerability of Purkinje Cells Generated from Spinocerebellar Ataxia Type 6 Patient-Derived iPSCs. Cell reports *17*, 1482-1490.
Ishikawa, K., Fujigasaki, H., Saegusa, H., Ohwada, K., Fujita, T., Iwamoto, H., Komatsuzaki, Y., Toru, S., Toriyama, H., Watanabe, M., *et al.* (1999). Abundant expression and cytoplasmic aggregations of [alpha]1A voltage-dependent calcium channel protein associated with neurodegeneration in spinocerebellar ataxia type 6. Human molecular genetics *8*, 1185-1193.
Ishikawa, K., Owada, K., Ishida, K., Fujigasaki, H., Shun Li, M., Tsunemi, T., Ohkoshi, N., Toru, S., Mizutani, T., Hayashi, M., *et al.* (2001). Cytoplasmic and nuclear polyglutamine aggregates in SCA6 Purkinje cells. Neurology *56*, 1753-1756.
Ito, M. (2001). Cerebellar long-term depression: characterization, signal transduction, and functional roles. Physiological reviews *81*, 1143-1195.
Iwaki, A., Kawano, Y., Miura, S., Shibata, H., Matsuse, D., Li, W., Furuya, H., Ohyagi, Y., Taniwaki, T., Kira, J., *et al.* (2008). Heterozygous deletion of ITPR1, but not SUMF1, in spinocerebellar ataxia type 16. Journal of medical genetics *45*, 32-35.
Jellinger, K.A. (2001). Cell death mechanisms in neurodegeneration. Journal of cellular and molecular medicine *5*, 1-17.
Jezierska, J., Goedhart, J., Kampinga, H.H., Reits, E.A., and Verbeek, D.S. (2014). SCA14 mutation V138E leads to partly unfolded PKCγ associated with an exposed C-terminus, altered kinetics, phosphorylation and enhanced insolubilization. Journal of Neurochemistry *128*, 741-751.
Ji, J., Hassler, M.L., Shimobayashi, E., Paka, N., Streit, R., and Kapfhammer, J.P. (2014). Increased protein kinase C gamma activity induces Purkinje cell pathology in a mouse model of spinocerebellar ataxia 14. Neurobiology of disease *70*, 1-11.
Jiang, H., Cheng, D., Liu, W., Peng, J., and Feng, J. (2010). Protein kinase C inhibits autophagy and phosphorylates LC3. Biochemical and biophysical research communications *395*, 471-476.
Jiang, T., Tan, M.-S., Tan, L., and Yu, J.-T. (2014). Application of next-generation sequencing technologies in Neurology. Annals of Translational Medicine *2*, 125.
Jiang, W., Bikard, D., Cox, D., Zhang, F., and Marraffini, L.A. (2013). RNA-guided editing of bacterial genomes using CRISPR-Cas systems. Nature biotechnology *31*, 233-239.
Jinek, M., East, A., Cheng, A., Lin, S., Ma, E., and Doudna, J. (2013). RNA-programmed genome editing in human cells. eLife *2*, e00471.
Johnson, J.E., Giorgione, J., and Newton, A.C. (2000). The C1 and C2 domains of protein kinase C are independent membrane targeting modules, with specificity for phosphatidylserine conferred by the C1 domain. Biochemistry *39*, 11360-11369.
Joyner, A.L. (1996). Engrailed, Wnt and Pax genes regulate midbrain--hindbrain development. Trends in genetics : TIG *12*, 15-20.
Jun, K., Piedras-Renteria, E.S., Smith, S.M., Wheeler, D.B., Lee, S.B., Lee, T.G., Chin, H., Adams, M.E., Scheller, R.H., Tsien, R.W., *et al.* (1999). Ablation of P/Q-type Ca(2+) channel currents, altered synaptic transmission, and progressive ataxia in mice lacking the alpha(1A)-subunit. Proceedings of the National Academy of Sciences of the United States of America *96*, 15245-15250.
Kabayama, H., Nakamura, T., Takeuchi, M., Iwasaki, H., Taniguchi, M., Tokushige, N., and Mikoshiba, K. (2009). Ca2+ induces macropinocytosis via F-actin depolymerization during growth cone collapse. Molecular and cellular neurosciences *40*, 27-38.
Kannan, N., Haste, N., Taylor, S.S., and Neuwald, A.F. (2007). The hallmark of AGC kinase functional divergence is its C-terminal tail, a cis-acting regulatory module. Proceedings of the National Academy of Sciences of the United States of America *104*, 1272-1277.
Kano, M., Hashimoto, K., Chen, C., Abeliovich, A., Aiba, A., Kurihara, H., Watanabe, M., Inoue, Y., and Tonegawa, S. (1995). Impaired synapse elimination during cerebellar development in PKC gamma mutant mice. Cell *83*, 1223-1231.

Kano, M., Hashimoto, K., Kurihara, H., Watanabe, M., Inoue, Y., Aiba, A., and Tonegawa, S. (1997). Persistent multiple climbing fiber innervation of cerebellar Purkinje cells in mice lacking mGluR1. Neuron *18*, 71-79.
Kano, M., Hashimoto, K., and Tabata, T. (2008). Type-1 metabotropic glutamate receptor in cerebellar Purkinje cells: a key molecule responsible for long-term depression, endocannabinoid signalling and synapse elimination. Philosophical Transactions of the Royal Society B: Biological Sciences *363*, 2173-2186.
Kano, M., Hashimoto, K., Watanabe, M., Kurihara, H., Offermanns, S., Jiang, H., Wu, Y., Jun, K., Shin, H.S., Inoue, Y., *et al.* (1998). Phospholipase cbeta4 is specifically involved in climbing fiber synapse elimination in the developing cerebellum. Proceedings of the National Academy of Sciences of the United States of America *95*, 15724-15729.
Kapfhammer, J.P. (2004). Cellular and molecular control of dendritic growth and development of cerebellar Purkinje cells. Progress in histochemistry and cytochemistry *39*, 131-182.
Karam, S.D., Burrows, R.C., Logan, C., Koblar, S., Pasquale, E.B., and Bothwell, M. (2000). Eph receptors and ephrins in the developing chick cerebellum: relationship to sagittal patterning and granule cell migration. The Journal of neuroscience : the official journal of the Society for Neuroscience *20*, 6488-6500.
Karzbrun, E., Kshirsagar, A., Cohen, S.R., Hanna, J.H., and Reiner, O. (2018). Human brain organoids on a chip reveal the physics of folding. Nature Physics.
Kashiwabuchi, N., Ikeda, K., Araki, K., Hirano, T., Shibuki, K., Takayama, C., Inoue, Y., Kutsuwada, T., Yagi, T., Kang, Y., *et al.* (1995). Impairment of motor coordination, Purkinje cell synapse formation, and cerebellar long-term depression in GluR delta 2 mutant mice. Cell *81*, 245-252.
Kasumu, A., and Bezprozvanny, I. (2012). Deranged calcium signaling in Purkinje cells and pathogenesis in spinocerebellar ataxia 2 (SCA2) and other ataxias. Cerebellum *11*, 630-639.
Kawaguchi, S.Y., and Hirano, T. (2013). Gating of long-term depression by Ca2+/calmodulin-dependent protein kinase II through enhanced cGMP signalling in cerebellar Purkinje cells. The Journal of physiology *591*, 1707-1730.
Kawaguchi, Y., Okamoto, T., Taniwaki, M., Aizawa, M., Inoue, M., Katayama, S., Kawakami, H., Nakamura, S., Nishimura, M., Akiguchi, I., *et al.* (1994). CAG expansions in a novel gene for Machado-Joseph disease at chromosome 14q32.1. Nat Genet *8*, 221-228.
Kazanietz, M.G., Wang, S., Milne, G.W.A., Lewin, N.E., Liu, H.L., and Blumberg, P.M. (1995). Residues in the Second Cysteine-rich Region of Protein Kinase C δ Relevant to Phorbol Ester Binding as Revealed by Site-directed Mutagenesis. Journal of Biological Chemistry *270*, 21852-21859.
Kazi, J.U. (2011). The mechanism of protein kinase C regulation. Frontiers in Biology *6*, 328.
Kelava, I., and Lancaster, M.A. (2016). Dishing out mini-brains: Current progress and future prospects in brain organoid research. Dev Biol *420*, 199-209.
Kessels, H.W., and Malinow, R. (2009). Synaptic AMPA receptor plasticity and behavior. Neuron *61*, 340-350.
Kikkawa, U., Takai, Y., Tanaka, Y., Miyake, R., and Nishizuka, Y. (1983). Protein kinase C as a possible receptor protein of tumor-promoting phorbol esters. The Journal of biological chemistry *258*, 11442-11445.
Kim, C.H., Braud, S., Isaac, J.T., and Roche, K.W. (2005). Protein kinase C phosphorylation of the metabotropic glutamate receptor mGluR5 on Serine 839 regulates Ca2+ oscillations. The Journal of biological chemistry *280*, 25409-25415.
Kim, C.H., Chung, H.J., Lee, H.K., and Huganir, R.L. (2001). Interaction of the AMPA receptor subunit GluR2/3 with PDZ domains regulates hippocampal long-term depression. Proceedings of the National Academy of Sciences of the United States of America *98*, 11725-11730.
Kim, G.H., Kim, J.E., Rhie, S.J., and Yoon, S. (2015). The Role of Oxidative Stress in Neurodegenerative Diseases. Experimental neurobiology *24*, 325-340.

Kinoshita-Kikuta, E., Aoki, Y., Kinoshita, E., and Koike, T. (2007). Label-free kinase profiling using phosphate affinity polyacrylamide gel electrophoresis. Molecular & cellular proteomics : MCP *6*, 356-366.
Kinoshita, E., Kinoshita-Kikuta, E., Takiyama, K., and Koike, T. (2006). Phosphate-binding tag, a new tool to visualize phosphorylated proteins. Molecular & cellular proteomics : MCP *5*, 749-757.
Klebe, S., Durr, A., Rentschler, A., Hahn-Barma, V., Abele, M., Bouslam, N., Schols, L., Jedynak, P., Forlani, S., Denis, E., *et al.* (2005). New mutations in protein kinase Cgamma associated with spinocerebellar ataxia type 14. Annals of neurology *58*, 720-729.
Kleinstiver, B.P., Pattanayak, V., Prew, M.S., Tsai, S.Q., Nguyen, N.T., Zheng, Z., and Joung, J.K. (2016). High-fidelity CRISPR–Cas9 nucleases with no detectable genome-wide off-target effects. Nature *529*, 490-495.
Kleinstiver, B.P., Prew, M.S., Tsai, S.Q., Topkar, V.V., Nguyen, N.T., Zheng, Z., Gonzales, A.P., Li, Z., Peterson, R.T., Yeh, J.R., *et al.* (2015). Engineered CRISPR-Cas9 nucleases with altered PAM specificities. Nature *523*, 481-485.
Klement, I.A., Skinner, P.J., Kaytor, M.D., Yi, H., Hersch, S.M., Clark, H.B., Zoghbi, H.Y., and Orr, H.T. (1998). Ataxin-1 nuclear localization and aggregation: role in polyglutamine-induced disease in SCA1 transgenic mice. Cell *95*, 41-53.
Knight, M.A., Hernandez, D., Diede, S.J., Dauwerse, H.G., Rafferty, I., van de Leemput, J., Forrest, S.M., Gardner, R.J., Storey, E., van Ommen, G.J., *et al.* (2008). A duplication at chromosome 11q12.2-11q12.3 is associated with spinocerebellar ataxia type 20. Human molecular genetics *17*, 3847-3853.
Kobayashi, H., Abe, K., Matsuura, T., Ikeda, Y., Hitomi, T., Akechi, Y., Habu, T., Liu, W., Okuda, H., and Koizumi, A. (2011). Expansion of intronic GGCCTG hexanucleotide repeat in NOP56 causes SCA36, a type of spinocerebellar ataxia accompanied by motor neuron involvement. American journal of human genetics *89*, 121-130.
Koekkoek, S.K., Hulscher, H.C., Dortland, B.R., Hensbroek, R.A., Elgersma, Y., Ruigrok, T.J., and De Zeeuw, C.I. (2003). Cerebellar LTD and learning-dependent timing of conditioned eyelid responses. Science *301*, 1736-1739.
Koeppen, A.H. (2005). The pathogenesis of spinocerebellar ataxia. Cerebellum *4*, 62-73.
Kohout, S.C., Corbalan-Garcia, S., Torrecillas, A., Gomez-Fernandez, J.C., and Falke, J.J. (2002). C2 domains of protein kinase C isoforms alpha, beta, and gamma: activation parameters and calcium stoichiometries of the membrane-bound state. Biochemistry *41*, 11411-11424.
Koht, J., Stevanin, G., Durr, A., Mundwiller, E., Brice, A., and Tallaksen, C.M. (2012). SCA14 in Norway, two families with autosomal dominant cerebellar ataxia and a novel mutation in the PRKCG gene. Acta neurologica Scandinavica *125*, 116-122.
Kolpak, A.L., Jiang, J., Guo, D., Standley, C., Bellve, K., Fogarty, K., and Bao, Z.Z. (2009). Negative guidance factor-induced macropinocytosis in the growth cone plays a critical role in repulsive axon turning. The Journal of neuroscience : the official journal of the Society for Neuroscience *29*, 10488-10498.
Komor, A.C., Kim, Y.B., Packer, M.S., Zuris, J.A., and Liu, D.R. (2016). Programmable editing of a target base in genomic DNA without double-stranded DNA cleavage. Nature *533*, 420-424.
Konig, B., DiNitto, P.A., and Blumberg, P.M. (1985). Stoichiometric binding of diacylglycerol to the phorbol ester receptor. Journal of cellular biochemistry *29*, 37-44.
Koob, M.D., Moseley, M.L., Schut, L.J., Benzow, K.A., Bird, T.D., Day, J.W., and Ranum, L.P. (1999). An untranslated CTG expansion causes a novel form of spinocerebellar ataxia (SCA8). Nat Genet *21*, 379-384.
Kose, A., Saito, N., Ito, H., Kikkawa, U., Nishizuka, Y., and Tanaka, C. (1988). Electron microscopic localization of type I protein kinase C in rat Purkinje cells. The Journal of neuroscience : the official journal of the Society for Neuroscience *8*, 4262-4268.

Kouranova, E., Forbes, K., Zhao, G., Warren, J., Bartels, A., Wu, Y., and Cui, X. (2016). CRISPRs for Optimal Targeting: Delivery of CRISPR Components as DNA, RNA, and Protein into Cultured Cells and Single-Cell Embryos. Human gene therapy *27*, 464-475.
Krishnakumar, R., and Blelloch, R.H. (2013). Epigenetics of cellular reprogramming. Current opinion in genetics & development *23*, 548-555.
Kuroda, S., Schweighofer, N., and Kawato, M. (2001). Exploration of Signal Transduction Pathways in Cerebellar Long-Term Depression by Kinetic Simulation. The Journal of Neuroscience *21*, 5693-5702.
Kwon, Y.T., and Ciechanover, A. (2017). The Ubiquitin Code in the Ubiquitin-Proteasome System and Autophagy. Trends in biochemical sciences *42*, 873-886.
Lamm, N., Ben-David, U., Golan-Lev, T., Storchova, Z., Benvenisty, N., and Kerem, B. (2016). Genomic Instability in Human Pluripotent Stem Cells Arises from Replicative Stress and Chromosome Condensation Defects. Cell stem cell *18*, 253-261.
Lancaster, M.A., Corsini, N.S., Wolfinger, S., Gustafson, E.H., Phillips, A.W., Burkard, T.R., Otani, T., Livesey, F.J., and Knoblich, J.A. (2017). Guided self-organization and cortical plate formation in human brain organoids. Nature biotechnology *35*, 659-666.
Lancaster, M.A., and Knoblich, J.A. (2014). Generation of cerebral organoids from human pluripotent stem cells. Nature protocols *9*, 2329-2340.
Larkfors, L., Lindsay, R.M., and Alderson, R.F. (1994). Ciliary neurotrophic factor enhances the survival of Purkinje cells in vitro. The European journal of neuroscience *6*, 1015-1025.
Larouche, M., Che, P.M., and Hawkes, R. (2006). Neurogranin expression identifies a novel array of Purkinje cell parasagittal stripes during mouse cerebellar development. The Journal of comparative neurology *494*, 215-227.
Larouche, M., and Hawkes, R. (2006). From clusters to stripes: the developmental origins of adult cerebellar compartmentation. Cerebellum *5*, 77-88.
Larsell, O. (1952). The morphogenesis and adult pattern of the lobules and fissures of the cerebellum of the white rat. The Journal of comparative neurology *97*, 281-356.
Larsson, C. (2006). Protein kinase C and the regulation of the actin cytoskeleton. Cellular signalling *18*, 276-284.
Latham, A., and Paul, D.H. (1971). Spontaneous activity of cerebellar Purkinje cells and their responses to impulses in climbing fibres. The Journal of physiology *213*, 135-156.
Laurent, L.C., Ulitsky, I., Slavin, I., Tran, H., Schork, A., Morey, R., Lynch, C., Harness, J.V., Lee, S., Barrero, M.J., *et al.* (2011). Dynamic changes in the copy number of pluripotency and cell proliferation genes in human ESCs and iPSCs during reprogramming and time in culture. Cell stem cell *8*, 106-118.
Lee, Y.C., Durr, A., Majczenko, K., Huang, Y.H., Liu, Y.C., Lien, C.C., Tsai, P.C., Ichikawa, Y., Goto, J., Monin, M.L., *et al.* (2012). Mutations in KCND3 cause spinocerebellar ataxia type 22. Annals of neurology *72*, 859-869.
Leitges, M., Kovac, J., Plomann, M., and Linden, D.J. (2004). A unique PDZ ligand in PKCalpha confers induction of cerebellar long-term synaptic depression. Neuron *44*, 585-594.
Leonard, T.A., Rozycki, B., Saidi, L.F., Hummer, G., and Hurley, J.H. (2011). Crystal structure and allosteric activation of protein kinase C betaII. Cell *144*, 55-66.
Leto, K., Arancillo, M., Becker, E.B.E., Buffo, A., Chiang, C., Ding, B., Dobyns, W.B., Dusart, I., Haldipur, P., Hatten, M.E., *et al.* (2016). Consensus Paper: Cerebellar Development. Cerebellum *15*, 789-828.
Li, H.F., Mochly-Rosen, D., and Kendig, J.J. (2005). Protein kinase Cgamma mediates ethanol withdrawal hyper-responsiveness of NMDA receptor currents in spinal cord motor neurons. British journal of pharmacology *144*, 301-307.
Li, N., and Zhang, W. (2017). Protein kinase C β inhibits autophagy and sensitizes cervical cancer Hela cells to cisplatin. Bioscience reports *37*, BSR20160445.
Liang, G., and Zhang, Y. (2013). Embryonic stem cell and induced pluripotent stem cell: an epigenetic perspective. Cell research *23*, 49-69.

Lim, J.P., and Gleeson, P.A. (2011). Macropinocytosis: an endocytic pathway for internalising large gulps. Immunology and cell biology *89*, 836-843.
Lin, D., Shanks, D., Prakash, O., and Takemoto, D.J. (2007). Protein kinase C gamma mutations in the C1B domain cause caspase-3-linked apoptosis in lens epithelial cells through gap junctions. Experimental eye research *85*, 113-122.
Lin, D., and Takemoto, D.J. (2005). Oxidative activation of protein kinase Cgamma through the C1 domain. Effects on gap junctions. The Journal of biological chemistry *280*, 13682-13693.
Lin, D., and Takemoto, D.J. (2007). Protection from Ataxia-linked Apoptosis by Gap Junction Inhibitors. Biochemical and biophysical research communications *362*, 982-987.
Lin, X., Antalffy, B., Kang, D., Orr, H.T., and Zoghbi, H.Y. (2000). Polyglutamine expansion down-regulates specific neuronal genes before pathologic changes in SCA1. Nat Neurosci *3*, 157-163.
Linda, K., Fiuza, C., and Nadif Kasri, N. (2017). The promise of induced pluripotent stem cells for neurodevelopmental disorders. Progress in neuro-psychopharmacology & biological psychiatry.
Linden, D.J., Murakami, K., and Routtenberg, A. (1986). A newly discovered protein kinase C activator (oleic acid) enhances long-term potentiation in the intact hippocampus. Brain research *379*, 358-363.
Linden, D.J., Sheu, F.S., Murakami, K., and Routtenberg, A. (1987). Enhancement of long-term potentiation by cis-unsaturated fatty acid: relation to protein kinase C and phospholipase A2. The Journal of neuroscience : the official journal of the Society for Neuroscience *7*, 3783-3792.
Lindholm, D., Castren, E., Tsoulfas, P., Kolbeck, R., Berzaghi Mda, P., Leingartner, A., Heisenberg, C.P., Tessarollo, L., Parada, L.F., and Thoenen, H. (1993). Neurotrophin-3 induced by tri-iodothyronine in cerebellar granule cells promotes Purkinje cell differentiation. The Journal of cell biology *122*, 443-450.
Liu, C., Mei, M., Li, Q., Roboti, P., Pang, Q., Ying, Z., Gao, F., Lowe, M., and Bao, S. (2017). Loss of the golgin GM130 causes Golgi disruption, Purkinje neuron loss, and ataxia in mice. Proceedings of the National Academy of Sciences *114*, 346-351.
Liu, J., Tang, T.S., Tu, H., Nelson, O., Herndon, E., Huynh, D.P., Pulst, S.M., and Bezprozvanny, I. (2009). Deranged calcium signaling and neurodegeneration in spinocerebellar ataxia type 2. The Journal of neuroscience : the official journal of the Society for Neuroscience *29*, 9148-9162.
Lu, Z., Liu, D., Hornia, A., Devonish, W., Pagano, M., and Foster, D.A. (1998). Activation of protein kinase C triggers its ubiquitination and degradation. Mol Cell Biol *18*, 839-845.
Lukovic, D., Moreno-Manzano, V., Rodriguez-Jimenez, F.J., Vilches, A., Sykova, E., Jendelova, P., Stojkovic, M., and Erceg, S. (2016). hiPSC Disease Modeling of Rare Hereditary Cerebellar Ataxias. The Neuroscientist : a review journal bringing neurobiology, neurology and psychiatry, Epub ahead of print.
Machold, R., and Fishell, G. (2005). Math1 is expressed in temporally discrete pools of cerebellar rhombic-lip neural progenitors. Neuron *48*, 17-24.
Malenka, R.C., Madison, D.V., and Nicoll, R.A. (1986). Potentiation of synaptic transmission in the hippocampus by phorbol esters. Nature *321*, 175-177.
Malinow, R., Schulman, H., and Tsien, R.W. (1989). Inhibition of postsynaptic PKC or CaMKII blocks induction but not expression of LTP. Science *245*, 862-866.
Marais, R.M., Nguyen, O., Woodgett, J.R., and Parker, P.J. (1990). Studies on the primary sequence requirements for PKC-alpha, -beta 1 and -gamma peptide substrates. FEBS letters *277*, 151-155.
Mariani, J., Crepel, F., Mikoshiba, K., Changeux, J.P., and Sotelo, C. (1977). Anatomical, physiological and biochemical studies of the cerebellum from Reeler mutant mouse. Philosophical transactions of the Royal Society of London Series B, Biological sciences *281*, 1-28.

Martinez-Barbera, J.P., Signore, M., Boyl, P.P., Puelles, E., Acampora, D., Gogoi, R., Schubert, F., Lumsden, A., and Simeone, A. (2001). Regionalisation of anterior neuroectoderm and its competence in responding to forebrain and midbrain inducing activities depend on mutual antagonism between OTX2 and GBX2. Development *128*, 4789-4800.
Martinez, S., Crossley, P.H., Cobos, I., Rubenstein, J.L., and Martin, G.R. (1999). FGF8 induces formation of an ectopic isthmic organizer and isthmocerebellar development via a repressive effect on Otx2 expression. Development *126*, 1189-1200.
Maruyama, T., Dougan, S.K., Truttmann, M.C., Bilate, A.M., Ingram, J.R., and Ploegh, H.L. (2015). Increasing the efficiency of precise genome editing with CRISPR-Cas9 by inhibition of nonhomologous end joining. Nature biotechnology *33*, 538-542.
Mason, C.A., Christakos, S., and Catalano, S.M. (1990). Early climbing fiber interactions with Purkinje cells in the postnatal mouse cerebellum. The Journal of comparative neurology *297*, 77-90.
Matilla-Duenas, A., Ashizawa, T., Brice, A., Magri, S., McFarland, K.N., Pandolfo, M., Pulst, S.M., Riess, O., Rubinsztein, D.C., Schmidt, J., *et al.* (2014). Consensus paper: pathological mechanisms underlying neurodegeneration in spinocerebellar ataxias. Cerebellum *13*, 269-302.
Matsuda, S., Launey, T., Mikawa, S., and Hirai, H. (2000). Disruption of AMPA receptor GluR2 clusters following long-term depression induction in cerebellar Purkinje neurons. The EMBO journal *19*, 2765-2774.
Matsuda, S., Mikawa, S., and Hirai, H. (1999). Phosphorylation of serine-880 in GluR2 by protein kinase C prevents its C terminus from binding with glutamate receptor-interacting protein. J Neurochem *73*, 1765-1768.
Matsuura, T., Yamagata, T., Burgess, D.L., Rasmussen, A., Grewal, R.P., Watase, K., Khajavi, M., McCall, A.E., Davis, C.F., Zu, L., *et al.* (2000). Large expansion of the ATTCT pentanucleotide repeat in spinocerebellar ataxia type 10. Nat Genet *26*, 191-194.
Mayshar, Y., Ben-David, U., Lavon, N., Biancotti, J.C., Yakir, B., Clark, A.T., Plath, K., Lowry, W.E., and Benvenisty, N. (2010). Identification and classification of chromosomal aberrations in human induced pluripotent stem cells. Cell stem cell *7*, 521-531.
Meera, P., Pulst, S.M., and Otis, T.S. (2016). Cellular and circuit mechanisms underlying spinocerebellar ataxias. The Journal of physiology *594*, 4653-4660.
Menzies, F.M., Fleming, A., Caricasole, A., Bento, C.F., Andrews, S.P., Ashkenazi, A., Fullgrabe, J., Jackson, A., Jimenez Sanchez, M., Karabiyik, C., *et al.* (2017). Autophagy and Neurodegeneration: Pathogenic Mechanisms and Therapeutic Opportunities. Neuron *93*, 1015-1034.
Metzger, F. (2010). Molecular and cellular control of dendrite maturation during brain development. Curr Mol Pharmacol *3*, 1-11.
Metzger, F., and Kapfhammer, J.P. (2000). Protein kinase C activity modulates dendritic differentiation of rat Purkinje cells in cerebellar slice cultures. The European journal of neuroscience *12*, 1993-2005.
Metzger, F., and Kapfhammer, J.P. (2003). Protein kinase C: its role in activity-dependent Purkinje cell dendritic development and plasticity. Cerebellum *2*, 206-214.
Metzger, F., Pieri, I., and Eisel, U.L. (2005). Lack of NMDA receptor subunit exchange alters Purkinje cell dendritic morphology in cerebellar slice cultures. Brain research Developmental brain research *155*, 165-168.
Miale, I.L., and Sidman, R.L. (1961). An autoradiographic analysis of histogenesis in the mouse cerebellum. Experimental neurology *4*, 277-296.
Michael-Titus, A., Revest, P., and Shortland, P. (2010). 9 - MOTOR SYSTEMS I: DESCENDING PATHWAYS AND CEREBELLUM. In The Nervous System (Second Edition), A. Michael-Titus, P. Revest, and P. Shortland, eds. (Churchill Livingstone), pp. 159-180.
Minaki, Y., Nakatani, T., Mizuhara, E., Inoue, T., and Ono, Y. (2008). Identification of a novel transcriptional corepressor, Corl2, as a cerebellar Purkinje cell-selective marker. Gene expression patterns : GEP *8*, 418-423.

Miyata, H., Chute, D.J., Fink, J., Villablanca, P., and Vinters, H.V. (2004). Lissencephaly with agenesis of corpus callosum and rudimentary dysplastic cerebellum: a subtype of lissencephaly with cerebellar hypoplasia. Acta neuropathologica *107*, 69-81.
Miyata, T., Ono, Y., Okamoto, M., Masaoka, M., Sakakibara, A., Kawaguchi, A., Hashimoto, M., and Ogawa, M. (2010). Migration, early axonogenesis, and Reelin-dependent layer-forming behavior of early/posterior-born Purkinje cells in the developing mouse lateral cerebellum. Neural development *5*, 23.
Mizuhara, E., Minaki, Y., Nakatani, T., Kumai, M., Inoue, T., Muguruma, K., Sasai, Y., and Ono, Y. (2010). Purkinje cells originate from cerebellar ventricular zone progenitors positive for Neph3 and E-cadherin. Dev Biol *338*, 202-214.
Mizushima, N., Yoshimorim, T., and Levine, B. (2010). Methods in Mammalian Autophagy Research. Cell *140*, 313-326.
Morales, D., and Hatten, M.E. (2006). Molecular markers of neuronal progenitors in the embryonic cerebellar anlage. The Journal of neuroscience : the official journal of the Society for Neuroscience *26*, 12226-12236.
Morita, H., Yoshida, K., Suzuki, K., and Ikeda, S. (2006). A Japanese case of SCA14 with the Gly128Asp mutation. Journal of human genetics *51*, 1118-1121.
Moriya, M., and Tanaka, S. (1994). Prominent expression of protein kinase C (gamma) mRNA in the dendrite-rich neuropil of mice cerebellum at the critical period for synaptogenesis. Neuroreport *5*, 929-932.
Morris, S.A., and Daley, G.Q. (2013). A blueprint for engineering cell fate: current technologies to reprogram cell identity. Cell research *23*, 33-48.
Morrison, M.E., and Mason, C.A. (1998). Granule Neuron Regulation of Purkinje Cell Development: Striking a Balance Between Neurotrophin and Glutamate Signaling. The Journal of Neuroscience *18*, 3563.
Mount, H.T., Dreyfus, C.F., and Black, I.B. (1994). Neurotrophin-3 selectively increases cultured Purkinje cell survival. Neuroreport *5*, 2497-2500.
Muguruma, K., Nishiyama, A., Kawakami, H., Hashimoto, K., and Sasai, Y. (2015). Self-organization of polarized cerebellar tissue in 3D culture of human pluripotent stem cells. Cell reports *10*, 537-550.
Muguruma, K., Nishiyama, A., Ono, Y., Miyawaki, H., Mizuhara, E., Hori, S., Kakizuka, A., Obata, K., Yanagawa, Y., Hirano, T., *et al.* (2010). Ontogeny-recapitulating generation and tissue integration of ES cell-derived Purkinje cells. Nat Neurosci *13*, 1171-1180.
Muller, M., Lee, C.M., Gasiunas, G., Davis, T.H., Cradick, T.J., Siksnys, V., Bao, G., Cathomen, T., and Mussolino, C. (2016). Streptococcus thermophilus CRISPR-Cas9 Systems Enable Specific Editing of the Human Genome. Molecular therapy : the journal of the American Society of Gene Therapy *24*, 636-644.
Musunuru, K. (2013). Genome editing of human pluripotent stem cells to generate human cellular disease models. Disease models & mechanisms *6*, 896-904.
Nakagawa, M., Koyanagi, M., Tanabe, K., Takahashi, K., Ichisaka, T., Aoi, T., Okita, K., Mochiduki, Y., Takizawa, N., and Yamanaka, S. (2008). Generation of induced pluripotent stem cells without Myc from mouse and human fibroblasts. Nature biotechnology *26*, 101-106.
Nakamura, H., Katahira, T., Matsunaga, E., and Sato, T. (2005). Isthmus organizer for midbrain and hindbrain development. Brain research Brain research reviews *49*, 120-126.
Nakamura, K., Jeong, S.Y., Uchihara, T., Anno, M., Nagashima, K., Nagashima, T., Ikeda, S., Tsuji, S., and Kanazawa, I. (2001). SCA17, a novel autosomal dominant cerebellar ataxia caused by an expanded polyglutamine in TATA-binding protein. Human molecular genetics *10*, 1441-1448.
Nakao, H., Nakao, K., Kano, M., and Aiba, A. (2007). Metabotropic glutamate receptor subtype-1 is essential for motor coordination in the adult cerebellum. Neuroscience research *57*, 538-543.
Nakazono, A., Adachi, N., Takahashi, H., Seki, T., Hamada, D., Ueyama, T., Sakai, N., and Saito, N. (2018). Pharmacological induction of heat shock proteins ameliorates toxicity of

mutant PKCgamma in spinocerebellar ataxia type 14. The Journal of biological chemistry *293*, 14758-14774.
Namba, K., Sugihara, I., and Hashimoto, M. (2011). Close correlation between the birth date of Purkinje cells and the longitudinal compartmentalization of the mouse adult cerebellum. The Journal of comparative neurology *519*, 2594-2614.
Narbonne, P., Miyamoto, K., and Gurdon, J.B. (2012). Reprogramming and development in nuclear transfer embryos and in interspecific systems. Current opinion in genetics & development *22*, 450-458.
Nemeth, A.H., Kwasniewska, A.C., Lise, S., Parolin Schnekenberg, R., Becker, E.B., Bera, K.D., Shanks, M.E., Gregory, L., Buck, D., Zameel Cader, M., *et al.* (2013). Next generation sequencing for molecular diagnosis of neurological disorders using ataxias as a model. Brain : a journal of neurology *136*, 3106-3118.
Newton, A.C. (2001). Protein kinase C: structural and spatial regulation by phosphorylation, cofactors, and macromolecular interactions. Chemical reviews *101*, 2353-2364.
Newton, A.C. (2003). Regulation of the ABC kinases by phosphorylation: protein kinase C as a paradigm. Biochemical Journal *370*, 361-371.
Newton, A.C. (2010). Protein kinase C: poised to signal. American journal of physiology Endocrinology and metabolism *298*, E395-402.
Newton, A.C. (2018). Protein kinase C: perfectly balanced. Critical reviews in biochemistry and molecular biology *53*, 208-230.
Nguyen, T.A., Takemoto, L.J., and Takemoto, D.J. (2004). Inhibition of gap junction activity through the release of the C1B domain of protein kinase Cgamma (PKCgamma) from 14-3-3: identification of PKCgamma-binding sites. The Journal of biological chemistry *279*, 52714-52725.
Nibbeling, E.A.R., Duarri, A., Verschuuren-Bemelmans, C.C., Fokkens, M.R., Karjalainen, J.M., Smeets, C., de Boer-Bergsma, J.J., van der Vries, G., Dooijes, D., Bampi, G.B., *et al.* (2017). Exome sequencing and network analysis identifies shared mechanisms underlying spinocerebellar ataxia. Brain : a journal of neurology.
Nishimura, K., Sano, M., Ohtaka, M., Furuta, B., Umemura, Y., Nakajima, Y., Ikehara, Y., Kobayashi, T., Segawa, H., Takayasu, S., *et al.* (2011). Development of defective and persistent Sendai virus vector: a unique gene delivery/expression system ideal for cell reprogramming. The Journal of biological chemistry *286*, 4760-4771.
Nishimura, T., Kaneko, S., Kawana-Tachikawa, A., Tajima, Y., Goto, H., Zhu, D., Nakayama-Hosoya, K., Iriguchi, S., Uemura, Y., Shimizu, T., *et al.* (2013). Generation of rejuvenated antigen-specific T cells by reprogramming to pluripotency and redifferentiation. Cell stem cell *12*, 114-126.
Nishizuka, Y. (1988). The molecular heterogeneity of protein kinase C and its implications for cellular regulation. Nature *334*, 661-665.
Nixon, J.B., and McPhail, L.C. (1999). Protein kinase C (PKC) isoforms translocate to Triton-insoluble fractions in stimulated human neutrophils: correlation of conventional PKC with activation of NADPH oxidase. Journal of immunology (Baltimore, Md : 1950) *163*, 4574-4582.
Nolte, D., Landendinger, M., Schmitt, E., and Muller, U. (2007). Spinocerebellar ataxia 14: novel mutation in exon 2 of PRKCG in a German family. Movement disorders : official journal of the Movement Disorder Society *22*, 265-267.
Oancea, E., and Meyer, T. (1998). Protein kinase C as a molecular machine for decoding calcium and diacylglycerol signals. Cell *95*, 307-318.
Offermanns, S., Hashimoto, K., Watanabe, M., Sun, W., Kurihara, H., Thompson, R.F., Inoue, Y., Kano, M., and Simon, M.I. (1997). Impaired motor coordination and persistent multiple climbing fiber innervation of cerebellar Purkinje cells in mice lacking Galphaq. Proceedings of the National Academy of Sciences of the United States of America *94*, 14089-14094.
Ogawa, K., Seki, T., Onji, T., Adachi, N., Tanaka, S., Hide, I., Saito, N., and Sakai, N. (2013). Mutant gammaPKC that causes spinocerebellar ataxia type 14 upregulates Hsp70, which

protects cells from the mutant's cytotoxicity. Biochemical and biophysical research communications *440*, 25-30.
Orr, H.T. (2012). Cell biology of spinocerebellar ataxia. The Journal of cell biology *197*, 167-177.
Orr, H.T., Chung, M.Y., Banfi, S., Kwiatkowski, T.J., Jr., Servadio, A., Beaudet, A.L., McCall, A.E., Duvick, L.A., Ranum, L.P., and Zoghbi, H.Y. (1993). Expansion of an unstable trinucleotide CAG repeat in spinocerebellar ataxia type 1. Nat Genet *4*, 221-226.
Ostrowski, L.A., Hall, A.C., and Mekhail, K. (2017). Ataxin-2: From RNA Control to Human Health and Disease. Genes *8*.
Ozaki, K., Doi, H., Mitsui, J., Sato, N., Iikuni, Y., Majima, T., Yamane, K., Irioka, T., Ishiura, H., Doi, K., *et al.* (2015). A Novel Mutation in ELOVL4 Leading to Spinocerebellar Ataxia (SCA) With the Hot Cross Bun Sign but Lacking Erythrokeratodermia: A Broadened Spectrum of SCA34. JAMA neurology *72*, 797-805.
Palay, S.L., and Chan-Palay, V. (1974). Cerebellar Cortex: Cytology and Organization (Berlin Heidelberg: Springer-Verlag Berlin Heidelberg).
Palesi, F., Tournier, J.-D., Calamante, F., Muhlert, N., Castellazzi, G., Chard, D., D'Angelo, E., and Wheeler-Kingshott, C.A.M. (2015). Contralateral cerebello-thalamo-cortical pathways with prominent involvement of associative areas in humans in vivo. Brain Structure & Function *220*, 3369-3384.
Pascual, M., Abasolo, I., Mingorance-Le Meur, A., Martinez, A., Del Rio, J.A., Wright, C.V., Real, F.X., and Soriano, E. (2007). Cerebellar GABAergic progenitors adopt an external granule cell-like phenotype in the absence of Ptf1a transcription factor expression. Proceedings of the National Academy of Sciences of the United States of America *104*, 5193-5198.
Patten, D.A., Germain, M., Kelly, M.A., and Slack, R.S. (2010). Reactive oxygen species: stuck in the middle of neurodegeneration. Journal of Alzheimer's disease : JAD *20 Suppl 2*, S357-367.
Patten, S.A., and Ali, D.W. (2009). PKCgamma-induced trafficking of AMPA receptors in embryonic zebrafish depends on NSF and PICK1. Proceedings of the National Academy of Sciences of the United States of America *106*, 6796-6801.
Payne, A.P., Campbell, J.M., Russell, D., Favor, G., Sutcliffe, R.G., Bennett, N.K., Davies, R.W., and Stone, T.W. (2000). The AS/AGU rat: a spontaneous model of disruption and degeneration in the nigrostriatal dopaminergic system. Journal of anatomy *196 (Pt 4)*, 629-633.
Payne, A.P., Sutcliffe, R.G., Campbell, J.M., Favor, G., Russell, D., Bennett, N.K., Clarke, D.J., Branton, R., Davies, R.W., Simpson, E., *et al.* (1998). Disordered locomotion in the AS/AGU mutant rat and the effects of L-dopa or fetal midbrain grafts. Movement disorders : official journal of the Movement Disorder Society *13*, 832-834.
Peng, C., Gathagan, R.J., Covell, D.J., Medellin, C., Stieber, A., Robinson, J.L., Zhang, B., Pitkin, R.M., Olufemi, M.F., Luk, K.C., *et al.* (2018). Cellular milieu imparts distinct pathological alpha-synuclein strains in alpha-synucleinopathies. Nature *557*, 558-563.
Perez, M.K., Paulson, H.L., Pendse, S.J., Saionz, S.J., Bonini, N.M., and Pittman, R.N. (1998). Recruitment and the role of nuclear localization in polyglutamine-mediated aggregation. The Journal of cell biology *143*, 1457-1470.
Pflieger, L.T., Dansithong, W., Paul, S., Scoles, D.R., Figueroa, K.P., Meera, P., Otis, T.S., Facelli, J.C., and Pulst, S.M. (2017). Gene co-expression network analysis for identifying modules and functionally enriched pathways in SCA2. Human molecular genetics *26*, 3069-3080.
Pike, A.C.W., Amos, A., Johansson, C., Sobott, F., Savitsky, P., Berridge, G., Fedorov, O., Umeano, C., Gorrec, F., Bunkoczi, G., *et al.* (2007). Crystal Structure of C2 Domain of Protein Kinase C Gamma.
Pulst, S.M., Nechiporuk, A., Nechiporuk, T., Gispert, S., Chen, X.N., Lopes-Cendes, I., Pearlman, S., Starkman, S., Orozco-Diaz, G., Lunkes, A., *et al.* (1996). Moderate expansion of

a normally biallelic trinucleotide repeat in spinocerebellar ataxia type 2. Nat Genet *14*, 269-276.
Quest, A.F., Bardes, E.S., and Bell, R.M. (1994). A phorbol ester binding domain of protein kinase C gamma. Deletion analysis of the Cys2 domain defines a minimal 43-amino acid peptide. The Journal of biological chemistry *269*, 2961-2970.
Rakic, P., and Sidman, R.L. (1973). Organization of cerebellar cortex secondary to deficit of granule cells in weaver mutant mice. The Journal of comparative neurology *152*, 133-161.
Ramakers, G.M., Gerendasy, D.D., and de Graan, P.N. (1999). Substrate phosphorylation in the protein kinase Cgamma knockout mouse. The Journal of biological chemistry *274*, 1873-1874.
Ramnani, N. (2006). The primate cortico-cerebellar system: anatomy and function. Nat Rev Neurosci *7*, 511-522.
Ramon y Cajal, S. (1911). Histologie du Système Nerveux de l'Homme et des Vertébrés, Vol 2, 2 edn (Paris: A. Maloine).
Ran, F.A., Cong, L., Yan, W.X., Scott, D.A., Gootenberg, J.S., Kriz, A.J., Zetsche, B., Shalem, O., Wu, X., Makarova, K.S., *et al.* (2015). In vivo genome editing using Staphylococcus aureus Cas9. Nature *520*, 186-191.
Ran, F.A., Hsu, P.D., Lin, C.Y., Gootenberg, J.S., Konermann, S., Trevino, A.E., Scott, D.A., Inoue, A., Matoba, S., Zhang, Y., *et al.* (2013a). Double nicking by RNA-guided CRISPR Cas9 for enhanced genome editing specificity. Cell *154*, 1380-1389.
Ran, F.A., Hsu, P.D., Wright, J., Agarwala, V., Scott, D.A., and Zhang, F. (2013b). Genome engineering using the CRISPR-Cas9 system. Nature protocols *8*, 2281-2308.
Reifers, F., Bohli, H., Walsh, E.C., Crossley, P.H., Stainier, D.Y., and Brand, M. (1998). Fgf8 is mutated in zebrafish acerebellar (ace) mutants and is required for maintenance of midbrain-hindbrain boundary development and somitogenesis. Development *125*, 2381-2395.
Riback, J.A., Katanski, C.D., Kear-Scott, J.L., Pilipenko, E.V., Rojek, A.E., Sosnick, T.R., and Drummond, D.A. (2017). Stress-Triggered Phase Separation Is an Adaptive, Evolutionarily Tuned Response. Cell *168*, 1028-1040.e1019.
Rice, D.S., and Curran, T. (2001). Role of the reelin signaling pathway in central nervous system development. Annu Rev Neurosci *24*, 1005-1039.
Richardson, C.D., Ray, G.J., DeWitt, M.A., Curie, G.L., and Corn, J.E. (2016). Enhancing homology-directed genome editing by catalytically active and inactive CRISPR-Cas9 using asymmetric donor DNA. Nature biotechnology *34*, 339-344.
Rico, B., Xu, B., and Reichardt, L.F. (2002). TrkB receptor signaling is required for establishment of GABAergic synapses in the cerebellum. Nat Neurosci *5*, 225-233.
Riesenberg, S., and Maricic, T. (2017). Targeting Repair Pathways With Small Molecules Increases Precise Genome Editing In Pluripotent Stem Cells. bioRxiv.
Rose, A.S., Bradley, A.R., Valasatava, Y., Duarte, J.M., Prli, A., #263, and Rose, P.W. (2016). Web-based molecular graphics for large complexes. In Proceedings of the 21st International Conference on Web3D Technology (Anaheim, California: ACM), pp. 185-186.
Rosenberg, R.N., and Khemani, P. (2015). Chapter 71 - The Inherited Ataxias. In Rosenberg's Molecular and Genetic Basis of Neurological and Psychiatric Disease (Fifth Edition), R.N.R.M. Pascual, ed. (Boston: Academic Press), pp. 811-832.
Ryter, S.W., Cloonan, S.M., and Choi, A.M. (2013). Autophagy: a critical regulator of cellular metabolism and homeostasis. Molecules and cells *36*, 7-16.
Sahebkar, A., Panahi, Y., Yaribeygi, H., and Javadi, B. (2018). Oxidative stress in neurodegenerative diseases: a review. CNS & neurological disorders drug targets.
Sailer, A., and Houlden, H. (2012). Recent advances in the genetics of cerebellar ataxias. Current neurology and neuroscience reports *12*, 227-236.
Sailer, A., Scholz, S.W., Gibbs, J.R., Tucci, A., Johnson, J.O., Wood, N.W., Plagnol, V., Hummerich, H., Ding, J., Hernandez, D., *et al.* (2012). Exome sequencing in an SCA14 family demonstrates its utility in diagnosing heterogeneous diseases. Neurology *79*, 127-131.

Saito, N., Kikkawa, U., Nishizuka, Y., and Tanaka, C. (1988). Distribution of protein kinase C-like immunoreactive neurons in rat brain. The Journal of neuroscience : the official journal of the Society for Neuroscience *8*, 369-382.
Saito, N., and Shirai, Y. (2002). Protein kinase C gamma (PKC gamma): function of neuron specific isotype. Journal of biochemistry *132*, 683-687.
Sakai, N., Saito, N., and Seki, T. (2011). Molecular pathophysiology of neurodegenerative disease caused by gammaPKC mutations. The world journal of biological psychiatry : the official journal of the World Federation of Societies of Biological Psychiatry *12 Suppl 1*, 95-98.
Sakai, N., Tsubokawa, H., Matsuzaki, M., Kajimoto, T., Takahashi, E., Ren, Y., Ohmori, S., Shirai, Y., Matsubayashi, H., Chen, J., *et al.* (2004). Propagation of γPKC translocation along the dendrites of Purkinje cell in γPKC-GFP transgenic mice. Genes to Cells *9*, 945-957.
Sakaki, K., Wu, J., and Kaufman, R.J. (2008). Protein kinase Ctheta is required for autophagy in response to stress in the endoplasmic reticulum. The Journal of biological chemistry *283*, 15370-15380.
Salamon, N., Sicotte, N., Drain, A., Frew, A., Alger, J.R., Jen, J., Perlman, S., and Salamon, G. (2007). White matter fiber tractography and color mapping of the normal human cerebellum with diffusion tensor imaging. Journal of neuroradiology Journal de neuroradiologie *34*, 115-128.
Saleh, S.M., Takemoto, L.J., Zoukhri, D., and Takemoto, D.J. (2001). PKC-gamma phosphorylation of connexin 46 in the lens cortex. Molecular vision *7*, 240-246.
Sanchez-Bautista, S., Corbalan-Garcia, S., Perez-Lara, A., and Gomez-Fernandez, J.C. (2009). A comparison of the membrane binding properties of C1B domains of PKCgamma, PKCdelta, and PKCepsilon. Biophysical journal *96*, 3638-3647.
Sanchez-Bautista, S., Marin-Vicente, C., Gomez-Fernandez, J.C., and Corbalan-Garcia, S. (2006). The C2 domain of PKCalpha is a Ca2+ -dependent PtdIns(4,5)P2 sensing domain: a new insight into an old pathway. Journal of molecular biology *362*, 901-914.
Sandford, E., and Burmeister, M. (2014a). Genes and genetic testing in hereditary ataxias. Genes *5*, 586-603.
Sandford, E., and Burmeister, M. (2014b). Genes and genetic testing in hereditary ataxias. Genes *5*, 586-603.
Sanpei, K., Takano, H., Igarashi, S., Sato, T., Oyake, M., Sasaki, H., Wakisaka, A., Tashiro, K., Ishida, Y., Ikeuchi, T., *et al.* (1996). Identification of the spinocerebellar ataxia type 2 gene using a direct identification of repeat expansion and cloning technique, DIRECT. Nat Genet *14*, 277-284.
Sarbassov, D.D., Ali, S.M., Kim, D.H., Guertin, D.A., Latek, R.R., Erdjument-Bromage, H., Tempst, P., and Sabatini, D.M. (2004). Rictor, a novel binding partner of mTOR, defines a rapamycin-insensitive and raptor-independent pathway that regulates the cytoskeleton. Current biology : CB *14*, 1296-1302.
Sato, N., Amino, T., Kobayashi, K., Asakawa, S., Ishiguro, T., Tsunemi, T., Takahashi, M., Matsuura, T., Flanigan, K.M., Iwasaki, S., *et al.* (2009). Spinocerebellar ataxia type 31 is associated with "inserted" penta-nucleotide repeats containing (TGGAA)n. American journal of human genetics *85*, 544-557.
Saudou, F., Finkbeiner, S., Devys, D., and Greenberg, M.E. (1998). Huntingtin acts in the nucleus to induce apoptosis but death does not correlate with the formation of intranuclear inclusions. Cell *95*, 55-66.
Schilling, K., Oberdick, J., Rossi, F., and Baader, S.L. (2008). Besides Purkinje cells and granule neurons: an appraisal of the cell biology of the interneurons of the cerebellar cortex. Histochemistry and cell biology *130*, 601-615.
Schlett, K., Pieri, I., Metzger, F., Marchetti, L., Steigerwald, F., Dere, E., Kirilly, D., Tárnok, K., Barabás, B., Kis Varga, Á., *et al.* (2004). Long-term NR2B expression in the cerebellum alters granule cell development and leads to NR2A down-regulation and motor deficits. Molecular and Cellular Neuroscience *27*, 215-226.

Schmahmann, J.D., and Sherman, J.C. (1998). The cerebellar cognitive affective syndrome. Brain : a journal of neurology *121 (Pt 4)*, 561-579.
Schmidt, T., Lindenberg, K.S., Krebs, A., Schols, L., Laccone, F., Herms, J., Rechsteiner, M., Riess, O., and Landwehrmeyer, G.B. (2002). Protein surveillance machinery in brains with spinocerebellar ataxia type 3: redistribution and differential recruitment of 26S proteasome subunits and chaperones to neuronal intranuclear inclusions. Annals of neurology *51*, 302-310.
Schonewille, M., Gao, Z., Boele, H.J., Veloz, M.F., Amerika, W.E., Simek, A.A., De Jeu, M.T., Steinberg, J.P., Takamiya, K., Hoebeek, F.E., *et al.* (2011). Reevaluating the role of LTD in cerebellar motor learning. Neuron *70*, 43-50.
Schorge, S., van de Leemput, J., Singleton, A., Houlden, H., and Hardy, J. (2010). Human ataxias: a genetic dissection of inositol triphosphate receptor (ITPR1)-dependent signaling. Trends Neurosci *33*, 211-219.
Schrenk, K., Kapfhammer, J.P., and Metzger, F. (2002). Altered dendritic development of cerebellar Purkinje cells in slice cultures from protein kinase Cgamma-deficient mice. Neuroscience *110*, 675-689.
Schwake, M., Schroder, B., and Saftig, P. (2013). Lysosomal membrane proteins and their central role in physiology. Traffic (Copenhagen, Denmark) *14*, 739-748.
Schwartz, P.M., Borghesani, P.R., Levy, R.L., Pomeroy, S.L., and Segal, R.A. (1997). Abnormal cerebellar development and foliation in BDNF-/- mice reveals a role for neurotrophins in CNS patterning. Neuron *19*, 269-281.
Seil, F.J. (1987). Enhanced Purkinje cell survival in granuloprival cerebellar cultures. Brain research *432*, 312-316.
Seixas, A.I., Loureiro, J.R., Costa, C., Ordonez-Ugalde, A., Marcelino, H., Oliveira, C.L., Loureiro, J.L., Dhingra, A., Brandao, E., Cruz, V.T., *et al.* (2017). A Pentanucleotide ATTTC Repeat Insertion in the Non-coding Region of DAB1, Mapping to SCA37, Causes Spinocerebellar Ataxia. American journal of human genetics *101*, 87-103.
Seki, T., Abe-Seki, N., Kikawada, T., Takahashi, H., Yamamoto, K., Adachi, N., Tanaka, S., Hide, I., Saito, N., and Sakai, N. (2010a). Effect of trehalose on the properties of mutant {gamma}PKC, which causes spinocerebellar ataxia type 14, in neuronal cell lines and cultured Purkinje cells. The Journal of biological chemistry *285*, 33252-33264.
Seki, T., Adachi, N., Ono, Y., Mochizuki, H., Hiramoto, K., Amano, T., Matsubayashi, H., Matsumoto, M., Kawakami, H., Saito, N., *et al.* (2005a). Mutant protein kinase Cgamma found in spinocerebellar ataxia type 14 is susceptible to aggregation and causes cell death. The Journal of biological chemistry *280*, 29096-29106.
Seki, T., Matsubayashi, H., Amano, T., Shirai, Y., Saito, N., and Sakai, N. (2005b). Phosphorylation of PKC activation loop plays an important role in receptor-mediated translocation of PKC. Genes to cells : devoted to molecular & cellular mechanisms *10*, 225-239.
Seki, T., Shimahara, T., Yamamoto, K., Abe, N., Amano, T., Adachi, N., Takahashi, H., Kashiwagi, K., Saito, N., and Sakai, N. (2009). Mutant gammaPKC found in spinocerebellar ataxia type 14 induces aggregate-independent maldevelopment of dendrites in primary cultured Purkinje cells. Neurobiology of disease *33*, 260-273.
Seki, T., Takahashi, H., Adachi, N., Abe, N., Shimahara, T., Saito, N., and Sakai, N. (2007). Aggregate formation of mutant protein kinase C gamma found in spinocerebellar ataxia type 14 impairs ubiquitin-proteasome system and induces endoplasmic reticulum stress. The European journal of neuroscience *26*, 3126-3140.
Seki, T., Takahashi, H., Yamamoto, K., Ogawa, K., Onji, T., Adachi, N., Tanaka, S., Hide, I., Saito, N., and Sakai, N. (2010b). Congo red, an amyloid-inhibiting compound, alleviates various types of cellular dysfunction triggered by mutant protein kinase cgamma that causes spinocerebellar ataxia type 14 (SCA14) by inhibiting oligomerization and aggregation. Journal of pharmacological sciences *114*, 206-216.

Serra, H.G., Byam, C.E., Lande, J.D., Tousey, S.K., Zoghbi, H.Y., and Orr, H.T. (2004). Gene profiling links SCA1 pathophysiology to glutamate signaling in Purkinje cells of transgenic mice. Human molecular genetics *13*, 2535-2543.
Serra, H.G., Duvick, L., Zu, T., Carlson, K., Stevens, S., Jorgensen, N., Lysholm, A., Burright, E., Zoghbi, H.Y., Clark, H.B., *et al.* (2006). RORalpha-mediated Purkinje cell development determines disease severity in adult SCA1 mice. Cell *127*, 697-708.
Seto, Y., Nakatani, T., Masuyama, N., Taya, S., Kumai, M., Minaki, Y., Hamaguchi, A., Inoue, Y.U., Inoue, T., Miyashita, S., *et al.* (2014). Temporal identity transition from Purkinje cell progenitors to GABAergic interneuron progenitors in the cerebellum. Nature communications *5*, 3337.
Shimada, A., Mason, C.A., and Morrison, M.E. (1998). TrkB signaling modulates spine density and morphology independent of dendrite structure in cultured neonatal Purkinje cells. The Journal of neuroscience : the official journal of the Society for Neuroscience *18*, 8559-8570.
Shimobayashi, E., and Kapfhammer, J.P. (2017). Increased biological activity of protein Kinase C gamma is not required in Spinocerebellar ataxia 14. Mol Brain *10*, 34.
Shimobayashi, E., Wagner, W., and Kapfhammer, J.P. (2016). Carbonic Anhydrase 8 Expression in Purkinje Cells Is Controlled by PKCgamma Activity and Regulates Purkinje Cell Dendritic Growth. Molecular neurobiology *53*, 5149-5160.
Shimohama, S., Saitoh, T., and Gage, F.H. (1990). Differential expression of protein kinase C isozymes in rat cerebellum. Journal of chemical neuroanatomy *3*, 367-375.
Shuvaev, A.N., Horiuchi, H., Seki, T., Goenawan, H., Irie, T., Iizuka, A., Sakai, N., and Hirai, H. (2011). Mutant PKCgamma in spinocerebellar ataxia type 14 disrupts synapse elimination and long-term depression in Purkinje cells in vivo. The Journal of neuroscience : the official journal of the Society for Neuroscience *31*, 14324-14334.
Siller, R., Greenhough, S., Park, I.H., and Sullivan, G.J. (2013). Modelling human disease with pluripotent stem cells. Current gene therapy *13*, 99-110.
Sillitoe, R.V., and Joyner, A.L. (2007). Morphology, molecular codes, and circuitry produce the three-dimensional complexity of the cerebellum. Annual review of cell and developmental biology *23*, 549-577.
Simeone, A. (2000). Positioning the isthmic organizer where Otx2 and Gbx2meet. Trends in genetics : TIG *16*, 237-240.
Sirzen-Zelenskaya, A., Zeyse, J., and Kapfhammer, J.P. (2006). Activation of class I metabotropic glutamate receptors limits dendritic growth of Purkinje cells in organotypic slice cultures. The European journal of neuroscience *24*, 2978-2986.
Sisodia, S.S. (1998). Nuclear inclusions in glutamine repeat disorders: are they pernicious, coincidental, or beneficial? Cell *95*, 1-4.
Skinner, P.J., Vierra-Green, C.A., Clark, H.B., Zoghbi, H.Y., and Orr, H.T. (2001). Altered Trafficking of Membrane Proteins in Purkinje Cells of SCA1 Transgenic Mice. The American Journal of Pathology *159*, 905-913.
Slaymaker, I.M., Gao, L., Zetsche, B., Scott, D.A., Yan, W.X., and Zhang, F. (2015). Rationally engineered Cas9 nucleases with improved specificity. Science *351*, 84.
Slaymaker, I.M., Gao, L., Zetsche, B., Scott, D.A., Yan, W.X., and Zhang, F. (2016). Rationally engineered Cas9 nucleases with improved specificity. Science *351*, 84-88.
Smith, J.R., Vallier, L., Lupo, G., Alexander, M., Harris, W.A., and Pedersen, R.A. (2008). Inhibition of Activin/Nodal signaling promotes specification of human embryonic stem cells into neuroectoderm. Dev Biol *313*, 107-117.
Smith, Z.D., Sindhu, C., and Meissner, A. (2016). Molecular features of cellular reprogramming and development. Nature reviews Molecular cell biology *17*, 139-154.
Snider, R.S., and Eldred, E. (1952). Cerebrocerebellar relationships in the monkey. J Neurophysiol *15*, 27-40.
Sohl, G., Odermatt, B., Maxeiner, S., Degen, J., and Willecke, K. (2004). New insights into the expression and function of neural connexins with transgenic mouse mutant. Brain Res Brain Res Rev *47*, 245-259.

Song, F., and Stieger, K. (2017). Optimizing the DNA Donor Template for Homology-Directed Repair of Double-Strand Breaks. Molecular Therapy Nucleic Acids *7*, 53-60.
Sotelo, C. (1973). Permanence and fate of paramembranous synaptic specializations in "mutants" experimental animals. Brain research *62*, 345-351.
Sotelo, C. (1975). Anatomical, physiological and biochemical studies of the cerebellum from mutant mice. II. Morphological study of cerebellar cortical neurons and circuits in the weaver mouse. Brain research *94*, 19-44.
Sotelo, C., and Changeux, J.P. (1974). Bergmann fibers and granular cell migration in the cerebellum of homozygous weaver mutant mouse. Brain research *77*, 484-491.
Sotelo, C., and Rossi, F. (2013). Purkinje Cell Migration and Differentiation. In Handbook of the Cerebellum and Cerebellar Disorders, M. Manto, J.D. Schmahmann, F. Rossi, D.L. Gruol, and N. Koibuchi, eds. (Dordrecht: Springer Netherlands), pp. 147-178.
Stadtfeld, M., Maherali, N., Breault, D.T., and Hochedlinger, K. (2008). Defining molecular cornerstones during fibroblast to iPS cell reprogramming in mouse. Cell stem cell *2*, 230-240.
Steinberg, S.F. (2008). Structural basis of protein kinase C isoform function. Physiological reviews *88*, 1341-1378.
Steinmayr, M., Andre, E., Conquet, F., Rondi-Reig, L., Delhaye-Bouchaud, N., Auclair, N., Daniel, H., Crepel, F., Mariani, J., Sotelo, C., *et al.* (1998). staggerer phenotype in retinoid-related orphan receptor alpha-deficient mice. Proceedings of the National Academy of Sciences of the United States of America *95*, 3960-3965.
Sterneckert, J.L., Reinhardt, P., and Scholer, H.R. (2014). Investigating human disease using stem cell models. Nature reviews Genetics *15*, 625-639.
Stevanin, G., Hahn, V., Lohmann, E., Bouslam, N., Gouttard, M., Soumphonphakdy, C., Welter, M.L., Ollagnon-Roman, E., Lemainque, A., Ruberg, M., *et al.* (2004). Mutation in the catalytic domain of protein kinase C gamma and extension of the phenotype associated with spinocerebellar ataxia type 14. Archives of neurology *61*, 1242-1248.
Stoodley, C.J., MacMore, J.P., Makris, N., Sherman, J.C., and Schmahmann, J.D. (2016). Location of lesion determines motor vs. cognitive consequences in patients with cerebellar stroke. NeuroImage Clinical *12*, 765-775.
Stoodley, C.J., and Schmahmann, J.D. (2010). Evidence for topographic organization in the cerebellum of motor control versus cognitive and affective processing. Cortex; a journal devoted to the study of the nervous system and behavior *46*, 831-844.
Stoodley, C.J., Valera, E.M., and Schmahmann, J.D. (2012). Functional topography of the cerebellum for motor and cognitive tasks: an fMRI study. NeuroImage *59*, 1560-1570.
Strasser, V., Fasching, D., Hauser, C., Mayer, H., Bock, H.H., Hiesberger, T., Herz, J., Weeber, E.J., Sweatt, J.D., Pramatarova, A., *et al.* (2004). Receptor clustering is involved in Reelin signaling. Mol Cell Biol *24*, 1378-1386.
Sugawara, T., Hisatsune, C., Miyamoto, H., Ogawa, N., and Mikoshiba, K. (2017). Regulation of spinogenesis in mature Purkinje cells via mGluR/PKC-mediated phosphorylation of CaMKIIbeta. Proceedings of the National Academy of Sciences of the United States of America *114*, E5256-e5265.
Sundberg, M., Tochitsky, I., Buchholz, D.E., Winden, K., Kujala, V., Kapur, K., Cataltepe, D., Turner, D., Han, M.J., Woolf, C.J., *et al.* (2018). Purkinje cells derived from TSC patients display hypoexcitability and synaptic deficits associated with reduced FMRP levels and reversed by rapamycin. Molecular psychiatry.
Tada, M., Tada, T., Lefebvre, L., Barton, S.C., and Surani, M.A. (1997). Embryonic germ cells induce epigenetic reprogramming of somatic nucleus in hybrid cells. The EMBO journal *16*, 6510-6520.
Takahashi, H., Adachi, N., Shirafuji, T., Danno, S., Ueyama, T., Vendruscolo, M., Shuvaev, A.N., Sugimoto, T., Seki, T., Hamada, D., *et al.* (2015). Identification and characterization of PKCgamma, a kinase associated with SCA14, as an amyloidogenic protein. Human molecular genetics *24*, 525-539.

Takahashi, K., Tanabe, K., Ohnuki, M., Narita, M., Ichisaka, T., Tomoda, K., and Yamanaka, S. (2007). Induction of pluripotent stem cells from adult human fibroblasts by defined factors. Cell *131*, 861-872.
Takahashi, K., and Yamanaka, S. (2006). Induction of pluripotent stem cells from mouse embryonic and adult fibroblast cultures by defined factors. Cell *126*, 663-676.
Takahashi, N., Shuvaev, A.N., Konno, A., Matsuzaki, Y., Watanave, M., and Hirai, H. (2017). Regulatory connection between the expression level of classical protein kinase C and pruning of climbing fibers from cerebellar Purkinje cells. J Neurochem.
Tanabe, W., Suzuki, S., Muto, Y., Inoue, M., Kigawa, T., Terada, T., Shirouzu, M., and Yokoyama, S. (2007). Solution structure of the phorbol esters/diacylglycerol binding domain of protein kinase C gamma (Protein Data Bank).
Tanaka, K., and Augustine, G.J. (2008). A positive feedback signal transduction loop determines timing of cerebellar long-term depression. Neuron *59*, 608-620.
Tanaka, K., Khiroug, L., Santamaria, F., Doi, T., Ogasawara, H., Ellis-Davies, G.C., Kawato, M., and Augustine, G.J. (2007). Ca2+ requirements for cerebellar long-term synaptic depression: role for a postsynaptic leaky integrator. Neuron *54*, 787-800.
Tarnok, K., Czondor, K., Jelitai, M., Czirok, A., and Schlett, K. (2008). NMDA receptor NR2B subunit over-expression increases cerebellar granule cell migratory activity. J Neurochem *104*, 818-829.
Taroni, F., Chiapparini, L., and Mariotti, C. (2013). Autosomal Dominant Spinocerebellar Ataxias and Episodic Ataxias. In Handbook of the Cerebellum and Cerebellar Disorders, M. Manto, J. Schmahmann, F. Rossi, D. Gruol, and N. Koibuchi, eds. (Springer Netherlands), pp. 2193-2267.
Tatsukawa, T., Chimura, T., Miyakawa, H., and Yamaguchi, K. (2006). Involvement of basal protein kinase C and extracellular signal-regulated kinase 1/2 activities in constitutive internalization of AMPA receptors in cerebellar Purkinje cells. The Journal of neuroscience : the official journal of the Society for Neuroscience *26*, 4820-4825.
Thomson, J.A., Itskovitz-Eldor, J., Shapiro, S.S., Waknitz, M.A., Swiergiel, J.J., Marshall, V.S., and Jones, J.M. (1998). Embryonic stem cell lines derived from human blastocysts. Science *282*, 1145-1147.
Tissir, F., and Goffinet, A.M. (2003). Reelin and brain development. Nat Rev Neurosci *4*, 496-505.
Todorov, B., Kros, L., Shyti, R., Plak, P., Haasdijk, E.D., Raike, R.S., Frants, R.R., Hess, E.J., Hoebeek, F.E., De Zeeuw, C.I., *et al.* (2012). Purkinje cell-specific ablation of Cav2.1 channels is sufficient to cause cerebellar ataxia in mice. Cerebellum *11*, 246-258.
Tofaris, G.K., Razzaq, A., Ghetti, B., Lilley, K.S., and Spillantini, M.G. (2003). Ubiquitination of alpha-synuclein in Lewy bodies is a pathological event not associated with impairment of proteasome function. The Journal of biological chemistry *278*, 44405-44411.
Torres-Aleman, I., Pons, S., and Arevalo, M.A. (1994). The insulin-like growth factor I system in the rat cerebellum: developmental regulation and role in neuronal survival and differentiation. J Neurosci Res *39*, 117-126.
Torres-Aleman, I., Pons, S., and Santos-Benito, F.F. (1992). Survival of Purkinje Cells in Cerebellar Cultures is Increased by Insulin-like Growth Factor I. The European journal of neuroscience *4*, 864-869.
Trebak, M., Hempel, N., Wedel, B.J., Smyth, J.T., Bird, G.S., and Putney, J.W., Jr. (2005). Negative regulation of TRPC3 channels by protein kinase C-mediated phosphorylation of serine 712. Molecular pharmacology *67*, 558-563.
Trommsdorff, M., Gotthardt, M., Hiesberger, T., Shelton, J., Stockinger, W., Nimpf, J., Hammer, R.E., Richardson, J.A., and Herz, J. (1999). Reeler/Disabled-like disruption of neuronal migration in knockout mice lacking the VLDL receptor and ApoE receptor 2. Cell *97*, 689-701.

Trzesniewski, J., Altmann, S., Jager, L., and Kapfhammer, J.P. (2018). Reduced Purkinje cell size is compatible with near normal morphology and function of the cerebellar cortex in a mouse model of spinocerebellar ataxia. Experimental neurology.
Tsai, C.C., Kao, H.Y., Mitzutani, A., Banayo, E., Rajan, H., McKeown, M., and Evans, R.M. (2004). Ataxin 1, a SCA1 neurodegenerative disorder protein, is functionally linked to the silencing mediator of retinoid and thyroid hormone receptors. Proceedings of the National Academy of Sciences of the United States of America *101*, 4047-4052.
Tsai, S.Q., Zheng, Z., Nguyen, N.T., Liebers, M., Topkar, V.V., Thapar, V., Wyvekens, N., Khayter, C., Iafrate, A.J., Le, L.P., *et al.* (2015). GUIDE-seq enables genome-wide profiling of off-target cleavage by CRISPR-Cas nucleases. Nature biotechnology *33*, 187-197.
Tsoi, H., Yu, A.C., Chen, Z.S., Ng, N.K., Chan, A.Y., Yuen, L.Y., Abrigo, J.M., Tsang, S.Y., Tsui, S.K., Tong, T.M., *et al.* (2014). A novel missense mutation in CCDC88C activates the JNK pathway and causes a dominant form of spinocerebellar ataxia. Journal of medical genetics *51*, 590-595.
Uchihara, T., Fujigasaki, H., Koyano, S., Nakamura, A., Yagishita, S., and Iwabuchi, K. (2001). Non-expanded polyglutamine proteins in intranuclear inclusions of hereditary ataxias--triple-labeling immunofluorescence study. Acta neuropathologica *102*, 149-152.
Ueda, T., Seki, T., Katanazaka, K., Sekiguchi, K., Kobayashi, K., Kanda, F., and Toda, T. (2013). A novel mutation in the C2 domain of protein kinase C gamma associated with spinocerebellar ataxia type 14. Journal of neurology *260*, 1664-1666.
van de Leemput, J., Chandran, J., Knight, M.A., Holtzclaw, L.A., Scholz, S., Cookson, M.R., Houlden, H., Gwinn-Hardy, K., Fung, H.C., Lin, X., *et al.* (2007). Deletion at ITPR1 underlies ataxia in mice and spinocerebellar ataxia 15 in humans. PLoS genetics *3*, e108.
van de Loo, S., Eich, F., Nonis, D., Auburger, G., and Nowock, J. (2009). Ataxin-2 associates with rough endoplasmic reticulum. Experimental neurology *215*, 110-118.
van de Warrenburg, B.P., Verbeek, D.S., Piersma, S.J., Hennekam, F.A., Pearson, P.L., Knoers, N.V., Kremer, H.P., and Sinke, R.J. (2003). Identification of a novel SCA14 mutation in a Dutch autosomal dominant cerebellar ataxia family. Neurology *61*, 1760-1765.
van Gaalen, J., Vermeer, S., van Veluw, M., van de Warrenburg, B.P., and Dooijes, D. (2013). A de novo SCA14 mutation in an isolated case of late-onset cerebellar ataxia. Movement disorders : official journal of the Movement Disorder Society *28*, 1902-1903.
van Swieten, J.C., Brusse, E., de Graaf, B.M., Krieger, E., van de Graaf, R., de Koning, I., Maat-Kievit, A., Leegwater, P., Dooijes, D., Oostra, B.A., *et al.* (2003). A mutation in the fibroblast growth factor 14 gene is associated with autosomal dominant cerebellar ataxia [corrected]. American journal of human genetics *72*, 191-199.
Venkatachalam, K., Zheng, F., and Gill, D.L. (2003). Regulation of canonical transient receptor potential (TRPC) channel function by diacylglycerol and protein kinase C. The Journal of biological chemistry *278*, 29031-29040.
Verbeek, D.S., Goedhart, J., Bruinsma, L., Sinke, R.J., and Reits, E.A. (2008). PKC gamma mutations in spinocerebellar ataxia type 14 affect C1 domain accessibility and kinase activity leading to aberrant MAPK signaling. Journal of cell science *121*, 2339-2349.
Verbeek, D.S., Knight, M.A., Harmison, G.G., Fischbeck, K.H., and Howell, B.W. (2005). Protein kinase C gamma mutations in spinocerebellar ataxia 14 increase kinase activity and alter membrane targeting. Brain : a journal of neurology *128*, 436-442.
VerPlank, J.J.S., Lokireddy, S., Feltri, M.L., Goldberg, A.L., and Wrabetz, L. (2017). Impairment of protein degradation and proteasome function in hereditary neuropathies. Glia.
Vlak, M.H., Sinke, R.J., Rabelink, G.M., Kremer, B.P., and van de Warrenburg, B.P. (2006). Novel PRKCG/SCA14 mutation in a Dutch spinocerebellar ataxia family: expanding the phenotype. Movement disorders : official journal of the Movement Disorder Society *21*, 1025-1028.
Voogd, J., and Glickstein, M. (1998). The anatomy of the cerebellum. Trends Neurosci *21*, 370-375.

Wang, F., Xu, C., Reece, E.A., Li, X., Wu, Y., Harman, C., Yu, J., Dong, D., Wang, C., Yang, P., *et al.* (2017). Protein kinase C-alpha suppresses autophagy and induces neural tube defects via miR-129-2 in diabetic pregnancy. Nature communications *8*, 15182.
Wang, J.L., Yang, X., Xia, K., Hu, Z.M., Weng, L., Jin, X., Jiang, H., Zhang, P., Shen, L., Guo, J.F., *et al.* (2010). TGM6 identified as a novel causative gene of spinocerebellar ataxias using exome sequencing. Brain : a journal of neurology *133*, 3510-3518.
Wang, K., Xu, R., Schrandt, J., Shah, P., Gong, Y.Z., Preston, C., Wang, L., Yi, J.K., Lin, C.L., Sun, W., *et al.* (2015a). Alkaline Ceramidase 3 Deficiency Results in Purkinje Cell Degeneration and Cerebellar Ataxia Due to Dyshomeostasis of Sphingolipids in the Brain. PLoS genetics *11*, e1005591.
Wang, S., Wang, B., Pan, N., Fu, L., Wang, C., Song, G., An, J., Liu, Z., Zhu, W., Guan, Y., *et al.* (2015b). Differentiation of human induced pluripotent stem cells to mature functional Purkinje neurons. Scientific reports *5*, 9232.
Wang, V.Y., Rose, M.F., and Zoghbi, H.Y. (2005). Math1 expression redefines the rhombic lip derivatives and reveals novel lineages within the brainstem and cerebellum. Neuron *48*, 31-43.
Wang, Y., Wang, Y., Zhang, H., Gao, Y., Huang, C., Zhou, A., Zhou, Y., and Li, Y. (2016). Sequential posttranslational modifications regulate PKC degradation. Molecular biology of the cell *27*, 410-420.
Watanabe, M., Buth, J.E., Vishlaghi, N., de la Torre-Ubieta, L., Taxidis, J., Khakh, B.S., Coppola, G., Pearson, C.A., Yamauchi, K., Gong, D., *et al.* (2017). Self-Organized Cerebral Organoids with Human-Specific Features Predict Effective Drugs to Combat Zika Virus Infection. Cell reports *21*, 517-532.
Waters, M.F., Minassian, N.A., Stevanin, G., Figueroa, K.P., Bannister, J.P., Nolte, D., Mock, A.F., Evidente, V.G., Fee, D.B., Muller, U., *et al.* (2006). Mutations in voltage-gated potassium channel KCNC3 cause degenerative and developmental central nervous system phenotypes. Nat Genet *38*, 447-451.
Watson, L.M., Bamber, E., Schnekenberg, R.P., Williams, J., Bettencourt, C., Lickiss, J., Jayawant, S., Fawcett, K., Clokie, S., Wallis, Y., *et al.* (2017). Dominant Mutations in GRM1 Cause Spinocerebellar Ataxia Type 44. American journal of human genetics *101*, 451-458.
Watson, L.M., Wong, M.M., and Becker, E.B. (2015a). Induced pluripotent stem cell technology for modelling and therapy of cerebellar ataxia. *5*.
Watson, L.M., Wong, M.M.K., and Becker, E.B.E. (2015b). Induced pluripotent stem cell technology for modelling and therapy of cerebellar ataxia. Open biology *5*, 150056.
Watson, L.M., Wong, M.M.K., Vowles, J., Cowley, S.A., and Becker, E.B.E. (2018). A Simplified Method for Generating Purkinje Cells from Human-Induced Pluripotent Stem Cells. Cerebellum, 1-9.
Wedding, I.M., Koht, J., Dietrichs, E., Landro, N.I., and Tallaksen, C.M. (2013). Cognition is only minimally impaired in Spinocerebellar ataxia type 14 (SCA14): a neuropsychological study of ten Norwegian subjects compared to intrafamilial controls and population norm. BMC neurology *13*, 186.
Wetsel, W.C., Khan, W.A., Merchenthaler, I., Rivera, H., Halpern, A.E., Phung, H.M., Negro-Vilar, A., and Hannun, Y.A. (1992). Tissue and cellular distribution of the extended family of protein kinase C isoenzymes. The Journal of cell biology *117*, 121-133.
Wieczorek, S., Arning, L., Gizewski, E.R., Alheite, I., and Timmann, D. (2007). Benign SCA14 phenotype in a German patient associated with a missense mutation in exon 3 of the PRKCG gene. Movement disorders : official journal of the Movement Disorder Society *22*, 2135-2136.
Wiegert, J.S., and Bading, H. (2011). Activity-dependent calcium signaling and ERK-MAP kinases in neurons: a link to structural plasticity of the nucleus and gene transcription regulation. Cell Calcium *49*, 296-305.
Williams, R., and Coluccio, L.M. (1995). Phosphorylation of myosin-I from rat liver by protein kinase C reduces calmodulin binding. Biochemical and biophysical research communications *216*, 90-102.

Wingate, R.J., and Hatten, M.E. (1999). The role of the rhombic lip in avian cerebellum development. Development *126*, 4395-4404.
Witter, L., Rudolph, S., Pressler, R.T., Lahlaf, S.I., and Regehr, W.G. (2016). Purkinje cell collaterals enable output signals from the cerebellar cortex to feed back to Purkinje cells and interneurons. Neuron *91*, 312-319.
Wong, M.M.K., Watson, L.M., and Becker, E.B.E. (2017). Recent advances in modelling of cerebellar ataxia using induced pluripotent stem cells. Journal of neurology & neuromedicine *2*, 11-15.
Woodward, D.J., Hoffer, B.J., Siggins, G.R., and Oliver, A.P. (1971). Inhibition of Purkinje cells in the frog cerebellum. II. Evidence for GABA as the inhibitory transmitter. Brain research *33*, 91-100.
Xia, J., Chung, H.J., Wihler, C., Huganir, R.L., and Linden, D.J. (2000). Cerebellar long-term depression requires PKC-regulated interactions between GluR2/3 and PDZ domain-containing proteins. Neuron *28*, 499-510.
Xiao, D.M., Pak, J.H., Wang, X., Sato, T., Huang, F.L., Chen, H.C., and Huang, K.P. (2000). Phosphorylation of HMG-I by protein kinase C attenuates its binding affinity to the promoter regions of protein kinase C gamma and neurogranin/RC3 genes. J Neurochem *74*, 392-399.
Xu, R.X., Pawelczyk, T., Xia, T.H., and Brown, S.C. (1997). NMR structure of a protein kinase C-gamma phorbol-binding domain and study of protein-lipid micelle interactions. Biochemistry *36*, 10709-10717.
Yabe, I., Sasaki, H., Chen, D.H., Raskind, W.H., Bird, T.D., Yamashita, I., Tsuji, S., Kikuchi, S., and Tashiro, K. (2003). Spinocerebellar ataxia type 14 caused by a mutation in protein kinase C gamma. Archives of neurology *60*, 1749-1751.
Yagi, K., Shirai, Y., Hirai, M., Sakai, N., and Saito, N. (2004). Phospholipase A2 products retain a neuron specific gamma isoform of PKC on the plasma membrane through the C1 domain--a molecular mechanism for sustained enzyme activity. Neurochemistry international *45*, 39-47.
Yamada, M., Seto, Y., Taya, S., Owa, T., Inoue, Y.U., Inoue, T., Kawaguchi, Y., Nabeshima, Y., and Hoshino, M. (2014). Specification of spatial identities of cerebellar neuron progenitors by ptf1a and atoh1 for proper production of GABAergic and glutamatergic neurons. The Journal of neuroscience : the official journal of the Society for Neuroscience *34*, 4786-4800.
Yamaguchi, K., Itohara, S., and Ito, M. (2016). Reassessment of long-term depression in cerebellar Purkinje cells in mice carrying mutated GluA2 C terminus. Proceedings of the National Academy of Sciences of the United States of America *113*, 10192-10197.
Yamaguchi, Y., Shirai, Y., Matsubara, T., Sanse, K., Kuriyama, M., Oshiro, N., Yoshino, K., Yonezawa, K., Ono, Y., and Saito, N. (2006). Phosphorylation and up-regulation of diacylglycerol kinase gamma via its interaction with protein kinase C gamma. The Journal of biological chemistry *281*, 31627-31637.
Yamamoto, K., Seki, T., Adachi, N., Takahashi, T., Tanaka, S., Hide, I., Saito, N., and Sakai, N. (2010). Mutant protein kinase C gamma that causes spinocerebellar ataxia type 14 (SCA14) is selectively degraded by autophagy. Genes to cells : devoted to molecular & cellular mechanisms *15*, 425-438.
Yamamoto, K., Seki, T., Yamamoto, H., Adachi, N., Tanaka, S., Hide, I., Saito, N., and Sakai, N. (2014). Deregulation of the actin cytoskeleton and macropinocytosis in response to phorbol ester by the mutant protein kinase C gamma that causes spinocerebellar ataxia type 14. Frontiers in physiology *5*, 126.
Yamashita, I., Sasaki, H., Yabe, I., Fukazawa, T., Nogoshi, S., Komeichi, K., Takada, A., Shiraishi, K., Takiyama, Y., Nishizawa, M., *et al.* (2000). A novel locus for dominant cerebellar ataxia (SCA14) maps to a 10.2-cM interval flanked by D19S206 and D19S605 on chromosome 19q13.4-qter. Annals of neurology *48*, 156-163.
Yang, H., Wang, H., and Jaenisch, R. (2014). Generating genetically modified mice using CRISPR/Cas-mediated genome engineering. Nature protocols *9*, 1956-1968.

Yang, L., Guell, M., Byrne, S., Yang, J.L., De Los Angeles, A., Mali, P., Aach, J., Kim-Kiselak, C., Briggs, A.W., Rios, X., *et al.* (2013a). Optimization of scarless human stem cell genome editing. Nucleic acids research *41*, 9049-9061.
Yang, Y., Muzny, D.M., Reid, J.G., Bainbridge, M.N., Willis, A., Ward, P.A., Braxton, A., Beuten, J., Xia, F., Niu, Z., *et al.* (2013b). Clinical whole-exome sequencing for the diagnosis of mendelian disorders. The New England journal of medicine *369*, 1502-1511.
Ye, W., Shimamura, K., Rubenstein, J.L., Hynes, M.A., and Rosenthal, A. (1998). FGF and Shh signals control dopaminergic and serotonergic cell fate in the anterior neural plate. Cell *93*, 755-766.
Yu, C., Liu, Y., Ma, T., Liu, K., Xu, S., Zhang, Y., Liu, H., La Russa, M., Xie, M., Ding, S., *et al.* (2015). Small molecules enhance CRISPR genome editing in pluripotent stem cells. Cell stem cell *16*, 142-147.
Yu, J., Vodyanik, M.A., Smuga-Otto, K., Antosiewicz-Bourget, J., Frane, J.L., Tian, S., Nie, J., Jonsdottir, G.A., Ruotti, V., Stewart, R., *et al.* (2007). Induced pluripotent stem cell lines derived from human somatic cells. Science *318*, 1917-1920.
Yuasa, S., Kawamura, K., Ono, K., Yamakuni, T., and Takahashi, Y. (1991). Development and migration of Purkinje cells in the mouse cerebellar primordium. Anatomy and embryology *184*, 195-212.
Zander, C., Takahashi, J., El Hachimi, K.H., Fujigasaki, H., Albanese, V., Lebre, A.S., Stevanin, G., Duyckaerts, C., and Brice, A. (2001). Similarities between spinocerebellar ataxia type 7 (SCA7) cell models and human brain: proteins recruited in inclusions and activation of caspase-3. Human molecular genetics *10*, 2569-2579.
Zetsche, B., Gootenberg, J.S., Abudayyeh, O.O., Slaymaker, I.M., Makarova, K.S., Essletzbichler, P., Volz, S.E., Joung, J., van der Oost, J., Regev, A., *et al.* (2015). Cpf1 is a single RNA-guided endonuclease of a class 2 CRISPR-Cas system. Cell *163*, 759-771.
Zhang, G., Kazanietz, M.G., Blumberg, P.M., and Hurley, J.H. (1995). Crystal structure of the cys2 activator-binding domain of protein kinase C delta in complex with phorbol ester. Cell *81*, 917-924.
Zhang, J.P., Li, X.L., Li, G.H., Chen, W., Arakaki, C., Botimer, G.D., Baylink, D., Zhang, L., Wen, W., Fu, Y.W., *et al.* (2017a). Efficient precise knockin with a double cut HDR donor after CRISPR/Cas9-mediated double-stranded DNA cleavage. Genome biology *18*, 35.
Zhang, X.H., Tee, L.Y., Wang, X.G., Huang, Q.S., and Yang, S.H. (2015). Off-target Effects in CRISPR/Cas9-mediated Genome Engineering. Mol Ther Nucleic Acids *4*, e264.
Zhang, Y., Snider, A., Willard, L., Takemoto, D.J., and Lin, D. (2009). Loss of Purkinje cells in the PKCgamma H101Y transgenic mouse. Biochemical and biophysical research communications *378*, 524-528.
Zhang, Z., Zhang, Y., Gao, F., Han, S., Cheah, K.S., Tse, H.F., and Lian, Q. (2017b). CRISPR/Cas9 Genome-Editing System in Human Stem Cells: Current Status and Future Prospects. Mol Ther Nucleic Acids *9*, 230-241.
Zhao, L., Spassieva, S.D., Jucius, T.J., Shultz, L.D., Shick, H.E., Macklin, W.B., Hannun, Y.A., Obeid, L.M., and Ackerman, S.L. (2011). A deficiency of ceramide biosynthesis causes cerebellar purkinje cell neurodegeneration and lipofuscin accumulation. PLoS genetics *7*, e1002063.
Zhao, Y., Kwan, K.M., Mailloux, C.M., Lee, W.K., Grinberg, A., Wurst, W., Behringer, R.R., and Westphal, H. (2007). LIM-homeodomain proteins Lhx1 and Lhx5, and their cofactor Ldb1, control Purkinje cell differentiation in the developing cerebellum. Proceedings of the National Academy of Sciences of the United States of America *104*, 13182-13186.
Zheng, Q., Huang, T., Zhang, L., Zhou, Y., Luo, H., Xu, H., and Wang, X. (2016). Dysregulation of Ubiquitin-Proteasome System in Neurodegenerative Diseases. Frontiers in Aging Neuroscience *8*, 303.
Zhou, H., Lin, Z., Voges, K., Ju, C., Gao, Z., Bosman, L.W., Ruigrok, T.J., Hoebeek, F.E., De Zeeuw, C.I., and Schonewille, M. (2014). Cerebellar modules operate at different frequencies. eLife *3*, e02536.

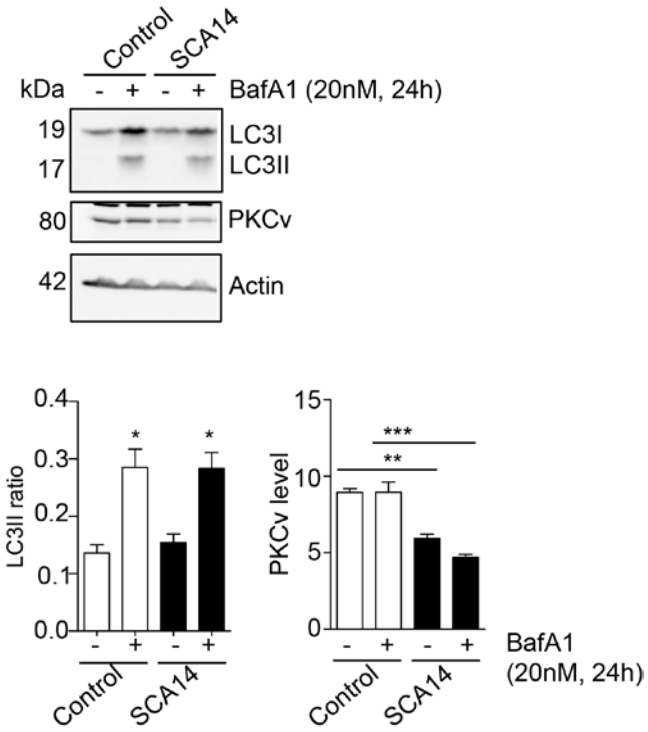
Zhou, H., Voges, K., Lin, Z., Ju, C., and Schonewille, M. (2015). Differential Purkinje cell simple spike activity and pausing behavior related to cerebellar modules. J Neurophysiol *113*, 2524-2536.
Zhuchenko, O., Bailey, J., Bonnen, P., Ashizawa, T., Stockton, D.W., Amos, C., Dobyns, W.B., Subramony, S.H., Zoghbi, H.Y., and Lee, C.C. (1997). Autosomal dominant cerebellar ataxia (SCA6) associated with small polyglutamine expansions in the alpha 1A-voltage-dependent calcium channel. Nat Genet *15*, 62-69.
Ziv, O., Zaritsky, A., Yaffe, Y., Mutukula, N., Edri, R., and Elkabetz, Y. (2015). Quantitative Live Imaging of Human Embryonic Stem Cell Derived Neural Rosettes Reveals Structure-Function Dynamics Coupled to Cortical Development. PLoS computational biology *11*, e1004453.
Zordan, P., Croci, L., Hawkes, R., and Consalez, G.G. (2008). Comparative analysis of proneural gene expression in the embryonic cerebellum. Developmental dynamics : an official publication of the American Association of Anatomists *237*, 1726-1735.

Appendix

Supplementary Table 5.1 Demographics and post-mortem interval for control and SCA14 brains used in this study.

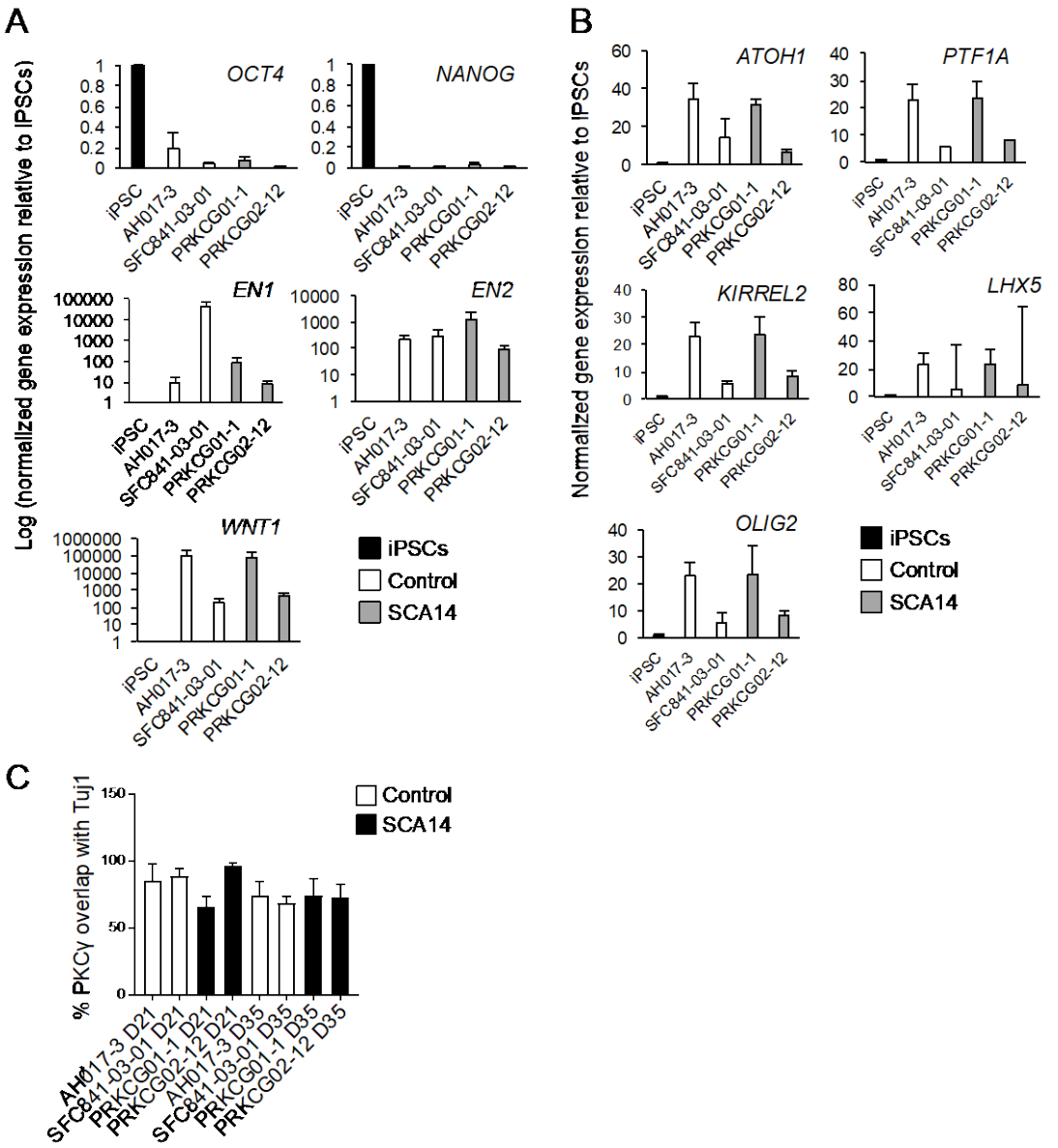
Samples	Sex	Age (years)	Post-mortem interval (days)
Control 1	M	75	2
Control 2	F	91	2
Control 3	M	100	3
SCA14-H101Q	M	103	Unavailable

F: female; M: male.



Supplementary Figure 5.1: PKCγ is not degraded via autophagy.

One control line (AH017-3) and one patient iPSC clone carrying the H101Q mutation (SCA14-2-14) were used in each experiment, i.e. bafilomycin A1 (BafA1) treatment to inhibit autophagosome-lysosome fusion. iPSCs were treated with 20nM BafA1 for 24 hours. The experiment was repeated for three times and cell lysates were prepared and subject to immunoblotting LC3 and PKCγ (upper panel). Representative immunoblots are shown. LC3I represents free cytosolic cleaved LC3. LC3II represents LC3 that is anchored to the autophagosome membrane and indicates autophagosome load. Actin: loading control. Ratio of LC3II/total LC3 levels and PKCγ at 24 hours post-BafA1 treatment was quantified (lower panel. Although autophagosome-lysosome fusion was inhibited, PKCγ levels remained constant (control, white bars) or slightly reduced (SCA14, black bars). (*$p<0.5$, *$p<0.01$, *$p<0.001$, error bars represent S.E.M., two way-ANOVA followed by Bonferroni's post-hoc test).



Supplementary Figure 6.2: Results of cerebellar progenitors derived from individual iPSC clones.

(A) Gene expression of cerebellar progenitors derived from different control and SCA14 iPSC clones after 21 days in suspension culture. The expression of early markers of midbrain-hindbrain proximity regions *EN1*, *EN2* and *WNT1* were upregulated while the pluripotency markers *OCT4* and *NANOG* were downregulated. Control and SCA14 cerebellar progenitors showed similar expression levels of all markers assessed. (B) Gene expression of cerebellar progenitors derived from different control and SCA14 iPSC clones after 35 days in suspension culture. Control and SCA14 cerebellar progenitors showed similar expression levels of markers of glutamatergic neuronal precursors *ATOH1* and GABAergic neuronal progenitors *PTF1A*. Markers of Purkinje cell progenitors *KIRREL2*, *LHX5* and *OLIG2* were also expressed. (C) Quantification of co-localisation between PKCγ and neuron-specific Class III β-tubulin (Tuj1). Gene expression is shown normalised to β-actin and relative to iPSCs (set to one). Results are representative of at least six clone differentiations of two control iPSC lines and two patient iPSC lines; error bars represent S.E.M.. One-way ANOVA followed by Bonferroni's post-hoc test were performed.